Targeting Retinoblastoma tumour suppressor deficiency in Leiomyosarcoma

Irene Sechi

St Hilda's College

A thesis submitted to the University of Oxford
for the degree of Doctor of Philosophy
Hilary Term 2024



Supervisors: Professor Vincenzo D'Angiolella (Primary)
Professor Eileen Parkes (Secondary)

MRC Oxford Institute for Radiation Oncology
Department of Oncology
University of Oxford

Targeting Rb tumour suppressor deficiency in Leiomyosarcoma

Irene Sechi

St Hilda's College, University of Oxford

Abstract

Leiomyosarcoma (LMS) is an aggressive malignant tumour of soft tissue with poor prognosis. Current treatment for LMS involves surgical resection followed by radiotherapy; however, prognosis remains poor in 40% of the cases. The frequent occurrence of mutations in *TP53* and Retinoblastoma (*RB1*) genes in LMS suggests disruptions in normal cell cycle pathways controlling checkpoints and DNA repair mechanisms. In this study, we aimed to identify drugs that exhibit a synthetic lethality effect with *RB1* gene mutations in LMS.

A comprehensive screening approach was used, wherein a panel of LMS *RB1* gene-deficient cell lines was exposed to the Oncology drug library, including 384 inhibitors. A cell proliferation resazurin assay was optimized to identify the drug response. Drug screen data and validation experiments revealed that inhibitors targeting Heat Shock Protein 90 (HSP90) were selectively active against LMS cell lines with *RB1* gene depletion in our drug screen.

Total proteome analysis was carried out to elucidate molecular pathways behind the cytotoxicity of alvespimycin (17-DMAG) in RB1-deficient LMS cells. Data were validated by western blot analysis and flow cytometry, resulting in the proposal of a model wherein targeting Rb loss engaged with a unique dependency on HSP90 for cell survival.

The identification of this synthetic lethal interaction between Rb deficiency and HSP90 inhibition, along with the discovery of a drug candidate, opens potential novel treatment options for RB1-deficient malignancies, particularly among LMS patients. This study provided new insights into potential therapeutic strategies and underscored the importance of personalized medicine approaches for improving outcomes in patients with aggressive soft tissue tumours like LMS.

Acknowledgements

I am greatly grateful to Prof. Vincenzo D'Angiolella whose constant guidance, support, and belief in my abilities have been the cornerstone of this work. Your mentorship has not only shaped my academic journey but has also inspired me to work hard and get results with enthusiasm and creativity.

I extend my gratitude to the funding institute Sarcoma-UK for their generous support. The investment in our collective interest in deepening knowledge on sarcoma research has empowered me to pursue my passion enthusiastically.

To my dedicated labmates, whose insights and encouragement have enriched every steps of this journey, thank you. The collaboration and shared dedication have always created an environment of growth and great teamwork.

To my beloved family, whose unconditional love, understanding, and encouragement have been my rock throughout this work. Your unwavering support, patience, and sacrifices have been the driving force behind my achievements, and for that, I am deeply grateful.

And to my beautiful crazy gang of friends, whose encouragement, laughter, and the positive vibes provided the great amount of laugh and salsa music, thank you. To my wonderful friends Marta, Miranda, Saif, and everyone I shared this journey, your friendship has been a pure source of joy reminding me of the importance of feeling home in another country.

This accomplishment would not have been possible without the collective support and encouragement of each one of you. Thank you for believing in me and for being an integral part of this remarkable journey.

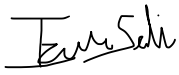
~ Nothing is impossible ~

Declaration of Originality

I declare the research work presented in this thesis is of my own composition, unless stated otherwise by reference or acknowledgement. Any information derived from the published or unpublished work of others has been acknowledged in the text, and references are listed in the bibliography. This work has not been submitted, in whole or in part, in any previous applications for a degree.

Date Signature

4/04/2024



Statement of Impact

I started my PhD studies at the Oncology Department, University of Oxford, in Oxford, in October 2020, supervised by Prof. Anderson J Ryan. At that time my research area was focused on investigating the potential use of novel therapeutic strategies targeting sarcoma tumour with *RB1* gene depletion. However, two external events occurred. First, COVID-19 restrictions slowed down the lab work as the working hours and the support from more senior colleague were limited due to COVID disruptions. Second, my supervisor announced his retirement. Prof. Vincenzo D'Angiolella kindly welcomed me in his team allowing me to continue working on sarcoma research as planned on Sarcoma-UK scholarship who funded the research lab work.

List of Abbreviations

ATCC	American Type Culture Collection
ATM	ataxia-telangiectasia mutated
ATP	adenine triphosphate
ATR	ataxia-telangiectasia and Rad3-related
ATRi	ATR inhibitor/ inhibition
ATRIP	ATR interacting protein
C	Celsius
CCNA2	cyclin A2
CCNE1	cyclin E1
CCNF	Cyclin F
CDC	cell division cycle
CDK	cyclin dependent kinase
CHK1 CHEK1,	checkpoint kinase 1
CHK2 CHEK2,	checkpoint kinase 2
CIN	Chromosome Instability
CO2	carbon dioxide
CV	crystal violet
DDR	DNA damage response
dH2O	distilled water
DMEM	Dulbecco's modified Eagle's medium
DMSO	dimethyl sulfoxide
DNA	deoxyribonucleic acid
dNTP	deoxynucleotide triphosphate
DSB	double-strand break
FBS	foetal bovine serum
EDTA	ethylenediaminetetraacetic acid
EMT	Epithelial Mesenchymal Transition
FACS	fluorescence-activated cell sorting
g	gram(s)
Gln	glutamine
G1	phase gap phase of cell cycle before DNA replication

G2	phase gap phase of cell cycle before mitosis
hr	hour(s)
H2O	water
HCl hydrochloric acid	hydrochloric acid
IC50	half-maximal inhibitory concentration
KAP1	Krüppel-associated box-associated co-repressor 1
kDa	kilo-Dalton
L	litre
LMS	Leiomyosarcoma
M	molarity
MSCs	Mesenchymal Stem cells
m	metre
min	minute(s)
M phase	mitosis
mAb	monoclonal antibody
Na_3VO_4	sodium orthovanadate
NaCl	Sodium chloride
NaF	sodium fluoride
NaOH	sodium hydroxide
NSCLC	non-small cell lung cancer
OS	Osteosarcoma
p53	(TP53) tumour protein 53
pAb	polyclonal antibody
PARP	poly (ADP ribose)-polymerase
pATM	phosphor-ATM
PBS	phosphate buffered saline
PBS-T	phosphate buffered saline with Tween 20
pCHK1	phospho-CHK1
pCHK2	phospho-CHK2
PI	propidium iodide
PI3K	Phosphatidylinositol 3-kinase
PIKK	phosphatidylinositol 3-kinase-related kinase
pKAP1	phospho-KAP1

PTEN	Phosphatase and tensin homolog
Rb	Retinoblastoma protein
RNA	ribonucleic acid
RNR	ribonucleotide reductase
RPA	replication protein
RRM2	Ribonucleotide Reductase Regulatory Subunit M2
RT	room temperature
Runx2	Runt-related transcription factor 2
S phase	DNA replication or synthesis phase of the cell cycle
SDS	sodium dodecyl sulphate
sec(s)	second(s)
SEM	standard error of the mean
Ser	serine
SL	Synthetic lethality
ssDNA	single-stranded DNA
STS	Soft tissue sarcoma
t	time
TBS	tris-buffered saline
TBS-T	tris-buffered saline with Tween 20
TGS	Tumour suppressor gene
TFDP	transcription factor dimerization partner
UV	ultraviolet
γH2AX	phosphorylated histone H2AX

List of Figure

Figure 1.1 Cyclins and CDKs as the main regulators of the cell cycle. 24
Figure 1.2. The Retinoblastoma-E2F pathway. 25
Figure 1.3. Schematic representation of the ATPase cycle of HSP90. 30
Figure 1.4. The aims of the research study 37

Figure 2.1. The TLCV2-RB1 LentiCRISPR system 42
Figure 2.2. The pCW57.1 inducible system. 43
Figure 2.3. The Gateway cloning system. 45

Figure 3.1. Leiomyosarcoma cell lines with stably integrated TLCV2 or TLCV2-RB1 inducible systems. 61
Figure 3.2. Rb knockout in SK-LMS-1 and RKN cell lines. 62
Figure 3.3. Cas9 levels after doxycycline induction. 63
Figure 3.4. Clones with complete *RB1* gene knockout in SK-LMS-1 and RKN cell lines. 64
Figure 3.5. Rb loss promotes proliferation in vitro. 65
Figure 3.6. SKUT-1 cells with the integration of novel inducible system PCW57.1-RB1. 67
Figure 3.7. Rb loss does alter cell cycle biomarkers levels. 68
Figure 3.8. Replication stress/DNA damage repair pathways in LMS cell lines. 70

Figure 4.1. Drug discovery using high through-put drug screen. 73
Figure 4.2. Drug Screen hits identification. 77
Figure 4.3. Drug screen data of SK-LMS-1 cells (30nM). 78
Figure 4.4. Validation of the top hit HSP90 inhibitor, Alvespimycin. 79
Figure 4.5. Validation of the synthetic lethality effect of Alvespimycin. 80
Figure 4. 6. Viability of LMS cell lines upon DDRi inhibitors 82

Figure 5.1. HSP90 inhibitors examined in the drug screen assay. 86
Figure 5.2. The synthetic lethality effect of the HSP90i, Luminespib. 87
Figure 5.3. The synthetic lethality effect of HSP90i in SKUT-1 cell line. 89
Figure 5.4. Cell viability assessment in SKUT-1 cells upon HSP90i. 90
Figure 5.5. siRNA HSP90 knockdown and assessment of HSP90 half-life. 91
Figure 5.6. HSP90 degradation analysis by PROTAC BP3. 92
Figure 5.7. HSPs expression levels validation. 93

Figure 5.8. Cell cycle was not altered by Rb loss and HSP90 inhibition. 95
Figure 5. 9. HSP90 inhibitors treatment promotes apoptosis......97
Figure 5.10. Assessment of apoptosis activation by Flow cytometry analysis......99
Figure 5.11. Process of p62-mediated selective autophagy. 101
Figure 5.12. HSP90 inhibitors activate autophagy pathway......103
Figure 5.13 . HSP90i does not induce cell death by DNA damage response pathways......105

Figure 6.1. S-Trap sample processing technology and mass spectrometry analysis. 107
Figure 6.2. Cell line and drug treatment validation before mass spectrometry analysis......108
Figure 6.3. Rb status examination by mass spectrometry. 109
Figure 6.4. Missing values comparison by mass spectrometry analysis. 110
Figure 6.5. Principal component analysis (PCA) plot for SK-LMS-1 cells (RB1+/-) and with HSP90 inhibition......111
Figure 6.6. Illustration of volcano plots comparing protein expression fluctuation in SK-LMS-1 cells and Rb protein main interactors......114
Figure 6.7. Total proteomic profiles of SK-LMS-1 No-RB1 vs. RB1 cells. 117
Figure 6.8. Metascape's enrichment pathways analysis of SK-LMS-1 cells 118
Figure 6.9. GO Biological Processes of SK-LMS-1 Rb lacking cells......119
Figure 6.10. Proteomic profiling and Enrichment pathways analysis of HSP90i-treated SK-LMS-1 cells (No-RB1 vs RB1). 122
Figure 6.11. Enrichment Pathways Analysis of HSP90i-treated SK-LMS-1 cells (No-RB1 vs RB1). 123
Figure 6.12. GO Biological Processes of HSP90i-treated Rb-null cells. 124
Figure 6.13. Comparison of No-RB1 HSP90i-Treated and Untreated Proteome Profiles.....127
Figure 6.14. Metascape's enrichment data analysis 128
Figure 6.15. GO Biological Processes of HSP90i-treated Rb-null cells. 128
Figure 6.16 Enrichment pathways analysis and GO Biological process......130

Figure 7.1. FAS-apoptotic extrinsic pathway, c-FLIP antiapoptotic activity and HSP90 inhibition......140
Figure 7. 2. Synthetic lethality hypothesis......146

List of Table

Table 1.1. The most common bone sarcoma and STS subtypes. 17

Table 2.1. Leiomyosarcoma Cell line 39
Table 2.2. Plasmids used in the study. 43
Table 2.3. List of components for TAE buffer (1X). Stock solution was stored at 4℃. 48
Table 2.4. Primer used in this study. 49
Table 2.5. Crystal violet staining solution components 50
Table 2.6. Drugs selected for drug screen validation experiments. 52
Table 2.7. Buffers and solutions used in immunoblotting 53
Table 2.8. Primary antibodies used for immunoblotting analysis. 53
Table 2.9. Secondary antibodies used for two-colour detection with infrared fluorescence 54

Table 4.1. The table shows the IC50 values (μM) of the identified hits in each LMS cell line. 77
Table 4.2. Top 10 hits identified in SK-LMS-1 cell line. 78
Table 4.3. IC50 Value of HSP90 inhibitor 17-DMAG 80
Table 4.4. IC50 values of LMS cells upon DDR inhibitors 83

Table 5.1. Delta-Z values of each HSP90 inhibitor used in the drug screen. 87
Table 5.2. IC50 values of Luminespib tested in SK-LMS-1 RB1+/- cells. 88
Table 5.3. IC50 values of SKUT-1 RB1 +/- cells upon HSP90i treatment. 89

Table of Contents

Declaration of Originality 4
Statement of Impact 5
List of Abbreviations 6
List of Figure 9
List of Table 11
CHAPTER 1 16
Introduction 16
1.1. Sarcoma, state of art and classification 16
1.1.1. Soft Tissue Sarcoma 16
1.1.2. Leiomyosarcoma 18
1.1.3. Genetic features in leiomyosarcoma: RB1 gene deficiency 19
1.1.4. Current diagnosis and treatment of leiomyosarcoma 21
1.2.1. Retinoblastoma as a master regulator of the G1-S phase transition 23
1.2.2. The impact of losing Retinoblastoma pathway 26
1.3. Protein homeostasis 27
1.3.1. The role of protein homeostasis in the cell cycle 27
1.3.2. The HSPs chaperones family: structure, regulation, and function. 28
1.3.3. The role of HSP90 in cancer 31
1.4. Synthetic Lethality – Definition and applications 32
1.4.1. The principle of synthetic lethality interaction 32
1.4.2. The high –throughput drug screens 33
1.4.3. Reported synthetic lethality interactions with RB1 gene deficient tumours 35
1.5. Aims of the research project and Hypothesis 36
1.5.1. Targeting RB1 gene deficiency in leiomyosarcoma 36
1.5.2. The generation of an isogenic cell model for Rb loss 36
1.5.3. The identification of novel therapies based on synthetic lethality effect 37
CHAPTER 2 39
Materials and Methods 39
2.1. Cell Culture 39
2.1.1. Leiomyosarcoma cell lines 39
2.1.2. Cell counting and seeding 39
2.1.3. Cryopreservation and thawing cells 39
2.1.4. Harvesting cells 40
2.1.5. siRNA targeting HSP90AA1 gene knockdown 40
2.1.6. Cycloheximide chase assay 41

2.2. Plasmids used in the research study *41*
2.2.1. The Lenti-CRISPR TLCV2 system *41*
2.2.2. The inducible pCW57.1 system *42*
2.2.3. Lentiviral transfection *43*
2.2.4. Gateway cloning *44*
2.2.5. Preparation of medium and agar plates *46*
2.2.6. pCW57.1-RB1 a novel plasmid *46*
2.2.7. Transformation E. Coli – LR Clonase reaction *46*
2.3. DNA sequencing *47*
2.4. DNA agarose gel electrophoresis *47*
2.5. qPCR *48*
2.6. Cell viability assays *49*
2.6.1. Cell Viability assays using Resazurin *49*
2.6.2. Colonies formation assay *49*
2.6.3. Real time Live Cell Microscopy with IncuCyte-Imaging system *50*
2.7. Drug Treatment *50*
2.7.1. High Throughput Drug Screening: The Small Oncology Library *50*
2.7.2. Compounds used for drug screen validation *51*
2.8. Protein Analysis *52*
2.8.1. Protein extraction, SDS-PAGE and western blotting *52*
2.8.2. Immunoblotting and Protein Detection *53*
2.9. Silver staining gel electrophoresis *55*
2.10. Flow Cytometry analysis *55*
2.10.1. Annexin-V for apoptosis cell analysis *55*
2.11. Total Proteome Mass Spectrometry Analysis *56*
2.12. Statistical analysis *57*
CHAPTER 3 58
Results 58
3.1. Developing isogenic RB1+/- cell lines for the study of SL interactions *58*
3.1.1. The panel of leiomyosarcoma cell lines *58*
3.1.2. Genetic heterogeneity of the leiomyosarcoma cell lines *58*
3.2. Generation of isogenic cell line models to study Rb loss *59*
3.2.1. Genetic depletion of Rb in SK-LMS-1 and RKN cell lines *59*
3.2.2. The role of Rb depletion in SK-LMS-1 and RKN cells *65*
3.3. The introduction of the RB1 gene in SKUT-1 cell line *66*

3.4. Further characterisation of the LMS Rb isogenic models *68*
3.4.1. Effects on cyclins *68*
3.4.2. Rb loss in DNA replication stress and DNA damage *69*
3.5. Key Findings *71*
CHAPTER 4 72
4.1. Identification of Synthetic lethality effects with Rb depletion *72*
4.2. Investigation of novel synthetic lethality interactions using a high through-put drug screen *72*
4.2.1. Oncology Drug Library and Rb loss targeted drug screening assay *73*
4.2.2. Identification of potential hits from the drug screen across LMS cell lines *74*
4.3. Validation of synthetic lethality effect *79*
4.3.1. HSP90 inhibition is synthetic lethal in SK-LMS-1 cell line lacking Rb *79*
4.3.2. Investigation of potential synthetic lethality effects using DDR modulators *81*
4.4. Key Findings *84*
CHAPTER 5 85
5.1. HSP90 inhibition is synthetic lethal with Rb loss *85*
5.1.1. Synthetic lethality effect with others HSP90 inhibitors *85*
5.1.2. Synthetic lethality effect with HSP90i in other cell line and different cell system *88*
5.1.3. HSP90 inhibition using different methods (siRNA and PROTACS) *90*
5.2. Cell signalling analysis *93*
5.2.1. HSP90 and HSP70 ..... *93*
5.2.2. The impact of HSP90 inhibition in the cell cycle *94*
5.2.3. Exploring mechanisms of cell death induced by HSP90 inhibition *95*
5.2.4. HSP90i induces cell death by apoptosis activation *96*
5.2.5. HSP90i does not induce cell death by autophagy and other processes *100*
5.2.6. HSP90i does not induce cell death by DNA damage response pathways *103*
5.3. Key findings *106*
CHAPTER 6 107
6.1. The identification of cell death mechanisms *107*
6.1.1. Total proteome mass spectrometry analysis *107*
6.2. Samples preparation for proteome profiling of deficient and proficient Rb cells *107*
6.2.1. Samples validation for proteome profiling of deficient and proficient Rb cells *108*
6.3. Total proteomic profile of SK-LMS-1 cells Rb proficient/deficient *115*
6.4. Total proteomic profile of SK-LMS-1 RB1 +/- cells with HSP90 inhibitor *119*
6.5. Proteome Profiles of HSP90i-Treated vs. Untreated Rb lacking cells *124*
6.6. Proteome Profiles of HSP90i-Treated vs Untreated Rb proficient cells *129*

6.7. Investigation of the Total Proteome data *130*

6.8. Key findings *132*

CHAPTER 7 134

Discussion 134

7.1. Novel therapeutic approaches in leiomyosarcoma *134*

7.1.1 Synthetic lethality effects with Rb tumour suppressor deficiency *134*

7.1.2. The inhibition of HSP90 is synthetic lethal with Rb loss *136*

7.1.3. Apoptotic cell death mechanisms induced by HSP90 inhibition *138*

7.2. The potential of HSP90 inhibition in cancer therapy *141*

7.2.1. HSP90 inhibitors are promising in preclinical and clinical settings *141*

7.3.2. Potential use of HSP90 inhibitors in sarcoma *143*

7.4. Summary and Conclusions *145*

REFERENCES 148

APPENDICES 177

Compound Screening Library – The small Oncology Library tested at 30 nM in SK-LMS-1 cell line. 177

CHAPTER 1

Introduction

1.1. Sarcoma, state of art and classification

1.1.1. Soft Tissue Sarcoma

Sarcomas comprise a heterogeneous subtype of tumours that arise from transformed cells of mesenchymal origins. Indeed, sarcomas arise from mesenchymal tissues, including soft tissue and bone, as primary locations. (Antonescu 2006; Alessandro Gronchi et al. 2017; Matushansky and Maki 2005) Although sarcomas are classified as a rare adult tumour affecting only 1% of all human malignancies, the highest incidence is recorded among rare paediatric malignancies, representing 12-15% of all paediatric tumours. (Grünewald et al. 2020; Stiller et al. 2013) According to the anatomical site of occurrences, sarcomas are generally categorised in soft tissue sarcomas (STS) and bone tumours. Table 1 summarises the major sarcoma subtypes and their main features. Overall, 5 years survival is estimated at 60% and it strongly depends on the disease stage. (H. G. Lyu et al. 2019; Stevens et al. 2008; Stiller et al. 2006)

Soft Tissue Sarcomas have been grouped in two major classes based on genomic, histologic, and/or immunohistochemical features. (Nacev et al. 2020) In terms of genomic characteristics, the first class includes sarcomas with specific genetic alterations and simple karyotypes, such as reciprocal chromosomal translocations and specific oncogenic mutations. This sarcoma subset presents a high prevalence of p53 checkpoint abnormalities, including p53 inactivating mutations, homozygous deletion in CDKN2A, MDM2 amplifications, etc. The second class includes sarcomas characterised by non-specific genetic alterations and unbalanced karyotypes. Chromosomal deletions, amplifications, gains/losses of whole chromosomes and aneuploidy are included in this class. Cumulative chromosomal abnormalities have been associated to high-grade tumours. (Mertens et al. 2002) Significant advances in investigating the molecular genetics of different sarcomas led to an

improved tumour classification and improved prognostication. However, there is a significant gap between the molecular mechanisms of mesenchymal tumour types and targeted therapeutic approaches. (George 2019; Taylor et al. 2011) Current treatments are based on well-established therapeutic regimens combining multi-agent chemotherapy. Conventional chemotherapeutic methods currently may result in treatment failure due to multidrug resistance mechanisms. In addition, chemotherapy is vexed by significant side effects and long-term effects in children. Notably, improvements in survival have been modest. (Gronchi et al. 2017) Surgery represents the mainstay of therapy for limited/localised stage disease, whether outcomes are usually poor for patients with an advanced/metastatic disease. (Taylor et al. 2011; Alessandro Gronchi et al. 2017)

A comprehensive identification of the genetic alterations of sarcomas might contribute to the development of novel therapies. The recognition of gene mutations existing within sarcomas is crucial for the advance of innovative and effective therapeutic strategies. (Gao et al. 2018; Abeshouse et al. 2017; Groisberg et al. 2017)

Table 1.1. The most common bone sarcoma and STS subtypes.
(modified from WHO Classification of Tumours: Soft Tissue and Bone Tumours, 2020, (Teng 2005))

Sarcoma Subtype	Localisation	Main features
Bone tumours		
Chondrosarcoma CHS	Cartilage, bone surface, central bone	Chondrocytes in a chondroid matrix with calcified foci
Ewing Sarcoma EW	Long flat bones	Undifferentiated cells with immune cells infiltration
Osteosarcoma OS	Bone surface or central bone	Neoplastic cells with mesenchymal morphology and frequent polymorphisms; Complex karyotype
Soft Tissue Sarcomas (STSs)		
Fibrosarcoma	Deep soft tissue of extremities, head, neck	Monomorphic fibroblastic cells in collagenous matrix
Gastrointestinal stromal tumours GIST	Gastrointestinal track	Undifferentiated cells spectrum with cells and mixed histology (spindle, epithelioid)
Leiomyosarcoma	Peritoneum and uterus	Mesenchymal, spindle shaped

LMS		cells; Highly complex karyotype and genomic instability
Liposarcoma LPS	Variable (retroperitoneal space)	High heterogeneity among cells included in a vascularized stroma
Rhabdomyosarcoma RMS	Variable	Mesenchymal phenotype cells with altered myogenic differentiation
Synovial Sarcoma SS	Deep soft tissue of extremities	Spindle cells with altered mesenchymal or epithelial differentiation

1.1.2. Leiomyosarcoma

Leiomyosarcoma (LMS) is a rare, highly malignant sarcoma tumour, accounting for 1-2% of all uterine malignancies with an estimated incidence of 0.4/100000 women per year. (Juhasz-Böss et al. 2018; Koivisto-Korander et al. 2012; Toro et al. 2006) LMS exhibits several degrees of smooth muscle differentiation and generally originates from the smooth muscle layer of the uterus, known as the myometrium tissue. (Dei Tos et al. 1996; X. Guo et al. 2015; Juhasz-Böss et al. 2018) Leiomyosarcoma occurs in five specific anatomic sites: retroperitoneum, deep extremity, uterus, blood vessels and superficial dermis. (Yang et al. 2009) It is common to distinguish between extra-uterine LMS (arising in the retroperitoneum, walls of blood vessels, gastrointestinal tracts) or uterine-LMS as the two groups present differences in clinicopathological features such as the histological grade, tumour size, and depth. (Kasper et al. 2021; Bathan et al. 2013; Serrano and George 2013; George et al. 2022)

LMS is a particularly aggressive malignancy and metastasis can occur in half of the patients despite initial surgery resections. Clinical responses and survival outcomes observed in patients depended on the histological, clinical, and molecular heterogeneity of LMS. (A. T. J. Lee et al. 2019; E. Merry et al. 2021; Anderson et al. 2021) Prognosis is based on tumour staging and anatomical localisation, with patients presenting metastasis having a low chance of successful drug treatment. Metastasis of

LMS arises for 31% in extremities, 58% in abdomen and for the 50-71 % in the uterus. (Mbatani, Olawaiye, and Prat 2018; Gladdy et al. 2013) Histological features can be categorized into spindle, myxoid, and epithelioid variants or a mix of these three histotypes. The spindle type tissue looks like smooth muscle with elongated spindle cells organised in intersecting fascicular packets with eosinophilic cytoplasm and a wide number of pleomorphic cells (Demicco et al., 2015) Myxoid LMS exhibits scant cytoplasm and altered nuclei morphology, while epithelioid LMS tumours are often hypercellular. Well-differentiated LMS tumours commonly exhibit spindle type tissue. In contrast, moderately or poorly differentiated LMS shows low levels of smooth muscle features. (Oliva 2016) Diagnoses of uterine LMS could be easily mistaken as benign myometrial leiomyomas. (Sanada et al. 2022; Zheng et al. 2020; Z. Zhang et al. 2020) Non-uterine smooth muscle tumours are commonly considered malignant, as benign leiomyomas do not occur in extra-uterine locations. (Kostov et al. 2021)

1.1.3. Genetic features in leiomyosarcoma: *RB1* gene deficiency

Cytogenetic studies have classified leiomyosarcoma as a soft-tissue tumours with a complex karyotype. The heterogeneous genetic landscape reflects low chances of survival for LMS patients. The pathogenesis of leiomyosarcoma reveals wide heterogeneity between cells within the same patient. (Abeshouse et al. 2017; Hattinger et al. 2019) Genetic aberrations considered as hallmarks of this disease include structural chromosomal aberrations, abnormalities affecting the tumour suppressor network, DNA damage response pathways, and alternative lengthening of telomeres (ALT). (Cuppens et al. 2018; Raish et al. 2012) Genomic studies have reported that LMS presents loss of gene function at specific chromosomal regions such as 10q11–21.2 encoding *PTEN*, 13q14.3-q21.1 encoding *RB1* and 17p13 which encodes *TP53.* (Nacev et al. 2020; Cuppens et al. 2018; Chudasama et al. 2018) Inactivating genetic aberrations such as mutations and gene deletions in *TP53* and *RB1* are highly common in LMS (92% and 94% respectively), while 57% of LMS shows inactivating aberrations in *PTEN*. (Chudasama et al. 2018) Anomalies in the RB1-cyclin D1 pathway, including *RB1, CCND1, CCND3* and *CDKN2A,* were reported to be present in approximately 90% of

LMS tumours, associating with poor prognosis. (Anderson et al. 2021; J. Yang et al. 2009) Moreover, LMS mutations occur in genes encoding the alpha thalassemia/mental retardation syndrome X-linked (ATRX). (Guo et al. 2015; Mäkinen et al. 2016; Tsuyoshi and Yoshida 2018) Analysis of a pan-cancer cohort indicated LMS shows homologous recombination (HR) deficiency due to mutations in BRACA1/2 genes in 5% of cases, followed by gene deletion in PTEN, ATM, CHEK1, XRCC3, CHEK2, RAD51. (Jonsson et al. 2019; Nacev et al. 2020) LMS patients presenting as genomic mutations in DNA damage response (DDR)-associated genes showed the worst prognosis compared to those missing these gene alterations. (Rosenbaum et al. 2020)

Overall, *TP53* and *RB1* genes inactivation denotes a unifying feature of LMS development. (Chudasama et al. 2018; Groisberg et al. 2017; Mäkinen et al. 2016) Chudasama et al developed exosome and transcriptome sequencing analysis in LMS revealing *TP53* and *RB1* depletion was due to genetic mechanisms such as chromosomal rearrangements in 50 % of sporadic leiomyosarcoma. Mutations in the *TP53* gene, the guardian of the genome (Sherr and McCormick 2002; Mantovani, Collavin, and Del Sal 2019), can promote aberrant cell cycle regulation, inhibit senescence, and cell apoptosis, thereby exposing the cells to genomic instability. (Ito et al. 2011; Masuda et al. 1987; Würl et al. 1999) Mutations associated with either one or both Rb and p53 pathways abrogate regulation of G1 to S-phase transition during the cell cycle. (López-Guerrero et al. 2004; Nath et al. 2015; Kent and Leone 2019) An uncontrolled G1-S phase transition in the cell cycle promotes chromosomal abnormalities exposing the genome to DNA damage accumulation. (Benassi et al. 1997; Leng et al. 1997; Jackson and Bartek 2009; Bartek, Lukas, and Lukas 2004)

The identification of oncogenes and the depletion of tumour suppressor deepen our knowledge of the basis of sarcomagenesis and enable the investigation of novel targeted therapies. Our research study aimed to identify selective treatments for LMS with defined genetic features.

1.1.4. Current diagnosis and treatment of leiomyosarcoma

Surgical resection remains the keystone of therapy for patients diagnosed with localised LMS. The optimal approach involves complete excision with substantial negative margins. However, performing surgical resections in retroperitoneal LMS remains challenging. (Hensley 2011) For patients with u-LMS, hysterectomy is still recommended especially when disease is restricted to the uterus area.

Surgery may by complemented by neo-adjuvant or adjuvant radiotherapy and chemotherapy. (Alessandro Gronchi et al. 2017; Linch et al. 2014; Casali et al. 2018) Clinical trials studies have investigated the advantage of implementing adjuvant chemotherapy following surgical removal to prevent recurrences. Data regarding the use of radiotherapy in localised STS in the extremity and trunk can be controversial. There is very limited clinical data on radiotherapy when LMS occurs in the retroperitoneal area. As a result, adjuvant chemotherapy is not regularly recommended. Neoadjuvant chemotherapy is also still under evaluation. (Le Cesne et al. 2014; Pasquali et al. 2022; A. Gronchi et al. 2021)

Overall, doxorubicin-based chemotherapy continues to be the primary treatment for advanced-stage soft tissue sarcoma, including LMS. Positive responses have been reported in patients with metastatic LMS who underwent doxorubicin treatment. (D'Ambrosio et al. 2020; Tap et al. 2020; Judson et al. 2014) Additional chemotherapeutics have been investigated in combination with doxorubicin or as monotherapy such as gemcitabine, taxanes, trabectedin, pazopanib, and eribulin. However, doxorubicin remains the main chemotherapeutic agent to have significant responses in patients with advanced LMS. (Linch et al. 2014)

Among the broadly established immunotherapeutic approaches with promising results in various subtypes of cancers, the immune checkpoint blockade (ICB), also known as immune checkpoint inhibitors (ICIs) has been investigated in sarcomas. Inhibitory immune checkpoints (ICs) play a key role in regulating and suppressing the immune system to prevent autoimmunity. Currently, numerous

clinical trials are exploring ICIs potential benefits in several type of sarcomas including leiomyosarcoma. (De Wispelaere et al. 2021) Despite the advances in immunotherapy over the past decade, immunotherapeutic approaches shown no effective results and have not been incorporated into standard treatment protocols for sarcomas. (Birdi et al. 2021; Siozopoulou et al. 2021) This underscores the need to develop novel therapies based on predictive biomarkers that can categorise sarcoma patients who might benefit of ICIs treatment.

Hormonal therapies targeting the estrogen and progesterone receptors may also represent an effective therapeutic alternative in LMS. Both estrogen and progesterone receptors are highly expressed in uterine sarcoma patients, representing a favourable prognostic factor demonstrating an improved overall survival. (Leitao et al. 2012; Thanopoulou et al. 2014) Clinical trials based on the use of aromatase inhibitors, progestins and gonadotropin-releasing hormone analogues have indicated that hormone dependency is only partial and not entirely effective. Overall, the outcome of hormone therapies in LMS has been limited, and the quality of data associated with them is low, so these therapeutic agents are falling out of favour. (Maccaroni et al. 2022)

Given the potential BRCAness feature in soft tissue sarcoma, including LMS, further clinical assessments have been focused on evaluating poly-(ADP-ribose) polymerase (PARP) inhibitors in clinical settings. Olaparib is the first PARP inhibitor approved to treat BRCA1/2 mutated ovarian cancers, BRCA1/2 mutant HER2-negative breast cancer, and advanced pancreatic cancer. (Kaufman et al. 2015; Bryant et al. 2005) Furthermore, PARP inhibitors have exhibited activity in other cancers showing HR deficiency and/or mutations in DDR-associated genes. (Eric Pujade-Lauraine et al. 2017) However, preclinical observations in LMS indicated that Olaparib showed a modest effect in patients with relapsed bone and soft tissue sarcoma. (Grignani et al. 2018; H. Li et al. 2020)

In conclusion, LMS is a complicate disease to treat, especially in advanced stages. Chemotherapeutic regimens for localised disease should be optimised, and the potential introduction of new targeted

therapy such as PARP inhibitors needs to be explored. Further investigations are also needed to comprehend the biological basis of drug responses and resistance mechanisms in LMS. The molecular heterogeneity of this disease requires the identification of novel drug targets alongside biomarkers to identify specific patient populations that would benefit of an improved chance of survival. Given the poor benefit of conventional therapies, we believe novel treatments must be developed based on the common genetic alterations detected in LMS. The loss of tumour suppressors can be exploited in synthetic lethal approaches.

1.2.1. Retinoblastoma as a master regulator of the G1-S phase transition

Cell cycle is a well-orchestrated process divided in phases (G1, S, G2, M) that directs the duplication and distribution of genetic material to the next cell generation. Each step is controlled by checkpoints that regulate the execution of each transitional phase (fig.1.1). The transition among cell cycle phases is driven by cyclin-dependent kinases (CDKs). Each cell cycle phase is driven by distinct CDKs complexes, which contain a catalytic kinase (CDKs) and a cyclin that selects substrates for phosphorylation. CDK-cyclin complexes serve as the engine of the cell cycle, driving phase transitions. Their expression varies at each cell cycle phases, ensuring irreversibility and checkpoint controls (fig.1.1). (S. Kim et al. 2022; Resnitzky and Reed 1995)

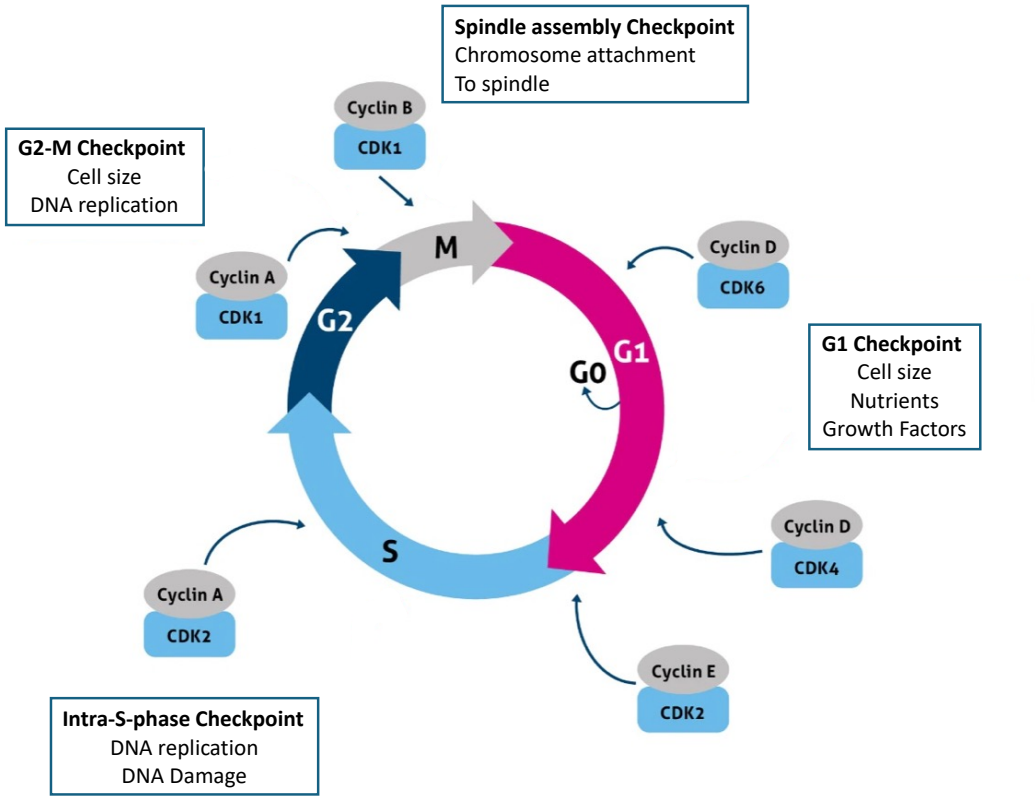


Figure 1.1 Cyclins and CDKs as the main regulators of the cell cycle.
Scheme showing the different cyclins/CDK partners regulating cell cycle progression and respective cell cycle checkpoints controlling the different regulatory pathway of the cell cycle. Adapted from Proteintech.

Cell cycle entry from quiescence is promoted by cyclin-dependent kinase 4 and 6 (CDK4/6) partnering with cyclin D. (Pennycook and Barr 2020a; Henley and Dick 2012; Heldt et al. 2018) During G1 phase, mitogenic signalling stimulates cyclin D expression, which interacts and activates the CDK4/6 (fig.1.2). In turn, the active form of cyclin D-CDK4/6 phosphorylates and inactivates Rb. In its active form, Rb complexes with E2Fs, DNA-binding transcription factors. Once Rb is phosphorylated, E2Fs are released from the Rb complex and stimulate transcription of genes encoding positive cell cycle regulators such as cyclin E1, cyclin A2 and others (fig.1.2). (Lundberg and

Weinberg 1998; Sherr and McCormick 2002) Cyclin E/A interacts with CDK2 which phosphorylates Rb in a positive feedback loop, further inactivating Rb. (Matson and Cook 2017; Fisher 2016; S. Kim et al. 2022; Pennycook and Barr 2020a) The CDK2-posivite feedback establishes the irreversible progression into the cell cycle. (Pennycook and Barr 2020b; Johnson and Skotheim 2013; Zetterberg, Larsson, and Wiman 1995) This is considered the most critical step of the G1-S phase transition regulated by the CDK2-Rb-E2F pathway, referred to as the restriction point of the cell cycle. (Kent and Leone 2019; Bertoli, Skotheim, and De Bruin 2013) Thus, Rb acts as a tumour suppressor inhibiting the cell cycle entry. (Weinberg 1995) Interference in the G1/S control and disruption of the restriction point are considered hallmarks of cancer and can occur through Rb loss or hyperactivation of CDKs. (Rubin, Sage, and Skotheim 2020; Resnitzky et al. 1994; Lukas et al. 1997)

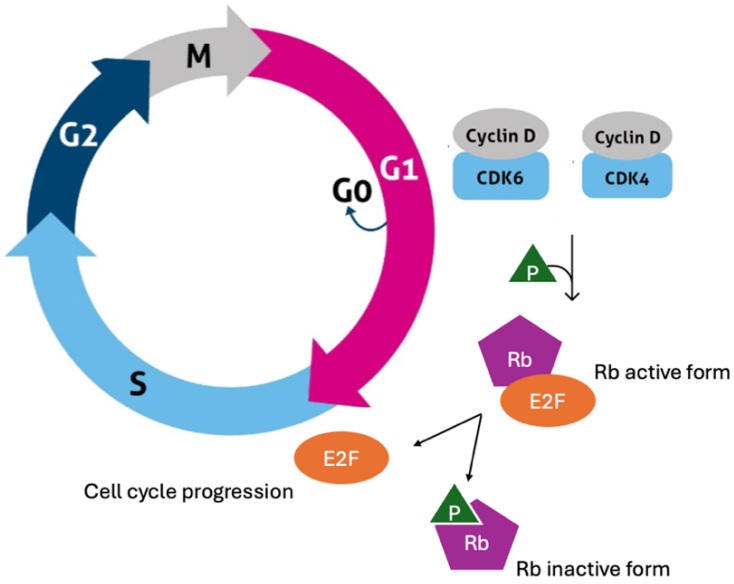


Figure 1.2. The Retinoblastoma-E2F pathway.

Phosphorylation by Cyclin D-CDK4/6 induce conformational changes to the structure of Rb that consequently release E2F, which regulates the expression of S phase genes promoting cell cycle progression. Adapted from Proteintech.

During the mid-late S/G2 phase, expression levels of E2Fs gradually decline in a negative feedback loop promoted by atypical repressors such as E2F7/8 (Chen, Tsai, and Leone 2009; Clijsters et al. 2020) and by the phosphorylation reaction catalysed by cyclin A-CKD2 on E2F to stop its transcription activity. (Bertoli, Skotheim, and De Bruin 2013; Fischer and Müller 2017; Pagano, Draetta, and Jansen-Dürr 1992) Members of the INK4 family including $p16^{Ink4a}$, a tumour suppressor that restricts the phosphorylation of Rb, inactivate cyclin D-CDK4/6. Additionally, the $SCF^{cyclin\ F}$ machinery coordinates the fluctuations of protein levels during late G1-S and G2 phase, including E2F family proteins. (Burdova et al. 2019; D'Angiolella, Esencay, and Pagano 2013b; Clijsters et al. 2019b) Unlike other cyclins, cyclin F does not bind to or activate any CDKs. Cyclin F has an F-box domain acting as an E3 ubiquitin ligase. The F-box domain mediates the interaction of cyclin F with Skp1, which in turn binds to Cullin1 (Cul1), resulting in the Skp1–Cul1–F-box multi-subunit ubiquitin ligase complex. (Cardozo and Pagano 2004; L. Wang et al. 2014) $SCF^{cyclin\ F}$ targets for the degradation of E2Fs factors during G2 phase, resetting cell cycle control for the next G1/S phase transition.

1.2.2. The impact of losing Retinoblastoma pathway

The CDK-Rb-E2F axis plays a fundamental role in regulating the cell cycle progression and safeguarding genomic stability. Functional inactivation of Rb or alterations in any components of the CDK-Rb-E2F axis promote the oncogenic activity of E2F, leading to DNA damage and genomic instability. Through E2F activity, loss of Rb creates a cellular environment that enables abnormal cell proliferation and cancer development. (Sherr and McCormick 2002) The continuous activity of E2Fs implies abnormal expression of multiple proteins that influence the DNA replication process. (Kent and Leone 2019; Chen, Tsai, and Leone 2009; Fischer and Müller 2017) Bestor et al. published that DNA damage arising in case of Rb inactivation is an indirect consequence of replication fork stalling due to E2F deregulation. Overall, Rb loss triggers the stalling of replication forks, an increase of DNA damage, and alterations in chromosome structure. Replication fork stalling may leave un-replicated regions of the genome, promoting the occurrence of double strand breaks (DSBs) that, if not repaired,

delay mitotic progression and chromosome segregation. (Bester et al. 2011) Chromosome instability and aneuploidy due to Rb loss led to genomic instability. (Nath et al. 2015; Ly et al. 2019) Furthermore, replication forks stalling triggered by Rb loss may affect the replication of repetitive genome regions, such as centromeres and telomeres. Alterations in centromere structure contribute to incorrect chromosome mis-attachment to the mitotic spindle, increasing the likelihood of errors during chromosome segregation. (Manning and Dyson 2012a; Manning, Longworth, and Dyson 2010; Longworth et al. 2008)

Furthermore, additional studies have shown that E2F1 and E2F2 regulate genes that activate angiogenesis, extracellular matrix remodelling, and tumour cell interactions, promoting tumour invasion and metastasis. Dysregulation of E2Fs not only participates in early tumour development but also can mediate the transition to malignant metastatic carcinomas. Additionally, E2F1 influences cancer metabolism by enhancing glycolysis and controlling oxidative metabolic genes, critical for tumour cell proliferation under hypoxic and nutrient-limited conditions. (Kent and Leone 2019)

Overall, the loss of Rb function promotes the acquisition of a malignant phenotype mediated by E2Fs' activity. While promoting cancer progression, the constant activation of E2Fs might also give rise to significant genomic instability, rendering cells vulnerable to DNA damage repair inhibitors. (Weber and Ryan 2015; C. Merry et al. 2010) DNA damage, CIN, oxidative stress or E2F activation have inspired the development of DNA damage response (DDR) inhibitors. This may represent an exciting opportunity to target sarcomas by exploiting genetic differences that exist between normal and tumour cells. (Koppenhafer et al. 2020; Hattinger et al. 2019; S. E. Jones et al. 2017)

1.3. Protein homeostasis

1.3.1. The role of protein homeostasis in the cell cycle

Proteins are fundamental players in cellular operations, constantly undergoing folding, assembly, and disassembly processes, trafficking to specific subcellular compartments. Additionally, old proteins

must be cleared to ensure their proper function. Thus, protein homeostasis is essential for cell survival. The protein turnover process, mediated by ubiquitination, ensures that cells respond promptly to stimuli and adapt to changing environments, thereby preserving optimal cell functionality. (López-Otín et al. 2023; Hipp, Kasturi, and Hartl 2019a) It is not surprising that the efficiency of the proteostasis network decreases with aging, leading to several pathological conditions. (Hipp, Kasturi, and Hartl 2019a) Disruptions of crucial cellular processes can cause abnormal intracellular protein accumulation (e. g. damaged misfolded proteins or aggresomes). (López-Otín et al. 2023) To restore proteostasis, cells orchestrate a quality control network of signalling pathways that sense and resolve disruptions in the total proteome. (Hipp, Kasturi, and Hartl 2019b; Kaushik and Cuervo 2015; Brandvold and Morimoto 2015) Molecular chaperones, the ubiquitin proteosome system, and the autophagy-lysosomal machinery cooperate to promote effective protein folding and discard aberrant or misfolded proteins, thereby counteracting potential dynamic stress events that are otherwise toxic to the cells. (Y. E. Kim et al. 2013; Brandvold and Morimoto 2015) While disruptions in this process might lead to aging, several approaches have been developed to exploit the altered protein homeostasis in cancer. (Morimoto and Cuervo 2014; Costa-Mattioli and Walter 2020)

1.3.2. The HSPs chaperones family: structure, regulation, and function.

The physiological cellular processes of oxidation tend to induce protein misfolding by mispairing critical residues for folding (for instance, cysteines residues). (Ngo et al. 2022) Cells have developed molecular chaperones that counteract this process by promoting the clearance of misfolded proteins. Chaperone proteins represent about 1–2% of the total mammalian cellular proteins under non-stress conditions. (Whitesell and Lindquist 2005) Chaperones are also referred to as heat shock proteins as their synthesis increases under high temperature. The function of chaperones is not only to clear misfolded proteins but also to assist in the folding of newly synthetised proteins and ensure conformational rearrangements. This includes the eventual dissociation and refolding of stress-denatured proteins. (Brandvold and Morimoto 2015; Kim et al. 2013) Furthermore, chaperones

cooperate with the proteosome degradation machinery to discard aberrant misfolded proteins. (Morimoto and Cuervo 2014; Costa-Mattioli and Walter 2020)

Heat shock proteins can be classified based on their molecular weight as HSP40, HSP60, HSP70s, HSP90s, HSP100s, and small HSPs. Among the many HSPs, HSP90 is a highly abundant conserved molecular chaperone which is present within the cells in 4 isoforms: HSP90α/β isoforms are allocated to the cytosol, GRP94 localised in the endoplasmic reticulum, and TRAP1 (tumour necrosis factor receptor-associated protein 1) in mitochondria. Given they derived from gene duplication, the two cytosolic isoforms (HSP90α/β) show high homology (85% sequence identity) which leads to the interchangeable use of the term HSP90 for both unless specified. (Biebl and Buchner 2019) The tight regulation of HSP90 is crucial for cellular physiology preservation. (Zhang et al. 2022; Chatterjee and Burns 2017)

HSP90 is formed by three domains: a highly conserved ATP binding domain at the N-terminus (NTD), a middle regulatory domain (MDT), and a C-terminal dimerization domain (CDT). ATP binding and hydrolysis reactions induce changes in the conformational state of HSP90 which allow the interaction with client proteins or co-chaperones. During the ATPase cycle, HSP90 changes from an ATP-free open to an ATP-bound closed conformation (fig.1.3). These ATP-dependent conformational changes allow client proteins' association and their folding process. (Mickler et al. 2009; Shiau et al. 2006)

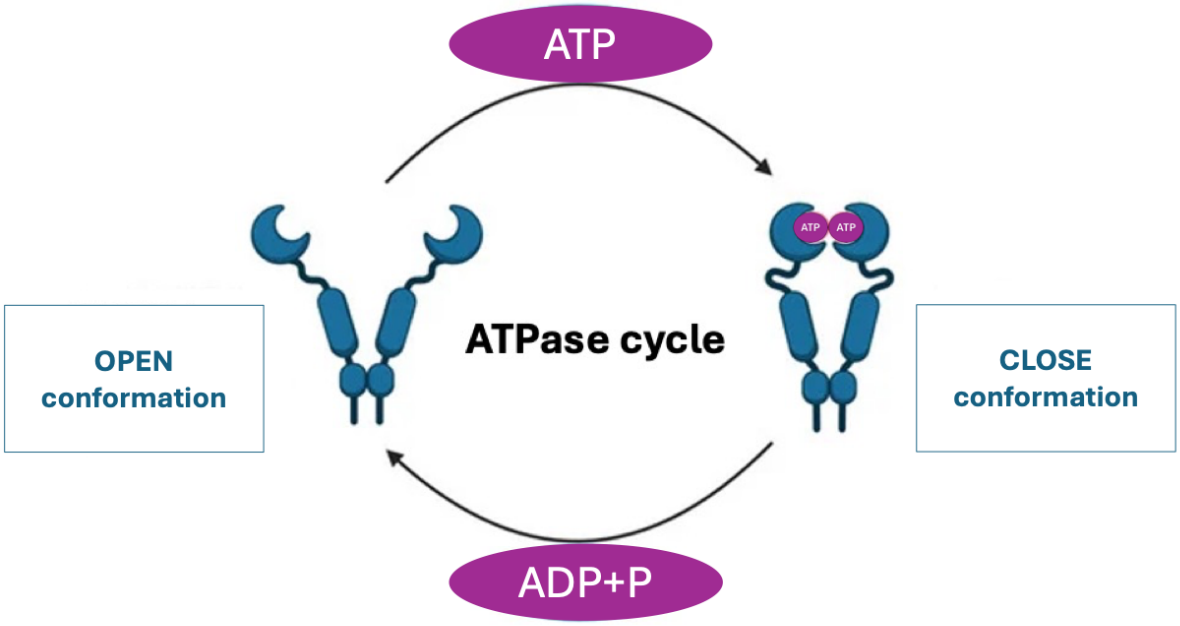


Figure 1.3. Schematic representation of the ATPase cycle of HSP90.
ATP binding and ATP hydrolysis to ADP result in a structurally transient conformational adaptation of HSP90 chaperone from an open to a close state. Dissociation of ADP restores HSP90 to its open conformation. Modified from Youssef et al. 2023.

HSP90 interacts with a large range of client proteins. Client proteins are interacting partners of HSPs through non-covalent binding. For instance, client proteins of HSP90 comprise receptor tyrosine kinases (HER2, EGFR, IGF-1R), as well as signalling proteins (AKT and SRC), transcription factors like steroid receptors (BCL-6, CAR), cell cycle regulatory proteins (CDK4 and CDK6) and structural proteins, such as actin and tubulin. This highlights the crucial role of HSP90 in cell signalling. (Biebl and Buchner 2019; Hoter, El-Sabban, and Naim 2018)

Furthermore, HSP90 promotes the correct folding of the tumour suppressor p53. The interaction between HSP90 and p53 plays a crucial role in cell survival and cancer development. (Alexandrova et al. 2015) Notably, the mutant form of the p53 tumour suppressor leads to oncogenic activities via gain-of-function processes, correlating with genomic instability, tumorigenesis, metastasis and cancer progression. Differently from wild type p53, mutant p53 escapes protein degradation interacting with

HSP90, undergoing constitutive protein stabilisation in tumours. The pharmacological inhibition of HSP90 appeared to be a promising approach to target mutant p53 harbouring cancers. (Müller et al. 2004)

Co-chaperones represent the main co-player of HSP90 regulators. These molecules assist HSP90 in performing its functions. Co-chaperones interact to N-terminal domain of HSP90, assisting in the ATP hydrolysis reactions and facilitating the folding of client proteins. (Biebl and Buchner 2019; Prodromou and Bjorklund 2022) There are various co-chaperones such as p50/Cdc37, HSP90-organizing protein (HOP/Sti1, p23, Aha1 and HSP70), as well as a range of immunophilins, that are required by HSP90 to function. They are grouped into two classes: TRP-domain-containing co-chaperones and TRP-less co-chaperones. The TRP (tetratricopeptide repeat) domain comprises 34 amino acids repeats integrated together in a bunch of helix-turn-helix motifs, functioning as a binding site for the HSP90 C-terminal MEEVD (Met-Glu-Glu-Val-Asp) motif. (Scheufler et al. 2000). The main co-chaperones including the TRP domain is HOP (Hsp70/Hsp90 organizing protein) and PPIase (peptidyl-proline isomerase, PP5). Co-chaperones TPR-less domain differs by the specific binding sites on the surface of the HSP90 dimer. This class of co-chaperones comprises AHA1 (“activator of Hsp90 ATPase”), CDC37 (a “cell division cycle control” protein), and PTGES3 (prostaglandin E synthase 3 cytosolic, so-called p23 protein). Additionally, HSPs can be regulated by post-translational modifications (PTMs). PTMs, such as phosphorylation, acetylation, SUMOylation, S-nitrosylation, methylation, and ubiquitylation, can affect HSPs in two roles: facilitating access to the binding site or the domain interactions between dimers. (Mollapour and Neckers 2012)

1.3.3. The role of HSP90 in cancer

HSP90 plays a crucial role in assisting the folding of client proteins required for the proliferation and survival of cancer cells. A wide range of client proteins, including signalling kinases, steroid hormone receptors, and transcription factors, participate in signal transduction, transcriptional regulation, cell cycle control and other cell signalling processes. Moreover, most of HSP90 client proteins play

oncogenic roles in cancer. The clientele comprises many oncogenic kinases such as EGFR, CDK4, BRAF, HER2, AKT, MET, MEK, and BCR-ABL (breakpoint cluster region-Abelson), as well as transcription factors such as estrogen and androgen receptors, p53 and HIF-1α. Other cancer-dependent client proteins include survivin and the catalytic subunit of telomerase hTERT. (Taipale, Jarosz, and Lindquist 2010; Workman et al. 2007a) HSP90 is often highly expressed in cancer, likely reflecting the contribution of chaperones to cancer progression. Thus, several pharmacological approaches have been developed to inhibit HSP90. (Hoter, El-Sabban, and Naim 2018; Whitesell and Lindquist 2005; Biebl and Buchner 2019; Jian Zhang et al. 2022)

The inhibition of HSP90 would allow the simultaneous depletion of oncogenic proteins through the ubiquitin-proteasome pathway. This approach targets a broad spectrum of cancer dependencies, challenging key cancer pathological processes such as cell growth, evasion of apoptosis, angiogenesis, invasion, and metastasis. (Z. N. Li and Luo 2023)

1.4. Synthetic Lethality – Definition and applications

1.4.1. The principle of synthetic lethality interaction

The principle of synthetic lethality (SL) refers to a condition in which the simultaneous loss of two non-lethal genes results in cell death. (Setton et al. 2021a; Mullard 2017) Neither of the single genes is lethal when considered individually, but the absence of both genes is lethal. Since cancer cells could present loss of gene function in tumour suppressor genes, pharmacological inhibition of a second gene may induce cell death. (Huang et al. 2020; Setton et al. 2021b) This approach allows targeting only cancer cells (that lose the gene) sparing normal cells (which have it) offering great potential for clinical implication. The discovery of the lethal effects of PARP inhibitors in a BRCA1/2 mutation initiated the development of similar therapeutic strategies. Olaparib is the first suitable PARP inhibitor to enter the clinic for the treatment of recurrent high-grade serious ovarian cancer. (Lord and Ashworth 2017)

Synthetic lethality is considered a powerful approach to exploit specific genetic vulnerabilities in cancer cells, while sparing normal tissues.

1.4.2. The high –throughput drug screens

The synthetic lethality (SL) approaches in cancer are appealing as cancer cells often lose genes, and in some cases, entire chromosomes. To discover potential novel drug candidates in synthetic lethality approaches targeting specific genetic alterations, high throughput drug screens are conducted using large chemogenomic drug libraries. (Coussens et al. 2017) Drug libraries can be screened in a panel of cancer cells to validate that synthetic lethality is consistent and reproducible across many cancer models. (Ghandi et al. 2019; A. Lin and Sheltzer, 2020) Depletion induced by RNAi, CRISPR gene editing approaches or loss-of-function gene in cells are common tools used to facilitate the identification of genes synthetic lethal upon chemical compounds. (Edwards et al. 2015). Large scale projects to identify SLs have been undertaken by consortia and are collected in websites such as www.depmap.org.

The use of well-designed chemogenomic library represents a mainstream approach to introduce novel therapies into the clinic. (Hughes et al. 2011) The drug candidate can also be referred as a hit of the drug screen. Hits can function either on their own or by playing synergistic effects with other drugs. Furthermore, HTS may evidence the opportunity to repurpose the use of existing drugs currently used in clinic for other disease. (Ghandi et al. 2019; Mohammadi et al. 2020) Collections of chemical drugs targeting specific gene families such as kinases, methyltransferases, and others, have been established. Initiatives led by the Structural Genomics Consortium (SGC) at the University of Oxford have focused on developing novel probes collections to use in HTS drug screens. (L. H. Jones and Bunnage 2017) In particular, automated robotic systems have been optimised to handle large screens of compounds.

We can distinguish between phenotypic cell-based and biochemical target-based assays. In a phenotypic cell-based drug screen, compounds are expected to induce a specific cellular responses or changes in cell phenotype such as alterations in morphology, viability, or other biological features. This method is quite valuable when mechanisms of action are not very well understood. The target-based drug screen is another approach where compounds are chosen for their well-known interaction with a molecular target linked with the disease. Here, the screening process aims to observe any changes of the biological targets which may include proteins, enzymes, or receptors.

Data analysis informatic tools process the high volume of data, leading to the identification of potential hits, which is followed by preclinical validation. First, chemical structure may be modified to increase the potency and efficacy of the hits and drug properties. Next, biology approaches and bioinformatic tools play a significant role in validating the potency of the drug candidate and exploring its potential use in the clinic. Biological or physiological assays have been utilised to validate drug responses within a panel of cell lines with specific mutations, however, animal studies are crucial to validate the promise of the approach. For instance, animal studies are fundamental for assessing the safety and toxicity of the chemicals, providing important insights to determine the appropriate dosage level. Successful compounds may move to preclinical studies to evaluate their safety (Phase I), pharmacokinetics, and toxicity (Phase II). Once, side effects and efficacy have been evaluated in Phase III, the chemical agent may enter in clinical trials. (Mammadova, Mermer, and Kocabaş 2021a; Edwards et al. 2015)

Despite several challenges, the use of chemogenomic library screens has increased in recent years, becoming a fundamental tool for drug discovery. (Mammadova, Mermer, and Kocabaş 2021b; Athanasiadis et al. 2023) This method accelerates drug discovery by investigating chemical compounds in a very short time and with limited costs. Moreover, the use of automated technologies, biological and physiological assessment play an essential role in identifying novel drug candidates, which may represent therapeutic alternatives in cancer.

1.4.3. Reported synthetic lethality interactions with RB1 gene deficient tumours

The presence of an oncogene in a tumour represents a defined vulnerability that can be exploited in targeted approaches. However, it is often the case that cancer cells lack specific activated oncogenes and are transformed mainly through the loss of tumour suppressors. The SL approach allows targeting cancer cells where tumour suppressors are lost, sparing the normal tissues. (Setton et al. 2021a; L. Liu et al. 2018) As mentioned above, Rb is lost in numerous cancers and, other laboratories have undertaken approaches to identify drugs or drug targets synthetic lethal with Rb loss. It has recently been reported in the literature that the inhibition of Aurora kinase B is synthetic lethal with the loss of *RB1* in lung cancer SCLC cell lines. A CRISPR/Cas9-based screening was utilised in SCLC lines bearing inactivating Rb mutations, comparing them to cells where Rb expression was induced. The screen identified the loss of Aurora B as a synthetic lethal target, promoting cell death with *RB1* loss in SCLC cells. (Oser et al. 2019; Gong et al. 2019) Aurora kinases participate in centrosome maturation, regulate spindle assembly, control centrosome orientation and cytokinesis during mitosis. Since cells without Rb progress faster into mitosis, the inhibition of Aurora kinase B might impair the correct execution of mitosis, resulting in cell death. (Manning and Dyson 2012b)

Additionally, Rb loss induces DNA replication stress through the accumulation of E2F, which triggers DNA damage response pathways. In these circumstances, cancer cells depend on checkpoints to preserve cell survival. (Kitajima, Li, and Takahashi 2020; Shamma et al. 2009) It has indeed been reported that the removal of CHK1 leads to synthetic lethal effects with Rb loss due to S phase collapse. (Witkiewicz et al. 2018)

The inactivation of the *RB1* gene could lead to unstable mitotic fidelity and a weakened DNA damage response in tumour cells. This vulnerability can be exploited by pharmaceutical agents targeting these abnormalities, triggering cell death upon chromosomal instability (CIN). In advanced prostate cancer, where *RB1* and *BRCA2* are frequently depleted, these tumours show high sensitivity to PARP inhibitors. (Chakraborty et al. 2020) However, it has not been validated whether Rb loss alone makes

cells susceptible to PARP inhibition. Similarly, the loss of Rb together with K-Ras mutation sensitises cancer cells to platinum-based-chemotherapy, especially in pancreatic cancer. (Hijioka et al. 2017a; Treré et al. 2009) Additionally, Rb inactivation induces a better drug response to the topoisomerase inhibitor irinotecan. (Coussy et al. 2020)

In summary, while the loss of *RB1* gene function is generally associated with a poor prognosis, it may also promote clinically significant vulnerabilities in cancer cells. The aberrancies linked to Rb loss, including DNA damage occurrences, chromosomal instability (CIN), oxidative stress, and hyperactivation of the E2F transcription factor, create opportunities for exploiting synthetic lethality. Notably, the absence of Rb is observed in a diverse range of tumours at different stages, which makes potential synthetic lethality screenings worthy to identify effective and innovative therapeutic strategies.

1.5. Aims of the research project and Hypothesis

1.5.1. Targeting *RB1* gene deficiency in leiomyosarcoma

The concept of synthetic lethality opens new opportunities for the development of drugs targeting cancer-specific mutations identified in a specific type of tumour. The main aim of this research study is to identify therapeutic strategies targeting retinoblastoma tumour suppressor deficiency in leiomyosarcoma tumour cells, an attempt that has not been undertaken before in this tumour.

1.5.2. The generation of an isogenic cell model for Rb loss

The initial objective was to generate isogenic cell models of *RB1* gene deficient leiomyosarcoma tumours. The generation of a panel of cell lines proficient and deficient for the *RB1* gene was achieved by introducing specific gene losses into a well-characterised LMS cell line. The CRISPR/Cas9 genome-editing method was employed to introduce *RB1* depletion mutations into inherently *RB1*-proficient leiomyosarcoma cell lines. A complementary approach was used in cells intrinsically carrying *RB1* gene-inactivating mutations. In this case, the expression of Rb was induced

from an exogenous promoter after the addition of doxycycline. Our cell line models recapitulate the genetic complexity of LMS and represent the first model of Rb loss in this tumour type. We hope these models will be utilised by other laboratories in similar approaches.

1.5.3. The identification of novel therapies based on synthetic lethality effect

To advance leiomyosarcoma cancer treatment, we aimed to uncover and authenticate novel drug candidates exploiting the concept of synthetic lethality due to the presence of specific vulnerabilities arising from Rb loss within our cell models. The outline of the study is presented in figure 1.4. We first generated isogenic LMS cell models for Rb loss, followed by the development of a high-throughput drug screen. The drug screen was designed based on a phenotypic-based approach to systematically investigate a drug library of 384 compounds, including chemotherapeutics already used in the clinic, in clinical trials or still under scientific investigation. The identification of potential hits from the drug screen data was followed by conducting preclinical investigations to gain a comprehensive understanding of the molecular targets' activity and the pathways affected by the selected hits. These findings could also provide insights into which mechanism of action facilitates the synthetic lethality interaction with Rb loss. In addition to providing a model to study Rb gene loss in LMS, our study highlights a potential treatment approach for LMS using HSP90 inhibitors (HSP90i) in a clinical setting.

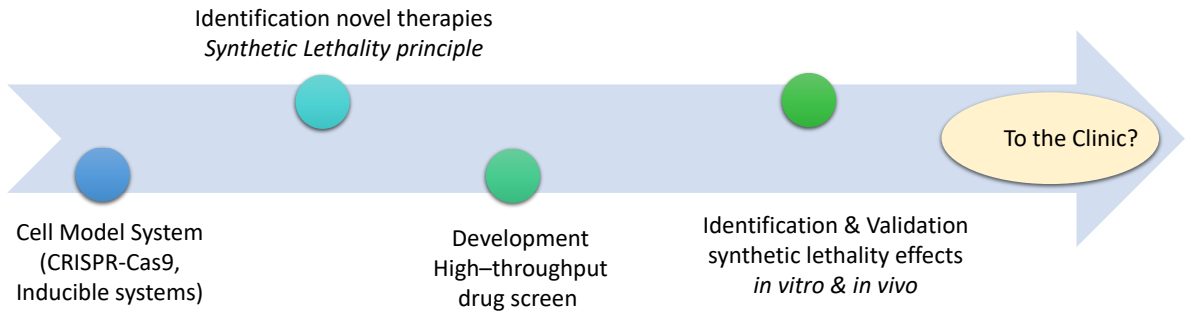


Figure 1.4. The aims of the research study

Schematic illustrating the aims of the research study starting from the generation of the cell model system for RB1+/- LMS cells used to identify novel synthetic lethal interactors with Rb loss in the

high-throughput drug screen. Consequently, synthetic lethality effects of the hits identified by the drug screen should be validated *in vitro*. The highest expectation of the research study would be to present these hits to the clinic.

CHAPTER 2

Materials and Methods

2.1. Cell Culture

2.1.1. Leiomyosarcoma cell lines

The Leiomyosarcoma cell lines are listed in Table 2.1. The cells lines were maintained in Dulbecco's Modified Eagle's Limiting Medium (GIBCO, #41965039), supplemented with 10% Fetal bovine serum (EU approved, Tetracycline Free PAN, Biotech, #30–3602), or fetal bovine serum (Sigma-Aldrich, #F9665) for HEK293T cells, and 100 U penicillin / 100 µg/ml streptomycin (Millipore). The cell lines have been tested negative for mycoplasma with MycoAlert ® Detecion Kit (Lonza, #LT-07418).

Table 2.1. Leiomyosarcoma Cell line

Leiomyosarcoma Cell Line	Tissue Type	Obtain from
RKN	Ovary	Tebu-bio, JCRB0176
SK-LMS-1	Uterus	ATCC, HTB-88
SKUT-1	Vulva	ATCC, HTB-114
HEK-293T	Kidney	ATCC, CRL-3216

2.1.2. Cell counting and seeding

Cell density and viability were measured using the LUNA-II™ automated cell counter (Logos biosystem). A 1:1 mixture of a cell suspension and 0.4% trypan blue solution (Life Technologies) was added to a Luna-Countess cell counting chamber slide and inserted into the Luna-Countess automated cell counter. Alternatively, all cells were counted manually with a hemocytometer counting chamber (Marienfeld Neubauer-improved #0640030) under a light microscope.

2.1.3. Cryopreservation and thawing cells

For long term storage, cells were grown to 70-80% confluency treated with Trypsin/EDTA (AppliChem, #A48920500) as described above. Following standard passaging, cells were collected in

culture medium and centrifuged at 300 g for 5 minutes. The cell pellet was re-suspended with freezing medium mix containing FBS with 10% (v/v) DMSO. 1 ml aliquots were stored in cryogenic vials within an isopropanol Mr. Frosty^{TM} Freezing Container (Themo Scientific) at -80°C, thereafter, transferred to a liquid nitrogen storage vessel for long term/permanent storage.

To recover frozen cells from liquid nitrogen storage, cryovials were moved from liquid nitrogen onto dry ice, defrosted quickly in a 37°C water bath with gentle agitation. The contents of the vial were transferred to Falcon tubes containing 10 ml prewarmed complete culture medium. After centrifugation at 250 g for 5 minutes, cell pellet was gently resuspended in an appropriate amount of prewarmed culture medium to be successfully transferred into plates/ flasks (6-well: 3 ml; T25: 8 ml; T75: 16 ml) and incubated overnight to allow cell surface attachment. The cells were split once or twice before seeding in any future experiments.

2.1.4. Harvesting cells

The medium was discarded, and the plates/dishes were rinsed 1-2 times with an appropriate amount of DPBS. Plates/dishes were then placed on ice, and cells were lysed by adding lysis buffer. Cells were then scraped off from the surface using a cell scraper and transferred into Eppendorf tubes. RIPA buffer was chosen as suitable lysis buffer as it enables the extraction of membrane, nuclear and cytoplasmic proteins. It was supplemented with proteinase inhibitors: phenylmethylsulphonyl fluoride (DTT, 1:1000), protease inhibitor cocktail (PIN 1:500, Sigma, P8340), phenylmethyl sulphonyl fluoride (PMSF, 1:1000), β–glycerophosphate (BGP, 1:100), okadaic acid (1:1000). After DPBS washing and spinning down at 400 g for 5 minutes in a microcentrifuge, samples were either stored frozen at -20°C to -80°C or processed promptly to downstream applications.

2.1.5. siRNA targeting HSP90AA1 gene knockdown

SK-LMS-1 cells were seeded and allowed to reach 60-80% confluence over 24 h before transfection. Transfection was performed using HiPerfect Transfection Reagent (Qiagen, #301704) following the

manufacturer's instructions. The siRNA used in this study was ON-TARGET-plus Human HSP90AA1 siRNA (Dharmacon, #L-005186-00-0005).

2.1.6. Cycloheximide chase assay

Cells were seeded in 10cm-dishes and allowed to reach 60% confluence after 24 hours of incubation. Subsequently, cells were treated with 50 µg/ml of Cycloheximide to inhibit ribosomal protein synthesis. Cell samples were collected at the indicated time points over 24-hour period, and the half-life of the Rb protein was monitored by Western blot (WB).

2.2. Plasmids used in the research study

2.2.1. The Lenti-CRISPR TLCV2 system

To induce the CRISPR knockout of the gene of interest (*RB1*), two SK-LMS-1 and two RKN cell lines were generated through lentivirus transduction, derived from their respective parental SK-LMS-1 and RKN cell lines. An inducible TLCV2-RB1 vector (Addgene, #87836, Fig.2.1, table 2.2) was utilised to facilitate the removal of the *RB1* Retinoblastoma gene by activating the expression of Cas9 upon addition of doxycycline. The TLCV2 vector (Addgene, #87360, Fig 2.1) served as a control, as it does not express sgRNAs targeting Rb. Both vectors contained a puromycin resistance cassette. (Barger, Branick, Chee, & Karpf, 2019; Nicolay et al., 2015) The LentiCRISPR TLCV2 v2 is an all-in-one inducible system, where doxycycline (Sigma-Aldrich, #D3447) induces CAS9-2A-eGFP expression in a concentration manner. The U6 promoter drives constitutive expression of an sgRNA targeting the human *RB1* gene in TLCV2-RB1, or an untargeted sgRNA in the TLCV2 vector.

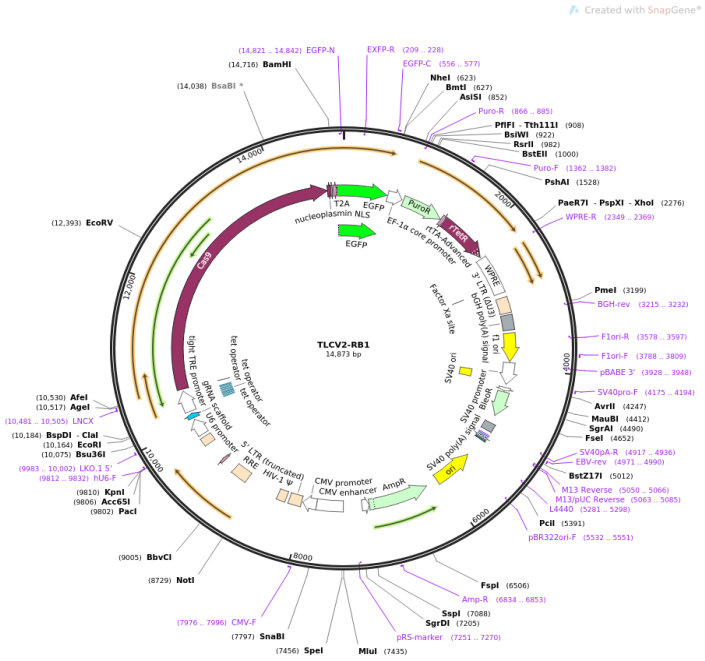


Figure 2.1. The TLCV2-RB1 LentiCRISPR system

LentiCRISPR v2 is an all-in-one inducible system. The addition of doxycycline induces Cas9-2A-eGFP expression. The U6 promoter facilitates constitutive expression of an sgRNA targeting human *RB1*. Expression of sgRNA and puromycin is activated by constitutive promoters. (Adapted from Addgene).

2.2.2. The inducible pCW57.1 system

The pCW57.1-RB1 plasmid was employed to transfect the SKUT-1 cell line, which harbours inactivation mutations in the *RB1* gene (Fig.2.2, table 2.2). The pCW57.1 plasmid, a generous gift from David Root (Addgene, #41393), is a lentiviral vector that expresses rtTA-VP16-2A-puro from the PGK promoter. It can facilitate *RB1* gene expression upon addition of doxycycline. *RB1* gene sequence was introduced into the pCW57.1 destination vector from an entry vector pDON-233-RB1 (Addgene, #81857) using gateway recombination cloning technology (ThermoFisher, #11791100).

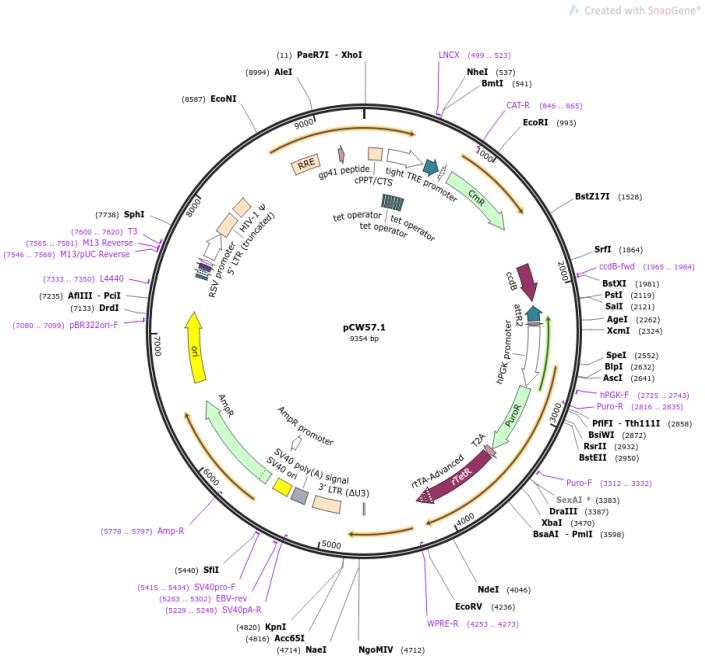


Figure 2.2. The pCW57.1 inducible system.

The plasmid expresses rtTA-VP16-2A-puro from the PGK promoter, and it functions as an 'all-in-one' dox-on system. pCW57.1 was generously provided by David Root. (Adapted from Addgene)

Table 2.2. Plasmids used in the study.

Plasmid	Company
TLCV2-RB1	Addgene #87836
TLCV2	Addgene #87360
pCW57.1	Addgene #41393
pDONR-223_RB1_WT	Addgene #81857

2.2.3. Lentiviral transfection

To perform the removal of the *RB1* gene, LentiCRISPR viruses TLCV2 and TLCV2-RB1 were generated in HEK-293T cells to transduce the SK-LMS-1 and RKN cell lines. Similarly, viral particles containing pCW57.1-RB1 were produced in HEK-293T cells to infect the SKUT-1 cell line and insert the *RB1* gene into the genome of this cell line. The transfer plasmid (TLCV2, TLCV2-RB1 or pCW57.1), the packaging plasmid (psPAX2, Addgene #12260), and the envelope plasmid (pMD2.G, Addgene #12259) were purified using the QIAprep Spin Miniprep Kit (Qiagen, Germantown, MD, USA) and propagated in culture for storage in glycerol at -80°C (500 µL).

HEK-293T cells were seeded in complete culture medium in 10cm-dishes to reach 70-95% cell confluency within 24 hours. On the day of transfection, 2 µg of the transfer vector, 1.5 µg of the packaging plasmid psPAX2, and 1.5 µg of the envelope plasmid pMD2.G were combined in a 1.2-centrifuge tube with 400 µL Opti-MEM I Reduced Serum Medium (Thermo Fisher Scientific). Subsequently, 15 µl of the transfection reagent Polyethylenimine (PEI, Polysciences, #23966) was added. The PEI solution was prepared by dissolving 125 mg of PEI powder in 50 ml of 1×PBS and filtered using a 0.22 µm membrane. Aliquots were stored at - 80°C. The transfection mixture was vortexed and incubated for 15 min at room temperature before adding dropwise to the cells. After 24 hours, the medium was replaced with complete culture medium to allow low basal levels of target gene expression. The following day, 48 hours post-transfection, virion-containing medium was collected from HEK-293T cells, loaded onto a syringe, and filtered using a 0.45 µm filter. The filtered medium containing virions was collected into a new 15 ml falcon tube for storage at - 80 °C or for use in infecting the appropriate target cell line in the presence of polybrene (4 µg/ml, Sigma). The next day, infected target cell lines were washed with PBS, and complete fresh medium was replaced. After 48 hours post-infection, puromycin was added to the cells at a final concentration of 2.5 µg/ml to induce cell selection. Infected cells were cultured for approximately ten days in presence of puromycin; for maintenance, cells were cultured at a reduced puromycin concentration of 1.25 µg/ml.

2.2.4. Gateway cloning

The Gateway Technology is an *in vitro* cloning method dependent on bacteriophage tyrosine recombinases known as lambda integrases. (Landy, 1989). These enzymes catalyse recombination reactions, resulting in the excision and integration of linear DNA sequences (donor vector) into entry plasmid vectors. (Ptashne,1992) Recombination reactions occur with high accuracy and specificity at *att* DNA sites that flank cloning sites, selectively exchanging between two DNA strand sequences. The entry plasmid is designed to ensure that the gene of interest is positioned between attL1 and attL2 following the attB/attP recombination reaction. Destination vectors are strategically engineered to incorporate the *ccdb* gene, which serves as a negative selectable marker positioned by attR1 and

attR2. The negative selectable marker encodes a toxic protein that leads to bacteria cell death, allowing only those bacteria with the successfully cloned gene to survive.

Recombination reactions can occur within both the lytic and lysogenic pathway. The lytic pathway involves host cell lysis and viral release, catalysed by the bacteriophage λ Int, Excisionase (Xis) proteins, and the E. coli Integration Host Factor (IHF) protein (LR Clonase ™ enzyme mix). The lysogenic pathway involves the integration of the viral genome into the host chromosomes without cell lysis. This reaction is catalysed by the bacteriophage λ Integrase (Int) and E. coli Integration Host Factor (IHF) proteins (BP Clonase ™ enzyme mix).

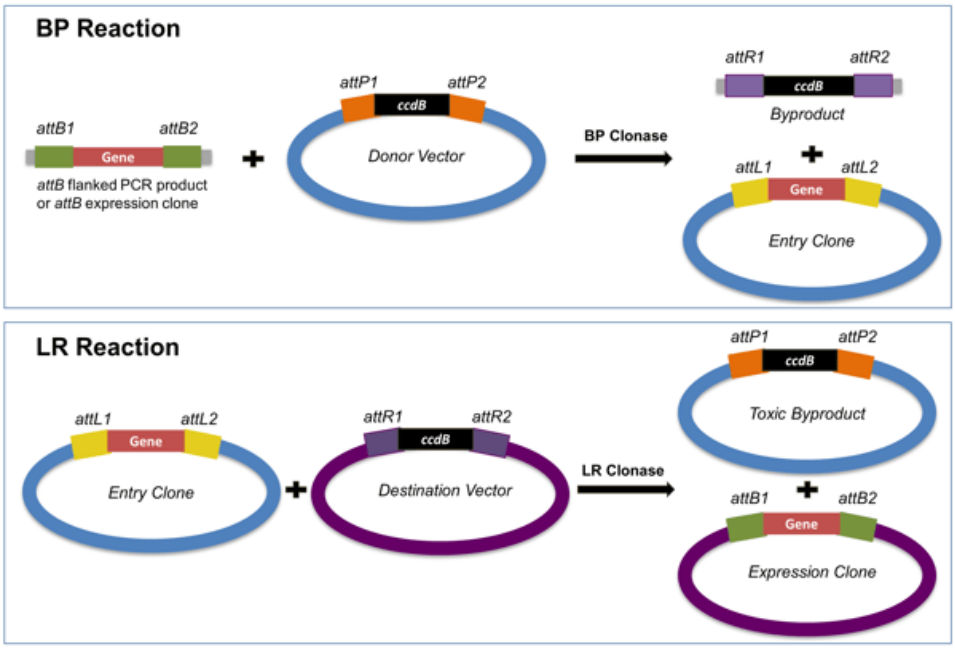


Figure 2.3. The Gateway cloning system.
BP reaction (Top). The gene of interest is cloned into the donor vector using the attB/attP recombination reaction, resulting in the gene of interest flanking between attL1 and attL2 hybrid sites. **LR reaction (Bottom)**. The gene of interest is transferred from the entry vector to the destination vector using the attR/attL recombination reaction, positioning the gene of interest between attB1 and attB2. (Adapted from Addgene)

2.2.5. Preparation of medium and agar plates

Bacteria were cultured in Luria-Bertani (LB) broth. LB agar was prepared by suspending 35 g of LB agar in 1 L of distilled water and sterilised by autoclaving. The LB agar was heated until it reached the boiling point, then supplemented with the appropriate antibiotic. The agar solution was dispensed into sterile 10-cm Petri dishes in a sterile environment (~20 ml/plate). Plates were left at room temperature before being moved to 4°C storage.

2.2.6. pCW57.1-RB1 a novel plasmid

The gateway recombination cloning technology (ThermoFisher, #11791100) was used to generate the novel plasmid pCW57.1-RB1. This implied an LR clonase reaction (Invitrogen) to transfer the entry vector pDON-233-RB1 (Addgene, #81857) into the destination vector pCW57.1 (Addgene, #41393). For the LR recombination reaction, 5 µl of the entry clone pDON-233-RB1 and 2 µl of the destination vector pCW57.1 were combined in a 1.5 ml-Eppendorf tube. TE buffer pH 8.0 (10 mM Tris-HCl, pH 8.0, 1 mM EDTA) was added to reach a final volume of 16 µl. The mixture was supplemented with 4 µl of LR clonase enzyme mix (Invitrogen, #11791019), vortexed, and then incubated at room temperature for 1 hour. After incubation, 2 µl of proteinase K solution (2µg/µl) was added to the reaction mixture, which was then vortexed and incubated at 37°C for 10 min. Competent E. coli bacteria were transformed with the reaction mixture, and antibiotic-resistant expression clones were selected.

2.2.7. Transformation E. Coli – LR Clonase reaction

Competent E. coli cells were aliquoted in 50 µl in 1.5ml-eppendorf tube and stored at -80°C. Upon thawing on ice, 4 µl of the LR Clonase reaction mixture was added to the competent E. coli cells. The tubes were briefly mixed by gently tapping them twice, followed by a 30-minutes incubation on ice. Subsequently, the cells were heat-shocked at 42°C in a water bath for 30 seconds before being immediately returned to ice for 2 minutes. Then, 200 µl of S.O.C medium (Invitrogen™, #15544034) was added to the cells. The cells were incubated in a shaker set at 37° C for 1 hour with constant

shaking at 5 g. After incubation, 50 µl of the mixture was spread onto LB agar plates containing the appropriate antibiotic. The plates were then incubated overnight at 37°C to allow bacterial colonies to form.

The following day, single bacterial colonies were picked from the LB agar plate and allowed to grow in agar medium overnight at 37°C in a shaking incubator. On the subsequent day, tubes containing the bacterial solution were centrifugated at 300 g for 10 minutes, and the supernatant was discarded while the bacteria pellet was stored at - 80°C. Plasmids were isolated from the bacteria and purified using a mini prep kit (Quiagen, #27106) following the manufacturer's procedure. The DNA concentration was validated by measuring the optical density (OD) at A_{260} using the SPECTROstar Nano spectrophotometer (BMG LabTech). The ratio of absorbance at 260 nm and 280 nm was used to assess the purity of the DNA. A ratio of approximately 1.8 is generally recognised as "pure" for DNA; if the ratio is lower, it may indicate the presence of proteins or other contaminants that absorb at or near 280 nm.

2.3. DNA sequencing

To validate the integration of the sequence of the *RB1* gene sequence into the pCW57.1 vector and confirm the integrity of the entire construct, DNA sequences were verified by Sanger sequencing.

2.4. DNA agarose gel electrophoresis

The DNA agarose gel electrophoresis technique is commonly used to separate DNA molecules based on their size. When an electric field is applied, DNA fragments, which carry a negative charge due to the phosphate groups, migrate towards the positively charged anode. Since DNA molecules have a uniform mass/charge ratio, they undergo separation based on size within the agarose gel. The separation of DNA fragments is inversely proportional to their molecular weight: small fragments migrate faster and through the gel than larger ones.

For DNA analysis, 1% (w/v) agarose gels were used. The agarose gels were prepared by melting 1 g of agarose in 100 ml of 1x TAE buffer. After cooling, 10 µl of SYBR Safe DNA Gel Stain (Stratech Scientific Ltd) was added for every 100 ml of agarose mixture. DNA samples were appropriately diluted with 6x DNA Gel Loading Dye (Thermo Fisher Scientific) and loaded onto the gel alongside a Generuler 1 kb DNA molecular weight marker (Thermo Fisher Scientific). Gel electrophoresis was performed in 1x TAE buffer at 120V. After the separation process, the DNA molecules were visualized using the iBright™ FL1500 Imaging System (Thermo Fisher Scientific).

Table 2.3. List of components for TAE buffer (1X). Stock solution was stored at 4℃.

Component	Final Concentration
Tris[a] (pH 7.5)	40 mM
Acetic acid[b]	20 mM
EDTA[c]	1mM

a. VWR, E691-500ml
b. Sigma-Aldrich, M5661-50G
c. AppliChem, A48920500

2.5. qPCR

For real time gene expression quantification, the HotStarTaq®Master Mix Kit (#203446, 203443 and 203445) was utilised, which includes buffers and reagents. The primers used in this study are described in table 2.4. The PCR mix comprises 1 µM of each forward and reverse primer, 2.5 units of HotStarTaq Master Mix, with RNAse-free water added to reach a total volume of 50 µl. The reaction mix was gently mixed by pipetting up and down a few times before being distributed at appropriate volumes into PCR tubes. Subsequently, template DNA (<1 µg/50 µl reaction) was added to each individual PCR reaction mix. The PCR tubes were then placed into the QuantStudio™ 5 Real-Time PCR System (Thermo Fisher Scientific, #A28140) programmed for an initial heat activation at 95°C for 5 min to activate HotStarTaq DNA Polymerase. This was followed by 25 cycles of 98°C for 10 sec, then primer annealing temperature at 52°C for 20 sec, extension at 72°C for 30 sec per kb of

template, and a final extension at 72°C for 2 min. After completion, the reaction mixture was kept at 4 °C until further use.

Table 2.4. Primer used in this study.

Gene Symbol	Accession Number	Forward primer 5'-3'	Reverse primer 5'-3'	Company
RB1	VC00021N	GCCTCTCGTCAGGCTTGAG	CAGTCCTAACTGGAGTGTGTGGA	Merk

2.6. Cell viability assays

2.6.1. Cell Viability assays using Resazurin

Cells were seeded at an optimised cell density of 1000 cells per well and in triplicate in 96-well plates (Costar, flat bottom; Corning Incorporated) following overnight incubation to allow re-attachment. Subsequently, cells were treated with drugs and 0.01% DMSO (vehicle control) at the indicated concentrations. After five days, relative cell proliferation was assessed using resazurin (0.125 mg/ml in dH2O; Sigma-Aldrich). Only metabolically active cells can reduce resazurin to the highly fluorescent resorufin molecule. The fluorescence intensity is directly proportional to the number of viable cells. Fluorescence was detected by using POLARstar Omega plate reader (BMG Labtech GmbH; Ortenberg, Germany) with excitation at 544 nm, emission at 590 nm, and at a gain of 1000. The average values of the triplicate blank wells were subtracted from all other wells, and the resulting data were normalized to the average of the vehicle-treated wells. Data analysis and graph were generated using Microsoft Excel 2013 and GraphPad Prism® 7 (GraphPad Software, La Jolla, CA, USA).

2.6.2. Colonies formation assay

Cells were seeded at a very low cell density, aiming for 100 cells per well in triplicates in 10cm-dishes and incubated overnight to allow attachment. After 24 hours, cells were treated at the indicated drug concentrations and then incubated at 37°C for 7-10 days to allow growth. To investigate cell

sensitivity to drug treatment, cells were incubated for a time equivalent to at least six potential cell divisions. On the final day, when untreated cells reached 90% cell confluence, the medium was removed, and cells were washed with 5 ml of 1xPBS each. Subsequently, they were stained with 5 ml crystal violet solution for 10 min on a rocker set to very low speed. After pouring out the crystal violet, the wells were carefully rinsed in H_2O and dried. Cells were then visualised with digital development with the iBright™ FL1500 Imaging System (Invitrogen).

Table 2.5. Crystal violet staining solution components

Component	Final Concentration
Crystal violet (powder)	0.5 g
Methanol*	20%
H_2O	100ml

* Thermo Fisher Scientific, #10164663

2.6.3. Real time Live Cell Microscopy with IncuCyte-Imaging system

Cells were seeded in flat bottom 96-well plates to reach 70% confluence after 5 days incubation at 37°C, CO2 (5%). The 96-well plates were then inserted into the Real time Live Cell Microscopy system with IncuCyte-Imaging system (Sartorius). Four fields were imaged per well under 10× magnification every 24 h for 5 days. A sample of these images was collected as an image collection, and using the IncuCyte-Imaging software, phase contrast, object, size, filters, and hole filling were adjusted to optimise precision in-cell detection. These settings were then applied to every image. The images were analysed using the IncuCyte-Imaging software to yield cell confluence data.

2.7. Drug Treatment

2.7.1. High Throughput Drug Screening: The Small Oncology Library

The Oncology library (384 compounds, indicated in the appendix) was screened in duplicate at concentrations of 30 nM, 0.3 μM and 3 μM alone in SK-LMS-1, RKN, SKUT-1 cells, which were

proficient and deficient for the *RB1* gene, respectively. Cells were seeded at pre-optimised densities in 384-well plates using Perkin Elmer Janus liquid handling workstations. After 24-hour incubation at 37°C, cells were treated with the drug library, consisting of 384 compounds including cell cycle inhibitors, replication inhibitors, DNA repair inhibitors and standard chemotherapeutics, or with 1 μM gemcitabine used as positive control, using the Perkin Elmer Janus liquid handling workstations. Following s 72-hour incubation at 37°C, DMEM medium was replace with DMEM containing 1mM resazurin (Cell Titer Blue, Promega). Cells were then incubated for an additional 2 hours at 37°C, and the fluorescence intensity of resazurin was measured using the EnVision multilabel plate reader (PerkinElmer).

The raw data underwent normalized to account for negative controls and the edge effect, with background subtraction implemented to prevent artifacts and ensure reproducibility. Delta-Z (ΔZ) values were calculated using the positive control for viability inhibition, representing the difference between Rb-proficient and Rb-deficient cells. Cell viability was assessed by comparing normalised proficient and non-proficient cells, generating a ΔZ list for each compound concentration. Hits were prioritised based on their ΔZ value, ranked from the lowest to the highest, indicating drug sensitivity in Rb-deficient LMS cell lines. Potential hits were identified as drugs that sensitised the Rb-deficient LMS cells at one or more concentrations, with a false positive possibility of ≤ 0.05.

2.7.2. Compounds used for drug screen validation

The inhibitors identified as potential hits from the drug screen data analysis were employed to explore potential synthetic lethality interactions in LMS cell lines. These compounds were initially prepared as 10 mM stock solutions in 100% DMSO, with aliquots stored for a extended periods at -80°C, or alternatively at -20°C for shorter durations.

Table 2.6. Drugs selected for drug screen validation experiments.

Target	Compound	Company
ATR	VE821	SelleckChem
CHK1	LY2606318	Stratech Scientific Ltd
HSP90	Alvespimycin, 17-DMAG	SelleckChem
HSP90	Luminespib, NVP-AUY922	SelleckChem
WEE1	MK-1775	SelleckChem

2.8. Protein Analysis

2.8.1. Protein extraction, SDS-PAGE and western blotting

To prepare cell-extracts, cells were lysed in RIPA lysis buffer supplemented with the following: phenylmethylsulphonyl fluoride (DTT, 1:1000), protease inhibitor cocktail (PIN 1:500, Sigma, P8340), phenylmethyl sulphonyl fluoride (PMSF, 1:1000), β–glycerophosphate (BGP, 1:100), okadaic acid (1:1000). After centrifugation at 250 g for 15 minutes at 4°C, the supernatant of each sample was transferred to fresh microcentrifuge tubes, and the pellets were discarded. Protein concentration in the cell lysates was measured using Lowry Protein Assay Kit (Bio-Rad) following the manufacturer's instructions with bovine serum albumin (BSA, Sigma) used as a protein standard. A standard curve was constructed using BSA with concentrations ranking from 0 to 1 mg/ml, and the absorbance readings were measured at 750 nm using a microplate reader (SPECTROstar Omega plate reader, BMG Labtech GmbH). All standards and samples were measured in duplicate, and Microsoft Excel 2013 was used for computing the unknown sample concentrations and designing the standard curve.

Once protein concentration was calculated, protein samples were diluted in distilled water to achieve equal protein concentrations in each sample. 4x Laemmli sample loading buffer (Sigma-Aldrich) was added to the samples before incubation at 95℃ for 5 mins in a dry heating block. 10 µg of protein per lane was loaded onto a precast Bolt™ 4 to 12%, Bis-Tris, 1.0 mm Mini Protein Gels (ThermoFisher,

NW04125BOX) alongside PageRulerTM Prestained Protein Ladder (ThermoFisher, #26617). The gel was run at 180V for 30 min with Tris/Glycine/SDS running buffer (BioRad). Proteins were then transferred to PVDF membranes (Millipore) using a wet transfer system with cold 1x Tris/Glycine buffer (BioRad) containing 20% methanol (v/v; Sigma-Aldrich) at 100 V for 40 min with an ice pack cooler and magnetic stirrer.

2.8.2. Immunoblotting and Protein Detection

After transferring proteins to PVDF membranes, the membranes were stained with Ponceau S solution (Sigma-Aldrich), carefully cut where appropriate, and washed twice with PBS or PBS-T for 5 minutes. Subsequently, they were incubated in blocking buffer (5% Silk Milk Powder in TBS) for 45 minutes at room temperature. Diluted primary antibodies were then added, and the membranes were incubated overnight at 4°C. The following day, membranes were washed three times for 5 minutes each in PBS-T and then incubated with the appropriate secondary antibody diluted in 5% Silk Milk Powder in PBS-T for 60 minutes at room temperature. After another round of washing (3 x 5min) in PBS-T, blot development was carried out using the iBright™ FL1500 Imaging System (Invitrogen).

For loading control, the same membranes were probed with Anti-GAPDH (ThermoFisher Scientific MA5–15738) or Anti-alpha Tubulin (TU-02) antibody (Santa Cruz Biotechnology, # sc-8035).

Table 2.7. Buffers and solutions used in immunoblotting

Buffer	Composition
PBS (1X)	PBS[a]
PBS-T	1x PBS, 0.1% (v/v) Tween-20 [b]

a. Life Technologies, #14200083
b. Fisher Scientific #10485733

Table 2.8. Primary antibodies used for immunoblotting analysis.

Specification (Name)	Species/clonality	Dilutions	Company
α-Tubulin	Mouse	1:1000 (PBS)	Santa Cruz, #sc-23948
CDK4	Rabbit	1:1000 (PBS)	Cell Signalling, # 12790S
Phosphor-CHK1 ser317	Mouse	1:1000 (PBS)	Cell Signalling, #12302S
CHK1	Rabbit	1:1000 (PBS)	Cell Signalling, #2360S
Cleaved-Caspase 3	Rabbit	1:1000(5%BSA)	Cell Signalling, #9664T
Cleaved-PARP	Rabbit	1:1000(5%BSA)	Cell Signalling, #94885
Cyclin A2	Rabbit	1:1000 (PBS)	Abcam, #ab16726
Cyclin D1	Rabbit	1:1000 (PBS)	Abcam, ab16663
Cyclin E1	Mouse	1:1000 (PBS)	Cell Signalling, #4129S
Cyclin F	Mouse	1:1000 (PBS)	Bethyl, #A303-406A
E2F1	Mouse	1:1000 (PBS)	Santa Cruz, #sc-251
HSP70	Rabbit	1:1000 (PBS)	Cell Signalling, #4872S
HSP90	Rabbit	1:1000 (PBS)	Cell Signalling, #4874S
KAP1	Rabbit	1:1000 (PBS)	Abcam, #ab10484
LC3I-II	Mouse	1:1000 (PBS)	Cell Signalling, #83546
SQSTM1/p62	Mouse	1:1000 (PBS)	Cell Signalling, #23214
Phospho CHK1 ser317	Rabbit	1:1000 (5% BSA)	Cell Signalling, #12302S
Phospho KAP1Ser824	Rabbit	1:1000 (5% BSA)	Abcam, #ab70369
Phospho RPA ser32/33	Rabbit	1:1000 (5% BSA)	Bethyl, #A300-246A-M
Phospho RPA ser4/8	Rabbit	1:1000 (5% BSA)	Bethyl, #A300-245A-T
Rb Retinoblastoma	Mouse	1:1000 (PBS)	Cell Signalling,
RPA	Mouse	1:1000 (PBS)	Abcam, #ab2175
RRM2	Mouse	1:1000 (PBS)	Santa Cruz, #sc398294
Vinculin	Rabbit	1:1000 (PBS)	Cell Signalling,

Table 2.9. Secondary antibodies used for two-colour detection with infrared fluorescence

Specification (Name)	Species/clonality	Dilutions	Company
DyLight 680	Goat anti-Mouse IgG (H+L)	1:3000	ThermoFisher, #A32730
Alexa Fluor Plus 800	Goat anti Rabbit IgG (H+L)	1:3000	Millipore, #AP307P

2.9. Silver staining gel electrophoresis

The invitrogen novex SilverQuest Silver Staining Kit (Fisher scientific, LC6070) was used for protein silver staining. After electrophoresis, the gel was carefully removed from the cassette and placed in a clean staining tray. The gel was gently rinsed with ultrapure water before being fixed with 100 mL of fixative solution for 20 minutes with gentle rotation. Next, the gel was washed in 30% ethanol for 10 minutes, followed by washing with 100 mL of Sensitizing solution. Once the gel had been incubated for 20 minutes at room temperature, the Sensitizing solution was rinsed away, and the gel was washed in 100 mL of 30% ethanol for another 10 minutes. After that, the gel was subjected to two 100 mL washes with ultrapure water for 10 minutes each before being incubated in 100 mL of Staining solution for 15 minutes.

2.10. Flow Cytometry analysis

2.10.1. Annexin-V for apoptosis cell analysis

To assess apoptosis pathway activation in Rb-deficient/proficient LMS cell lines, we utilised the Annexin V Apoptosis Detection Kit (Biolegend, #640934). Cells were seeded in 10cm-dishes to reach 30 % confluency the day after. The next day, cells were treated with optimised drug concentrations and incubated for 48 hours at 37°C. Cells were tripsinased, collected in 15 ml-tube and centrifuged at 1000 g for 5 min. The medium was discarded, and the pellet was washed twice with cold Biolegend's Cell Staining Buffer and resuspended in 1 ml Annexin V binding buffer at a concentration of 0.25-1.0 x 10^6 cells/ml. FITC Annexin V (2µL) and 7-AAD Viability Staining Solution (4 µL) were added to 100 µL of the cell suspension in a 1.5-ml Eppendorf tube. Samples were gently vortexed and incubated for 15 min at room temperature in the dark. Afterwards 400 µL of Annexin V Binding Buffer was added to each tube before Attune flow cytometer analysis with proper machine settings.

2.11. Total Proteome Mass Spectrometry Analysis

RB1 gene proficient and deficient cells were seeded to reach 30% cell confluence after 24 hours incubation. Next, cells were treated with Alvespimycin for 48 hours, then trypsinased, washed with PBS, and stored at – 80° C until further use.

Cells were lysed in 5% SDS buffer supplemented with protease inhibitors and phosphatase inhibitors, sonicated, and then aliquoted at the same amount of protein (50 µg) into a new tube. The following steps were conducted according to the manufacture's protocol of the S-trap micro column (Profiti, C02-micro-10). Proteins were reduced with 10 mM DTT and then alkylated with 25 mM chloroacetamide. Acidification of the samples was carried out with 1.2% phosphoric acid and mixed with binding buffer (100mM triethylammonium bicarbonate in 90% methanol) to a 1:7 ratio (sample: binding buffer). Samples were then loaded onto the micro-S-trap spin column and centrifuged for 30 sec at 4000g to allow the sample to pass through. Then the loading step was repeated again. Next, the column was washed three times with the binding buffer. 20 µl of 50 mM triethylammonium bicarbonate (TEAB) containing 1.25 µg of trypsin was then added to the column and incubated overnight at 37°C. Peptides were eluted sequentially with 40 µl 50 mM TEAB, 0.2% formic acid and 0.2% formic acid in 50% acetonitrile solution. The eluted solution was then dried using a SpeedVac vacuum concentrator. Before MS, samples were dissolved in 0.1% TFA in MS grade water. Samples were run by Dr Iolanda Vendrell, on Dionex Ultimate 3000 nano UPLC (Thermo Scientific) with a connected Orbitrap Fusion Lumos Tribid mass spectrometer (Thermo Scientific) for Total Proteome mass spectrometry analysis. Protein identification and label-free quantification were performed using the DIA-NN search engine (version 1.8) and Perseus (version 1.6.2.3), respectively. Protein group intensities and significant enrichment were plotted into Volcano plots (T-test: FDR = 0.05 for multiple-test correction, s0 = 0.1). Enriched-R and Metascape, comprehensive gene set enrichment analysis web servers, were used to look for the most impacted pathways in the total proteome mass spectrometry samples.

2.12. Statistical analysis

Microsoft Excel 2013 and GraphPad Prism® 7 (GraphPad Software, Inc.; La Jolla, CA, USA) were used for all statistical analyses, and all values are expressed as the mean ± standard error of the mean (SEM) of at least three independent experiments unless otherwise stated. IC50 values were calculated using GraphPad Prism® 7 (GraphPad Software, Inc.; La Jolla, CA, USA) and presented as the mean ± standard error of the mean (SEM) of at least three independent experiments.

CHAPTER 3

Results

3.1. Developing isogenic RB1+/- cell lines for the study of SL interactions

3.1.1. The panel of leiomyosarcoma cell lines

To discover potential synthetic lethality effects with *RB1* gene loss in leiomyosarcoma (LMS), we first identified an appropriate panel of LMS cell lines with the genetic diversity present in the disease. The genetic profiles of commercially available LMS cell lines were examined using DepMap data portal (https://depmap.org/portal/). The aim was to select a subset of LMS cell lines differing in their Rb status. SK-LMS-1 and RKN cell lines represented a suitable LMS cell model retaining a functional copy of the *RB1* gene. On the contrary, SKUT-1 cells were selected for Rb loss as they bear a frameshift deletion of the *RB1* gene (V654fs).

3.1.2. Genetic heterogeneity of the leiomyosarcoma cell lines

The genetic features of the leiomyosarcoma cell lines chosen for our research study were investigated by using DepMap to uncover crucial insights into the molecular basis of LMS that could contribute to the development of targeted therapies. The SK-LMS-1 cell line carries a functional *RB1* gene and histologically derives from vulvar leiomyosarcoma tissue. One of the distinct genetic features of this cell line is the inactivation of the *TP53* gene. The *TP53* gene encodes for the tumour suppressor p53, the master regulator of cell division playing a crucial role in preventing tumour development. In the contest of selecting *RB1* gene proficient LMS cell lines, the RKN cell line was included in our LMS panel. The RKN cell line originates from ovarian soft tissue sarcoma. The cells carry more oncogenic events such as the loss of *TP53* and *CDKN2A*, and activation of *KRAS* genes. The *KRAS* gene, belonging to the RAS family, regulates cell signalling pathways controlling cell growth and differentiation. A gain-of-function mutation in *KRAS* has the potential to enhance uncontrolled cell proliferation and participate in cancer development.

SKUT-1 cells derived from uterine corpus tissue, exhibited multiple mutations beside loss of Rb, including *TP53* gene inactivation. Loss-of-function mutations were detected in other crucial genes such as *PTEN* and *KMT2B*. *PTEN* is a tumour suppressor involved in cell survival and genomic stability. Its inactivation stimulates the PI3K/AKT pathway, increasing cell proliferation. The *KMT2B* gene encodes for a histone methyltransferase playing a key role in the epigenetic regulation of chromatin structure and transcriptional activation. These mutations suggest potential dysregulation in cell cycle control, tumour suppression and epigenetic regulation in SKUT-1 cells.

3.2. Generation of isogenic cell line models to study Rb loss

3.2.1. Genetic depletion of Rb in SK-LMS-1 and RKN cell lines

To establish isogenic cell models differing only in Rb status from parental LMS Rb-proficient cells (SK-LMS-1, RKN), we utilised the inducible lentiCRISPR TLCV2-RB1 vector (Addgene, #87836). In this system, Cas9 expression and GFP fluorescence are both induced by the addition of doxycycline, while the sgRNA targeting the human *RB1* gene is constitutively expressed. The TLCV2 vector (Addgene, #87360) was used as a control, which expresses a non-functional sgRNA (non-targeting control) (Fig.3.1a).

To identify the optimal timeline for inducing *RB1* gene loss, cells were seeded in 6-well plates in the presence of doxycycline (2 μg/ml) for 7 days. Fresh medium containing doxycycline was replenished every 3 days to maintain a constant antibiotic concentration. This system facilitated the visualization of cells with high Cas9 expression by measuring GFP fluorescence levels. Initially, GFP fluorescence levels were monitored after 1-, 3-, and 7-days of doxycycline induction. The data showed a gradual increase in GFP levels over time (Fig.3.1b). This approach allowed for the assessment of Cas9 expression over time, as GFP and Cas9 are expressed simultaneously from the same genetic construct. Subsequently, western blot analysis revealed that SK-LMS-1 and RKN cell lines transduced with the inducible lentiCRISPR TLCV2-RB1 construct exhibited an increase in Cas9 expression levels alongside the disappearance of Rb, indicative of CRISPR-mediated gene editing effects (Fig.3.1c).

Interestingly, TLCV2-RB1 cells required more than 7 days to generate a homogeneous *RB1* gene knockout cell population.

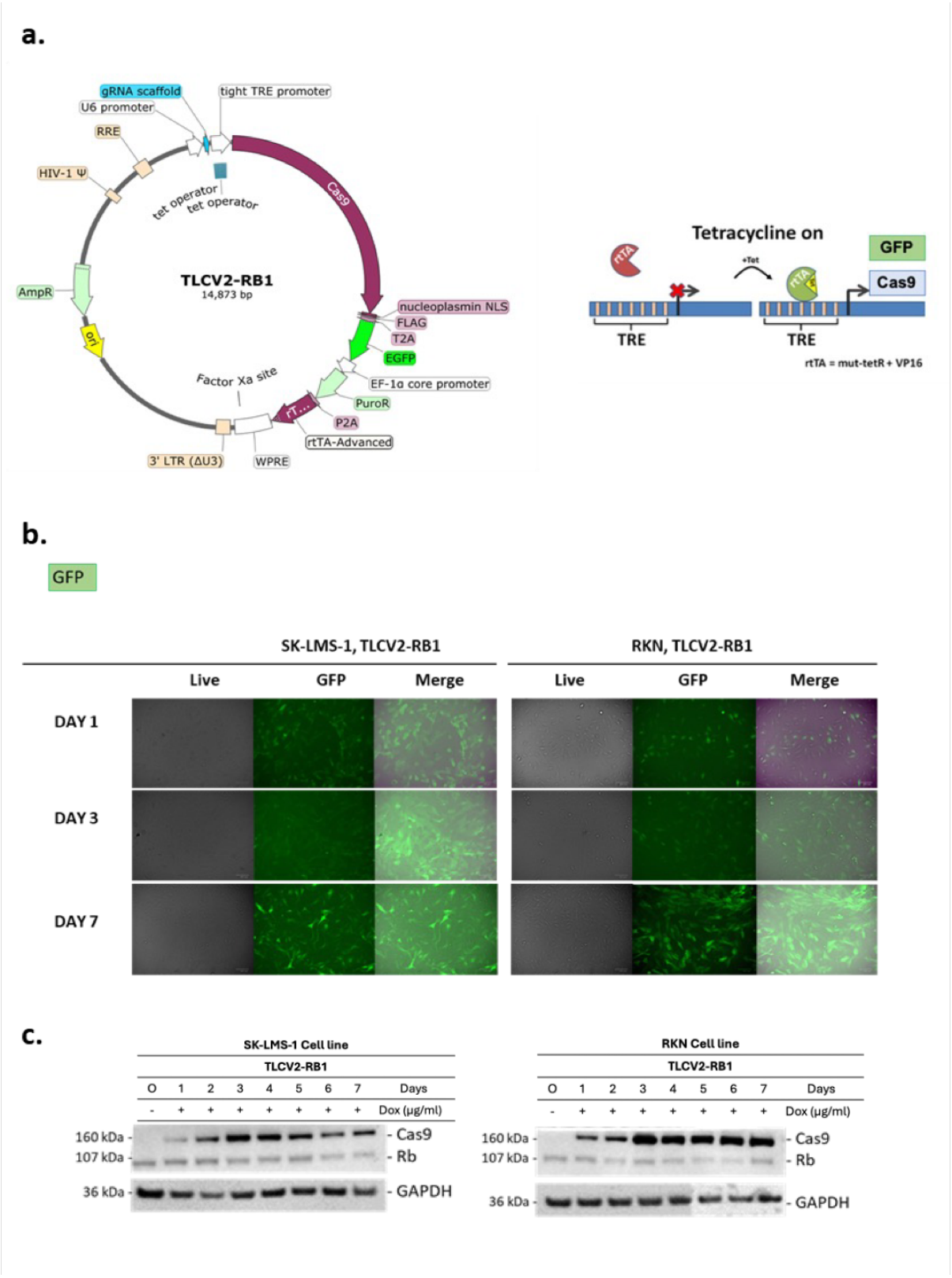


Figure 3.1. Leiomyosarcoma cell lines with stably integrated TLCV2 or TLCV2-RB1 inducible systems.

a. Schematic representation of TLCV2-RB1 TET-On inducible system. **b.** Imaging of GFP fluorescence in SK-LMS-1 and RKN cell lines with integrated TLCV2-RB1 inducible system after 1-,

3- and 7-days doxycycline (2 µg/ml) induction, using ZOE Cell Imager (Bio-Rad). **c.** Western blots showing Cas9 and Rb expression each day for 7 days of doxycycline (2 µg/ml) induction in SK-LMS-1 and RKN cell lines. GAPDH was used as a loading control.

Moreover, SK-LMS-1 and RKN cells harbouring the TLCV2-RB1 system were compared with control cells (TLCV2) to evaluate Rb loss expression levels. Rb expression decreased in the TLCV2-RB1 vector-infected cells after 7 day of doxycycline induction, whereas not significant change was observed in TLCV2 carrying cells. (Fig.3.2).

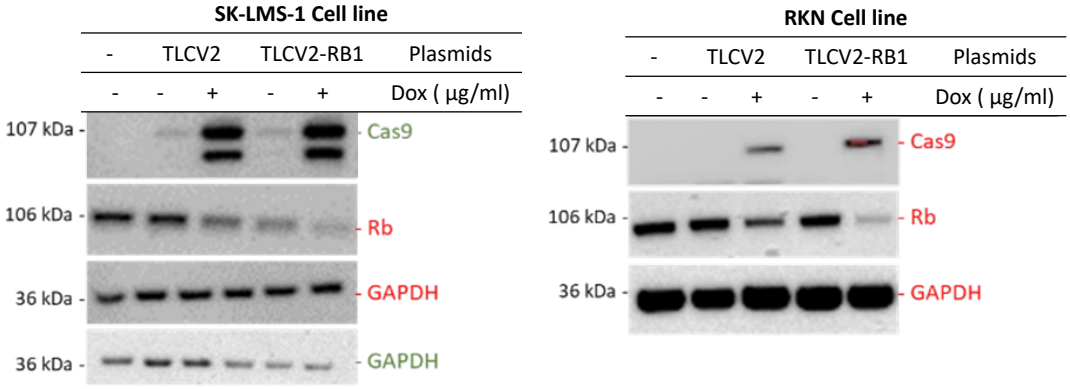


Figure 3.2. Rb knockout in SK-LMS-1 and RKN cell lines.
Cells with the TLCV2-RB1 system were compared with the control TLCV2 system to evaluate Rb loss. Cells were seeded in presence and absence of doxycycline (2 µg/ml) for 7 days followed by investigating Rb and Cas9 expression by Immunoblotting. GAPDH was used as a loading control. Colours of loading controls corresponded to the related coloured protein.

Next, we assessed whether Rb loss persisted following the removal of doxycycline. After 7 days of doxycycline induction, SK-LMS-1 TLCV2-RB1 cells were seeded in medium without doxycycline. Cas9 expression decreased after 3 days from doxycycline removal, and Rb levels were not restored, indicating efficient genome editing in the *RB1* gene (Fig.3.3).

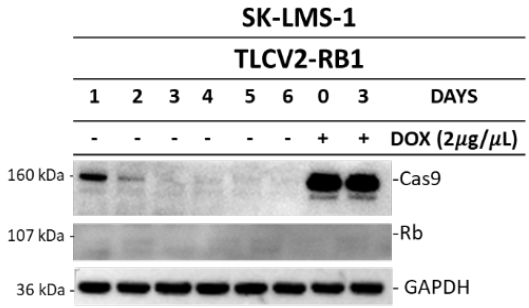


Figure 3.3. Cas9 levels after doxycycline induction.

After 7 days of doxycycline induction, SK-LMS-1 cells were seeded in 6 well plates, cells collection every 24 h for 6 days followed by immunoblotting investigation of Rb and Cas9 expression levels. Cells treated at 0 and 3 days with Dox were used as a control. GAPDH was used as a loading control.

To avoid cell population effect, single-cell clones were generated from the SK-LMS-1 and RKN cell lines transduced with TLCV2-RB1. After 7 days doxycycline induction, cells were seeded in 96-well plate at extremely low cell density, aiming for one cell per well. Western blot analysis confirmed that Rb was sufficiently depleted before seeding (Fig.3.4.a). Subsequently, cells were incubated at 37°C for two weeks to allow colony formation. Once individual cells began to grow into colonies, cells were transferred into larger culture vessels for further expansion. Clonal cell populations were then collected and analysed by western blot to confirm *RB1* gene knockout in SK-LMS-1 (Fig.3.4.b) and RKN cells (Fig.3.4.c). Interestingly, only a few clones exhibited Rb loss, indicating variability in the efficiency of gene depletion within the cell population.

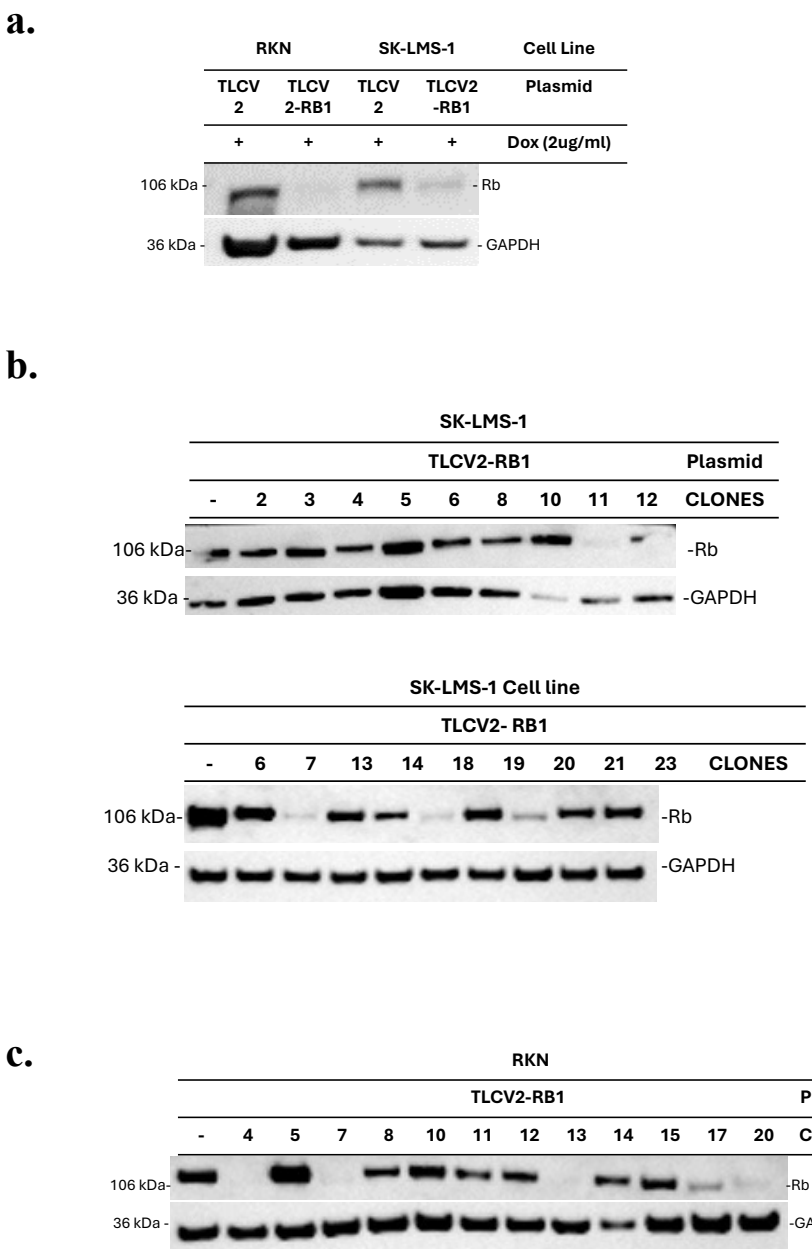


Figure 3.4. Clones with complete *RB1* gene knockout in SK-LMS-1 and RKN cell lines.

a. Western blot showing Rb expression levels in SK-LMS-1 and RKN cells carrying the TLCV2-RB1 system, after 7 days doxycycline induction before single cell clone experiments were performed. **b.** Immunoblots showing cell clones with the complete *RB1* gene knock out in SK-LMS-1 and **c.** in RKN cell line. First column showing positive control sample, GAPDH was used as a loading control. Representative data one independent experiments.

3.2.2. The role of Rb depletion in SK-LMS-1 and RKN cells

Rb is a well-established tumour suppressor known for its crucial role in regulating cell cycle progression. Consequently, we anticipated that our isogenic cells would exhibit an increased growth phenotype upon Rb loss. Cell proliferation was monitored over a period of 6 days, comparing TLCV2-control cells to TLCV2-RB1 cells with Rb loss. Remarkably, SK-LMS-1 RB1- cells exhibited a significant increase in growth, suggesting that Rb loss correlated with a tumorigenic phenotype and that Rb was functional in RB1+ cells (fig.3.5a). In contrast, RKN RB1+/- cells did not display any increase in cell growth, indicating that Rb was not functional in these cells (Fig.3.5b).

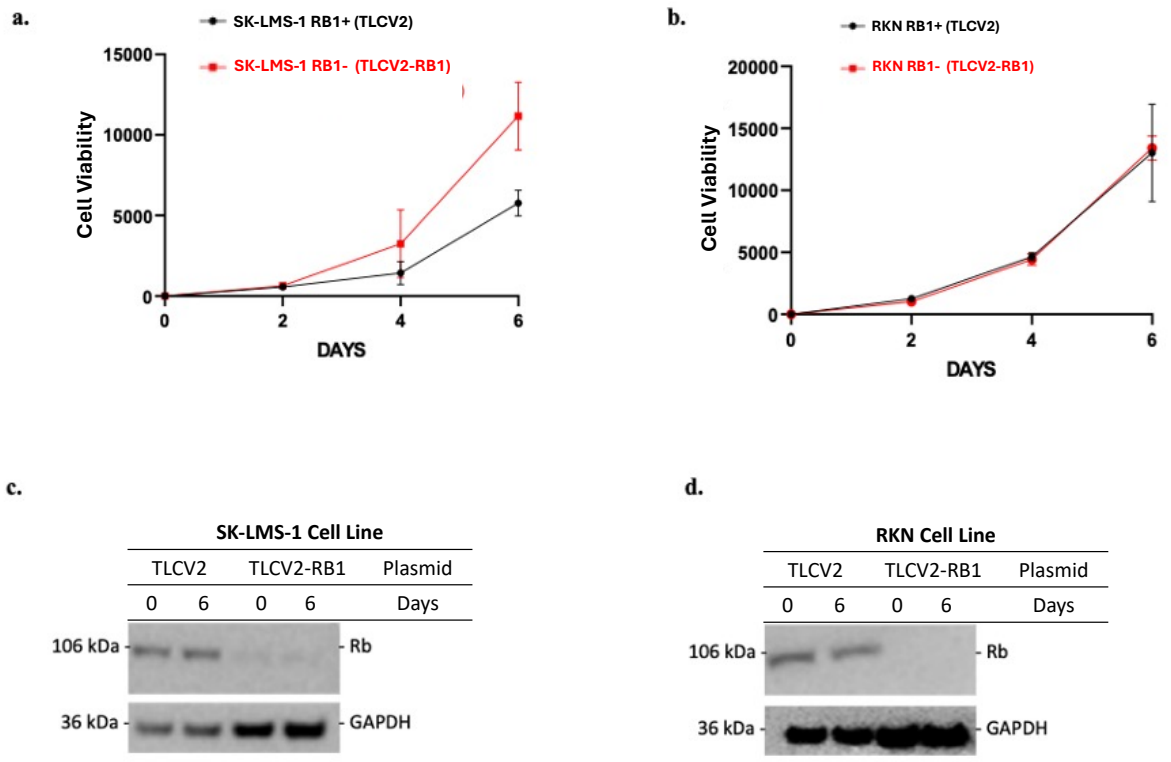


Figure 3.5. Rb loss promotes proliferation in vitro.

a. Viability of **(a)** RKN and **(b)** SK-LMS-1 cells, proficient/deficient for Rb, was evaluated with resazurin up to 6 day following doxycycline (2 µg/ml) induction. Western blot analysis confirm Rb removal up to 6 days following induction in (**c**) SK-LMS-1 and (**d**) RKN Rb proficient/deficient cells. GAPDH was used as a loading control. Representative data of n = 3 experiments.

3.3. The introduction of the *RB1* gene in SKUT-1 cell line

To complement loss of function investigations with gain-of-function studies, SKUT-1 cell lines were chosen due to their harbouring inactivating mutations in the *RB1* gene. Initially, attempts were made to insert the *RB1* gene into these cells using retroviral vectors constitutively expressing Rb. However, all cells infected with this system did not proliferate (data not shown), suggesting that reconstitution of Rb probable interfered with cell growth.

Therefore, we resorted to a vector system (pCW57.1, described in M&M), where Rb expression could be controlled by the addition of doxycycline. After establishing a stably integrated line with pCW57.1-RB1 or a control pCW57.1 vector lacking Rb, protein expression levels were evaluated by western blot analysis following the addition of doxycycline.

To determine the optimal doxycycline concentrations for inducing Rb expression, cells were treated with increasing concentrations of doxycycline (Fig.3.6a). The data indicated that doxycycline concentrations such as 1 or 2 μg/ml were suitable for inducing adequate levels of Rb expression in SKUT-1 cells after 24 hours. Subsequent western blot analysis investigated the best timeline to allow Rb expression. Data showed Rb was efficiently expressed after 24 hours of doxycycline treatment (Fig.3.6b). The concentration selected for subsequent experiments was 2 μg/ml to achieve a sustained induction of Rb. Additionally, we assessed that Rb expression was transient and persisted over 3 days following doxycycline induction. To maintain constant Rb expression levels, doxycycline induction had to be replaced every 3 days (fig.3.6c).

Furthermore, the proliferation rate of the SKUT-1 cell model system was measured (Fig.3.6d). Notably, we did not detect a significant difference in SKUT-1 cells after expression of Rb, likely reflecting other genetic alterations controlling G1/S transition. Indeed, it has been published that SKUT-1 cells exhibit high levels of cyclin Ds, due to depletion of the E3 ubiquitin ligase targeting them, AMBRA. (Maiani et al. 2021; Chaikovsky et al. 2021; Simoneschi et al. 2021) Although

SKUT-1 cells may not rely on Rb for growth, the model was selected for further studies due to the absence of potential confounding factors related to alterations in cell growth.

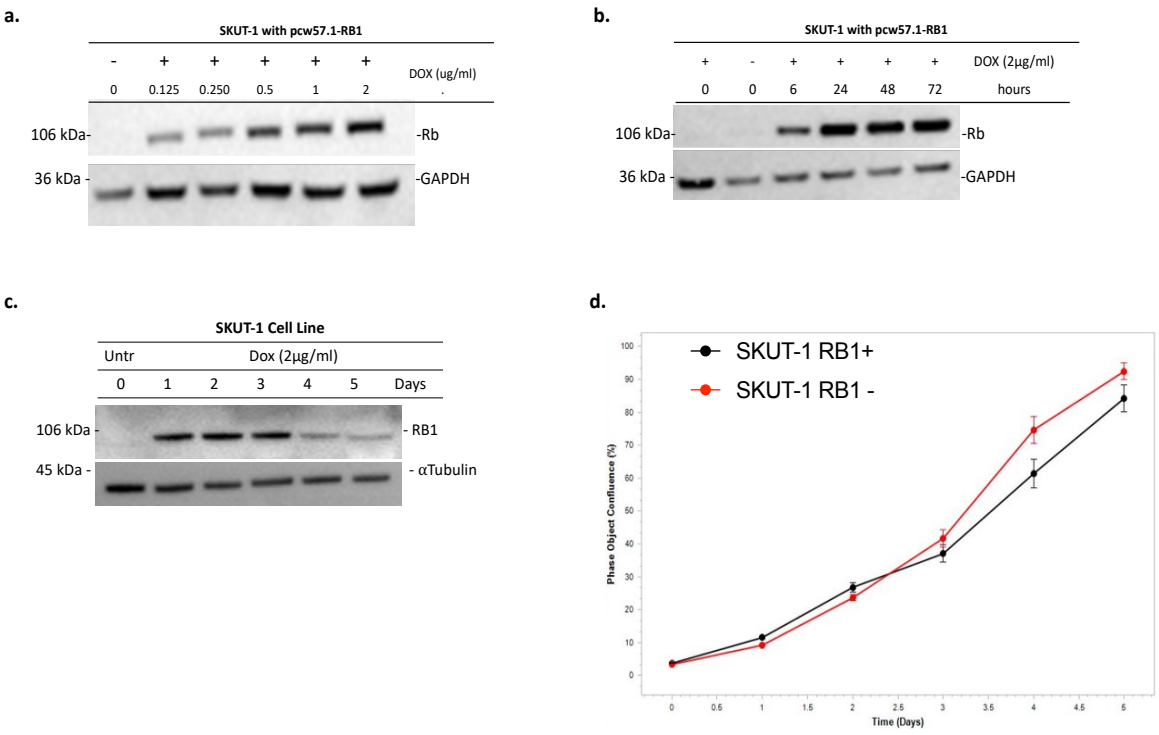


Figure 3.6. SKUT-1 cells with the integration of novel inducible system PCW57.1-RB1.

a. Western blot analysis showing Rb expression levels in SKUT-1 PCW57.1-RB1 cell line after 24 hours induction with increasing concentration of doxycycline. **b.** Cells were first treated with doxycycline (2 µg/ml) and the Rb expression levels over 3 days' time was investigated by immunoblot. **c.** western blot analysis showing Rb expression levels drop after 3 days from doxycycline induction (2 µg/ml). **d.** Cell growth rate was assessed in SKUT-1 cells RB1+/-, after 24 hours doxycycline induction and over a time of 6 days. Cell proliferation was assessed by Incucyte live cells imaging system. Representative experiment of three replicates.

3.4. Further characterisation of the LMS Rb isogenic models

3.4.1. Effects on cyclins

To investigate the potential effects of Rb loss on cell cycle progression, we examined the levels of cyclins by western blot analysis, considering the differences in growth rates observed in SK-LMS-1 and SKUT-1 cells. (fig.3.7).

The SK-LMS-1 and RKN cell lines, both proficient and with a complete knockout for the *RB1* gene, were seeded at an optimized cell density in 10cm-dishes. The SKUT-1 cell line carrying the pCW57.1-RB1 construct, was seeded in 10cm-dishes, in presence and in absence of doxycycline. After 24 hours, cell lysates were collected and subjected to western blot analysis. Although no major differences were observed in cyclin levels, our data showed that loss of Rb led to the accumulation of the transcription factor E2F1 in both SK-LMS-1 and RKN cells. Interestingly, the levels of E2F1 were comparable in SK-LMS-1 and RKN cells, but significantly reduced in the SKUT-1 cell line (fig.3.7).

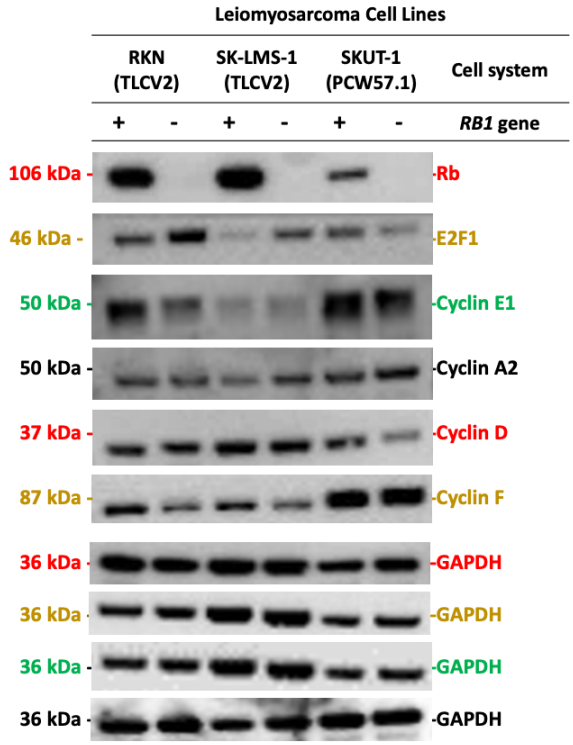


Figure 3.7. Rb loss does alter cell cycle biomarkers levels.

Biomarkers for cell cycle progression were evaluated by Immunoblotting in SK-LMS-1, RKN RB1+/- cells (TLCV2/ TLCV2-RB1 system, K/O clone), and SKUT-1 with the pCW57.1-RB1 cells system, with and with no 24 hours-doxycycline for Rb expression induction. GAPDH was used as loading control, colours of loading controls corresponded to the related coloured protein.

3.4.2. Rb loss in DNA replication stress and DNA damage

Alteration of Rb may lead to DNA damage through DNA replication stress. Therefore, we measured several markers of DNA damage induction and DNA replication stress by Western blot. The data presented in figure 3.8. shows that the panel of LMS cell lines displayed different responses. SK-LMS-1 cells presented activations of DNA damage response pathways with phosphorylated RPA at serine 4/8, selectively accumulating in Rb deficient cells. This indicated that Rb loss in these cells might promote the formation of DNA double-strand breaks, likely as a consequence of DNA replication stress induced by hyperactivation of E2F1. RKN cells presented very high levels of RPA serine 4/8 phosphorylation at basal levels, indicating that the DDR may be compromised in these cells, and they may bear a significant amount of genetic instability (fig.3.8). Indeed, mutation searches in Depmap revealed that these cells have mutations in ATM, an important kinase for the repair of DSBs. SKUT-1 cells did not present alterations in RPA phosphorylation consistent with DNA replication stress but exhibited increased CHK1 phosphorylation. Since CHK1 is crucial for checkpoint response, this is likely an indication of defective checkpoint control. (Bartek and Lukas 2003) Overall, our investigation highlighted that the SK-LMS-1 cell line exhibited features of a functional Rb, rendering this system highly suitable for further follow-up studies.

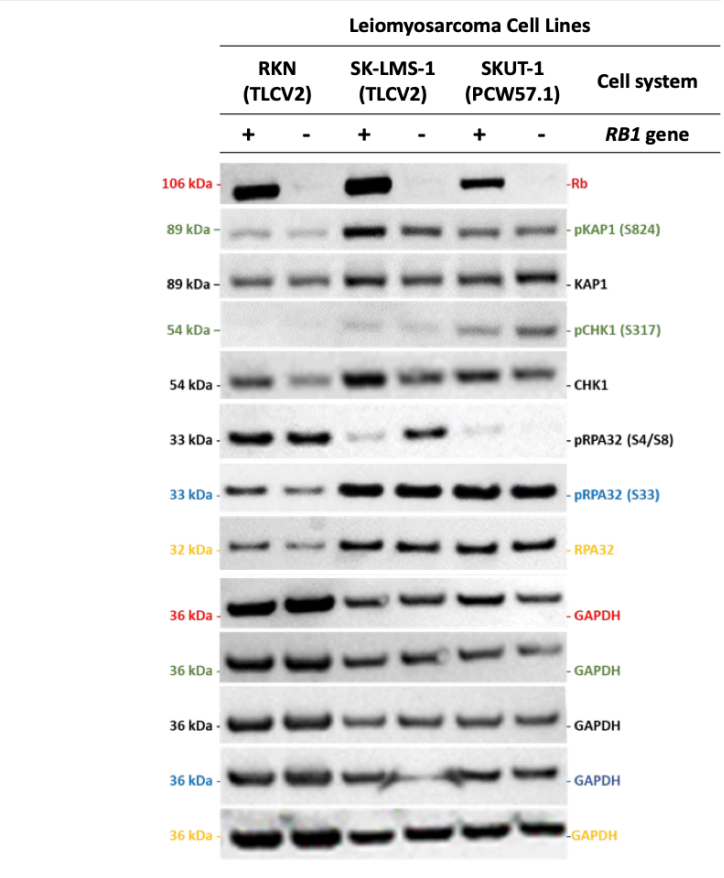


Figure 3.8. Replication stress/DNA damage repair pathways in LMS cell lines.

Markers were assessed by Immunoblotting in SK-LMS-1, RKN RB1+/- cells (TLCV2/ TLCV2-RB1 system, K/O clone), and SKUT-1 cells with the pCW57.1-RB1 cells system, with and with no 24hours-doxycycline-Rb expression induction. GAPDH was used as loading control, colours of loading control corresponded to the related coloured protein.

3.5. Key Findings

Commercially available LMS lines were carefully selected based on their Rb status. SK-LMS-1 and RKN cell lines, both proficient in the *RB1* gene, were chosen as representatives of Rb-proficient models. The SKUT-1 cell line, harbouring a frameshift mutation resulting in the loss of Rb function, was selected as a counterpart representing Rb-deficient cells.

Two distinct inducible cell systems were employed to induce the removal or the reinsertion of *RB1* gene (TLCV2-RB1 vs pCW57.1-RB1, respectively), ensuring comprehensive comparisons and investigations. Rb proficient cell lines were subjected to the lentivirus TLCV2-RB1 system, which utilises the CRISPR technique to induce complete knockout of the *RB1* gene. Furthermore, SKUT-1 cells lacking functional Rb were manipulated to reintroduce the gene using the inducible system pCW57.1-RB1.

Characterization experiments were conducted to explore various features of these cell lines, beginning with cell proliferation assays. The impact of Rb loss on cell growth rates was more pronounced in SK-LMS-1 and SKUT-1 cell line compared to RKN cells. Further experiments confirmed that the absence of Rb significantly influenced cell cycle progression and/or DNA replication in these models.

CHAPTER 4

4.1. Identification of Synthetic lethality effects with Rb depletion

4.2. Investigation of novel synthetic lethality interactions using a high through-put drug screen

Using the cell model systems described above, we performed a pharmacological high-throughput drug screen (HTS) to identify drug candidates that could be useful in targeting LMS cancer cells. The aim of the HTS assay was to identify drugs targeting proteins whose inhibition was synthetically lethal with Rb loss, thus promoting selective tumour cell death in leiomyosarcoma.

As described in figure 4.1, once target is validated, chemical libraries are tested in HTS. HTS are usually conducted with automated systems (robotics and liquid handling devices) to handle a considerable number of compounds in a short time (Fig.4.1). We chose a phenotypic screen approach as it is generally more successful in discovering novel drug candidates and requires the use of smaller libraries. (Swinney, 2013) Subsequently, validation experiments are required to assess the activity and efficacy of the identified drugs by performing biochemical and cell-based assays *in vitro* and *ex-vivo*. If these results are acceptable, biological drug responses are investigated within living organism (*in vivo*) to assess pharmacodynamic and pharmacokinetic qualities. Toxicology screening assays should also be conducted to verify drug safety. In some fortunate circumstance or in repurposing screens, drugs with high tolerability might be directly tested in the clinic (Fig.4.1).

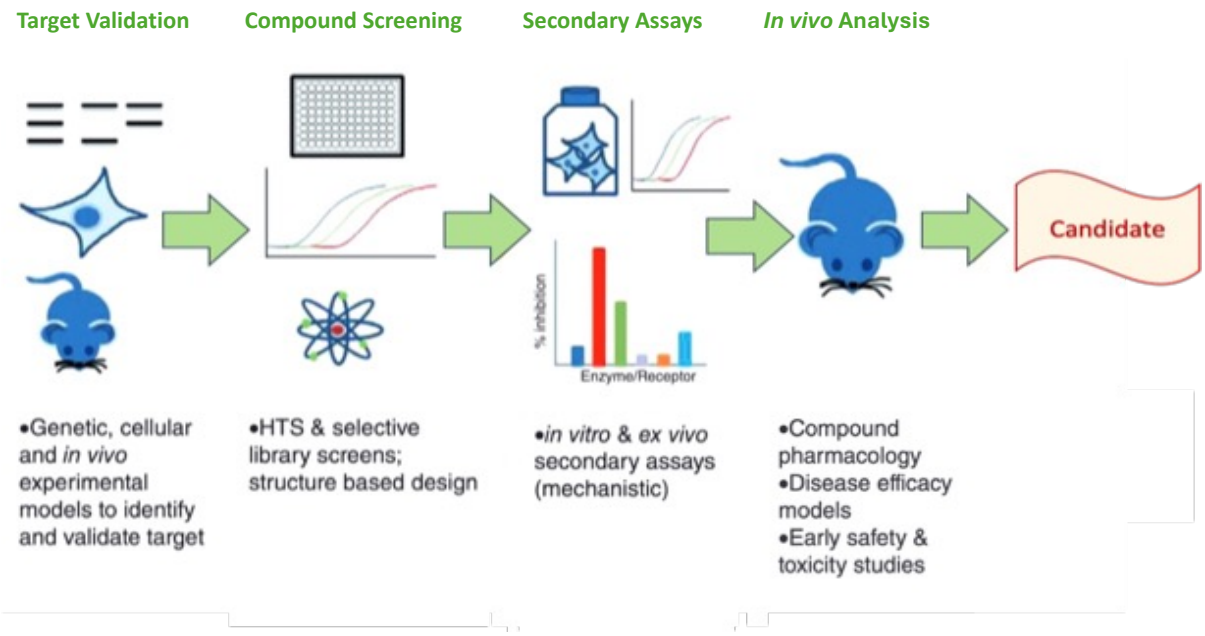


Figure 4.1. Drug discovery using high through-put drug screen.

The scheme outlines the progression of developing an HTS assay starting from preliminary experiments for validating the protein target, designing the HTS to identify potential drug candidates following drug pharmacology and toxicology studies for potential use in clinical trials. Modified from Hughes J et al. British Journal of Pharmacology, (2011).

4.2.1. Oncology Drug Library and Rb loss targeted drug screening assay

The panel of LMS cell lines generated in this study underwent screening using an anticancer compound library in a high-throughput screening manner, in collaboration with the Structural Genomics Consortium (SGC) and Prof D. Ebner (University of Oxford). The SGC assembles chemical compounds in drug libraries based on protein targets and biological pathways associated with various cancer types. The Oncology Drug library was chosen for our research study. This is a novel collection of 384 anticancer compounds in 384 well plates. This library includes both experimental and approved oncology-specific compounds for the purpose of drug screening and target investigations. It has been optimized in terms of library size, biological and chemical diversity, cellular activity, and target specificity.

The Oncology Drug Set library was tested in our panel of LMS lines, in duplicates at three different drug concentrations: 30 nM, 0.3 μM and 3 μM. The SK-LMS-1, RKN, and SKUT-1 cell lines, both Rb proficient and deficient (as shown in Wb analysis in fig.4.2a), were seeded at an optimised cell density (400 cells per well) in flat-bottom 384-well plates using Flex-drop (PerkinElmer, MA, USA). The following day, cells were treated with varying concentrations of each compound (0.03, 0.3, 3 μM) included in the drug library using Janus workstations (PerkinElmer, MA, USA). The biological assays chosen to assess the drug response was resazurin as a read out of cell viability. After 72 hours of incubation, alive cells were quantified with resazurin (10 μg/ml) by measuring fluorescence using a PerkinElmer Envision microplate reader (540 nm excitation/590 nm emission) (Fig.4.2b).

Following raw data analysis, drugs were ranked according to their delta-Z (ΔZ) score (from the lowest to the highest value), which represented the drug sensitivity ratio towards LMS Rb knock-out versus Rb proficient cells. A negative (ΔZ)-score indicated that compounds were highly effective in targeting Rb null cell lines. Compounds that did not show a dose response, or only showed a mild difference in cell viability compared to the control (DMSO), were excluded from the analysis. Effective drugs were defined as those sensitising Rb deficient LMS cells, with a false positive of ≤ 0.05. The aim was to select one or more compounds synthetically lethal in Rb deficient cells, holding potential for further explorations.

4.2.2. Identification of potential hits from the drug screen across LMS cell lines

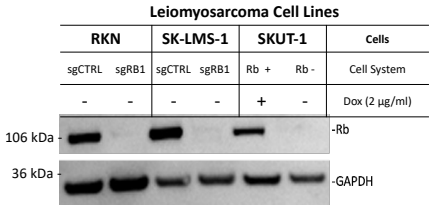
The drug screen identified several drug candidates selective in targeting Rb deficient cells. A summary of hits is presented in fig 4.2c. The identification of drug candidates in more than one LMS cell line provided confidence in the reliability of the hit/s.

Some drugs were particularly toxic for sarcoma cell lines, showing significant cell death at the concentrations tested (Table 4.1 showed the IC50). The drug screen revealed that the HSP90 inhibitor 17-DMAG effectively targeted both SK-LMS-1 and RKN cell lines, suggesting its potential

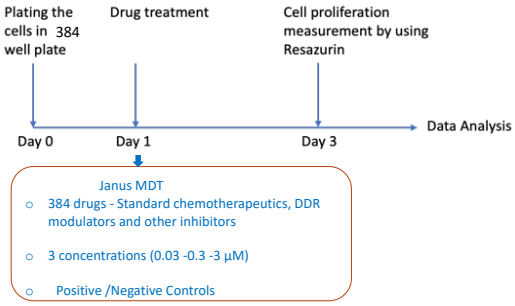
effectiveness and the need for further validation (Fig.4.2c,d). Data underscored DDR inhibitors as good candidates in both SK-LMS-1 and RKN cell lines (fig.4.2c,d). Both, the ATP-competitive CHK1 inhibitor PF477736 and the WEEI inhibitor MK1775 selectively targeted SK-LMS-1 cell line (fig.4.2c). Similarly to SK-LMS-1, RKN cells also showed high sensitivity towards CHK1 inhibitors (LY2603618) validating the hypothesis that DDR modulators may selectively be active in targeting LMS cells and require further investigations (Fig.4.2d).

Among the identified hits, HDAC inhibitors showed activity in LMS, such as Romidepsin in RKN and Panobinostat in SKUT-1 cells (fig.4.2d,e respectively). Other hits, such as the tubulin-binding agent ABT-751, showed efficacy exclusively in SK-LMS-1 (Fig.4.2c), as well as Homoharringtonine, known for its ability to inhibit protein synthesis, induced cell death specifically in RKN cells (fig.4.2d).

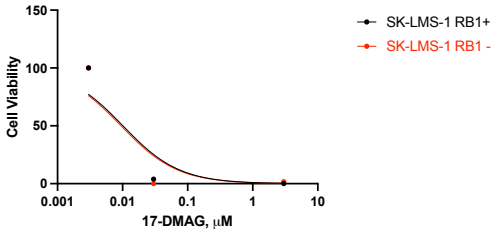
a.

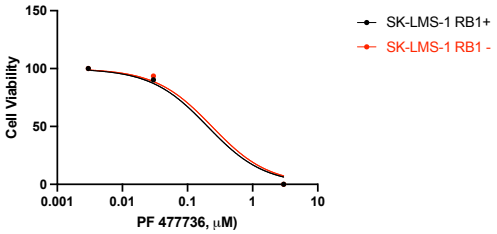


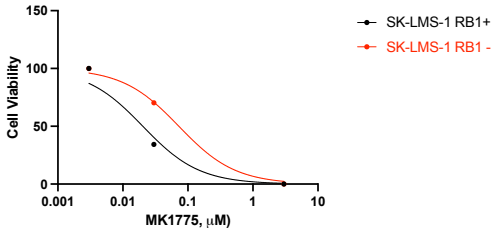
b.

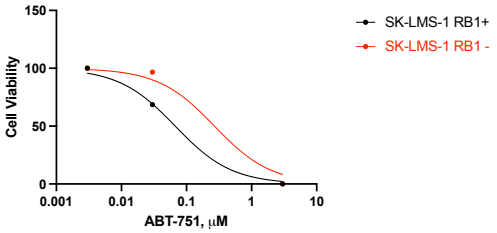


c. SK-LMS-1 cell line

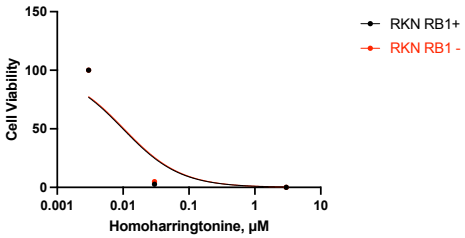


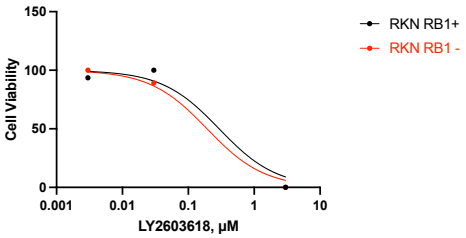


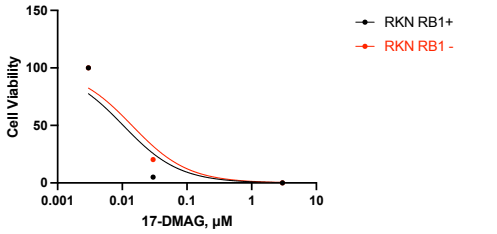


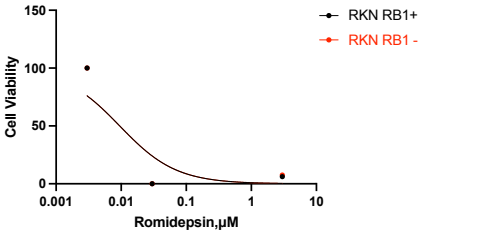


d. RKN cell line









e. SKUT-1 cell line

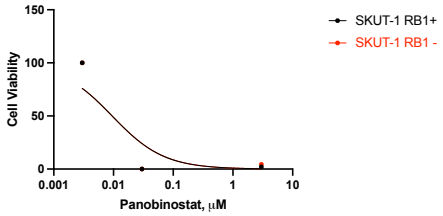


Figure 4.2. Drug Screen hits identification.

a. Western blot showing Rb status in the panel of LMS cell lines used for HTS screen. **b.** Timeline of drug screen from cell seeding 72 hours-drug treatment followed by resazurin viability assay and data analysis. **c.** Hits identified in SK-LMS-1 **d.** RKN **e.** SKUT-1 cell lines. Images were prepared by using GraphPad.

Table 4.1. The table shows the IC50 values (μM) of the identified hits in each LMS cell line.

Cell Lines	Drugs	Targets	IC50, RB1 +	IC50, RB1 -
SK-LMS-1	17-DMAG, Alvespimycin	HSP90	0.010	0.009
	ABT-751	Tubulin Synthesis	0.067	0.269
	MK1775	WEE1	0.02	0.07
	PF477736	CHK1	0.203	0.231
RKN	17-DMAG, Alvespimycin	HSP90	0.023	0.026
	Homoharringtonine	Protein Synthesis	0.009	0.010
	LY2606318, Rabusertib	CHK1	0.289	0.003
	Romidepsin	HDAC	0.009	0.009
SKUT-1	Panobinostat	HDAC	0.009	0.009

These data were generated using cell viability information collected in the drug screen, which focused on testing three drug concentrations: one excessively high, one moderate, and one very low (3 μM, 0.3 μM, and 0.03 μM, respectively). Drug effects depend on multiple factors such as mechanism of action, potency, and sensitivity towards our LMS cell lines. However, we needed to consider that

small molecules were likely to show some level of off-target pharmacology, especially when tested at high concentration. Overall, drugs tested at 3 μM displayed discordant data, as indicated by delta-Z values. At higher concentrations, we could not detect differences between Rb proficient and deficient cells. Thus, we focused specifically on data obtained at 30 nM concentration (Fig.4.3). Calculating the difference in cell viability between RB1+ vs RB1– cells by the Z-ratio, we observed a significant effect induced by 17-DMAG in Rb null cells to follow-up target validation. (Fig.4.3, Table 4.2.)

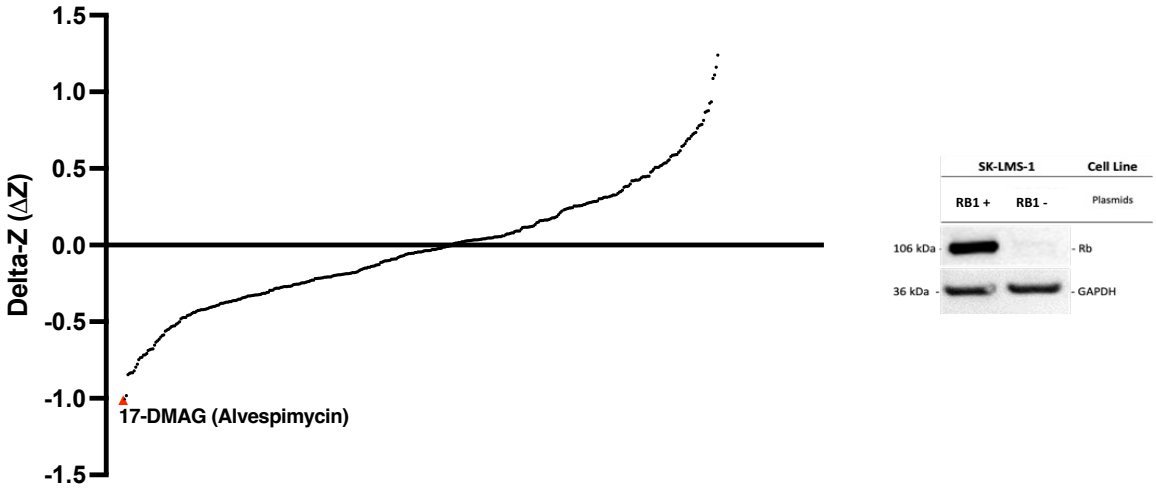


Figure 4.3. Drug screen data of SK-LMS-1 cells (30nM).

Drug screen analysis of SK-LMS-1 cell line treated with 384 compounds tested at 30 nM, ranked based on *Z*-score values, from most to least effective in inducing a synthetic lethal effect in Rb null cells. Cell viability was assessed 72 hours post-treatment using resazurin. Western blot analysis confirmed *RB1* gene knockout.

Table 4.2. Top 10 hits identified in SK-LMS-1 cell line.

Table illustrates drug screen hits ranked from lowest the to the highest *Z*-score values calculated from data analysis in SK-LMS-1 cells, 30 nM and 0.3 μM compounds concentration.

Compounds	Targets	Δz_30 nM	Δz_0.3 μM
17-DMAG (Alvespimycin)	HSP90	-1.256	-0.124
ABT-888 (Veliparib)	PARP	-1.011	0.064
CAL-101	p110δ kinase	-1.001	-0.455
Carfilzomib	Proteasome	-0.982	-0.028

Methylprednisolone	Glucocorticoid receptors (agonist)	-0.844	-0.335
Flutamide	Androgen receptors	-0.836	-0.307
Lenvatinib	Tyrosine kinases	-0.833	-0.285
OSI-906_Linsitinib	Insulin Receptors (IGF-1R)	-0.833	-0.318
Clofarabine	DNA polymerase, ribonucleotide reductase	-0.821	0.270

4.3. Validation of synthetic lethality effect

4.3.1. HSP90 inhibition is synthetic lethal in SK-LMS-1 cell line lacking Rb

Drug screen data revealed that the HSP90 inhibitor alvespimycin, also known as 17-DMAG, emerged as the top hit in targeting SK-LMS-1 cells lacking Rb. This result was observed when the drug library was tested at the lowest drug concentration (30 nM), allowing us to exclude potential off-target effect of the drug. To verify the potential synthetic lethality interactions between Rb loss and HSP90 inhibition by the chemical agent alvespimycin, cell viability of SK-LMS-1 TLCV2/TLCV2-RB1 cell lines, RB1+/- respectively, was examined by performing a resazurin cell viability assay. The data underscored that cells lacking Rb were strikingly more sensitive to the HSP90 inhibition, exhibiting an IC_{50} of 1 nM compared with Rb proficient cells (IC_{50} > 20 nM) (Table 4.3). Remarkably, alvespimycin treatment displayed high cytotoxic activity at the minimum drug concentrations. Thus, we can conclude that the general toxicity of the compound can be minimised in Rb null condition (Fig.4.4).

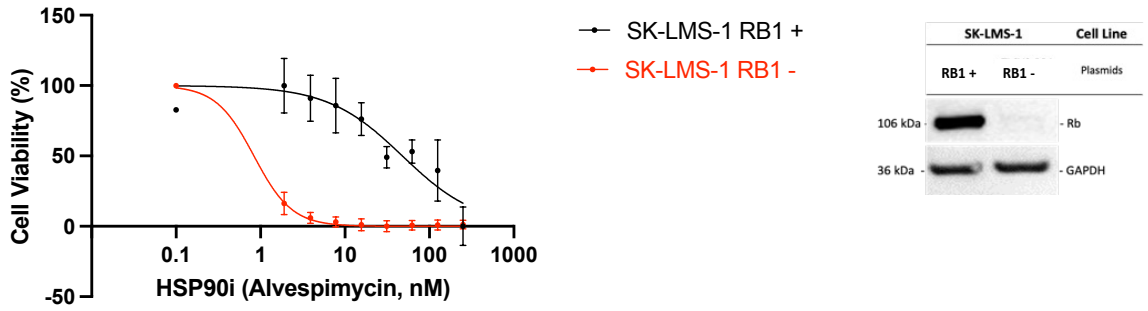


Figure 4.4. Validation of the top hit HSP90 inhibitor, Alvespimycin.

SK-LMS-1 RB1+/- cells were exposed for 5 days to increasing concentrations of alvespimycin (17-DMAG), respectively. Relative cell viability was assessed using the resazurin proliferation assay and normalised to DMSO treated controls. Graphs represent the mean of three independent experiments each performed with triplicates (± SEM). (**b**) Western blot analysis confirmed the stable *RB1* gene knockout of each proliferation assay of SK-LMS-1 cells. GAPDH was used as a loading control. Representative data of n = 3 experiments.

Table 4.3. IC50 Value of HSP90 inhibitor 17-DMAG

SK-LMS-1 cell line, IC_{50} Value, nM			
Target	Drugs	RB1 +	RB1 -
HSP90	Alvespimycin (17-DMAG)	47.88	0.8357

To understand the effect of prolonged treatment with alvespimycin, we measured cell viability using colony formation assays (Fig.4.5). As shown in figure 4.5, the data established that Rb loss was synthetic lethal with HSP90 inhibition. SK-LMS-1 cells lacking Rb showed an IC_{50} of 1-5 nM compared to the proficient cells. Rb proficient cells appeared to tolerate the damaging effects of the drug more effectively compared to the deficient cells displaying continuous cell proliferation up to 20 nM alvespimycin.

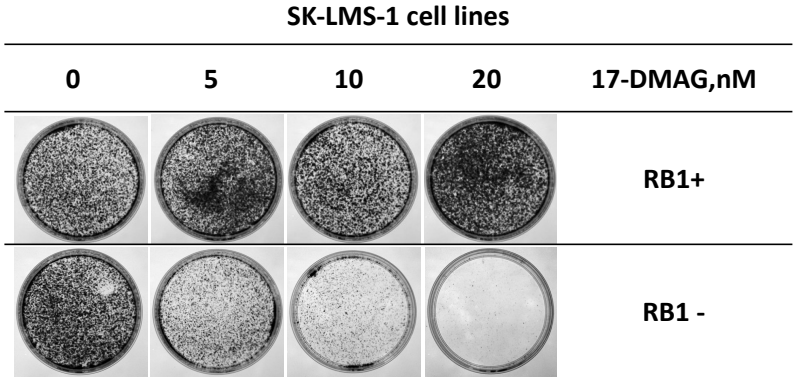


Figure 4.5. Validation of the synthetic lethality effect of Alvespimycin.

Cell survival of SK-LMS-1 RB1+/- cells was investigated with crystal violet staining, after 10 days HSP90 inhibitor treatment (Alvespimycin, 17-DMAG) tested at increasing drug concentrations.

4.3.2. Investigation of potential synthetic lethality effects using DDR modulators

Among the hits identified in the drug screen there were the DDR inhibitors belonging to the control of the G2/M checkpoint. The DNA damage response is a complex network of cellular signalling pathways activated in the presence of DNA damage. DNA damage events may render Rb-null cells selectively vulnerable to pharmacological inhibition of the ATR/CHK1 pathway. At the G2/M checkpoint, the kinase ATR phosphorylate CHK1, which in turn regulates WEE1 and CDKs to arrest cell cycle progression for checkpoint control. Thus, we tested the effect of cell death induced by ATRi, CHK1i and WEE1i in both RB1+/- SK-LMS-1 and RKN cells (fig.4.6, table 4.4 showing the IC50).

SK-LMS-1 cells exhibited increased sensitivity to CHK1i in Rb-deficient cells upon LY2603618 (CHK1i) (Fig.4.6a) compared with RKN. These differences can be explained by the fact that cells lacking a G1/S checkpoint might rely more on the G2/M checkpoint for survival. Furthermore, there was some sensitivity to WEE1i (fig. 4.6c) but not to ATRi (fig.4.6b) in SK-LMS-1 cells. Together, these data indicated sensitivity of LMS cells may be restricted to CHK1 inhibitors.

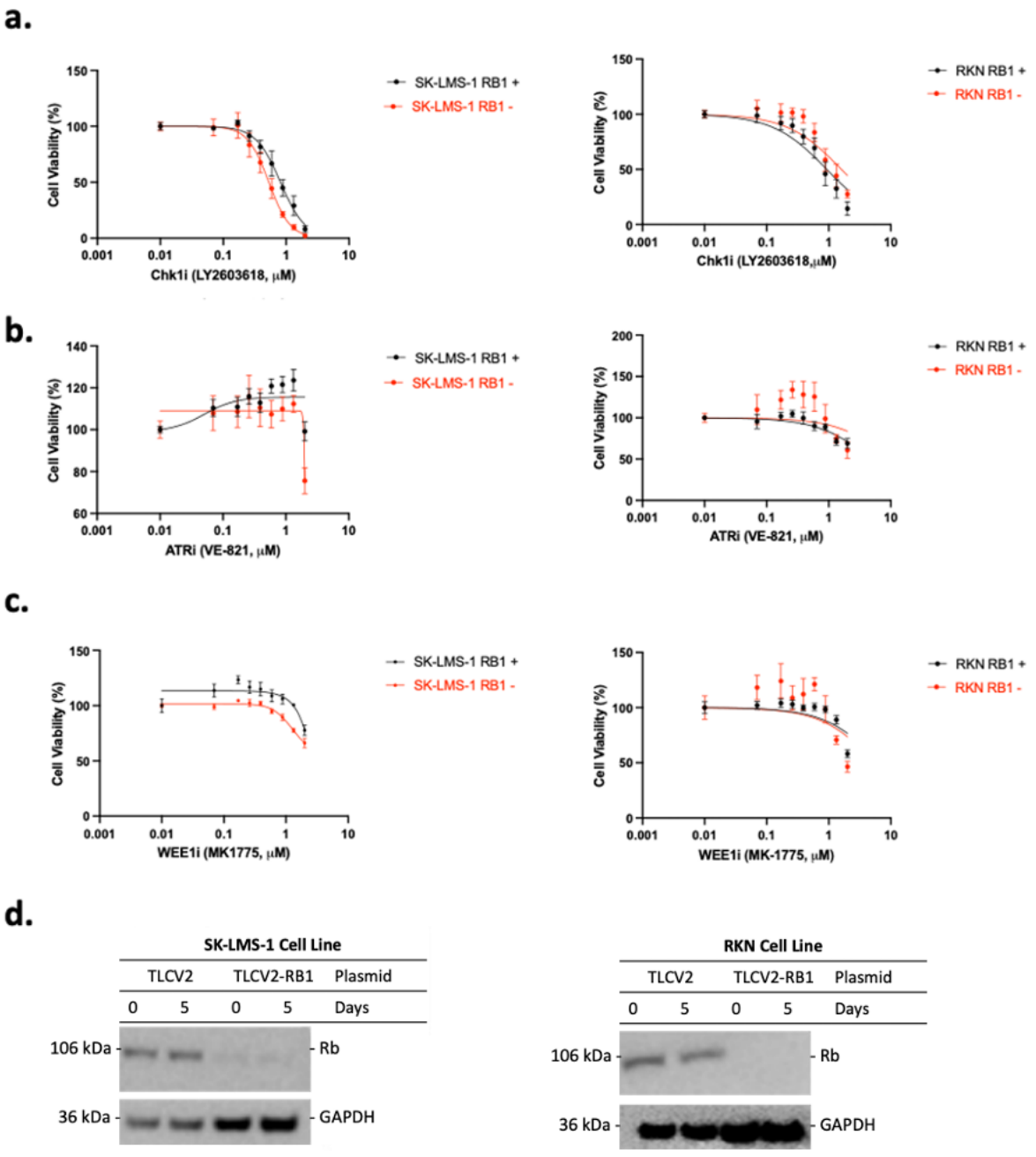


Figure 4.6. Viability of LMS cell lines upon DDRi inhibitors

SK-LMS-1 and RKN cells lacking Rb (TLCV2-RB1, RB1-) and the respective control (TLCV2, RB1+) were exposed for 5 days to increasing concentrations of **(a)** CHK1i: LY2603618; **(b)**, ATRi: VE821; **(c)** WEE1i: MK-1775, respectively. Relative cell viability was assessed using the resazurin proliferation assay and normalised to DMSO treated controls. Graphs represent the mean of three independent experiments each performed with triplicates (± SEM). Western blot analysis confirms the

RB1 gene K/O on day 0 and day 5 of each proliferation assay of SK-LMS-1 and RKN cells. GAPDH was used as a loading control. Representative data of n = 3 experiments.

Table 4.4. IC50 values of LMS cells upon DDR inhibitors

Tables illustrate IC50 values of SK-LMS-1 and RKN cells lacking Rb (RB1-) and the respective control (RB1+) after treatment using several DDR inhibitors as listed.

SK-LMS-1 cell line, IC_{50} Value, μM			
Target	Drugs	RB1 +	RB1 -
ATR	VE-821	0.0505	~2.029
CHK1	LY2603618	0.8124	0.5312
WEE1	MK-1775	indefinite	1.247
RKN cell line, IC_{50} Value, μM			
Target	Drugs	RB1 +	RB1 -
ATR	VE-821	4.916	10.30
CHK1	LY2603618	0.9306	1.598
WEE1	MK-1775	6.545	5.575

4.4. Key Findings

In this chapter, we described how drug discovery assay facilitated the identification of potential drug candidates from the tested drug library. We specifically focused on hits that exhibited sensitivity towards leiomyosarcoma cells lacking Rb. Validation experiments were conducted to confirm the hits identified in the drug screen performed at 30nM drug concentration. Cell viability data revealed that HSP90 inhibition selectively targeted Rb-deficient cells at a concentration of approximately 10nM, with an IC50 of 1 nM.

Furthermore, we explored the inhibition of the DNA damage response, a complex network of cellular pathways activated in response to DNA damage, as a potential strategy for targeting our panel of LMS cell lines. However, the LMS cell lines used in our study demonstrated only minor sensitivity towards this class of drugs targeting G2/M checkpoints mediators.

In conclusion, by exploiting the sensitivity of these cells to HSP90 inhibition, we aimed to elucidate the specific molecular alterations present in leiomyosarcoma cell. These alterations may play a critical role in the interplay leading to the synthetic lethality effect upon HSP90 inhibition.

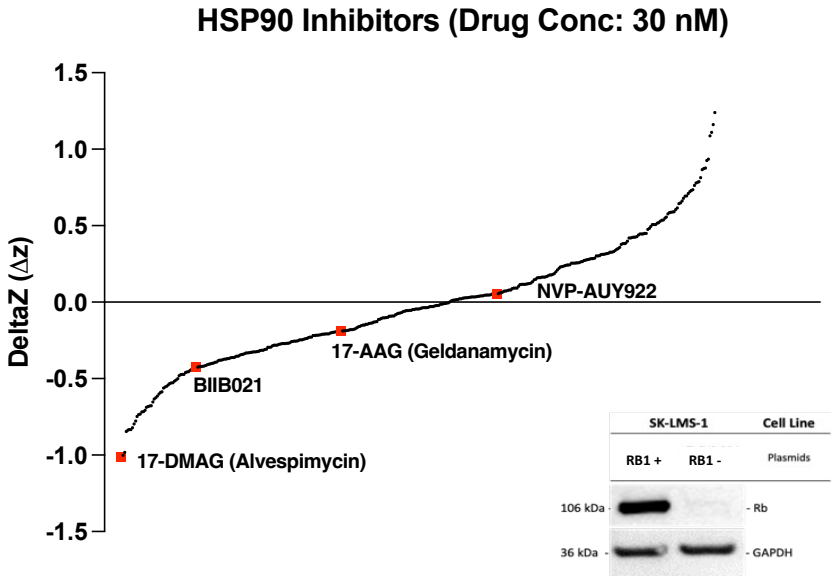
CHAPTER 5

5.1. HSP90 inhibition is synthetic lethal with Rb loss

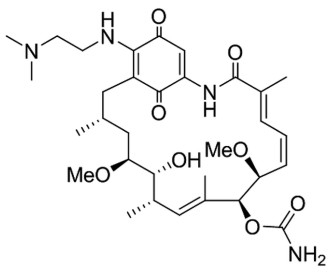
5.1.1. Synthetic lethality effect with others HSP90 inhibitors

In the previous chapter, we observed that alvespimycin selectively targets Rb null cells. While this data can be a bona fide synthetic lethal interaction between HSP90 and Rb, we needed to exclude the possibility of other targets besides HSP90. Therefore, among the HSP90 inhibitors tested in our drug screen (fig.5.1a, Delta-Zeta (Δz) value showed in table 5.1), we selected luminespib (NVP-AUY922) to validate synthetic lethality effects in Rb deficient SK-LMS-1 cell lines. This inhibitor was chosen for its distinct chemical structure (fig.5.1b), proven potency against HSP90 protein, and its status in clinical trials studies. (Zi Nan Li and Ying Luo 2023)

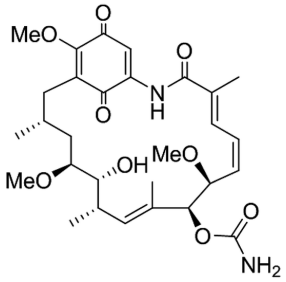
a.



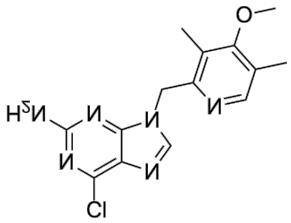
b.



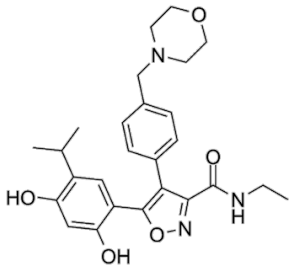
Alvespimycin (17-DMAG)



Geldanamycin (GA)



BIIB021



Luminespib (NVP-AUY922)

Figure 5.1. HSP90 inhibitors examined in the drug screen assay.

a. Drug screen data of SK-LMS-1 BR1 +/- cells treated with HSP90 inhibitors tested at 30 nM, ranked based on *Z*-score values, from most to least effective in inducing a synthetic lethal effect in Rb null cells. Cell viability was assessed 72 hours post-treatment using resazurin. **b.** Chemical structures of the HSP90 inhibitors examined in the drug screen assay.

Table 5.1. Delta-Z values of each HSP90 inhibitor used in the drug screen.

HSP90 inhibitors tested at 30 nM compounds concentration were ranked from the highest to the lowest *Z*-score values calculated from data analysis in SK-LMS-1 RB1- cells.

Compounds	Δz_30 nM	Δz_0.3 μM
17-AAG (Geldanamycin)	-0.189685182	0.006146482
17-DMAG (Alvespimycin)	-1.256	-0.124
BIIB021	-0.426154362	-0.106564652
NVP-AUY922 (Luminespib)	0.054751636	-0.063756767

Cell viability assay based on resazurin was utilised to assess the drug response of the HSP90i luminespib (NVP-AUY922) in SK-LMS-1 cells. Data revealed that luminespib selectively targets Rb null SK-LMS-1 cell line validating the synthetic lethal effect between Rb loss and HSP90i (fig.5.2). Luminespib was about three-fold more potent in targeting Rb null cells with an IC50 of 34 nM compared with Rb proficient (IC50: 88.94 nM) (table 5.2).

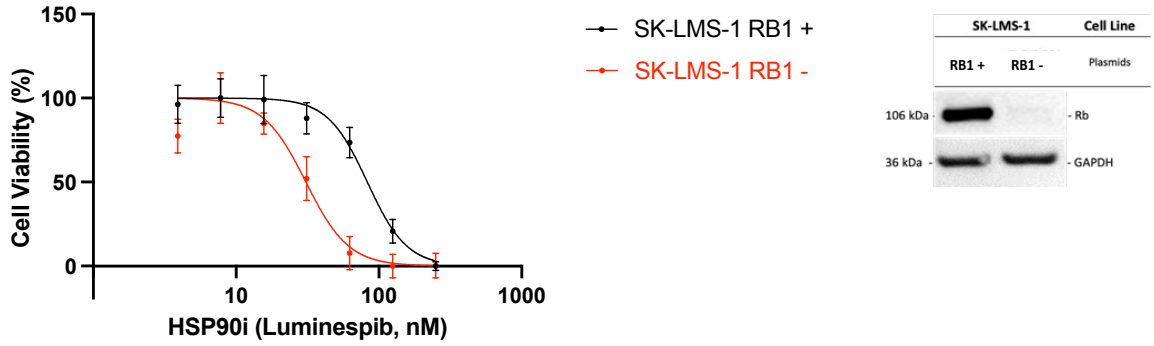


Figure 5.2. The synthetic lethality effect of the HSP90i, Luminespib.

SK-LMS-1 RB1+/- cells were exposed for 5 days to increasing concentrations of Luminespib (NVP-AYU922). Relative cell viability was assessed using the resazurin proliferation assay and normalised to DMSO treated controls. Graphs represent the mean of three independent experiments each

performed with triplicates (± SEM). Western blot analysis confirms the *RB1* K/O. GAPDH was used as a loading control. Representative data of n = 3 experiments.

Table 5.2. IC50 values of Luminespib tested in SK-LMS-1 RB1+/- cells.

SK-LMS-1 cell line, IC_{50} Value, nM			
Target	Drugs	RB1 +	RB1 -
HSP90	Luminespib (NVP-AUY922)	88.94	34.14

5.1.2. Synthetic lethality effect with HSP90i in other cell line and different cell system

As a complementary system to validate synthetic lethality between Rb loss and HSP90i, we tested SKUT-1 cell lines with an Rb-inducible cell system, described above (chapter 3.3). As shown in fig.5.3a,c, Rb expression was induced by doxycycline prior to starting the drug treatment with alvespimycin, and cell viability was assessed using resazurin. The data revealed that SKUT-1 cells lacking Rb showed an IC_{50} of 6.33 nM, notably lower than the proficient control cell line, which exhibited an IC_{50} of 34.26, confirming the synthetic lethality in a different model system (fig.5.3b, table 5.3 showing IC50).

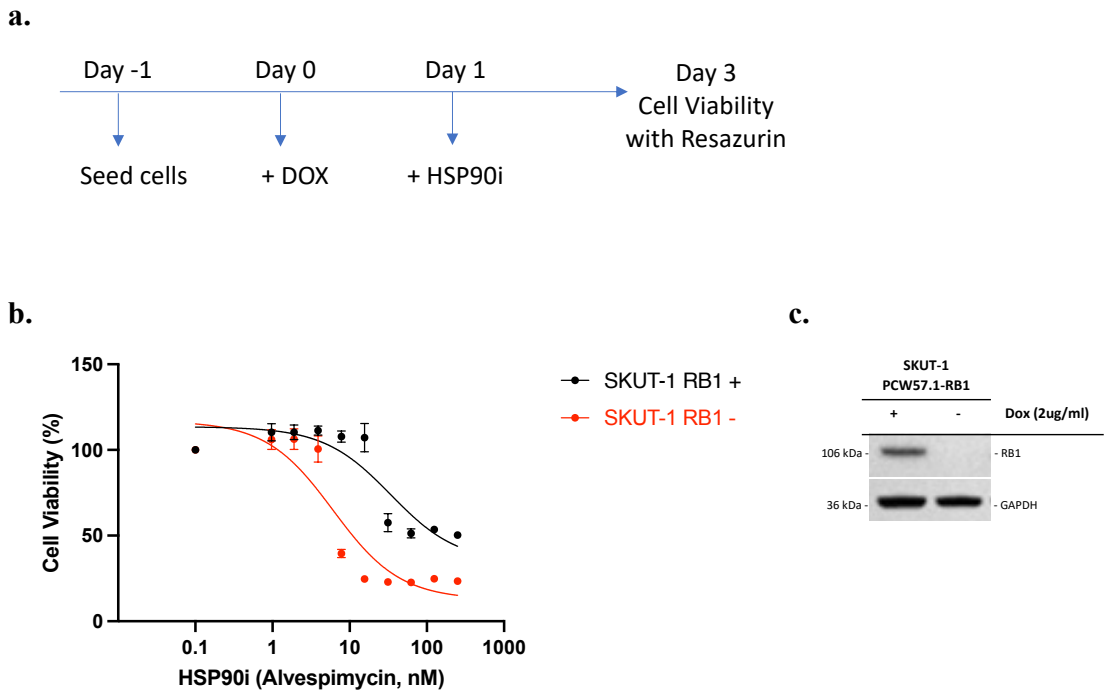


Figure 5.3. The synthetic lethality effect of HSP90i in SKUT-1 cell line.

a. Timeline of SKUT-1 cells RB1 +/- exposed for 3 days to increasing concentrations of alvespimycin. To generate RB1+ cells, cells were treated for 24 h Doxycycline before drug treatment. **b**. Cell viability was assessed using resazurin proliferation assay and normalised to DMSO treated controls. Graphs represent the mean of three independent experiments each performed with triplicates (± SEM). **c.** Western blot analysis confirmed the Rb expression at each proliferation assay of SKUT-1 cells. GAPDH was used as a loading control. Representative data of n = 3 experiments.

Table 5.3. IC50 values of SKUT-1 RB1 +/- cells upon HSP90i treatment.

SKUT-1 cell line, IC_{50} Value, nM			
Target	Drugs	RB1 +	RB1 -
HSP90	Alvespimycin (17-DMAG)	34.26	6.331

To further validate the drug response and determine the IC_{50} value upon prolonged exposure to the HSP90i, we assessed viability with a colony formation assay (fig.5.4). Cells treated with drug concentrations ranging from 1-5 nM demonstrated steady proliferation; however, only cells with Rb loss displayed a decrease in cell growth between 6-8 nM, consistent with the previous data recording

an IC_{50} of 6 nM (Table 5.3). Conversely, Rb-proficient SKUT-1 cells exhibited reduced viability at 10 nM. Both cell lines demonstrated 90% cell death at 20 nM (fig.5.4).

In conclusion, we were pleased to confirm the efficacy of the drug in cells with inherently mutated Rb. Indeed, in patients, Rb depletion is rare while mutations are frequent.

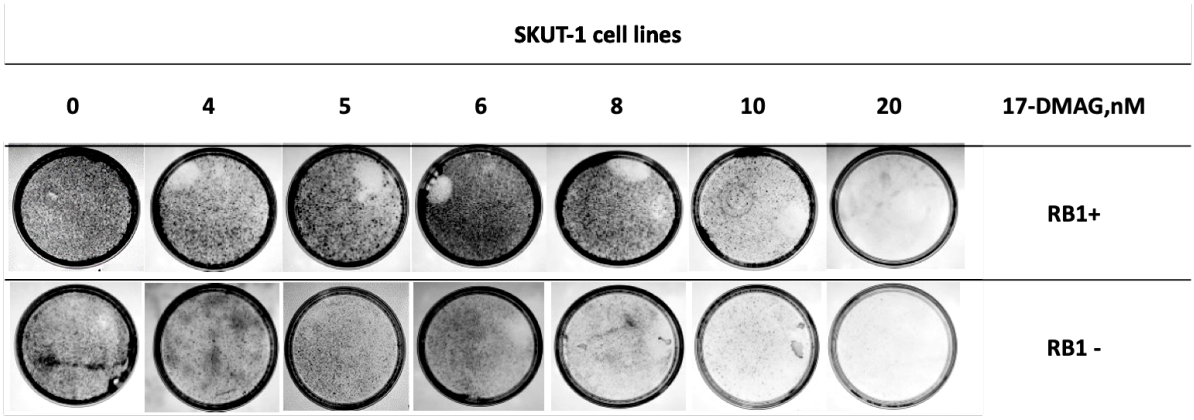


Figure 5.4. Cell viability assessment in SKUT-1 cells upon HSP90i.
Cell survival of SKUT-1 RB1+/- cells was examined with crystal violet staining, after 10 days HSP90 inhibitor alvespimycin (17-DMAG) treatment tested at increasing drug concentrations.

5.1.3. HSP90 inhibition using different methods (siRNA and PROTACS)

We attempted to validate the synthetic lethality (SL) between HSP90 inhibition and Rb loss using two model systems (TLCV2, pCW57.1) and two drugs (17-DMAG and NVP-AUY922). Although two distinct molecules might have similar off-targets, we aimed to ensure that our observation was specific to HSP90 inhibition. Instead of using pharmaceutical agents to inhibit HSP90 activity, we employed siRNA targeting HSP90AA1 gene to generate HSP90 gene knockdown.

Unfortunately, the siRNA did not successfully induce gene knockdown in our cells (fig.5.5a), which may reflect the high stability of the HSP90 protein. Indeed, it has been reported that the half-life of

HSP90α2 exceeds 100 hours, which could elucidate the lack of the observed knockdown effect. (Zecha et al. 2018)

To optimise the siRNA knockdown experiment, we next studied the stability and kinetics of HSP90 degradation by performing the cycloheximide (CHX) chase assay (fig.5.5b). Cycloheximide acts as a translation inhibitor and is commonly used to observe the temporal degradation of a protein by blocking ribosome translocation. It provides insights into protein stability, degradation pathways, and regulatory mechanisms. In our study, this method was chosen to gain a better understanding of the turnover rates and the half-life of the HSP90 protein. SK-LMS-1 cells were seeded and treated for 16 and 24 hours with CHX, (50 μg/ml). Cells were then collected, and HSP90 degradation was evaluated by western blot. As shown in fig.5.5.b, the half-life of the HSP90 protein was more than 24 hours. This observation suggested that inducing HSP90 depletion by siRNA was unlikely to occur in our cells, as the protein had an extremely long half-life, and its production was not under constant mRNA control.

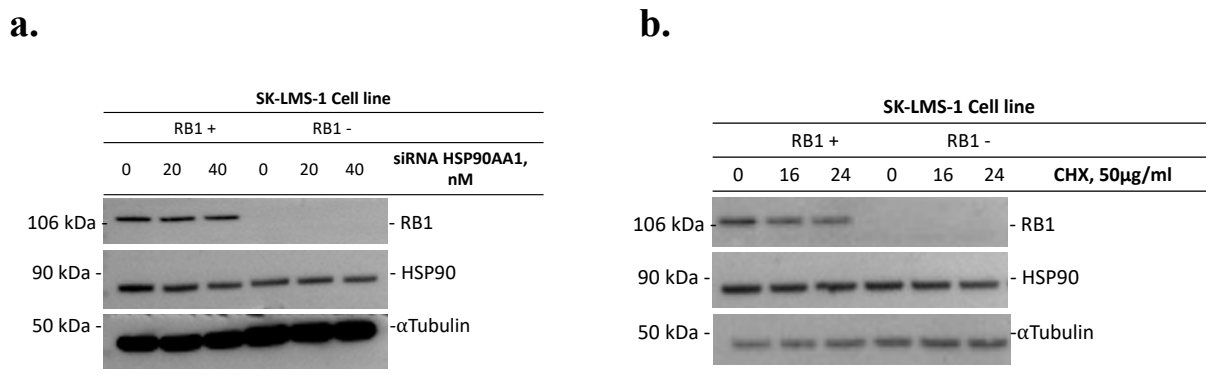


Figure 5.5. siRNA HSP90 knockdown and assessment of HSP90 half-life.

a. Western blot analysis illustrates the knockdown of HSP90 protein attempted using siRNA. **b.** HSP90 protein levels expression was monitored by immunoblotting analysis upon Cycloheximide (CHX) chase assay, in SK-LMS-1 RB1+/- cells. αTubulin was used as loading control.

Subsequently, we explored other methods to deplete HSP90 from cells. To this end, we chose to use the PROTAC HSP90-degrader BP3, which was claimed to induce potent and selective degradation of HSP90 (MedChemExpress, #HY-115997) (fig.5.6a). PROTACs are molecules designed to interact to specific target and recruit them to E3 ubiquitin ligases, leading to proteasomal degradation (fig.5.6b). However, western blot analysis revealed that BP3 was unsuccessful in degrading HSP90, indicating potential issues with the stability of BP3 or the reproducibility of reported experiments (fig.5.6c).

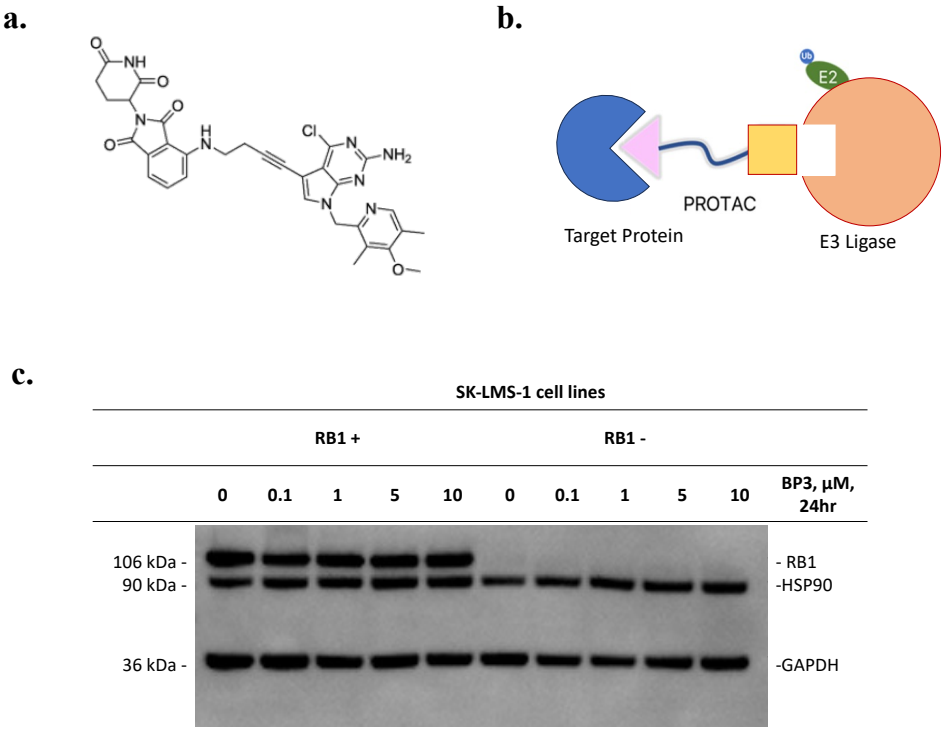


Figure 5.6. HSP90 degradation analysis by PROTAC BP3.

a. Chemical structure of PROTAC HSP90 degrader BP3 (Q. Liu et al. 2022). **b.** Schematic representation of PROTAC molecule mediating the interaction of the target protein and the E3 ligase. Ubiquitination reaction modifies the target protein promoting its degradation by the proteasome. Image courtesy of the Wang lab. **c.** Western blot illustrates 24 hours BP3 treatment was not effective in diminishing HSP90 protein levels in SK-LMS-1 RB1 +/- cells. GAPDH was used as loading control.

5.2. Cell signalling analysis

5.2.1. HSP90 and HSP70

To perform protein folding functions, HSP90 operates in conjunction with several co-chaperones. HSP70, another highly conserved ATP-dependent molecular chaperone, is involved in protein homeostasis process as well. Although HSP90 and HSP70 can independently perform co-chaperone activities, they may also cooperate in proteins remodelling processes. Given that HSP70 is considered the main collaborator of HSP90, we hypothesized that drug response could be influenced by HSP70 compensating for the inhibition of HSP90 due to alvespimycin treatment. Hence, we examined the levels of HSP proteins in both treated and untreated SK-LMS-1 RB1+/- cells using western blot analysis (fig.5.7).

As it shown in figure 5.7, the HSP90 inhibitor did not alter HSP70 levels at the lower concentrations in Rb proficient and deficient SK-LMS-1 cells. However, HSP70 accumulation occurred at a concentration of 50 nM in both deficient and control cells. This data reveals that alvespimycin treatment did not impact the total levels of HSP70 at drug concentrations lower than 50 nM.

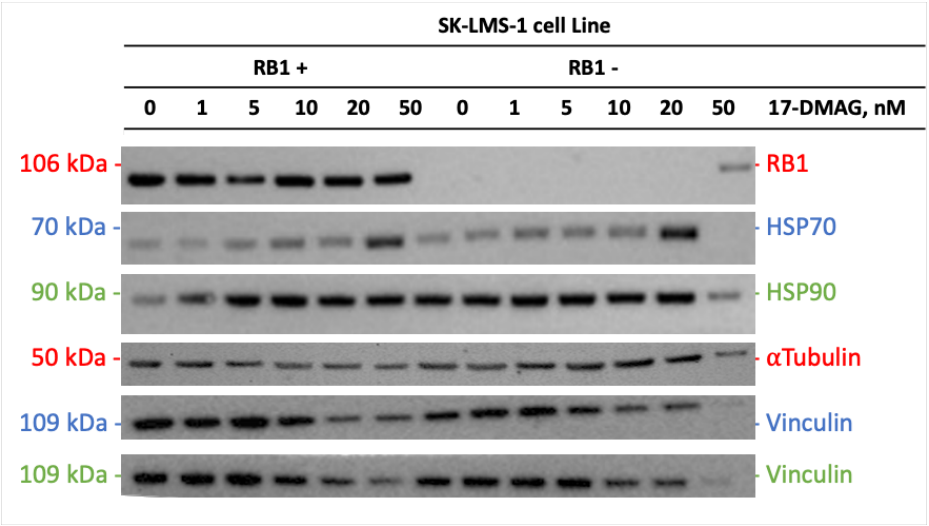


Figure 5.7. HSPs expression levels validation.

HSP70 or HSP90 expression levels upon increasing concentration of 17-DMAG were assessed by western blot analysis. DMSO-treated cells were used as a control and indicated as untreated cells with

HSP90i. Vinculin and αTubulin were used as loading control, colours of loading controls corresponded to the related coloured protein. Representative data of one independent experiments.

5.2.2. The impact of HSP90 inhibition in the cell cycle

To further investigate the impact of HSP90 inhibition in Rb deficient cells, we examined cell cycle alterations in LMS cells upon treatment with alvespimycin or luminespib. Levels of cell cycle biomarkers were evaluated by western blot analysis in both Rb proficient and deficient cells, treated or untreated with the HSP90 inhibitors.

Overall**,** there were no marked variations in cyclin expression levels between alvespimycin-treated and untreated cells, in both Rb-proficient and deficient cells (fig.5.8a,b). In contrast, cyclins such as cyclin D1, E1 and A2 decreased selectively upon treatment with 20 nM luminespib (fig.5.8b).

Considering that CDK4 is a client protein of HSP90, we expected changes in its expression levels under HSP90 inhibitor treatment. Indeed, CDK4 levels were remarkably reduced in Rb-deficient cells upon treatment with 20 nM alvespimycin or luminespib. These results were consistent across both drug treatments (fig.5.8a,b). To ensure that these findings were not cell line specific, we also investigated CDK4 expression levels in SKUT-1 cell line (pCW57.1-RB1 system, fig.5.8c,d). Rb expression was induced in this cell line by adding doxycycline one day before the experiment. Cells, both proficient and deficient (not induced), were treated with HSP90 inhibitors (alvespimycin or luminespib) and analysed by western blot. Consistent results were observed in the SKUT-1 cell line, with CDK4 expression decreasing upon treatment with 20 nM HSP90 inhibitors (fig.5.8c, d).

In summary, these findings suggested that Rb depleted cells increased sensitivity towards HSP90i, as evidenced by a more pronounced degradation of CDK4, which can serve as a read-out of drug activity in these cells.

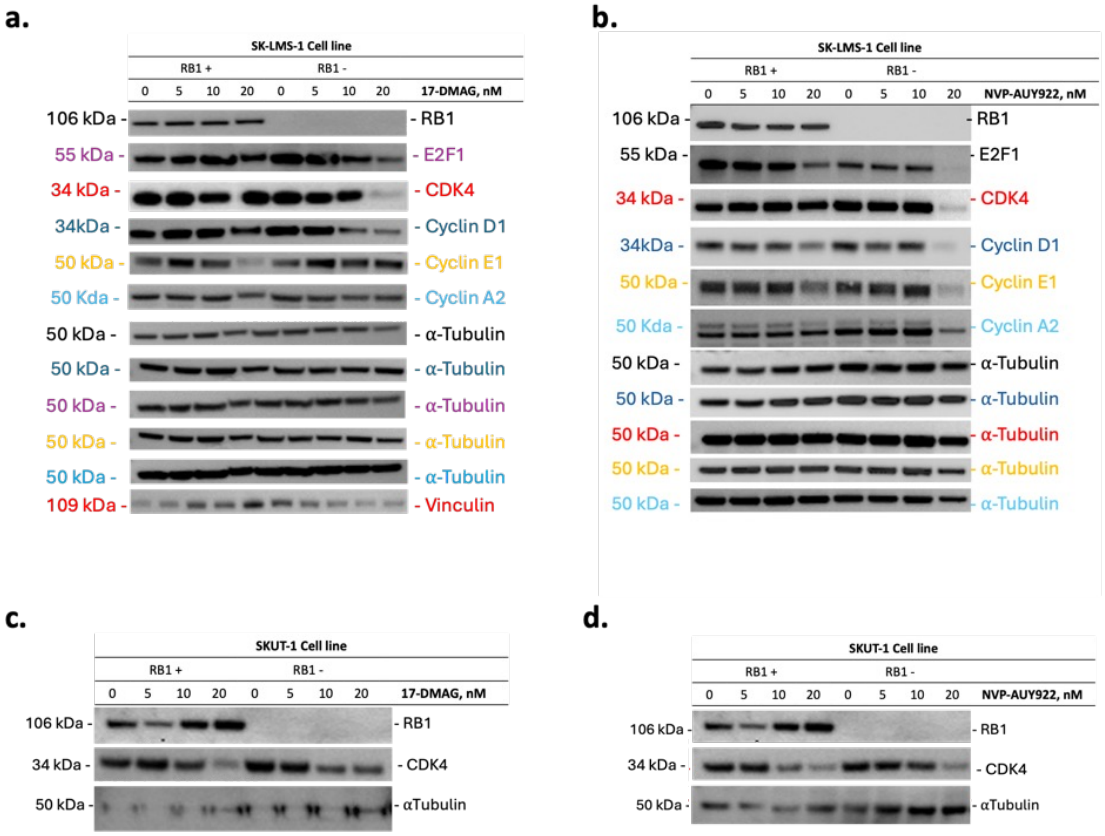


Figure 5.8. Cell cycle was not altered by Rb loss and HSP90 inhibition.

Cell cycle biomarkers expression levels were assessed by western blot analysis in SK-LMS-1 cells after 48-hour exposure of **a.** 17-DMAG and **b.** NVP-AUY922; in SKUT-1 cells **c.** 17-DMAG and **d.** NVP-AUY922 treatment. DMSO-treated cells were used as a control and indicated as untreated cells with HSP90i. Vinculin and αTubulin were used as loading control, colours of loading controls corresponded to the related coloured protein. Representative data of three independent experiments.

5.2.3. Exploring mechanisms of cell death induced by HSP90 inhibition

HSP90 plays a critical role in stabilising the folding of client proteins, many of which contribute to cell survival or anti-apoptotic pathways. Inhibition of HSP90 can disrupt the folding of these client proteins, leading to their degradation and potentially triggering programmed cell death (PCD). PCD comprises various pathways, including apoptosis, autophagy, necroptosis, pyroptosis and ferroptosis. Our hypothesis was that HSP90 inhibition may activate one or more PCD pathways in *RB1*-deficient

sarcoma cells. Understanding the molecular mechanisms of programmed cell death induced by HSP90 inhibition in cells lacking Rb could be crucial for unravelling the molecular mechanisms of selective lethality in *RB1* deficient cells.

5.2.4. HSP90i induces cell death by apoptosis activation

To evaluate whether the synthetic lethality effect mediated by HSP90 inhibition occurred through the apoptosis pathway in Rb lacking cells, we examined markers of cell death activation via western blot analysis after treating cells with alvespimycin at indicated concentrations (fig.5.9). Caspases, a family of cysteine acid proteases activated in a cascade-like manner, serve as key mediators of apoptosis. Caspase-3 is the main downstream protease that catalyses the enzymatic cleavage of many crucial cellular proteins involved in cell disassembly. Poly-(ADP-ribose) polymerase (PARP), a protein implicated in the DNA damage response, is among the substrates cleaved by caspase 3. The detection of cleaved-caspase 3 and cleaved-PARP by immunoblot analysis serves as an indicator of apoptosis pathway activation.

Western blot analysis revealed a significant increase in cleaved-caspase 3 expression levels, beginning at 10 nM in Rb deficient cells (fig.5.9a). This difference demonstrated a dose-dependent escalation, peaking at 50 nM. These findings suggested that the synthetic lethality effect between HSP90 inhibition and Rb loss may be mediated through the apoptosis pathway, as evidenced by the elevated levels of cleaved-caspase 3. Similarly, the levels of cleaved-caspase 3 increased in Rb-null cells with luminespib treatment (10 nM) (fig.5.9b), consistent with the effect observed with alvespimycin. However, it is important to note that the cleavage of PARP was relatively weak in Rb-null cells treated with luminespib. Despite this, cleaved caspase-3 levels were consistent and reproducible across treatments with both HSP90 inhibitors. This indicates that while PARP cleavage may be variable, caspase-3 activation performed as a more consistent indicator of apoptosis in this context.

In conclusion, our findings suggested that the activation of apoptosis was the underlying pathway for the synthetic lethal activity of HSP90 inhibition in cells lacking Rb.

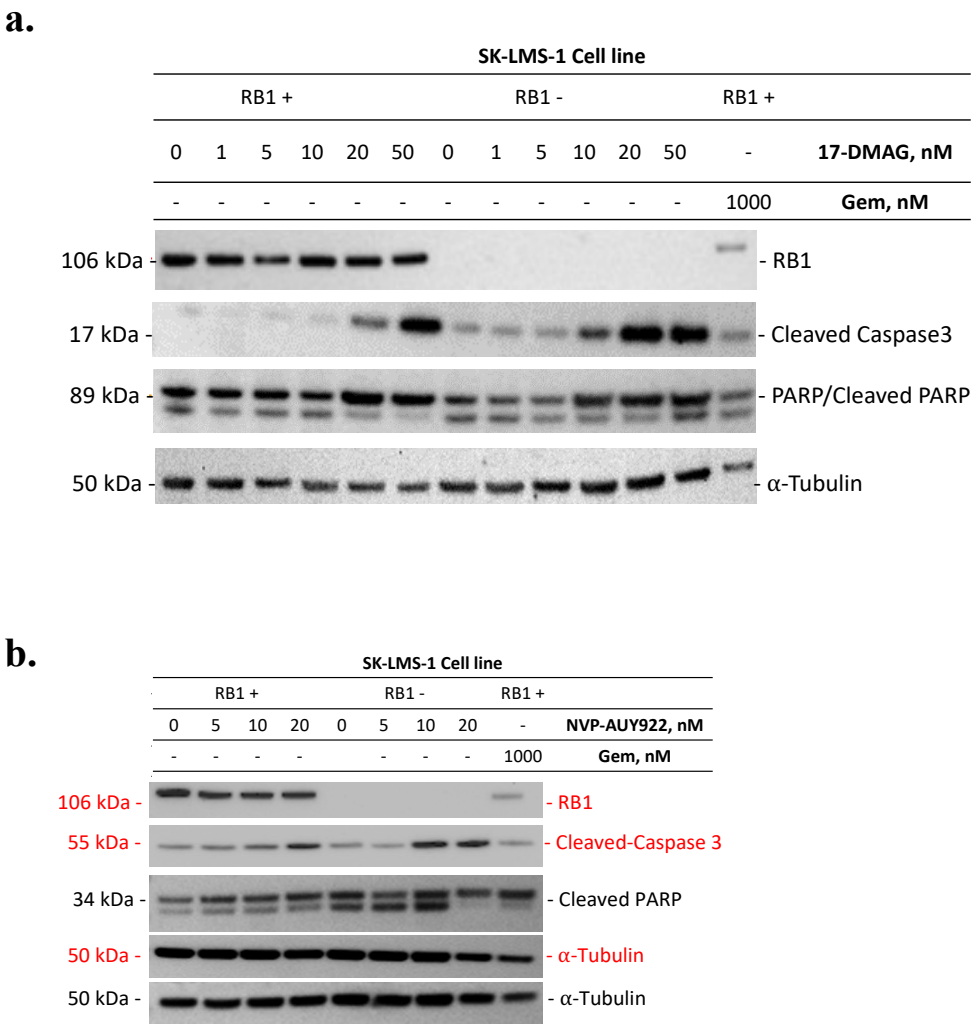


Figure 5. 9. HSP90 inhibitors treatment promotes apoptosis.

Western blots showed the increase of cleaved-caspase-3 and cleaved-PARP levels (apoptotic biomarkers) in *RB1* gene deficient SK-LMS-1 cells post 48-hour treatment with increasing concentrations of **a.** 17-DMAG and **b.** NVP-AUY922, compared to Rb proficient cells. DMSO-treated cells were used as a control and indicated as untreated cells with HSP90i. Control cells were treated with gemcitabine (1μM, 24h) used as a positive control for drug treated cells. αTubulin was used as loading control, colours of loading controls corresponded to the related coloured protein.

To further assess apoptosis pathway activation in Rb deficient/proficient cell lines upon HSP90i treatment, we quantified apoptotic cells using annexin V fluorescence and flow cytometry analysis (Biolegend, #640922). The fluorochrome-labelled annexin V binds to phosphatidylserine (PS), which is typically located on the intracellular leaflet of the cell membrane in healthy cells. During early apoptosis, PS transfers to the external leaflet of the membrane and interacts with annexin V. To distinguish apoptotic and necrotic cells, 7-amino-actinomycin D (7-AAD) was used to identify late-stage apoptotic cells (fig.5.10a). Data showed that the SK-LMS-1 cell line exhibited basal level of apoptotic pathway activation. Notably, HSP90 removal induced a two-fold increase in annexin V fluorescent cells compared to the untreated samples. Both treated cells (RB+/-) exhibited an increase in annexin V fluorescent. However, Rb null cells were selectively more affected by HSP90 inhibition (fig.5.10b,c,d).

In conclusion, the data established that the removal of HSP90 led to a significant enhancement of apoptotic cells. This effect was more pronounced in Rb null cells, suggesting a selective vulnerability of this cell population to HSP90 inhibition.

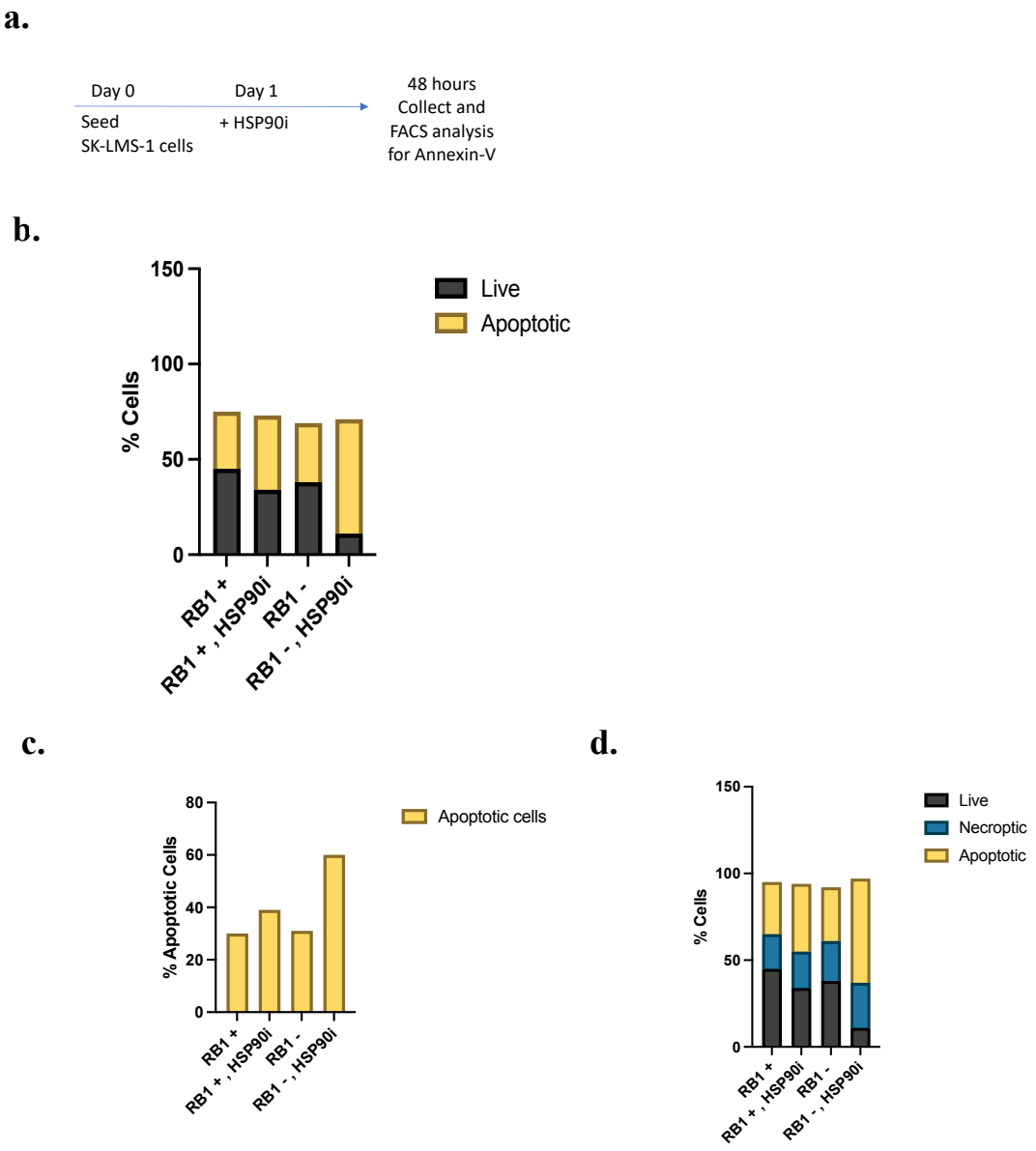


Figure 5.10. Assessment of apoptosis activation by Flow cytometry analysis.

a. Schematic timeline of the experiment starting from cell seeding, 48 h drug treatment with 17-DMAG (10nM) followed by collection and FACS analysis for Annexin V. Apoptotic cells distribution analysis was carried out by Annexin V staining Flow cytometry data analysis showing in **b.** both Live and Apoptotic cells increased upon HSP90 inhibition**, c.** only increase of apoptotic cells and **d.** Live, Necroptic and Apoptotic cells. Data of one representative experiments.

5.2.5. HSP90i does not induce cell death by autophagy and other processes

Next, we examined whether other programmed cell death mechanisms were implicated in the synthetic lethality effects observed in Rb lacking cells upon HSP90 inhibition. Autophagy was one of these mechanisms, as it can promote cell survival or trigger cell death under stress conditions. It preserves cellular homeostasis by degrading and recycling damaged or unnecessary cellular components, through the formation of vesicles called autophagosomes, which fuse with lysosomes for degradation (fig.5.11). Autophagic cell death is characterised by the massive accumulation of cellular components within autophagosomes. Potential activation of autophagy was evaluated by western blot analysis.

SK-LMS-1 cells were subjected to 48-hours of drug treatment, with alvespimycin or luminespib, at appropriate drug concentrations, and lysates were used to perform western blot analysis. To track autophagy in both treated and untreated cells, we monitored the expression levels of SQSTM1 (P62) and the conversion of LC3I to LC3II. SQSTM1 (P62) recognises ubiquitinated proteins designated for degradation and interacts with LC3-II. Members of the LC3 family, such as LC3B, are converted from a type I to a lipidated type II form to integrate into autophagosomes by interacting with cargo receptors like SQSTM1. This complex serves as a cargo protein receptor and promotes autophagosome formation. Autophagosomes fuse with lysosomes, and the cargo, including SQSTM1, undergoes degradation. This process leads to reduction in SQSTM1 levels and an increase in LC3B type II during autophagy, making its expression a common indicator for monitoring autophagic activity (fig.5.11).

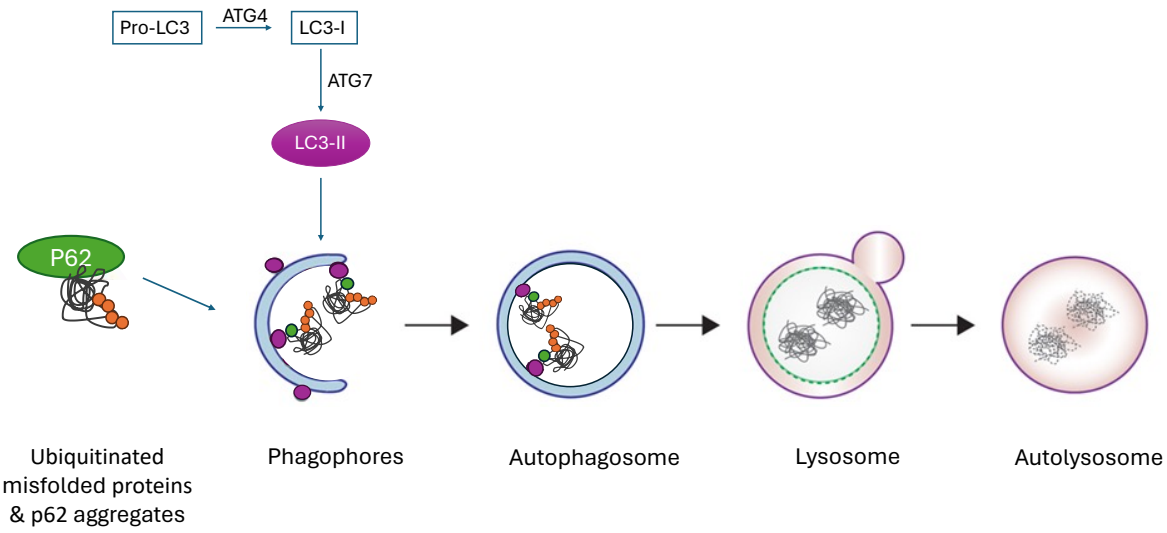


Figure 5.11. Process of p62-mediated selective autophagy.
Misfolded protein aggregates are recruited by p62 once ubiquitinated. Following intracellular or extracellular stimulation signals, phagophores continue to expand and encapsulate cytoplasmic components. Phagophores eventually form sealed spherical autophagosomes, which complex with LC3 in its lipidated form (LC3-II), interacting with p62 bodies. Autophagosomes then merge with lysosomes to form autolysosomes, promoting the degradation of aggregated protein. (Modified by Ichimura et al, Front Oncol. 2018)

Figure 5.12 illustrates that both LMS cell lines (SK-LMS-1, SKUT-1) exhibited a modest activation of autophagy following 48 hours treatment with HSP90 inhibitors (alvespimycin or luminespib) at the indicated concentrations. Notably, cells showed decreased SQSTM1 (P62) expression levels, as expected during autophagy activation, especially in Rb-deficient cells treated with 17-DMAG at 10 nM-20 nM, respectively. A decrease in LC3B-II expression was also observed starting at 10 nM 17-DMAG or NVP-AUY922 in both RB1+/- cells (fig.5.12). Although LC3I/II levels reflected the potential of autophagy activation in response to HSP90 inhibition, these data did not suggest that autophagy was the main mechanism driving cell death in this scenario. We concluded that, while autophagy may be activated, other mechanisms may be responsible for the synthetic lethality effect observed with HSP90 inhibition and Rb loss.

Subsequently, cell signalling biomarkers associated with alternative programmed cell death mechanisms were investigated in SK-LMS-1 cell line under the same drug treatment conditions. Necroptosis and pyroptosis were evaluated using a western blot approach, as well as ferroptosis (data not shown). Necroptosis is an alternative mechanism of programmed cell death initiated by specific signalling molecules like RIPK1, RIPK2 kinases, which activates the necrosome complex. This complex disrupts cell membrane integrity and induces the release of cytoplasmic contents. Pyroptosis involves gasdermin pores formation, which disrupts cell membrane permeabilization, resulting in cell swelling and rupture. Likewise, ferroptosis is characterized by membrane rupture and vesiculation, mitochondrial atrophy, reduced mitochondrial ridge, and an increased in membrane density. (Peng et al. 2022) In contrast, necrosis is an uncontrolled, passive form of cell death. Necrosis induces rupture of cell membrane and the release of intracellular contents. (Costigan, Hollville, and Martin 2023)

Western blot analysis in SK-LMS-1 cells did not detect any bands, suggesting these alternative mechanisms of programmed cell death were not activated. We excluded the possibility that HSP90 inhibition was mediating a lethal effect in Rb-deficient cells through alternative cell death processes unrelated to apoptosis.

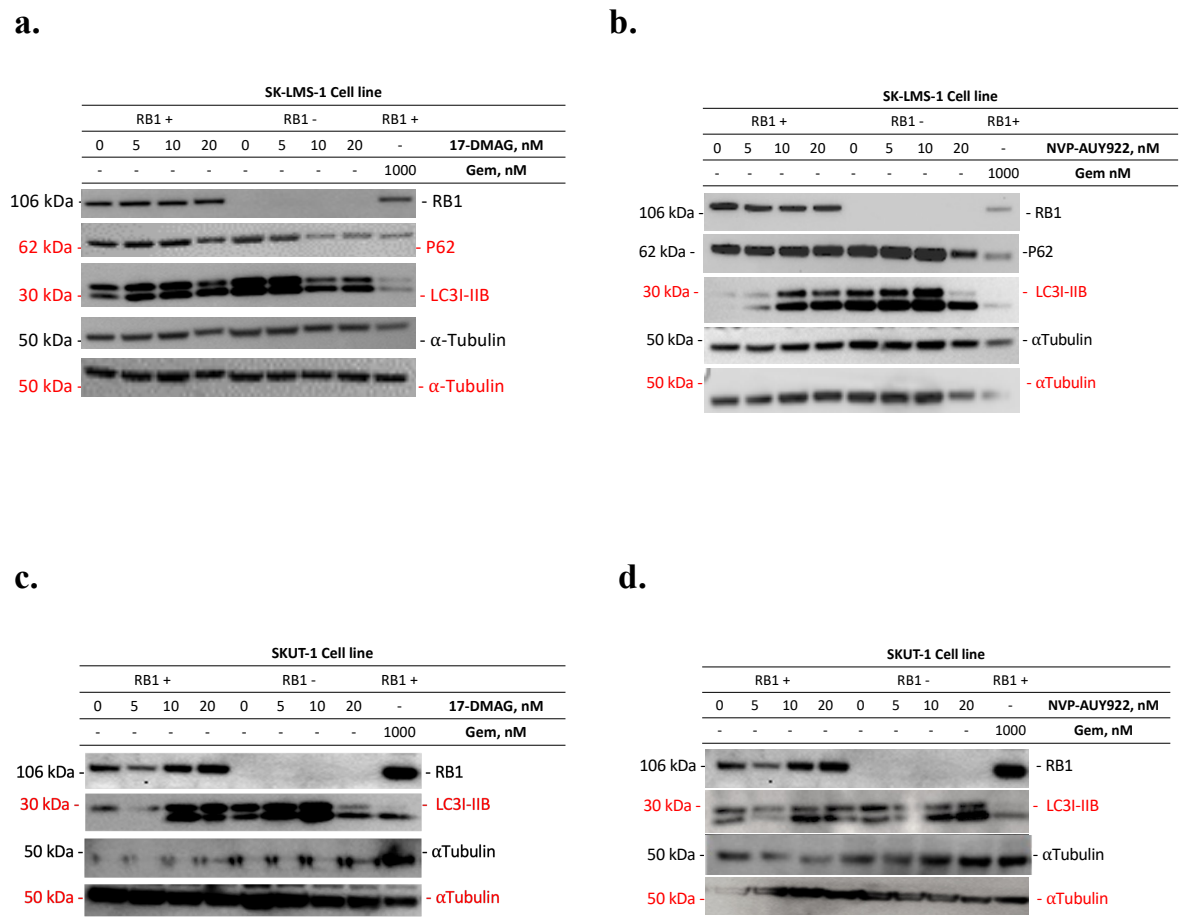


Figure 5.12. HSP90 inhibitors activate autophagy pathway.

Western blots illustrate autophagy biomarkers levels changed moderately in SK-LMS-1 RB1+/- cells after 48-hour exposure of **a.** 17-DMAG and **b.** NCP-AUY922, and in SKUT-1 RB1+/- cells upon **c.** 17-DMAG and **d.** NCP-AUY922 treatment. DMSO-treated cells were used as a control and indicated as untreated cells with HSP90i. Positive control cells were treated with gemcitabine (1μM, 24h). αTubulin was used as loading control, colours of loading controls corresponded to the related coloured protein. Representative data of three independent experiments.

5.2.6. HSP90i does not induce cell death by DNA damage response pathways

The absence of Rb and the disruption of efficient protein folding mediated by HSP90i, could contribute to the disruption of the DNA replication process, rendering cells more prone to DNA damage. Thus, we examined levels of replication stress/DNA damage biomarkers through western blot analysis (fig.5.13).

Expression levels of RPA protein phosphorylated in serine-33 or serine-4/8 were explored as biomarkers for DNA replication stress and double strands breaks, respectively. Phosphorylation of serine-33 on RPA is crucial for activating DNA repair processes by signalling the presence of DNA damaged and recruiting other repair proteins, including ATR (ataxia telangiectasia and Rad3-related) kinase, ATM (ataxia telangiectasia mutated) kinase, and DNA-PK (DNA-dependent protein kinase). Accumulation of RPA protein phosphorylated in serine-33 or serine-4/8 reflected the activation of ATR and DNA-PK kinase protein, respectively. However, our data showed no differences between RB1+ and RB1– cells in activating these DNA repair pathways in response to drug treatment (fig.5.13).

Additionally, we evaluated γH2AX levels as indicators of DNA double-strand breaks (DSBs). γH2AX signals the presence of DSBs and enhances the recruitment of DNA repair proteins to the damaged site to initiate the repair process (fig.5.13). ATM kinases are key mediators of the homologous recombination (HR) response to DNA double-strand breaks (DSBs) and phosphorylate various substrates, including KAP1, which serves as a biomarker for DSBs. While, γ-H2AX levels increased at the highest drug concentrations tested (20 and 50 nM), there was not a noticeable increase in phosphorylated KAP1 protein, suggesting ATM pathway might not be involved.

In conclusion, our findings suggested that HSP90i-induced cell death in Rb null cells may not occur due to DNA damage response pathways.

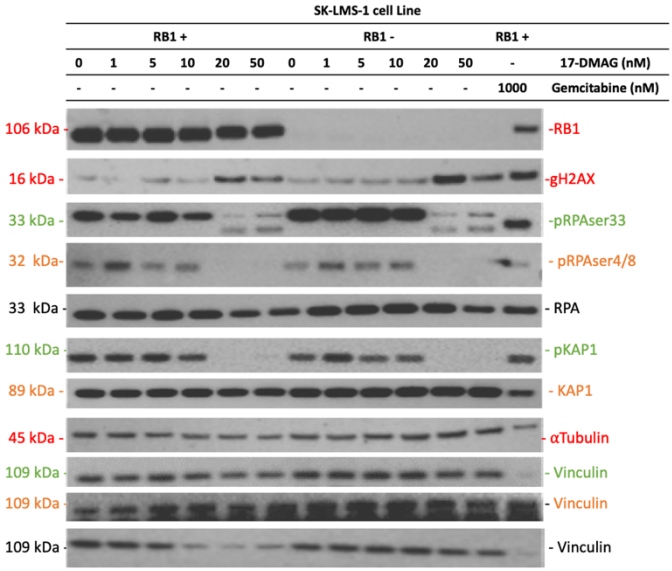


Figure 5.13 . HSP90i does not induce cell death by DNA damage response pathways.

DNA replication stress and DNA damage biomarkers expression levels were assessed by western blot analysis in SK-LMS-1 RB1+/- cells after 24-hour exposure of increasing concentration of 17-DMAG. DMSO-treated cells were used as a control and indicated as untreated cells with HSP90i. Positive control cells were treated with gemcitabine (1μM, 24h). Vinculin and αTubulin were used as loading control, colours of loading controls corresponded to the related coloured protein. Representative data of one independent experiments.

5.3. Key findings

This chapter established the synthetic lethality interaction between HSP90 removal and Rb loss as consistent and reproducible, while also providing crucial insights into the mechanism of cell death mediated by apoptosis.

Viability assays confirmed the reproducibility of the synthetic lethality effect when testing a different HSP90 inhibitor, such as luminespib, in SK-LMS-1 cells. This validation was further reinforced by observing the synthetic lethal effect also in the SKUT-1 cell line, indicating that this effect was consistently linked to Rb deficiency and not dependent on the cell line.

Furthermore, we explored cell signalling pathways by investigating molecular mechanisms. Western blot analysis indicated apoptosis as a potential mechanism for HSP90 inhibitor-induced cell death in Rb-deficient cells, supported by changes in apoptotic biomarkers levels such as cleaved-caspase-3.

Overall, this comprehensive examination provided a foundation for understanding the intricate interplay between HSP90 inhibition and genetic vulnerabilities in leiomyosarcoma, uncovering key cellular mechanisms employed by the cells in response to the drug.

CHAPTER 6

6.1. The identification of cell death mechanisms

6.1.1. Total proteome mass spectrometry analysis

In the previous chapters, we discussed the identification and validation of a synthetic lethal interaction between Rb loss and HSP90 inhibitors (HSP90i). However, the mechanisms driving this synthetic lethality effect induced by HSP90i in the context of Rb loss remain unknown. Therefore, we conducted an examination of the whole-cell proteome profiles in SK-LMS-1 cells upon treatment with the HSP90 inhibitor 17-DMAG using mass spectrometry. This quantitative proteomic approach allowed us to explore potential changes in the protein landscape due to HSP90 inhibition in our Rb null cell model. Samples proteins preparation was performed by Dr Yingying Ma in our lab, while mass spectrometry analysis was carried out in collaboration with Professor Benedikt M Kessler's group, specifically Dr Iolanda Vendrell (Target Discovery Institute, University of Oxford).

6.2. Samples preparation for proteome profiling of deficient and proficient Rb cells

In this study, we employed the suspension trapping method (S-trap) to generate the proteins samples analysed by mass spectrometry, as illustrated in figure 6.1. This method facilitates efficient SDS-based protein extraction, fast detergent removal, reactor-type protein digestion, and peptide clean-up as described in figure 6.1.

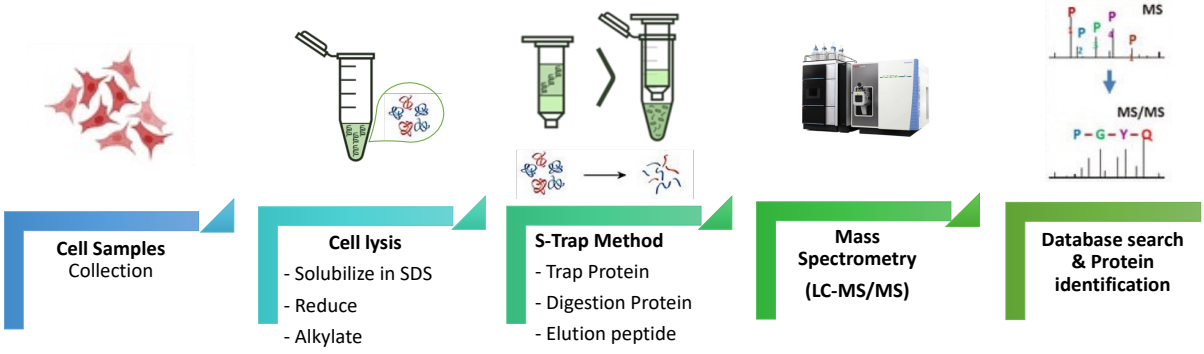


Figure 6.1. S-Trap sample processing technology and mass spectrometry analysis.

Schematic representation of S-Trap methodology requiring 1. Collection of cells samples, 2. Lysis of cells with 5% SDS solubilization and denaturation achieved by acidification (to reach pH<1), followed by reduction and alkylation reactions. 3. Trapping of proteins into the S-trap column, where they are digested into peptides by the protease mix buffer. 4. Purification of peptides, which are then eluted for MS analysis. 5. Database search and protein identification. Figures modified from Protifi website.

6.2.1. Samples validation for proteome profiling of deficient and proficient Rb cells

To verify that the cells responded as expected to the drug treatment, a small amount of the mass spectrometry protein lysates was analysed by western blot. We confirmed the knock-out of the *RB1* gene in the SK-LMS-1 cell line and that the HSP90 inhibitor 17-DMAG effectively stimulated an increase in the expression levels of apoptotic biomarkers. As a result, the presence or full knock out of *RB1* gene was successfully exhibited by the SK-LMS-1 *RB1*+/- cell samples, respectively. Additionally, the expression levels of cleaved-caspase-3, used as an indicator of cell death, increased more in HSP90i-treated SK-LMS-1 lacking Rb compared to the treated Rb proficient ones (Fig.6.2a). Furthermore, samples were stained by silver staining to assess protein abundance, revealing uniform loading among each sample (Fig.6.2b).

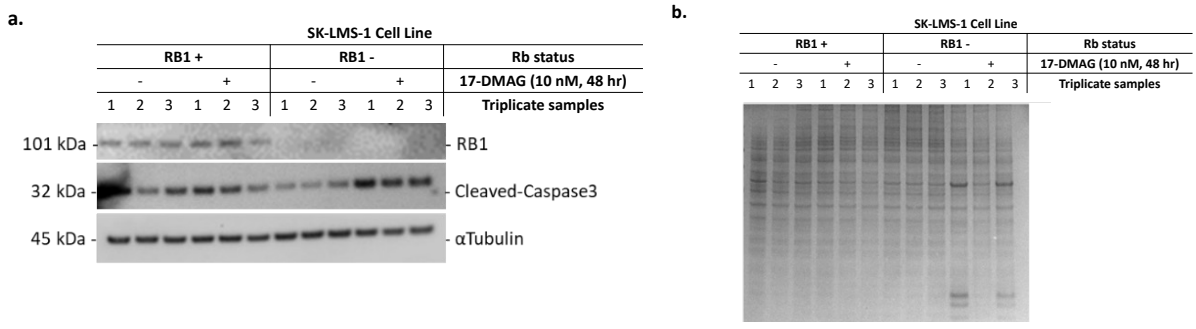


Figure 6.2. Cell line and drug treatment validation before mass spectrometry analysis.
a. Western blot showed Rb protein and cleaved-caspase-3 levels (apoptotic biomarker) in triplicate samples of SK-LMS-1 cells post 48-hour treatment with 10 nM HSP90i (17-DMAG). DMSO-treated cells were used as a control and indicated as untreated cells with HSP90i. **b.** Silver staining analysis revealed consistent protein concentrations among protein samples.

The *RB1* gene status in SK-LMS-1 RB1+/- cell line was also evaluated by mass spectrometry. Data analysis revealed that Rb protein was not detected in any of the triplicates of the *RB1* gene deficient samples, both untreated and HSP90i treated (indicated in figure as No-RB1, No-RB1_hsp, respectively). This confirmation indicated that the cell line represented a valid model for our investigations, and the protein samples preparation was performed correctly (fig.6.3).

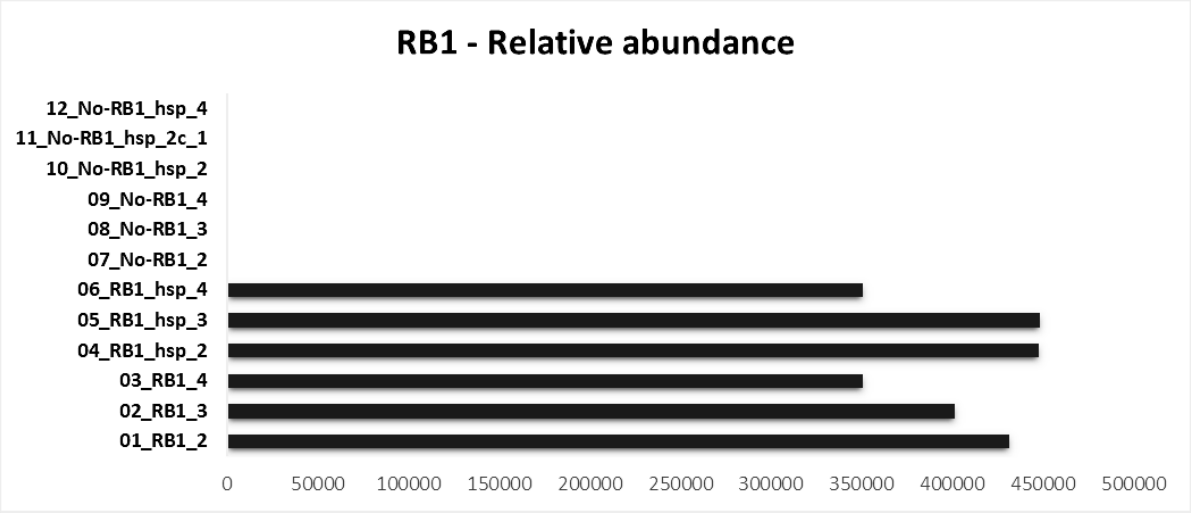


Figure 6.3. Rb status examination by mass spectrometry.
RB1 deficient cells, untreated and treated with HSP90i (No-RB1, No-RB1_hsp, respectively), showed the *RB1* gene knock out has worked. In proficient cells, Rb protein level was statistically significant in all comparisons (RB1, RB1_hsp, respectively).

To authenticate the quality of each sample used for total proteome analysis, missing values comparison (MVs) was performed (fig.6.4). The data indicated a very low number of missing value, showing a high level of consistency across the samples. Overall, the data presented a standard distribution. The number of imputed values was minimal, corresponding to low-abundance proteins due to the lower percentage of missing values.

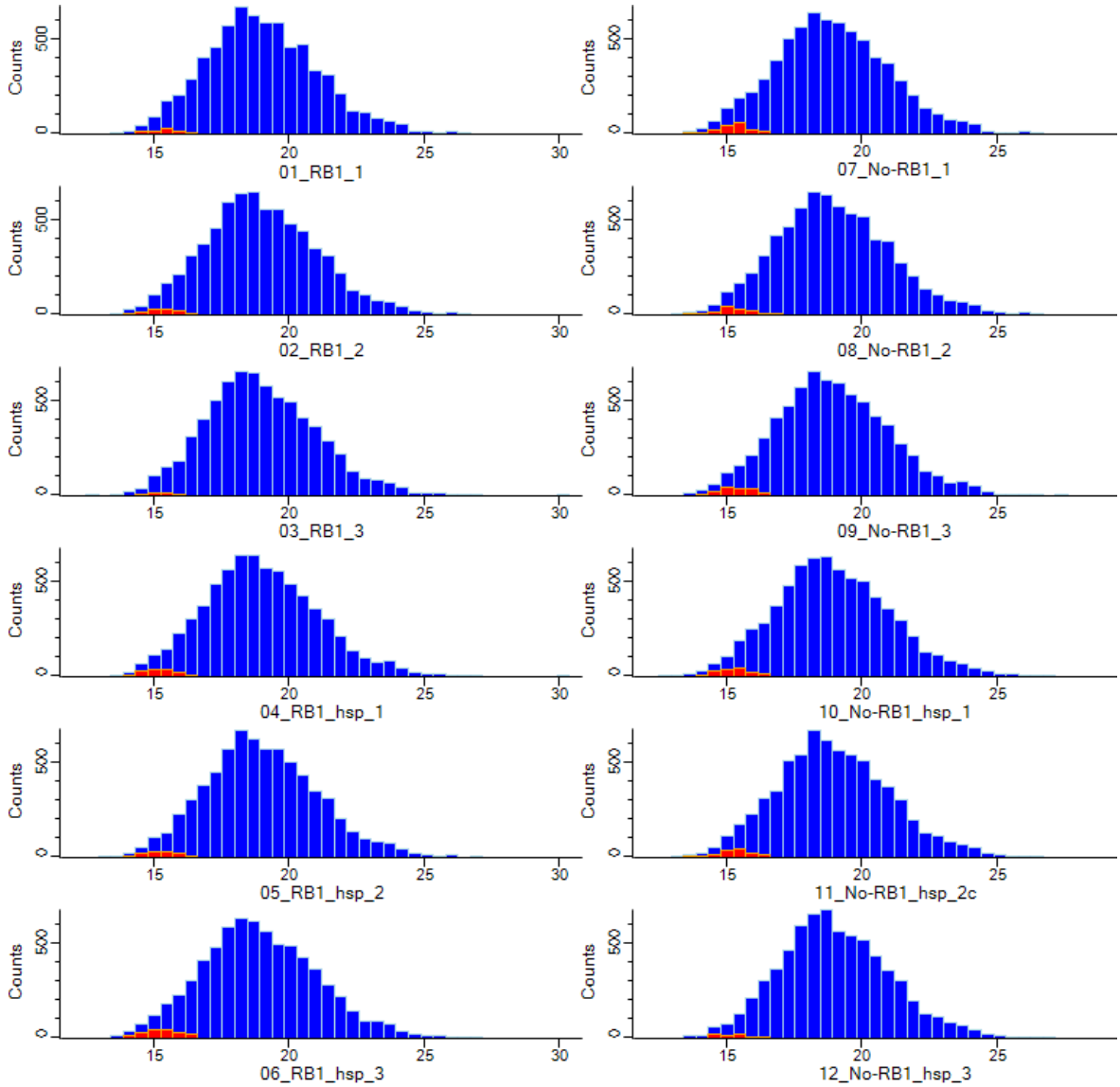


Figure 6.4. Missing values comparison by mass spectrometry analysis.

Bar plots represent the number of features (proteins, X-axis) detected at each intensity (counts per bin, Y-axis). Red bars illustrated where a missing value (feature not quantified) has been imputed in SK-LMS-1 cells untreated/treated Rb proficient (RB1/RB1_hsp respectively), or Rb deficient (No-RB1/No-RB1_hsp, respectively), in triplicate samples. Figures generated using Perseus software version 1.6.2.2.

Moreover, we conducted principal component analysis (PCA) (fig.6.5). PCA is a statistical procedure that summarises a large number of features into analogous features based on similar trends and patterns of each sample. In this analysis, the main features driving the separation of the principal

component were the presence or absence of the *RB1* gene. Additionally, PCA components were separated by HPS90 inhibition. The total proteome PCA graph displayed triplicate samples clustering together, indicating high consistency. PCA showed a clear separation between Rb proficient and deficient cell samples, whether treated or untreated with HSP90i, respectively, in each biological replicate (fig.6.5).

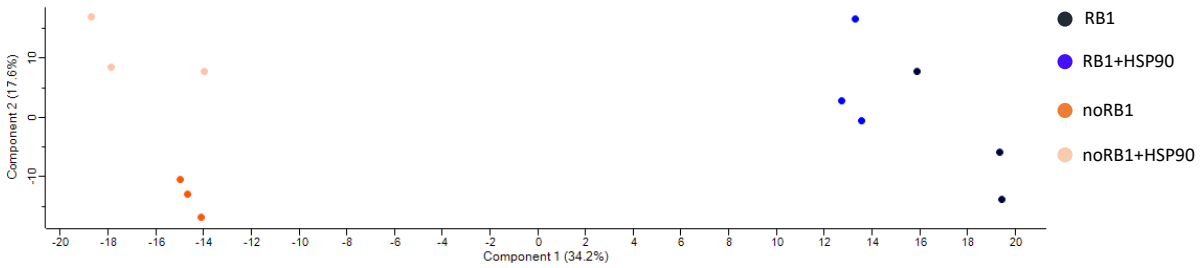


Figure 6.5. Principal component analysis (PCA) plot for SK-LMS-1 cells (RB1+/-) and with HSP90 inhibition.

The graph presented triplicate samples of SK-LMS-1 proficient (RB1) and deficient (noRB1) cells clustering by the Rb status and by drug treatment (17-DMAG, 10 nM, 48h). Figures generated using Perseus software version 1.6.2.2.

To interpret the proteomic data, volcano plots were employed to visualise differentially expressed proteins among the samples based on Rb status and on drug treatment. First, we analysed untreated samples (fig.6.6a). Rb proficient cells expressed proteins involved in molecule transport (NUP2, TMEM231), matrix development (CTHRC1), ubiquitination (UBE2L6) and proteostasis (CTSB). Rb loss induced the upregulation of proteins involved in mitotic chromosome (NCAPG2), cell adhesion (MMP3, MMP1, CERK) and cytoplasmic microtubule organization (CCD14, CLIP4) accompanied by oxidative stress response (KEAP1), inflammation and cell death mechanism (CD70, TNFRSF10D) (fig.6.6a). As expected, Rb loss had a significant impact on cell cycle regulatory pathways and cell survival.

Next, we evaluated the effects of HSP90 inhibition (fig.6.6b). Upon drug treatment, Rb proficient cells induced the expression of proteins involved in inflammation activation (LCP1, CASP1, NEO1), cell adhesion (CTHRC1, PODXL), cell metabolism (NAGLU) and cell transport (NUP2). Conversely, Rb-deficient cells responded to HSP90 inhibition by expressing proteins participating in autophagy (TMEM59, PLEKHB2, NDFIP2), accompanied by upregulation of those involved in cell adhesion, extracellular matrix development (PLG, ANTXR2, CERK) and fatty acid metabolism (ADIPOR1) (fig.6.6b). As a result, the removal of Rb and HSP90 promoted the activation of cellular stress mediatory pathways.

To gain more insights about the impact of HSP90 inhibition in promoting programmed cell death mechanisms in the context of Rb loss, we compared how protein expression changed upon drug treatment in RB1+/-, treated versus untreated, respectively (fig.6.6c/d). First, we examined RB1+ cells with/without drug treatment (fig.6.6c). Rb proficient cells showed a significant upregulation of HSP70 (HSPA1A, HSPA1), alongside proteins primarily involved with cell adhesion (MMP3, SEMA3E, VTN), microtubule/cytoskeleton organization (MLC1, CLIP4, COL8A1) and peptide transport (SLC1A5). Under drug treatment, Rb proficient cells enhanced expression of proteins involved in cell membrane adhesion and cytoskeleton development (MARCKS, PLD2, XIRP2), followed by others involved in cell cycle control at G1-S phase (LRWD1) and G2-M phase (ANAPC1) (fig.6.6c). This data may suggest Rb plays a crucial role in safeguarding cell survival, strengthening cell cycle control and maintaining cell structure integrity under HSP90 inhibition.

In contrast, Rb-deficient cells exhibited a different subset of upregulated proteins upon HSP90 inhibitor (fig.6.6d). Rb-deficient cells showed a high increase of chaperones such as HSP70 (HSPA1A), HSP47 (SERPINH1) and clusterin (CLU), suggesting the cells might be highly reliant on HSPs activity. This data highlighted the strong interplay between Rb loss and HSP90, in line with the synthetic lethality interaction we discovered. Another upregulated protein was ALDH1L2, involved in mitochondrial folate metabolism and transport, followed by others participating in cell adhesion

(VTN), cytoskeletal organization (COL8A1, MSFD11) and molecular transport (TAP1, HBA1, AHSG). Upon drug treatment, Rb null cells increased proteins that promote unfolded protein degradation through ubiquitination (ARRDC1), apoptosis (NAIF1) and autophagy (TECPR2) or peroxisome (TYSND1). Other proteins were involved in gene transcription and protein synthesis (CPSF1, URB2), telomerase maintenance (TOE1), cytoskeletal organisation (LLGL1, PLD2), development and differentiation of T cells (ZBTB17) (fig.6.6d). As a result, the survival of Rb null cells appeared to be strongly challenged by HSP90 depletion, leading to activation of cell death pathways.

In summary, the volcano plot served as a useful tool to investigate which biological pathways might be associated with protein expression changes underlying the role of Rb and in the context of HSP90 inhibition.

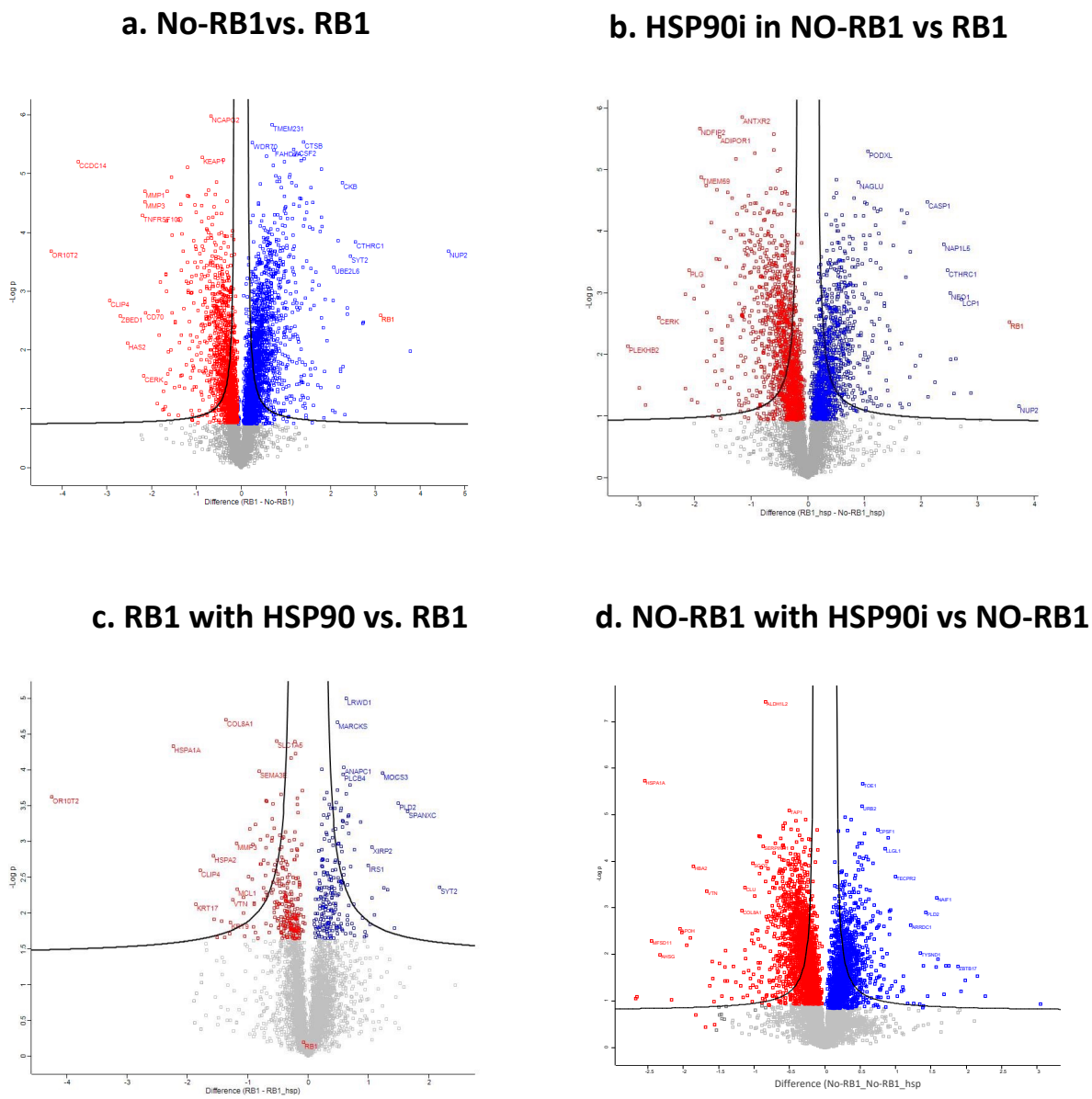


Figure 6.6. Illustration of volcano plots comparing protein expression fluctuation in SK-LMS-1 cells and Rb protein main interactors.

Volcano plots compared protein expression in SK-LMS-1 cells, respectively**: a.** untreated Rb deficient vs proficient **b.** HSP90i treated Rb deficient vs proficient **c.** HSP90i treated vs untreated Rb proficient **d.** HSP90i treated vs untreated Rb deficient**.** X-axis: fold change in Student-T-Test differences; Y-axis: -log (Student-T-Test-p-value).

6.3. Total proteomic profile of SK-LMS-1 cells Rb proficient/deficient

To investigate further the impact of Rb loss, the total proteomic profiles of SK-LMS-1 were compared within RB1- and RB1+ cells. Total proteome profiles data were utilised to construct a hierarchal heatmap clustergram based on the absence of Rb (fig.6.7a). This approach provided a comprehensive overview of proteins exhibiting significant expression changes linked to Rb status. Within the heatmap, proteins with similar expression profiles were summarised into two distinct clusters (fig.6.7b). Within the cluster, each protein's expression was regulated by Rb status. Cluster 676 represented 264 proteins, the upregulation of which was driven by Rb loss in RB1- cells. Cluster 675 represented 414 upregulated proteins in RB1+ cells (fig.6.7b).

To understand the biological implications of the upregulation of the protein datasets within the cluster 676 and 675, enrichment pathways data analysis was performed using multiple software such as Enriched-R and Metascape. The integration of multiple tools improved the consistency of the analysis (fig.6.7c/d).

Enrichment pathways analysis was assessed based on MgSDHallmark_2020 database using Enriched-R as a bioinformatics resource tool. Here, Rb lacking cells exhibited an enhancement of pathways linked to the transcription factor E2Fs family protein (fig.6.7c). This data was expected and previously validated by western blot analysis in Chapter 1 (fig.3.7). Coherent with this data, the G2-M phase checkpoint was present as one of the most enriched pathways. This result suggested an aberrant G1-S phase transition in the cell cycle, followed by a significant activation of the CHK2 checkpoint to avoid cell cycle progression and mitosis entry by RB1- cells. Moreover, the enrichment of mitotic spindle pathway activation suggested accumulation of S-replicating cells and abnormal cell cycle progression due to Rb loss. Rb proficient cells were upregulating a wide set of pathways commonly participating in tumour growth and tumour invasiveness such as the epithelial-mesenchymal transition pathway and complement activation (fig.6.7d). We could conclude we succeeded in generating a valid cell model for Rb loss using our LMS cell line.

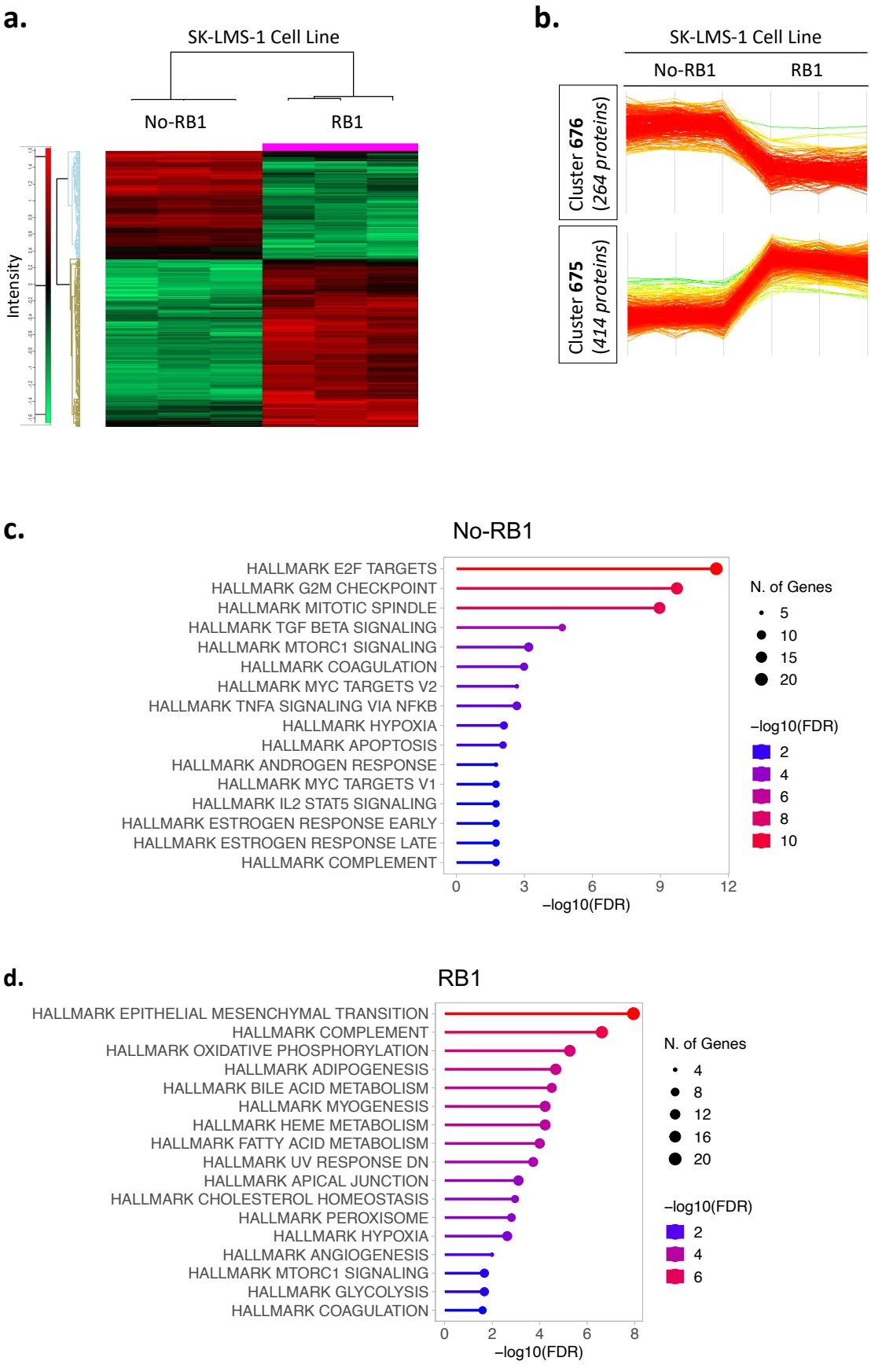

a.
SK-LMS-1 Cell Line
No-RB1
RB1
Intensity
b.
SK-LMS-1 Cell Line
No-RB1
RB1
Cluster 676 (264 proteins)
Cluster 675 (414 proteins)
c.
No-RB1
HALLMARK E2F TARGETS
HALLMARK G2M CHECKPOINT
HALLMARK MITOTIC SPINDLE
HALLMARK TGF BETA SIGNALING
HALLMARK MTORC1 SIGNALING
HALLMARK COAGULATION
HALLMARK MYC TARGETS V2
HALLMARK TNFA SIGNALING VIA NFKB
HALLMARK HYPOXIA
HALLMARK APOPTOSIS
HALLMARK ANDROGEN RESPONSE
HALLMARK MYC TARGETS V1
HALLMARK IL2 STAT5 SIGNALING
HALLMARK ESTROGEN RESPONSE EARLY
HALLMARK ESTROGEN RESPONSE LATE
HALLMARK COMPLEMENT
0
3
6
9
12
−log10(FDR)
N. of Genes
5
10
15
20
−log10(FDR)
2
4
6
8
10
d.
RB1
HALLMARK EPITHELIAL MESENCHYMAL TRANSITION
HALLMARK COMPLEMENT
HALLMARK OXIDATIVE PHOSPHORYLATION
HALLMARK ADIPOGENESIS
HALLMARK BILE ACID METABOLISM
HALLMARK MYOGENESIS
HALLMARK HEME METABOLISM
HALLMARK FATTY ACID METABOLISM
HALLMARK UV RESPONSE DN
HALLMARK APICAL JUNCTION
HALLMARK CHOLESTEROL HOMEOSTASIS
HALLMARK PEROXISOME
HALLMARK HYPOXIA
HALLMARK ANGIOGENESIS
HALLMARK MTORC1 SIGNALING
HALLMARK GLYCOLYSIS
HALLMARK COAGULATION
0
2
4
6
8
−log10(FDR)
N. of Genes
4
8
12
16
20
−log10(FDR)
2
4
6

Figure 6.7. Total proteomic profiles of SK-LMS-1 No-RB1 vs. RB1 cells.

a. The heatmap illustrates the proteome profile based on Rb loss in SK-LMS-1 Rb null cells (No-RB1) versus Rb proficient cells (RB1). The significant up-regulated proteins are indicated in red, the down-regulated are in green. Total proteome data were filtered by Anova q-value with Z-score presented as intensity. **b.** Cluster-grams show proteins differentially expressed due to Rb loss in two clusters (675,676), in SK-LMS-1 with RB1 and No-RB1 cell samples. Figures generated using Perseus software version 1.6.2.2. Enrichment pathways analysis showing upregulated pathways in **c.** No-RB1 (cluster 675) and **d.** RB1 (cluster 676); pathways are ranked based on p-value using Enriched-R software. Images were generated using Shinygo.

Metascape's enrichment pathways analysis was investigated using the MgSDHallmark_2020 database (fig.6.8.). Here, Rb null cells revealed a significant enhancement of the cell division pathway, followed by regulation of chromosome segregation and cell cycle (fig.6.8a). This data established that Rb loss plays a critical role in the deregulation of cell cycle progression. Interestingly, cells with functional Rb showed an increase in organic acid catabolic metabolism (fig.6.8b). As a result, Rb may play an essential role not only in cell cycle control but also in cell metabolism.

.

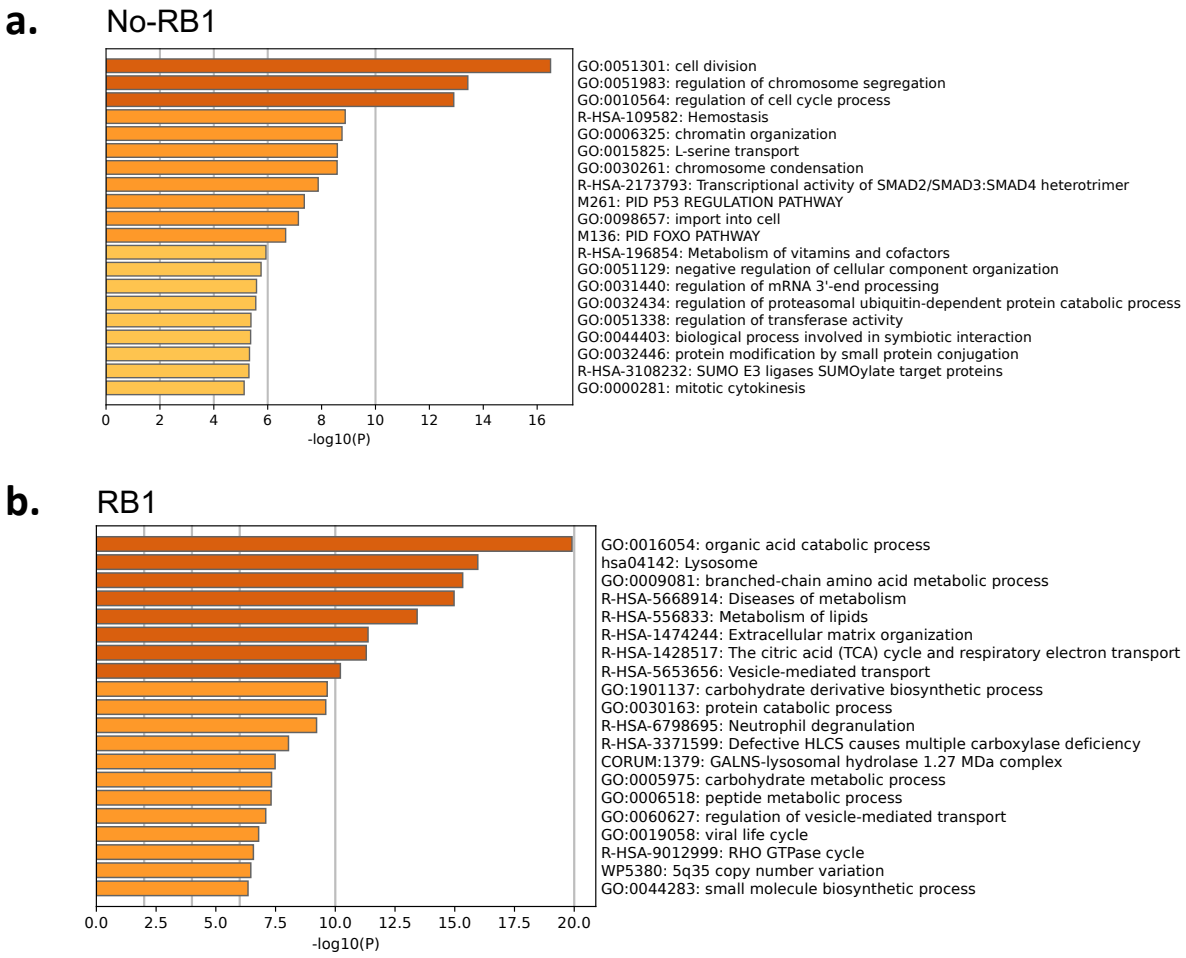


Figure 6.8. Metascape's enrichment pathways analysis of SK-LMS-1 cells

The figure highlights the outcomes of enrichment pathways analysis focusing on the proteome profiles of **a.** No-RB1 (cluster 676) and **b.** RB1 cells (cluster 675), developed using Metascape software, data are ranked by p-value.

To gain deeper insight into the impact of Rb loss in our cell system, gene ontology (GO) enrichment analysis was conducted (fig.6.9). Rb-lacking cells showed mitotic sister chromatid segregation (p-value: 1.8e-11) as the most represented category, followed by mitotic cell cycle regulatory pathways (p-value: 9.83e-08) and vascular transport (p-value: 1.44e-06). This data suggested genomic instability, accumulation genetic abnormalities, and tumour heterogenicity were potentially features of the Rb-lacking cells.

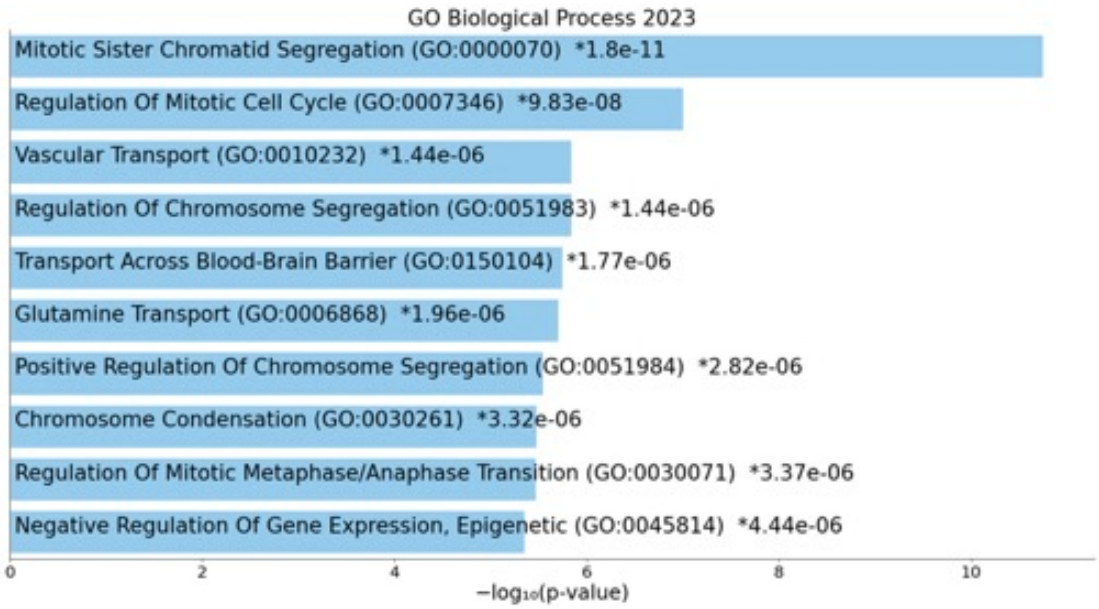


Figure 6.9. GO Biological Processes of SK-LMS-1 Rb lacking cells.
Gene Ontologies data analysis was performed in the context of proteomic data analysis for SK-LMS-1 cells without RB1 (cluster 676). Analysis and images were generated using Enriched-R, data are ranked by p-value.

6.4. Total proteomic profile of SK-LMS-1 *RB1* +/- cells with HSP90 inhibitor

To investigate which cellular mechanisms contributed to the synthetic lethality effect with Rb loss, the whole-cell proteome profiles of HSP90 inhibitor-treated SK-LMS-1 RB1+/- cells were compared using quantitative proteomics studies (fig.6.10). This approach allowed us to obtain different clusters corresponding to the proteins dysregulated in the different conditions tested. Treated SK-LMS-1 RB1+/- cells were organised in a heatmap showing the proteins significantly dysregulated by Rb loss (fig.6.10a). Within the heatmap, proteins with analogous expression profiles were summarised in two distinct gene clusters. Cluster 259 displayed the upregulation of 168 proteins triggered by Rb loss upon HSP90i treatment. Cluster 260 represented 94 proteins upregulated in RB1+ cells under the same drug conditions (fig.6.10b).

To identify which biological pathways may be affected by Rb loss in combination with HSP90 depletion, we performed enrichment pathways analysis focused on the gene datasets included in

clusters 259 and 260 (fig.6.10c/d). Enriched-R's enrichment pathways analysis based on the MgSDHallmark_2020 database highlighted apoptosis activation as the top enriched pathway in Rb null cells in response to HSP90 inhibitor treatment (fig.6.10c). Apoptosis is one of the programmed cell death pathways operating in cells. This observation is consistent with previous findings described in chapter 5 (fig.5.10). However, it is unclear whether apoptosis activation is a consequence or the cause of the observed increased cell death in Rb null cells.

Additionally, coagulation pathways accompanied by Heme metabolism appeared to be highly upregulated (fig.6.10c). Both coagulation pathways and Heme metabolism are highly reliant on the protein folding process mediated by HSP90 (Sumi and Ghosh 2022), and their upregulation likely reflected an increased reliance on protein folding upon Rb loss and HSP90i. IL6/JAK/STAT3 enrichment suggested Rb loss may induce an inflammatory response selectively under drug treatment conditions. In contrast, Rb proficient cells indicated G2-M checkpoint activation as one of the most enriched pathways upon HSP90 inhibitor treatment, followed by complement and mitotic spindle pathways. These pathways were also enriched in untreated conditions as shown in fig.6.7d, suggesting cells with functional Rb were less sensitive to HSP90 inhibition (fig.6.10d).

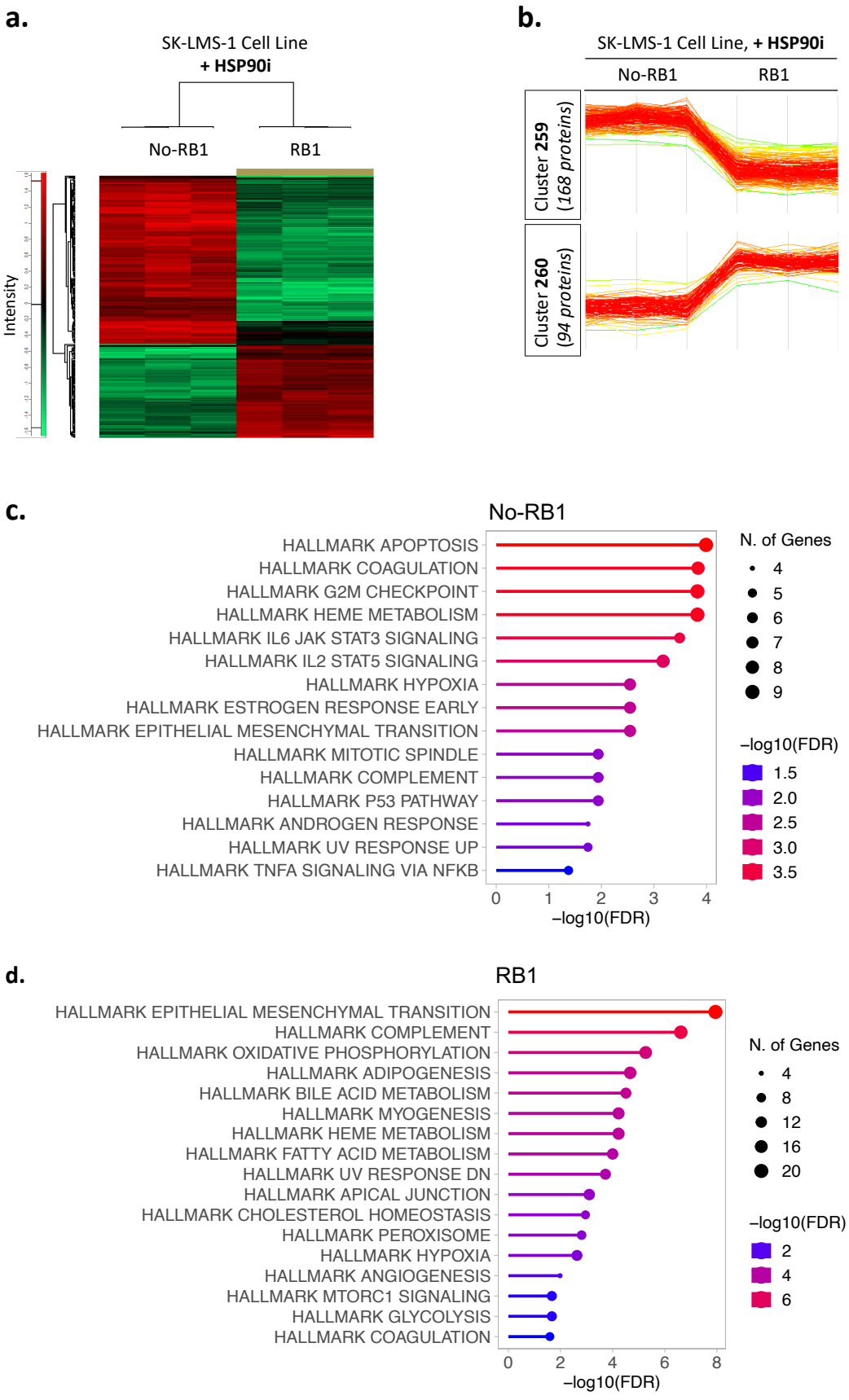

a.
SK-LMS-1 Cell Line
+ HSP90i
No-RB1
RB1
Intensity
b.
SK-LMS-1 Cell Line, + HSP90i
No-RB1
RB1
Cluster 259 (168 proteins)
Cluster 260 (94 proteins)
c.
No-RB1
HALLMARK APOPTOSIS
HALLMARK COAGULATION
HALLMARK G2M CHECKPOINT
HALLMARK HEME METABOLISM
HALLMARK IL6 JAK STAT3 SIGNALING
HALLMARK IL2 STAT5 SIGNALING
HALLMARK HYPOXIA
HALLMARK ESTROGEN RESPONSE EARLY
HALLMARK EPITHELIAL MESENCHYMAL TRANSITION
HALLMARK MITOTIC SPINDLE
HALLMARK COMPLEMENT
HALLMARK P53 PATHWAY
HALLMARK ANDROGEN RESPONSE
HALLMARK UV RESPONSE UP
HALLMARK TNFA SIGNALING VIA NFKB
0 1 2 3 4
–log10(FDR)
N. of Genes
4
5
6
7
8
9
–log10(FDR)
1.5
2.0
2.5
3.0
3.5
d.
RB1
HALLMARK EPITHELIAL MESENCHYMAL TRANSITION
HALLMARK COMPLEMENT
HALLMARK OXIDATIVE PHOSPHORYLATION
HALLMARK ADIPOGENESIS
HALLMARK BILE ACID METABOLISM
HALLMARK MYOGENESIS
HALLMARK HEME METABOLISM
HALLMARK FATTY ACID METABOLISM
HALLMARK UV RESPONSE DN
HALLMARK APICAL JUNCTION
HALLMARK CHOLESTEROL HOMEOSTASIS
HALLMARK PEROXISOME
HALLMARK HYPOXIA
HALLMARK ANGIOGENESIS
HALLMARK MTORC1 SIGNALING
HALLMARK GLYCOLYSIS
HALLMARK COAGULATION
0 2 4 6 8
–log10(FDR)
N. of Genes
4
8
12
16
20
–log10(FDR)
2
4
6

Figure 6.10. Proteomic profiling and Enrichment pathways analysis of HSP90i-treated SK-LMS-1 cells (No-RB1 vs RB1).

a. Heatmap compares proteome profile of SK-LMS-1 Rb-null cells (No-RB1) with Rb proficient cells (RB1) under 48h 17-DMAG treatment (HSP90i, 10 nM). Up-regulated proteins are indicated in red, the down-regulated in green. Data were filtered by Anova q-value with Z-score presented as intensity. **b.** Cluster-grams categorise differentially expressed proteins based on Rb loss into two clusters (259, 260), in SK-LMS-1 cells RB1/ No-RB1. Figures generated using Perseus software version 1.6.2.2. Bar chart illustrates enriched pathways in SK-LMS-1 **c.** RB1- cells and **d.** RB1+ cells, in response to HSP90i treatment. Enriched-R software was used for data search, data are ranked on p-value, figures generated using Shinygo software.

As shown in figure 6.11, Metascape's enrichment pathways analysis confirmed the analysis developed using Enriched-R. Apoptosis featured as the top enhanced pathway in Rb null cells upon drug treatment (fig.6.11a), while Rb proficient cells enriched pathways such as epithelial-mesenchymal transition (EMT) and complement activation (fig.6.11b), consistent with the Enriched-R's analysis (fig.6.10d).

In conclusion, Rb may play a crucial role in regulating specific cellular pathways potentially involved in mediating the drug response to HSP90 inhibitors (fig.6.11).

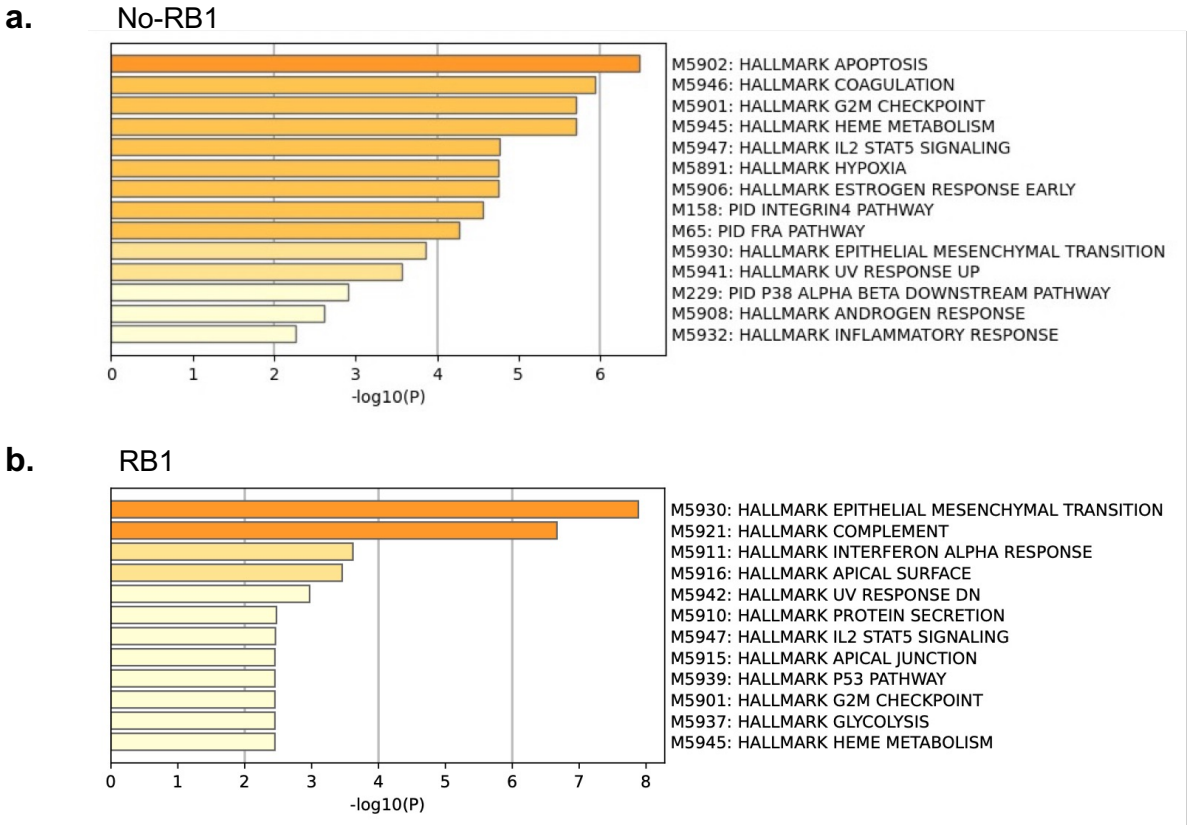


Figure 6.11. Enrichment Pathways Analysis of HSP90i-treated SK-LMS-1 cells (No-RB1 vs RB1).

Enriched pathways in response to HSP90i treatment in **a.** No-RB1 cells and **b.** RB1 cells. Metascape software was used for generating the images and data search based on MgSDHallmark_2020 database, the data are ranked by p-value.

Next, we conducted gene ontology (GO) analysis within the gene dataset based on the proteomic gene profiles of Rb-lacking cells under drug treatment (fig.6.12). Here, HSP90i-treated cells lacking Rb appeared to strengthen biological pathways involved in transporting cellular components such as amino acids, carboxylic acids, and glutamine. These data may validate that Rb has a role in positively controlling cell metabolism, as shown in fig.6.8b.

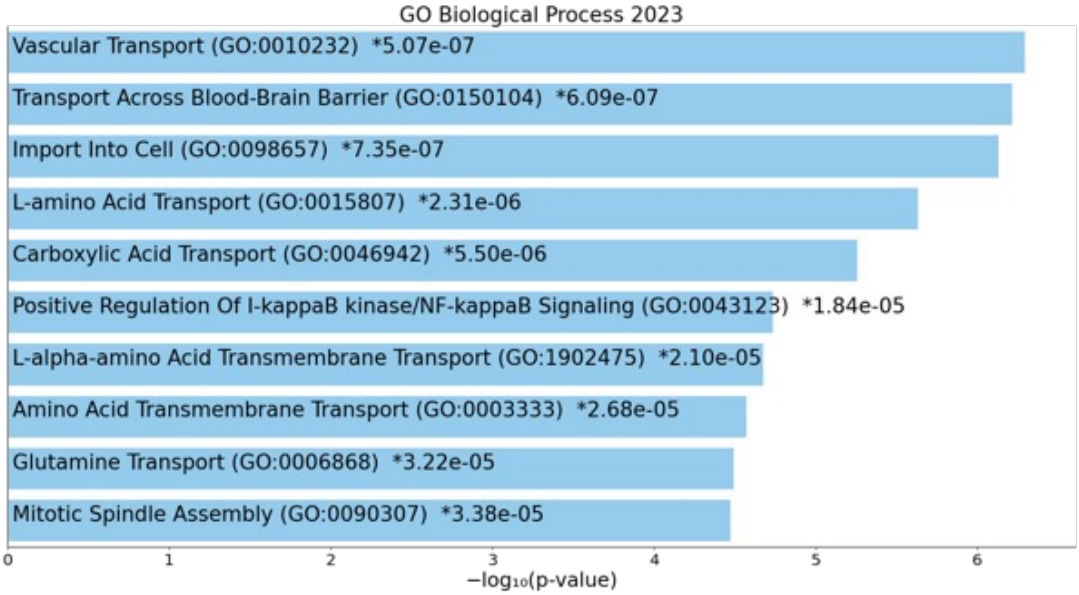


Figure 6.12. GO Biological Processes of HSP90i-treated Rb-null cells.
Gene Ontologies data analysis was performed examining upregulated protein of cluster 676 (without RB1) identified in SK-LMS-1 cells proteomic data analysis. Enriched-R software was used for generating the images and for data search based on MgSDHallmark_2020 database, data are ranked based on p-value.

6.5. Proteome Profiles of HSP90i-Treated vs. Untreated Rb lacking cells

To further explore the role of Rb loss in altering protein expression in response to HSP90 inhibitor treatment, we compared total proteome profiles of treated Rb-null cells with their untreated counterparts. As described before, we visualised significant differences in protein expression levels in a heatmap comparing treated Rb null cells to the untreated ones (fig.6.13a). Here, we identified cluster 573 showing the upregulation of 323 proteins upon HSP90i treatment, while cluster 574 indicated the upregulation of 143 proteins in untreated cells (fig.6.13b).

Enriched-R's pathways analysis showed a significant upregulation of proteins associated with apoptosis in HSP90i-treated cells (fig.6.13c). This data gave us confidence that apoptosis activation may be the main programmed cell death process triggered by Rb loss in combination with the pharmacological removal of HSP90. Additionally, G2-M checkpoints figured as the top hit enriched

pathways, followed by an increase in mitotic spindle and E2Fs targets activation consistent with the unique proteome profile of Rb-lacking cells shown in fig.6.7c, reflecting the impact of Rb loss in altering cell cycle progression. In contrast, DNA repair pathways figured as the top hit pathways in untreated Rb-null cells, followed only by E2Fs targets activation (cluster 574) (fig.6.13d). As shown in Chapter 3 fig.3.7, Rb depletion triggered the accumulation of E2F potentially inducing DNA replication stress and DNA damage (ssDNA, DSB) (Chapter 3, fig.3.8).

In conclusion, we hypothesized that the removal of HSP90 challenged Rb-lacking cells, disrupting cellular homeostasis, and activating apoptotic cell death, whether untreated Rb-null cells may be able to counteract the absence of Rb by promoting DNA repair pathways for cell survival.

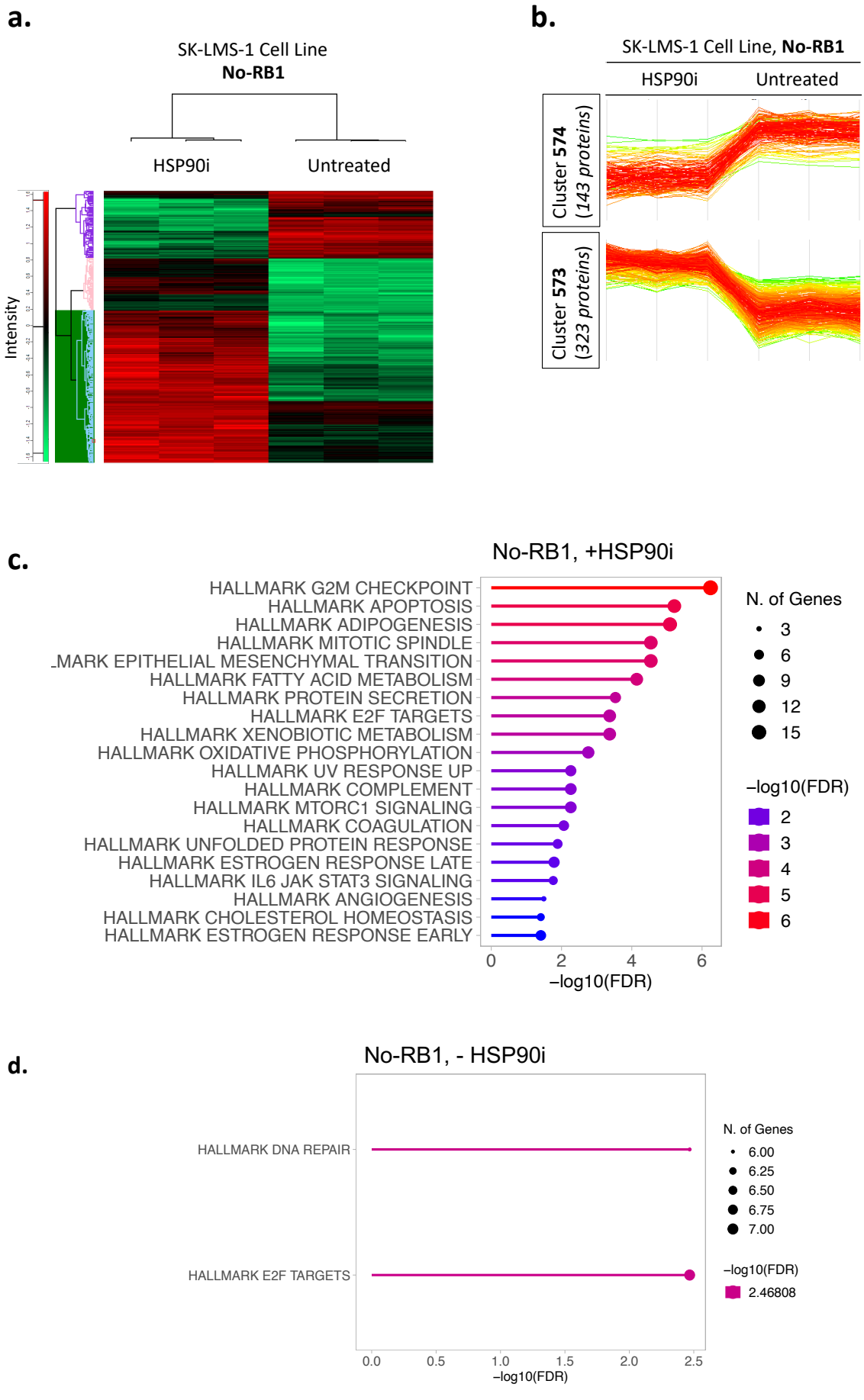

a.
SK-LMS-1 Cell Line
No-RB1
HSP90i
Untreated
Intensity
b.
SK-LMS-1 Cell Line, No-RB1
HSP90i
Untreated
Cluster 574 (143 proteins)
Cluster 573 (323 proteins)
c.
No-RB1, +HSP90i
HALLMARK G2M CHECKPOINT
HALLMARK APOPTOSIS
HALLMARK ADIPOGENESIS
HALLMARK MITOTIC SPINDLE
_MARK EPITHELIAL MESENCHYMAL TRANSITION
HALLMARK FATTY ACID METABOLISM
HALLMARK PROTEIN SECRETION
HALLMARK E2F TARGETS
HALLMARK XENOBIOTIC METABOLISM
HALLMARK OXIDATIVE PHOSPHORYLATION
HALLMARK UV RESPONSE UP
HALLMARK COMPLEMENT
HALLMARK MTORC1 SIGNALING
HALLMARK COAGULATION
HALLMARK UNFOLDED PROTEIN RESPONSE
HALLMARK ESTROGEN RESPONSE LATE
HALLMARK IL6 JAK STAT3 SIGNALING
HALLMARK ANGIOGENESIS
HALLMARK CHOLESTEROL HOMEOSTASIS
HALLMARK ESTROGEN RESPONSE EARLY
0
2
4
6
–log10(FDR)
N. of Genes
3
6
9
12
15
–log10(FDR)
2
3
4
5
6
d.
No-RB1, - HSP90i
HALLMARK DNA REPAIR
HALLMARK E2F TARGETS
0.0
0.5
1.0
1.5
2.0
2.5
–log10(FDR)
N. of Genes
6.00
6.25
6.50
6.75
7.00
–log10(FDR)
2.46808

Figure 6.13. Comparison of No-RB1 HSP90i-Treated and Untreated Proteome Profiles

a. The heatmap illustrates the proteomic profiles of SK-LMS-1 Rb lacking cells (No-RB1) post 10 nM 17-DMAG (HSP90i, 48hr) treatment compared to untreated conditions. The significant up-regulated proteins are indicated in red, the down-regulated are in green. Total proteome data were filtered by Anova q-value with Z-score presented as intensity. **b.** Cluster-grams categorise differentially expressed proteins into two clusters (573, 574), based on proteomic data of treated vs. untreated SK-LMS-1 Rb null cells. Figures generated using Perseus software version 1.6.2.2. Graphs illustrate significant pathways enrichment of **c.** treated Rb-null cells with HSP90i **d.** untreated SK-LMS-1 cells. Analysis was performed using Enriched-R based on MgSDHallmark_2020 database, data are ranked by p-value; figures generated using Shinygo software.

To confirm and validate our findings further, we conducted enrichment pathways analysis using Metascape (fig.6.14). As previous analysis has shown, apoptosis figured as one of the cellular pathways enriched the most in treated Rb null cells, together with the activation of G2-M checkpoints (fig.6.14a). Untreated cells enriched pathways involved in preventing replication stress and maintaining genome stability (fig.6.14b). (Rahul Bhowmick et al. 2023)

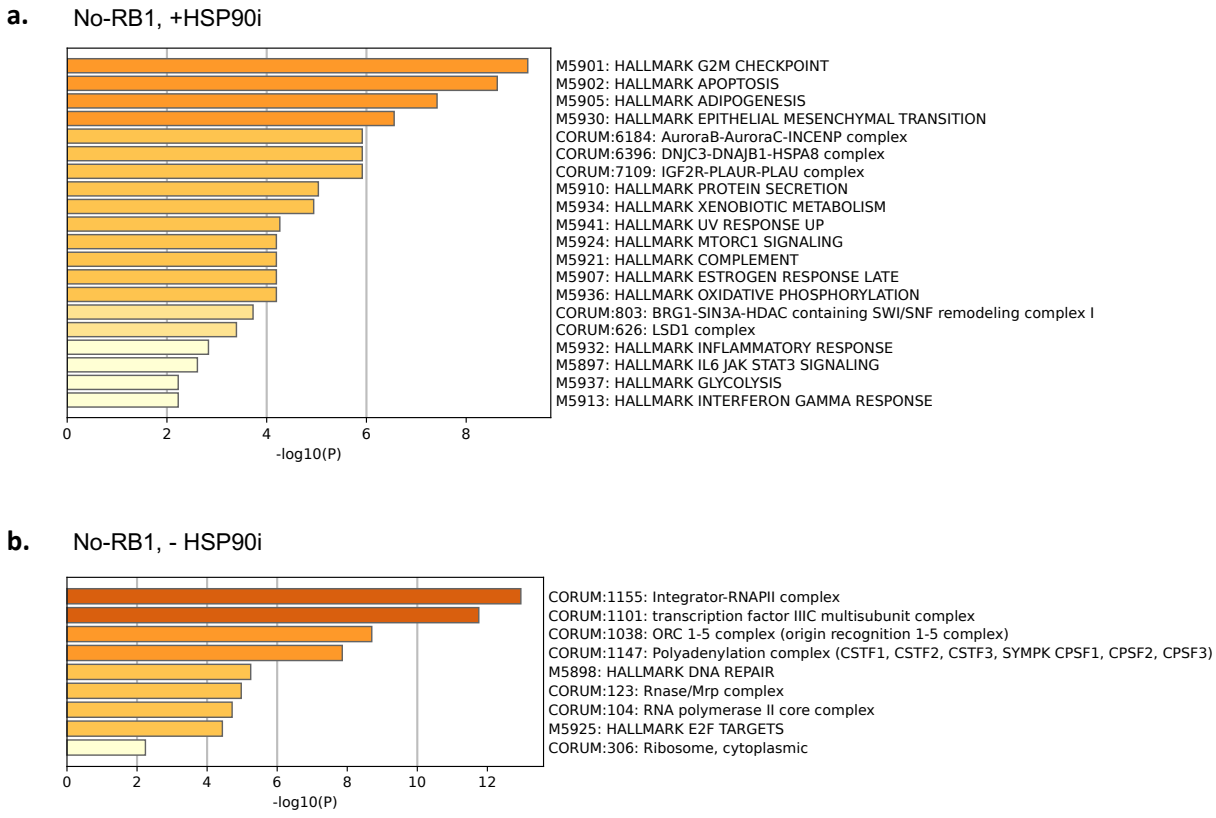


Figure 6.14. Metascape's enrichment data analysis

Top enriched pathways in cluster **a**. 574 **b**. 573. Analysis was performed using Metascape software, based on MgSDHallmark_2020 database, data are ranked by p-value, figures generated using Metascape software.

GO biological process analysis indicated Rb-null cells treated with the HSP90 inhibitor alvespimycin boosted cellular response pathways to contrast unfolded protein accumulation, this may include activation of the unfolded protein response (UPR) and upregulation of HSP70 chaperones (fig.6.15). Interestingly, several pathways governing mitosis control emerged. It is possible to speculate that cells lacking Rb encounter greater challenges in entering mitosis compared to their RB1+ counterparts, where the G1/S checkpoint can more effectively manage errors accumulated during the S phase. Additionally, it is conceivable that HSP90i disrupts mitotic control, leading to cell death RB1- cells.

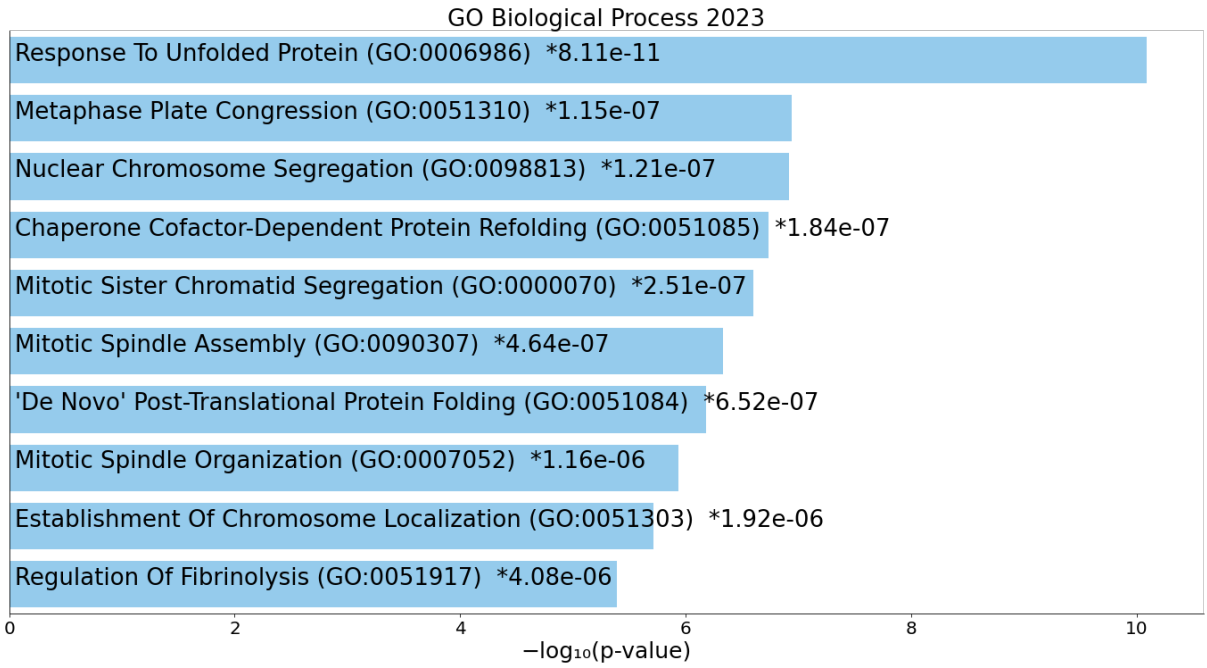


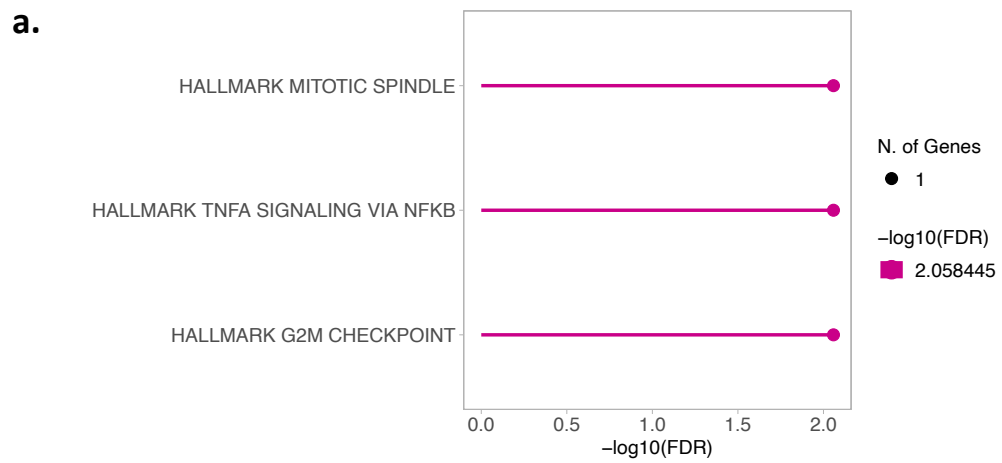
Figure 6.15. GO Biological Processes of HSP90i-treated Rb-null cells.

Gene Ontologies data analysis was performed examining upregulated protein of Rb-null cells treated with 17-DMAG, in SK-LMS-1 cells proteomic data analysis. Enriched-R software was used for generating the images and for data search based on MgSDHallmark_2020 database, data are ranked based on p-value.

6.6. Proteome Profiles of HSP90i-Treated vs Untreated Rb proficient cells

Total proteome profiles of treated Rb proficient cells were investigated by comparing changes in protein expression levels with their untreated equivalents (fig.6.16). Interestingly, the presence of functional Rb in treated cells resulted in the upregulation of MARCKS protein. MARCKS participates in multiple functions such as modulating cytoskeletal actin dynamics, vesicular trafficking, and signal transduction pathways. Moreover, it plays a key role in regulating cell migration, secretion, proliferation, and differentiation in many different tissues. (Van Itallie et al. 2018)

Enrichment pathways analysis developed by Enriched-R indicated that MARCKS was linked with a significant enhancement of mitotic spindle activation, followed by G2-M checkpoint and TNF-alpha signalling stimulation in response to drug treatment (fig.6.16a). Metascape's enrichment analysis did not provide a data graph as it required a set of proteins for its analysis. GO biological process were also explored by gene ontology investigations using Enriched-R (fig.6.16b). Here, actin filament organisation was the main enhanced cellular process in response to the drug treatment, confirming previous findings.



b.

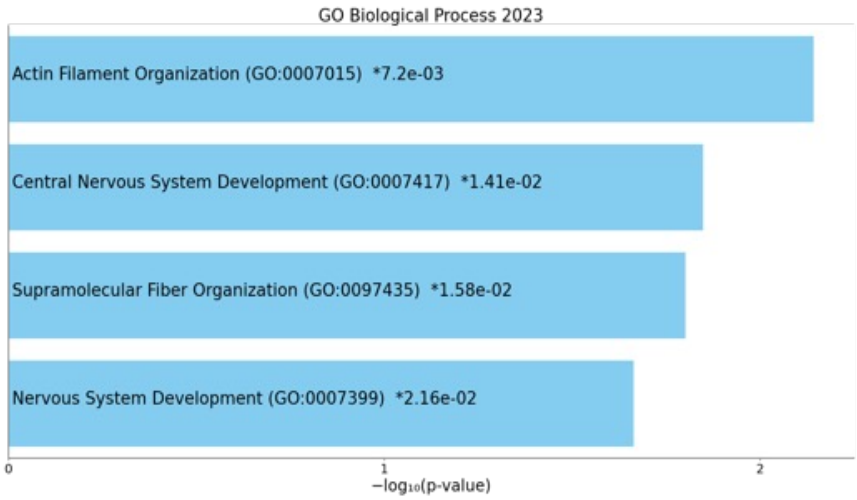


Figure 6.16 Enrichment pathways analysis and GO Biological process.

a. The figure illustrates the enrichment of three specific pathways in treated SK-LMS-1 cells with the HSP90 inhibitor (17-DMAG, 10nM, 48h). Graph was generated using Shinygo software. **b.** Bar chart provides insights in the GO biological processes activated by SK-LMS-1 cells expressing Rb under same conditions. Both analyses were performed using Enriched-R and based on MgSDHallmark_2020 database; data were ranked by p-value.

6.7. Investigation of the Total Proteome data

Reviewing the pool of proteins enriched in HSP90i-treated-Rb lacking-cells shown in Table 6.2, we identified FAS and JUN as proteins strongly interconnected with the apoptosis pathway. JUN, a negative regulator of apoptosis, was upregulated in our analysis. This finding indicated the presence of potent inducers of apoptosis that can overcome the effect of JUN activation. Notably, among the candidates identified to potentially fulfil such roles was FAS. FAS, a death domain–containing member of the tumour necrosis factor receptor (TNFR) family, plays a central role in regulating programmed cell death pathways in response to extrinsic stimuli. (Timmer, De Vries, and De Jong 2002) Interestingly, c-FLIP, the main negative regulator of death receptors-mediated apoptosis, is an HSP90 client protein. (Q. Wang et al. 2012; Park et al. 2008) Further studies should validate that the downregulation of c-FLIP due to the HSP90 inhibition may lead to an aberrant regulation of FAS, promoting apoptotic cell death in our LMS cell conditions. We hypothesised that Rb loss may

increase cell survival vulnerabilities to cellular stressor like HSP90 inhibition, and the subsequent degradation of c-FLIP potentially enhances susceptibility to apoptotic cell death. These findings might suggest the use of TNF/FAS agonists might induce similar drug response in LMS cell models lacking the tumour suppressor Rb. FasL agonists might hold promise for cancer therapy due to its potent apoptotic effects, however, its use is currently restricted by significant toxicity concerns.

Table 6.1. Up/Down-regulated pathways in SK-LMS-1 Rb lacking cells.

Table illustrates up/down regulated pathways based on their adjust-p-value indicating statistical significance and list of proteins identified as being associated with or contributing to the respective pathway.

Proteome profile of SK-LMS-1 Rb null cells upon HSP90i			
UP	**Down**	**Pathways**	**Enriched Protein datasets**
3.6510089		Apoptosis	JUN FAS IFNGR1 SLC20A1 HMOX1 TSPO APP PLAT IGF2R
3.5372156		Coagulation	TF MMP14 MMP1 SERPINC1 MAFF PLAT PLG A2M
3.3733793		G2-M Checkpoint	SQLE TPX2 SLC38A1 CENPF CCNT1 PRC1 NUSAP1 SLC7A1 AURKB
3.1653478		IL-6/JAK/STAT3 Signalling	JUN FAS IFNGR1 HMOX1 IL6ST A2M
2.7953614		Heme Metabolism	SDCBP SLC11A2 SLC2A1 HBD SLC7A11 ADIPOR1 LRP10 ABCG2
2.3048198		IL-2/STAT5 Signalling	P4HA1 IFNGR1 SERPINC1 MAFF SPRY4 IGF2R WLS
2.3048198		Hypoxia	JUN SCARB1 P4HA1 MAFF SLC2A1 HMOX1 KDELR3
	-4.778877	Epithelial Mesenchymal Transition	DAB2 ITGB5 ANPEP GPC1 FUCA1 ITGAV PCOLCE TGFBI CTHRC1
	-4.043699	Complement	LYN; ERAP2 SRC CASP1 CDH13 LAP3 CTSC CTSB
	-1.947256	Interferon Alpha Response	CASP1 UBE2L6 LAP3 CD47
	-1.947256	Apical Surface	LYN ATP8B1 DCBLD2
	-1.430023	UV Response	ABCC1 DAB2 PLCB4 ATRX
	-1.355125	Protein Secretion	NAPA PPT1 CTSC

6.8. Key findings

Mass spectrometry analysis provided a comprehensive exploration of the proteomic landscape in RB1+/- cells, highlighting the molecular effects associated with the absence of Rb. Enrichment pathways analysis based on the entire set of proteins aimed to gain more insights into the synthetic lethality interaction between Rb loss and HSP90 inhibition.

The analysis of untreated SK-LMS-1 cells (*RB1*+/-) revealed that Rb loss altered the expression of proteins involved in various biological processes, including cell cycle progression, abnormal activation of E2F targets, cell division, and mitotic spindle activation. Consistent results were obtained from analysis using Enriched-R and Metascape search tools, confirming the reliability of the Rb knock-out cell model in leiomyosarcoma.

Comparison of the whole proteome profiles of Rb proficient/deficient cells treated with HSP90 inhibitor showed that Rb null cells exhibited an increase in proteins mainly involved in apoptosis pathway activation. In contrast, Rb proficient cells appeared to be less responsive to the drug, indicating that functional Rb may guarantee cell survival despite HSP90 removal.

Moreover, the proteomic profiles of Rb null cells exhibited intriguing differences between treated and untreated conditions. Enriched pathways analysis validated that Rb-null cells induced apoptosis upon HSP90i treatment, whereas untreated Rb-null cells activated DNA repair pathways to promote cell survival. These findings underscored the potential pivotal role of Rb in promoting cell survival through DNA damage repair pathways activation in the contest of HSP90 inhibition.

The analysis of total proteome data also revealed the upregulation of FAS, a crucial apoptotic protein, in response to treatment with HSP90 inhibitors. One hypothesis suggested that alterations in negative apoptotic regulators, such as c-FLIP, might underlie this observation. Given that c-FLIP is a client protein of HSP90, its misfolding could lead to ubiquitination-mediated proteasomal degradation upon

HSP90i. Consequently, reduced levels of c-FLIP might facilitate abnormal FAS-mediated apoptosis following drug treatment.

In conclusion, quantitative mass spectrometry data acknowledged apoptosis as the mechanism of programmed cell death triggered in the presence of HSP90 inhibitor when Rb is lost. The sensitivity of Rb null cells to HSP90 inhibition may be attributed to the disruption of anti-apoptotic mediators such as c-FLIP, leading to apoptosis drug response mediated by upregulation of the FAS cascade.

CHAPTER 7

Discussion

7.1. Novel therapeutic approaches in leiomyosarcoma

Leiomyosarcoma, a heterogeneous soft tissue sarcoma originating from smooth muscle tissue and occurring in various anatomical locations, remains still a challenging disease to treat due to its poor patient prognosis, particularly in advanced stages and with limited therapeutic options available. Given the heterogeneity of LMS patients, standard chemotherapy regimens can fail to promote a consistent and durable response. Novel therapeutic strategies are urgently needed, especially those tailored to specific genetic alterations.

This research study explored potential novel therapeutic strategies in the context of the tumour suppressor Rb loss in LMS. One possible approach to target loss-of-function mutations or deletion of tumour suppressors is to identify synthetic lethal targets in such tumour cells.

7.1.1 Synthetic lethality effects with Rb tumour suppressor deficiency

The loss of the Retinoblastoma (Rb) gene is a distinctive feature observed in leiomyosarcoma tumour. (Chudasama et al. 2018) We hypothesised that potential synthetic lethality (SL) interactions could be worthy of investigation in LMS tumour lacking the tumour suppressor Rb.

We first generated and characterised different human isogenic cellular models of LMS carrying patient-relevant mutations, such as the loss of the tumour suppressor Rb. Isogenic cell models offer a versatile approach to explore the functional consequences of genetic mutations in a controlled setting. These models ensure genetic consistency among experimental conditions, enhancing the reproducibility and reliability of results. Additionally, they facilitate the identification of key molecular pathways involved in disease pathogenesis and support the development of targeted

therapies. Moreover, isogenic models aid in the identification of biomarkers for predicting drug response and advancing personalized medicine. (Sajjad et al. 2021)

Subsequently, we designed and screened a chemical drug library using a panel of the newly generated LMS cell lines proficient or deficient for Rb. High-throughput screens have been widely employed in drug discovery to identify chemical probes whose drug response might be applicable in clinical settings. (Coussens et al. 2017) This represented a powerful tool to identify novel synthetic lethal drug targets in our investigations of sarcomas.

Utilising a high-throughput screening approach, two independent studies have reported synthetic lethality interactions with Rb loss and with the inhibition of Aurora Kinases in lung cancer cell lines (SCLC). Pharmacogenomic screening revealed that the inhibition of Aurora kinase A induced striking cell death selectively in RB1-mutant SCLC cells. (Gong et al. 2019) A second study, a CRISPR/Cas9-based screening, demonstrated that the loss of Aurora kinase B was synthetic lethal with *RB1* gene loss in SCLC. (Oser et al. 2019) The mechanism of this lethal effect was attributed to the increased reliance of Rb deficient cells on the mitotic checkpoint. Targeting Aurora Kinases prevented the correct formation of the mitotic spindle and further exacerbated mitotic defects already present in RB1- cells. (J. Lyu et al. 2020; Borah and Reddy 2021; Oser et al. 2019b)

Furthermore, Liu et al. screened a kinome/phosphatase inhibitor library, including compounds cytotoxic to RB1, PTEN and Trp53-deficient TNBC cells, and selected a CDC25 inhibitor. (J. C. Liu et al. 2018) Since WEE1 and CDC25s cooperate to promote M phase progression (Lew and Kornbluth 1996), WEE1 inhibitors showed a similar synthetic lethal effect with Rb loss. (Lolli and Johnson 2005) It has been reported that the inactivation of the *RB1* gene induces S phase collapse in triple negative breast cancer (TNBC) cells when treated with inhibitors targeting CHK1. CHK1 is the main regulator of the G1/S phase checkpoint, whose activation is mediated by ATR pathway in response to replication stress. (Witkiewicz et al. 2018) Remarkably, the synthetic lethal effect induced

by CHK1i and CDC25Ai, analogous to the inhibition of Aurora Kinases, resulted in significant disruptions in mitosis, leading to selective cell death in Rb-negative cells.

The drug screen conducted in this study identified two classes of drugs showing promising potential: CHK1 inhibitors and HSP90 inhibitors. We could speculate that the sensitivity of LMS cell lines to CHK1 inhibitors may be attributed to mitotic aberrancies, similar to Aurora kinases or CDC25A inhibition. However, validation experiments revealed that CHK1 inhibitors showed a mild effect in targeting Rb-null cells in our LMS cell lines. Subsequently, our research study was focused on a striking synthetic lethality effect with the inhibition of the heat shock protein HSP90 in conjunction with Rb loss.

In this context, we had to consider that one of the HSP90 client proteins is the tumour suppressor p53. The inhibition of HSP90 would have led to significant disruption of the cell signalling pathways regulated by p53. (Müller et al. 2004) However, our panel of LMS cell lines harboured a mutant form of p53, resulting in a loss-of-function mutation. Therefore, we concluded that the synthetic lethality effect discovered was solely due to HSP90 inhibition, rather than a secondary effect related to p53.

7.1.2. The inhibition of HSP90 is synthetic lethal with Rb loss

Our primary objective was to validate the findings from the drug screening by assessing the effectiveness of HSP90 inhibitors in LMS cell lines. We selected two HSP90 inhibitors, alvespimycin and luminespib (17-DMAG and NVP-AUY922, respectively), which differ in molecular structure. *In vitro* experiments demonstrated that both 17-DMAG and NVP-AUY922 exerted potent inhibitory effects on the growth and proliferation of Rb null cells in a time- and dose-dependent manner. It is noteworthy that the concentration of HSP90i required to achieve the synthetic lethal effect was minimal in Rb lacking cells and may hold promise for translation into clinical practice. The IC50 of alvespymicin in Rb null cells was 1 nM, exhibiting a 20-fold difference in sensitivity compared to Rb proficient cells. In contrast, the other HSP90 inhibitor luminespib (NVP-AUY922), which is known to

be more potent, displayed a much smaller difference in sensitivity between RB1+/- cells. (Jensen et al. 2008) These data suggested that alvespimycin may induce off-target effects. Nevertheless, both drugs showed selectivity in targeting RB-null cells compared to Rb-proficient cells. Therefore, treatment optimisation might involve utilising minimal doses of HSP90 inhibitors, potentially reducing the severe toxic effects observed in clinical settings, and especially in the treatment of LMS tumours.

While numerous HSP inhibitors have been explored for cancer therapy, their effectiveness has been delayed by side effects, including hepatotoxicity and retinal dysfunction, which render them intolerable for cancer patients. Low drug concentrations may offer successful cancer treatment while mitigating side effects. (Chatterjee and Burns 2017) Studies in combining low doses of 17-DMAG with bortezomib has showed favourable outcomes in treating rhabdomyosarcoma, improving side effect profiles. Additionally, combining low doses of docetaxel with IPI-504 has demonstrated to enhance antitumoral properties in multiple non-small cell lung cancer xenograft models. (Peron, Bonvini, and Rosolen 2012; Acquaviva et al. 2012) Further investigations are needed to optimize combination therapies with appropriate dosages of HSP inhibitors.

Overall, our findings were reproducible in both SK-LMS-1 and SKUT-1 cell lines, indicating consistency across two different cell systems. The RKN cell line was excluded from validation experiments due to its complex karyotypes carrying an oncogenic KRAS mutation (G12V), which could have interfered with Rb loss. (Zhu et al. 2022b; Hijioka et al. 2017b)

To elucidate the molecular mechanisms underlying this synthetic lethality effect, we investigated cellular signalling pathways. Initially, we verified that the removal of HSP90 was not compensated by other heat shock proteins (HSPs) by examining the expression levels of HSP70, a heat shock protein that cooperates with HSP90 in protein folding, stabilization, activation, and proteolytic degradation processes. (Yun et al. 2020) Western blot analysis revealed a notable increase in HSP70 expression at

concentrations well above those inducing cell death, suggesting that the synthetic lethality effect with Rb loss was specifically triggered by HSP90 inhibitors at minimal concentrations.

Furthermore, we evaluated the impact of HSP90 inhibition on the cell cycle. We observed a reduction in the expression of CDK4, a client protein of HSP90, when Rb loss was combined with HSP90 inhibition. This decrease in CDK4 expression may be attributed to increased proteasomal degradation in response to HSP90 removal, which has been reported before. (Prodromou and Bjorklund 2022)
Subsequent signalling pathways analysis revealed that apoptosis was the main mechanism of cell death activated upon HSP90 inhibitor treatment in Rb null cells, prevailing over the activation of autophagy and DNA repair mechanisms. HSP90 plays a key role in coordinating the programmed cell death (PCD) network (Peng et al. 2022), as its client proteins regulate various PCD pathways, including necroptosis (RIP1, RIP3 and MLKL), apoptosis (Bcl-2 and cellular-FLICE inhibitory protein (FLIP)), autophagy (ULK1 and ATG7) and ferroptosis (GPX4 and ACLS4). (Peng et al. 2022) These findings deepen our understanding of the intricate mechanisms orchestrated by HSP90 and underscore its crucial role in shaping apoptotic cell fate in response to its inhibition in the context of Rb loss. Synthetic lethality with HSP90 inhibitors is complex to analyse given the pleiotropic effects of HSP90 inhibition. Therefore, individual observations regarding HSP90 inhibition should be independently validated in future studies.

7.1.3. Apoptotic cell death mechanisms induced by HSP90 inhibition

The comparative proteomic analysis, along with enrichment pathways analysis of the Rb null cells treated or untreated with the HSP90 inhibitor alvespimycin, revealed important insights on the biological implications of the synthetic lethality interaction between Rb loss and HSP90 inhibition. The simultaneous inactivation of Rb and HSP90 induced the upregulation of apoptotic pathways and G2/M checkpoints, while Rb lacking cells (HSP90 proficient) upregulated DNA damage repair pathways to preserve cell survival. Several studies have reported that alvespimycin triggers growth

inhibition *via* apoptosis across numerous cancer cells such as colon cancer cells, in medulloblastoma or cervical carcinoma cells. (Schwock et al. 2008; Ayrault et al. 2009; Ma et al. 2015)

In contrast, Rb proficient cells appeared less responsive to the drug, upregulating pathways such as the epithelial mesenchymal transition (EMT) and the activation of the complement pathways. One of the emerging roles of E2Fs in tumour progression includes epithelial-to-mesenchymal transition (EMT) signalling, invasion, and metastasis. (Chen, Tsai, and Leone 2009) The Rb/E2F axis can promote the EMT process, resulting in cytoskeleton restructuring and morphological changes. (Jusino et al. 2021; Jusino and Saavedra 2019) Additionally, complement activation may promote tumour progression *via* antiapoptotic mediators. (Ain et al. 2021; Dos Santos et al. 2017)

In our LMS cell model for Rb loss, the inhibition of HSP90 might disrupt mitotic control, as evidenced by gene enrichment analyses, thus leading to increased cell death and apoptosis in Rb-null cells treated with HSP90i. Examination of upregulated proteins in Rb lacking cells treated with the HSP90 inhibitor revealed Fas as one of the top proteins. Fas belongs to the subgroup of tumour necrosis factor receptor family that contains an intracellular cell death domain and mediates the activation of extrinsic apoptosis pathways. (Timmer, De Vries, and De Jong 2002) The interaction between Fas with Fas-ligands (Fas-L) leads to the formation of a death-inducing signalling complex (DISC) which recruits the Fas-associated death domain protein (FADD), caspase 8 and caspase 10 to trigger a downstream caspase cascade mediating apoptosis (fig.7.1a). (Jan and Chaudhry 2019) Its upregulation may be attributed to degradation of c-FLIP, a negative mediator of caspases 8/10 in DISC and an HSP90 client protein (fig.7.1b). (Min Woo et al. 2019) It has been reported that the inhibition of HSP90 leads to c-FLIP degradation by the ubiquitin-proteasome system, which would explain Fas upregulation in our experimental settings (fig.7.1c). (Q. Wang et al. 2012; Park et al. 2008) Further studies should validate that c-FLIP and HSP90 may represent promising targets to cause synthetic lethality in Rb-null cells. Fas upregulation may be a context-dependent effect in LMS, which would be worth investigating further.

These findings provided important insights into the complex interplay of Rb loss and HSP90 inhibition in LMS cells, indicating apoptosis as a potential mechanism of cell death induced by HSP90 inhibitors.

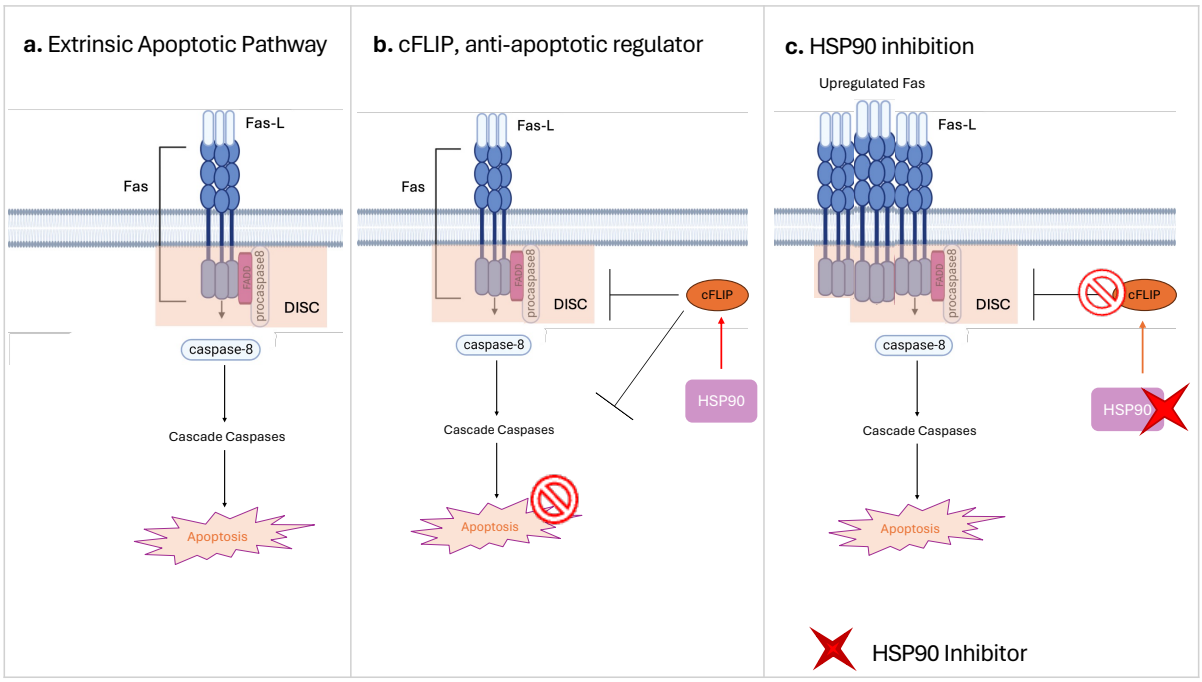


Figure 7.1. FAS-apoptotic extrinsic pathway, c-FLIP antiapoptotic activity and HSP90 inhibition.

a. Schematic representation of the extrinsic apoptotic pathway triggered by Fas-Fas-ligand interactions, leading to DISC formation and caspase 8 activation to promote apoptotic cell death. **b.** The second section illustrates that HSP90 promotes the correct folding of c-Flip which can act as a negative regulator of the FAS pathway impeding apoptosis. **c.** The third section, described that the HSP90 inhibition impacts on c-FLIP activity, promoting apoptosis. Modified by Yanrui Zhang et al, 2022.

7.2. The potential of HSP90 inhibition in cancer therapy

7.2.1. HSP90 inhibitors are promising in preclinical and clinical settings

HSP90 inhibition represents a promising anticancer strategy, offering a multitarget pharmacological approach. (Workman et al. 2007b; H. Liu et al. 2021; Scaltriti, Dawood, and Cortes 2012; Ernst et al. 2015) Significant progress has been made in developing small molecule inhibitors targeting HSP90, leading to preclinical and clinical studies. Currently, there are 17 distinct HSP90 inhibitors undergoing clinical trials. (Z. N. Li and Luo 2023; Brian S. J. Blagg 2020)

Geldanamycin, the first compound of this class of drugs discovered, competitively binds to the ATP/adenosine diphosphate (ADP)–binding site on HSP90 and impedes its intrinsic ATPase activity; however, it was too toxic for clinical use. 17-AAG, an analogue of geldanamycin with advanced binding affinity to the ATP binding site of HSP90, showed encouraging preclinical features due to its improved toxicity. It stimulates apoptosis and cell cycle arrest *in vitro* and in xenograft models. 17-AAG was the first HSP90i to undergo clinical trials. (Banerji et al. 2005) However, despite showing effective antitumour effects in early clinical trials, 17-AAG presented poor bioavailability. Among many derivatives synthetised starting from geldanamycin, Kosan Biosciences designed and developed 17-DMAG, which emerged for its improved physiochemical qualities. 17-DMAG interacts with the HSP90 ATP-binding motif, obstructing ATP binding and, leading to misfolding, ubiquitylation and the eventual degradation of the HSP90 client proteins by the proteasome.

Numerous preclinical studies investigated 17-DMAG efficacy in multiple malignancies. For instance, in murine models of acute myeloid leukaemia (AML), it diminishes HIF-1 and VEGF levels, blocking tumour progression. (Trepel et al. 2010) In human multiple myeloma (MM) cells, it induces apoptosis and autophagy by inhibiting the mTOR pathway and microtubule-associated proteins. (Palacios et al. 2010) Additionally, in hepatocellular carcinoma (HCC) cells, 17-DMAG inhibition affects cell cycle. (Jianming Zhang et al. 2016) In colon cancer cells, 17-DMAG leads to changes in several client proteins. (Ma et al. 2015) Given its promising potential, 17-DMAG entered in six Phase I clinical

trials. In the phase I trial of advanced solid tumours, 17-DMAG was administered intravenously at doses between 2.5–106 mg/m2 weekly. Here, one patient with refractory prostate (CRPC) cancer completely responded. Also, one patient with metastatic melanoma responded partially and three patients with chondrosarcoma and renal cancer exhibited stable disease. These findings were promising, however, 17-DMAG did not proceed into Phase II due to its side effects. (Pacey et al. 2011) In another phase I trial on acute myeloid leukaemia (AML) and chronic lymphocytic leukaemia (CLL), 17-DMAG was administered at a dosage of 24 mg/m2 twice a week, inducing an antileukemic activity in 4 of 17 patients assessed. (Maddocks et al. 2016; Lancet et al. 2010)

Second generation synthetic HSP90 inhibitors were developed based on the resorcinol structural scaffold. Vernalis and Novartis synthetised NVP-AUY922 (luminespib) characterised by a better compound solubility, high potency against HSP90 (K_d = 2nM), and high selectivity. Preclinical studies have shown NVP-AUY922 promoted growth inhibition in a broad panel of cancer cells (using nanomolar concentration) and xenograft models covering major cancer types and diverse oncogenic profiles. (Eccles et al. 2008a) It was also proved to reduce tumour growth, angiogenesis, and metastasis in a xenograft breast cancer mouse model. (Eccles et al. 2008b; Jensen et al. 2008)

NVP-AUY922 is currently in phase I/II single-agent and combination clinical trials in various malignancies, including NSCLC, ERBB2-positive advanced breast cancer, gastric cancer, and refractory GIST. One phase I dose-escalation study showed that NVP-AUY922 administered one-a-week resulted in steady disease in 10 of 171 patients with advanced solid tumours. (Sessa et al. 2013)
A phase II clinical study showed that NVP-AUY922 in combination with trastuzumab was safe and stabilising the disease in patients with ERBB2-positive metastatic breast cancer who were on trastuzumab-based therapy (rate at 74% of the cases).(Sharp, Jones, and Workman 2013) Another significant phase II study examined the efficacy of NVP-AUY922 in patients with previously treated advanced NSCLC with a recommended Phase II dose of 70 mg/m^2. (Sharp, Jones, and Workman

2013)NVP-AUY922 entered 25 clinical trials, both Phase I and II, with two trials currently on-going and one recruiting since February 2019. (Sharp, Jones, and Workman 2013)

One other major downside of using HSP90-targeted therapeutics is their impact on normal cellular physiology. High dosages of these inhibitors can lead to toxicity due to off-target effects or amplified on-target effects. Thus, HSP90 inhibitors have been explored in combination therapies to target cancer cell while minimizing dosages. (LoRusso et al. 2012; Barrott and Haystead 2013) The greatest clinical outcome has been evidenced with tanespimycin (a geldanamycin analogue) in combination with trastuzumab in HER2+ breast cancer patients. (Chandrakala et al. 2010) Likewise, NVP-AUY922 inhibits cell growth in HER2-positive and trastuzumab-resistant breast cancer cells. (Canonici et al. 2018) These results underscore the importance of using HSP90 inhibitors as targeted therapies and highlight the need for selecting a patient population to maximize the benefits of therapy and optimize dosing schedules of this class of compounds.

In our study, we highlighted the impact of using low doses of HSP90 inhibitors on Rb-deficient tumour cells. Notably, these inhibitors selectively triggered apoptosis in Rb-deficient cells while sparing the viability of the Rb-proficient cells. This synthetic lethality strategy offers potential for enhanced clinical outcomes by minimizing toxicity through low-dose administration and targeting patient populations most likely to benefit from the antitumorigenic effects of HSP90 inhibitors.

7.3.2. Potential use of HSP90 inhibitors in sarcoma

Addressing the urgent need to improve therapies in soft tissue sarcomas (STSs), several studies aimed to develop innovative therapeutic strategies, including targeting HSP90. Preclinical studies investigating HSP90 inhibition in soft tissue sarcoma have shown promising results. For instance, the HSP90 inhibitor 17-AAG decreases cell proliferation in spheroid culture models of synovial sarcoma. (Terry et al. 2005) Alvespimycin (17-DMAG) successfully decreased undifferentiated liposarcomas cell growth and invasiveness by disrupting the AKT/mTOR pathway *in vitro*. (Bekki et al. 2015)

Luminespib (NVP-AUY922) exhibited remarkable cytotoxic outcomes in cancer cell by disrupting Raf/MEK/ERK and PI3K signalling pathways, in different cell lines of myxoid (MLS402, MLS1765) and undifferentiated liposarcomas overexpressing HSP90 (SW872). (Steinmann et al. 2015)

HSP90 inhibition has also been investigated in clinical phase I trials as monotherapy in soft tissue sarcomas, including leiomyosarcoma. This phase 1 study determined the maximum tolerated doses (MTD) of the HSP90 inhibitor retaspimycin hydrochloride (IPI-504) in patients with gastrointestinal stromal tumours (GIST) and soft tissue sarcoma (STS). (Wagner et al. 2013) The HSP90 inhibitor was administered intravenously at doses ranging from 90-500 mg/m^2 twice a week for 2 week on/1 week off. Stable disease was observed in 70% of the cases (26/37) of patient with GIST and 59% (10/17) of patients with STS. (Wagner et al. 2013)

Overall, targeting HSP90 holds promise as potential alternative therapeutic approach to inhibit tumour growth, induce apoptosis, and overcome drug resistance in tumour malignancies, including soft tissue sarcomas. Our study demonstrated the efficacy of HSP90 inhibitors in leiomyosarcoma cell lines (*in vitro*) and additionally defined the patient population to target (*RB1* gene inactivation). Remarkably, the selection of patients with Rb deficiency may be crucial to optimise current treatment efficacy. Further research and clinical trials are needed to fully elucidate the therapeutic utility of HSP90 inhibitors in leiomyosarcoma treatment, especially in the context of Rb deficiency.

7.4. Summary and Conclusions

The research work presented in this thesis emphasized the synthetic lethality interaction mediated by the loss of the tumour suppressor retinoblastoma in combination with a specific class of inhibitors targeting Heat Shock Proteins (HSPs) in leiomyosarcoma. The drug screen and mass spectrometry data provided robust evidence of the reliability of our findings. Further investigations are warranted to fully elucidate the molecular mechanisms governing the HSP-mediated synthetic lethal interaction in Rb loss.

To elucidate the synthetic lethality between Rb loss and HSP90, we proposed a cell model as described in figure 7.2. Loss or mutation of Rb disrupts the precise regulation of the cell cycle, resulting in aberrant G1/S phase checkpoint and increased reliance on mitosis control (G2/M checkpoint). HSP90 plays a crucial role in the correct folding of several proteins involved in various cellular signalling pathways, including the mitotic checkpoint. Moreover, it regulates c-FLIP, a key protein that impedes apoptosis. We proposed that the combined effect of Rb loss and HSP90 inhibition promotes a synthetic lethality effect by further disrupting the mitotic checkpoint and enhancing activation of apoptosis pathways through upregulation of FAS (mediated by the reduction of c-FLIP levels). Consequently, while cell survival may be maintained through DDR pathways in RB1+ cells, RB1- cells rely solely on the mitotic checkpoint (Fig.7.2).

This synergistic interaction between Rb loss and HSP90 inhibition highlighted the intricate network of signalling pathways involved in tumour progression and underscored the therapeutic potential of targeting these pathways in cancer treatment, especially in leiomyosarcoma tumours lacking Rb.

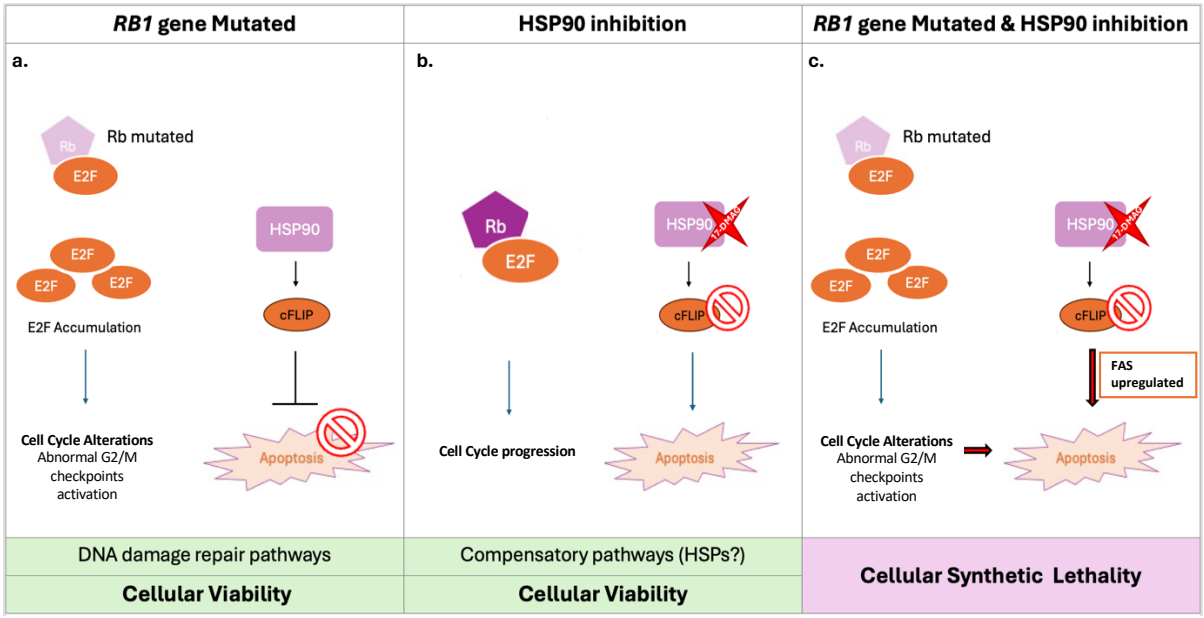


Figure 7. 2. Synthetic lethality hypothesis.

Schematic representation of the synthetic lethal effect between Rb and HSP90 inhibition. **a.** The loss or the mutation of Rb leads to E2F accumulation disrupting the cell cycle and promoting DNA damage occurrences. Cellular viability may be safeguard by DDR pathways activation, while c-FLIP impedes apoptosis. **b.** Inhibition of HSP90 can upregulate the Fas pathway by reducing c-FLIP expression. However, cellular viability may be preserved by compensatory pathways. **c.** The combination of Rb loss and HSP90 inhibition exacerbates disruptions in cellular pathways, leading to cell death. Modified by Yanrui Zhang et al, 2022

REFERENCES

Abeshouse, Adam, Clement Adebamowo, Sally N. Adebamowo, Rehan Akbani, Teniola Akeredolu, Adrian Ally, Matthew L. Anderson, et al. 2017. "Comprehensive and Integrated Genomic Characterization of Adult Soft Tissue Sarcomas." *Cell* 171 (4): 950-965.e28. https://doi.org/10.1016/j.cell.2017.10.014.

Acquaviva, Jaime, Donald L. Smith, Jim Sang, Julie C. Friedland, Suqin He, Manuel Sequeira, Chaohua Zhang, Yumiko Wada, and David A. Proia. 2012. "Targeting KRAS-Mutant Non-Small Cell Lung Cancer with the Hsp90 Inhibitor Ganetespib." *Molecular Cancer Therapeutics* 11 (12): 2633–43. https://doi.org/10.1158/1535-7163.MCT-12-0615.

Ain, Danyaal, Talha Shaikh, Samantha Manimala, and Berhane Ghebrehiwet. 2021. "The Role of Complement in the Tumor Microenvironment." *Faculty Reviews* 10 (November). https://doi.org/10.12703/r/10-80.

Alexandrova, E. M., A. R. Yallowitz, D. Li, S. Xu, R. Schulz, D. A. Proia, G. Lozano, M. Dobbelstein, and U. M. Moll. 2015. "Improving Survival by Exploiting Tumour Dependence on Stabilized Mutant P53 for Treatment." *Nature* 523 (7560): 352–56. https://doi.org/10.1038/nature14430.

Anderson, Nathaniel D., Yael Babichev, Fabio Fuligni, Federico Comitani, Mehdi Layeghifard, Rosemarie E. Venier, Stefan C. Dentro, et al. 2021. "Lineage-Defined Leiomyosarcoma Subtypes Emerge Years before Diagnosis and Determine Patient Survival." *Nature Communications* 12 (1). https://doi.org/10.1038/s41467-021-24677-6.

Antonescu, C. R. 2006. "The Role of Genetic Testing in Soft Tissue Sarcoma." *Histopathology* 48 (1): 13–21. https://doi.org/10.1111/j.1365-2559.2005.02285.x.

Athanasiadis, Paschalis, Balaguru Ravikumar, Neil O Carragher, Paul A Clemons, Timothy Johanssen, Daniel Ebner, and Tero Aittokallio. 2023. "Optimized Chemogenomic Library

Design Strategies for Precision Oncology." *IScience*. https://doi.org/10.1101/2020.11.30.403329.

Ayrault, Olivier, Michael D Godeny, Christopher Dillon, Frederique Zindy, Patrick Fitzgerald, Martine F Roussel, and Helen M Beere. 2009. "Inhibition of Hsp90 via 17-DMAG Induces Apoptosis in a P53-Dependent Manner to Prevent Medulloblastoma." www.pnas.org/cgi/content/full/.

Banerji, Udai, Anne O'Donnell, Michelle Scurr, Simon Pacey, Sarah Stapleton, Yasmin Asad, Laura Simmons, et al. 2005. "Phase I Pharmacokinetic and Pharmacodynamic Study of 17-Allylamino, 17-Demethoxygeldanamycin in Patients with Advanced Malignancies." *Journal of Clinical Oncology* 23 (18): 4152–61. https://doi.org/10.1200/JCO.2005.00.612.

Barrott, Jared J., and Timothy A.J. Haystead. 2013. "Hsp90, an Unlikely Ally in the War on Cancer." *FEBS Journal*. https://doi.org/10.1111/febs.12147.

Bartek, Jiri, Claudia Lukas, and Jiri Lukas. 2004. "Checking on DNA Damage in S Phase." *Nature Reviews Molecular Cell Biology* 5 (10): 792–804. https://doi.org/10.1038/nrm1493.

Bartek, Jiri, and Jiri Lukas. 2003. "Chk1 and Chk2 Kinases in Checkpoint Control and Cancer." *Cancer Cell* 3 (5): 421–29. https://doi.org/10.1016/S1535-6108(03)00110-7.

Bathan, Andrew J., Anastasia Constantinidou, Seth M. Pollack, and Robin L. Jones. 2013. "Diagnosis, Prognosis, and Management of Leiomyosarcoma: Recognition of Anatomic Variants." *Current Opinion in Oncology*. https://doi.org/10.1097/CCO.0b013e3283622c77.

Bekki, Hirofumi, Kenichi Kohashi, Akira Maekawa, Yuichi Yamada, Hidetaka Yamamoto, Katsumi Harimaya, Michiyuki Hakozaki, Kazuki Nabeshima, Yukihide Iwamoto, and Yoshinao Oda. 2015. "Elevated Expression of HSP90 and the Antitumor Effect of an HSP90 Inhibitor via Inactivation of the Akt/MTOR Pathway in Undifferentiated Pleomorphic Sarcoma." *BMC Cancer* 15 (1). https://doi.org/10.1186/s12885-015-1830-8.

Benassi, M. Serena, Lara Molendini, Gabriella Gamberi, M. Rosa Sollazzo, Paola Ragazzini, Mara Merli, Giovanna Magagnoli, et al. 1997. "Altered G1 Phase Regulation in Osteosarcoma."

International Journal of Cancer 74 (5): 518–22. https://doi.org/10.1002/(SICI)1097-0215(19971021)74:5<518::AID-IJC7>3.0.CO;2-6.

Bertoli, Cosetta, Jan M. Skotheim, and Robertus A.M. De Bruin. 2013. "Control of Cell Cycle Transcription during G1 and S Phases." *Nature Reviews Molecular Cell Biology* 14 (8): 518–28. https://doi.org/10.1038/nrm3629.

Bester, Assaf C., Maayan Roniger, Yifat S. Oren, Michael M. Im, Dan Sarni, Malka Chaoat, Aaron Bensimon, Gideon Zamir, Donna S. Shewach, and Batsheva Kerem. 2011. "Nucleotide Deficiency Promotes Genomic Instability in Early Stages of Cancer Development." *Cell* 145 (3): 435–46. https://doi.org/10.1016/j.cell.2011.03.044.

Biebl, Maximilian M., and Johannes Buchner. 2019. "Structure, Function, and Regulation of the Hsp90 Machinery." *Cold Spring Harbor Perspectives in Biology* 11 (9). https://doi.org/10.1101/cshperspect.a034017.

Birdi, Harsimrat Kaur, Anna Jirovec, Serena Cortés-Kaplan, Joel Werier, Carolyn Nessim, Jean Simon Diallo, and Michele Ardolino. 2021. "Immunotherapy for Sarcomas: New Frontiers and Unveiled Opportunities." *Journal for ImmunoTherapy of Cancer*. BMJ Publishing Group. https://doi.org/10.1136/jitc-2020-001580.

Borah, Naheed Arfin, and Mamatha M. Reddy. 2021. "Aurora Kinase B Inhibition: A Potential Therapeutic Strategy for Cancer." *Molecules*. MDPI AG. https://doi.org/10.3390/molecules26071981.

Brandvold, Kristoffer R., and Richard I. Morimoto. 2015. "The Chemical Biology of Molecular Chaperones - Implications for Modulation of Proteostasis." *Journal of Molecular Biology*. Academic Press. https://doi.org/10.1016/j.jmb.2015.05.010.

Brian S. J. Blagg, John Koren III. 2020. "The Right Tool for the Job: An Overview of Hsp90 Inhibitors." *Advances in Experimental Medicine and Biology*.

Bryant, Helen E, Niklas Schultz, Huw D Thomas, Kayan M Parker, Dan Flower, Elena Lopez, Suzanne Kyle, Mark Meuth, Nicola J Curtin, and Thomas Helleday. 2005. "Specific Killing of

BRCA2-Deficient Tumours with Inhibitors of Poly(ADP-Ribose) Polymerase." www.nature.com/nature.

Burdova, Kamila, Hongbin Yang, Roberta Faedda, Samuel Hume, Jagat Chauhan, Daniel Ebner, Benedikt M Kessler, et al. 2019. " E2F1 Proteolysis via SCF -cyclin F Underlies Synthetic Lethality between Cyclin F Loss and Chk1 Inhibition ." *The EMBO Journal* 38 (20). https://doi.org/10.15252/embj.2018101443.

Canonici, Alexandra, Zulfiqar Qadir, Neil T. Conlon, Denis M. Collins, Neil A. O'Brien, Naomi Walsh, Alex J. Eustace, Norma O'Donovan, and John Crown. 2018. "The HSP90 Inhibitor NVP-AUY922 Inhibits Growth of HER2 Positive and Trastuzumab-Resistant Breast Cancer Cells." *Investigational New Drugs* 36 (4): 581–89. https://doi.org/10.1007/s10637-017-0556-7.

Cardozo, Timothy, and Michele Pagano. 2004. "The SCF Ubiquitin Ligase: Insights into a Molecular Machine." *Nature Reviews Molecular Cell Biology* 5 (9): 739–51. https://doi.org/10.1038/nrm1471.

Casali, P. G., N. Abecassis, S. Bauer, R. Biagini, S. Bielack, S. Bonvalot, I. Boukovinas, et al. 2018. "Soft Tissue and Visceral Sarcomas: ESMO-EURACAN Clinical Practice Guidelines for Diagnosis, Treatment and Follow-Up." *Annals of Oncology* 29 (October):iv51–67. https://doi.org/10.1093/annonc/mdy096.

Cesne, A. Le, M. Ouali, M. G. Leahy, A. Santoro, H. J. Hoekstra, P. Hohenberger, F. Van Coevorden, et al. 2014. "Doxorubicin-Based Adjuvant Chemotherapy in Soft Tissue Sarcoma: Pooled Analysis of Two STBSG-EORTC Phase III Clinical Trials." *Annals of Oncology* 25 (12): 2425–32. https://doi.org/10.1093/annonc/mdu460.

Chaikovsky, Andrea C., Chuan Li, Edwin E. Jeng, Samuel Loebell, Myung Chang Lee, Christopher W. Murray, Ran Cheng, et al. 2021. "The AMBRA1 E3 Ligase Adaptor Regulates the Stability of Cyclin D." *Nature* 592 (7856): 794–98. https://doi.org/10.1038/s41586-021-03474-7.

Chakraborty, Goutam, Joshua Armenia, Ying Z. Mazzu, Subhiksha Nandakumar, Konrad H. Stopsack, Mohammad O. Atiq, Kazumasa Komura, et al. 2020. "Significance of BRCA2 and

RB1 Co-Loss in Aggressive Prostate Cancer Progression." *Clinical Cancer Research* 26 (8): 2047–64. https://doi.org/10.1158/1078-0432.CCR-19-1570.

Chandarlapaty, S., M. Scaltriti, P. Angelini, Q. Ye, M. Guzman, C. A. Hudis, L. Norton, et al. 2010. "Inhibitors of HSP90 Block P95-HER2 Signaling in Trastuzumab-Resistant Tumors and Suppress Their Growth." *Oncogene* 29 (3): 325–34. https://doi.org/10.1038/onc.2009.337.

Chatterjee, Suman, and Timothy F. Burns. 2017. "Targeting Heat Shock Proteins in Cancer: A Promising Therapeutic Approach." *International Journal of Molecular Sciences*. MDPI AG. https://doi.org/10.3390/ijms18091978.

Chen, Hui Zi, Shih Yin Tsai, and Gustavo Leone. 2009. "Emerging Roles of E2Fs in Cancer: An Exit from Cell Cycle Control." *Nature Reviews Cancer* 9 (11): 785–97. https://doi.org/10.1038/nrc2696.

Chudasama, Priya, Sadaf S. Mughal, Mathijs A. Sanders, Daniel Hübschmann, Inn Chung, Katharina I. Deeg, Siao Han Wong, et al. 2018. "Integrative Genomic and Transcriptomic Analysis of Leiomyosarcoma." *Nature Communications* 9 (1): 1–15. https://doi.org/10.1038/s41467-017-02602-0.

Clijsters, Linda, Claire Hoencamp, Jorg J A Calis, Antonio Marzio, M Shanna, Maria C Cuitino, Brad R Rosenberg, and Gustavo Leone. 2020. "The Degradation of the Three Activator E2Fs" 74 (6): 1264–77. https://doi.org/10.1016/j.molcel.2019.04.010.Cyclin.

Clijsters, Linda, Claire Hoencamp, Jorg J.A. Calis, Antonio Marzio, Shanna M. Handgraaf, Maria C. Cuitino, Brad R. Rosenberg, Gustavo Leone, and Michele Pagano. 2019. "Cyclin F Controls Cell-Cycle Transcriptional Outputs by Directing the Degradation of the Three Activator E2Fs." *Molecular Cell* 74 (6): 1264-1277.e7. https://doi.org/10.1016/j.molcel.2019.04.010.

"Clinical Oncology_20240203." n.d.

Costa-Mattioli, Mauro, and Peter Walter. 2020. "The Integrated Stress Response: From Mechanism to Disease." *Science (New York, N.Y.)*. NLM (Medline). https://doi.org/10.1126/science.aat5314.

Costigan, Aoife, Emilie Hollville, and Seamus J. Martin. 2023. “Discriminating Between Apoptosis, Necrosis, Necroptosis, and Ferroptosis by Microscopy and Flow Cytometry.” *Current Protocols* 3 (12). https://doi.org/10.1002/cpz1.951.

Coussens, Nathan P., John C. Braisted, Tyler Peryea, G. Sitta Sittampalam, Anton Simeonov, and Matthew D. Hall. 2017. “Small-Molecule Screens: A Gateway to Cancer Therapeutic Agents with Case Studies of Food and Drug Administration–Approved Drugs.” *Pharmacological Reviews* 69 (4): 479–96. https://doi.org/10.1124/pr.117.013755.

Coussy, Florence, Rania El-Botty, Sophie Château-Joubert, Ahmed Dahmani, Elodie Montaudon, Sophie Leboucher, Ludivine Morisset, et al. 2020. “BRCAness, SLFN11, and RB1 Loss Predict Response to Topoisomerase I Inhibitors in Triple-Negative Breast Cancers.” *Sci. Transl. Med*. Vol. 12. https://www.science.org.

Cuppens, Tine, Matthieu Moisse, Jeroen Depreeuw, Daniela Annibali, Eva Colas, Antonio Gil-Moreno, Jutta Huvila, et al. 2018. “Integrated Genome Analysis of Uterine Leiomyosarcoma to Identify Novel Driver Genes and Targetable Pathways.” *International Journal of Cancer* 142 (6): 1230–43. https://doi.org/10.1002/ijc.31129.

D’Ambrosio, Lorenzo, Nathan Touati, Jean Yves Blay, Giovanni Grignani, Ronan Flippot, Anna M. Czarnecka, Sophie Piperno-Neumann, et al. 2020. “Doxorubicin plus Dacarbazine, Doxorubicin plus Ifosfamide, or Doxorubicin Alone as a First-Line Treatment for Advanced Leiomyosarcoma: A Propensity Score Matching Analysis from the European Organization for Research and Treatment of Cancer Soft Tissue and Bone Sarcoma Group.” *Cancer* 126 (11): 2637–47. https://doi.org/10.1002/cncr.32795.

D’Angiolella, Vincenzo, Mine Esencay, and Michele Pagano. 2013. “A Cyclin without Cyclin-Dependent Kinases: Cyclin F Controls Genome Stability through Ubiquitin-Mediated Proteolysis.” *Trends in Cell Biology*. https://doi.org/10.1016/j.tcb.2012.10.011.

Dei Tos, Angelo P., Roberta Maestro, Claudio Doglioni, Sara Piccinin, Duilio Della Libera, Mauro Boiocchi, and Christopher D.M. Fletcher. 1996. “Tumor Suppressor Genes and Related Molecules in Leiomyosarcoma.” *American Journal of Pathology* 148 (4): 1037–45.

Dick, Frederick A., and Shawn Shun Cheng Li. 2019. “Drugging RB1 Deficiency: Synthetic Lethality with Aurora Kinases.” *Cancer Discovery* 9 (2): 169–72. https://doi.org/10.1158/2159-8290.CD-18-1448.

Eccles, Suzanne A., Andy Massey, Florence I. Raynaud, Swee Y. Sharp, Gary Box, Melanie Valenti, Lisa Patterson, et al. 2008a. “NVP-AUY922: A Novel Heat Shock Protein 90 Inhibitor Active against Xenograft Tumor Growth, Angiogenesis, and Metastasis.” *Cancer Research* 68 (8): 2850–60. https://doi.org/10.1158/0008-5472.CAN-07-5256.

———. 2008b. “NVP-AUY922: A Novel Heat Shock Protein 90 Inhibitor Active against Xenograft Tumor Growth, Angiogenesis, and Metastasis.” *Cancer Research* 68 (8): 2850–60. https://doi.org/10.1158/0008-5472.CAN-07-5256.

Edwards, Aled M., Cheryl H. Arrowsmith, Chas Bountra, Mark E. Bunnage, Marc Feldmann, Julian C. Knight, Dhavalkumar D. Patel, Panagiotis Prinos, Michael D. Taylor, and Michael Sundström. 2015. “Preclinical Target Validation Using Patient-Derived Cells.” *Nature Reviews Drug Discovery*. Nature Publishing Group. https://doi.org/10.1038/nrd4565.

Eric Pujade-Lauraine, Professor, Professor A Jonathan Ledermann, Susana Banerjee, Joyce Liu, Elizabeth S Lowe, Ralph Bloomfield, Patricia Pautier, and Istituto Tumori Pascale di Napoli. 2017. “SOLO2/ENGOT-Ov21: A Phase 3, Randomised, Double-Blind, Placebo-Controlled Trial of Olaparib Tablets as Maintenance Therapy in Patients with Platinum-Sensitive, Relapsed Ovarian Cancer and a BRCA1/2 Mutation.”

Ernst, Anne, Heike Anders, Heidi Kapfhammer, Michael Orth, Roman Hennel, Karin Seidl, Nicolas Winssinger, Claus Belka, Steffen Unkel, and Kirsten Lauber. 2015. “HSP90 Inhibition as a Means of Radiosensitizing Resistant, Aggressive Soft Tissue Sarcomas.” *Cancer Letters* 365 (2): 211–22. https://doi.org/10.1016/j.canlet.2015.05.024.

“European Journal of Surgical Oncology_20240203.” n.d.

Fischer, Martin, and Gerd A. Müller. 2017. “Cell Cycle Transcription Control: DREAM/MuvB and RB-E2F Complexes.” *Critical Reviews in Biochemistry and Molecular Biology* 52 (6): 638–62. https://doi.org/10.1080/10409238.2017.1360836.

Fisher, Robert P. 2016. “Getting to S: CDK Functions and Targets on the Path to Cell-Cycle Commitment.” *F1000Research*. F1000 Research Ltd. https://doi.org/10.12688/f1000research.9463.1.

Gao, Peng, Nicole A. Seebacher, Francis Hornicek, Zheng Guo, and Zhenfeng Duan. 2018. “Advances in Sarcoma Gene Mutations and Therapeutic Targets.” *Cancer Treatment Reviews* 62:98–109. https://doi.org/10.1016/j.ctrv.2017.11.001.

George, Suzanne. 2019. “Developments in Systemic Therapy for Soft Tissue and Bone Sarcomas.” *Journal of the National Comprehensive Cancer Network : JNCCN* 17 (55): 625–28. https://doi.org/10.6004/jnccn.2019.5020.

George, Suzanne, César Serrano, Martee L Hensley, and Isabelle Ray-Coquard. 2022. “JOURNAL OF CLINICAL ONCOLOGY Soft Tissue and Uterine Leiomyosarcoma.” *J Clin Oncol* 36:144–50. https://doi.org/10.1200/JCO.2017.

Ghandi, Mahmoud, Franklin W. Huang, Judit Jané-Valbuena, Gregory V. Kryukov, Christopher C. Lo, E. Robert McDonald, Jordi Barretina, et al. 2019. “Next-Generation Characterization of the Cancer Cell Line Encyclopedia.” *Nature* 569 (7757): 503–8. https://doi.org/10.1038/s41586-019-1186-3.

Gladdy, Rebecca A., Li Xuan Qin, Nicole Moraco, Narasimhan P. Agaram, Murray F. Brennan, and Samuel Singer. 2013. “Predictors of Survival and Recurrence in Primary Leiomyosarcoma.” *Annals of Surgical Oncology* 20 (6): 1851–57. https://doi.org/10.1245/s10434-013-2876-y.

Gong, Xueqian, Jian Du, Stephen H. Parsons, Farhana F. Merzoug, Yue Webster, Philip W. Iversen, Li Chun Chio, et al. 2019. “Aurora a Kinase Inhibition Is Synthetic Lethal with Loss of the RB1 Tumor Suppressor Gene.” *Cancer Discovery* 9 (2): 248–63. https://doi.org/10.1158/2159-8290.CD-18-0469.

Grignani, Giovanni, Lorenzo D’Ambrosio, Ymera Pignochino, Emanuela Palmerini, Massimo Zucchetti, Paola Boccone, Sandra Aliberti, et al. 2018. “Trabectedin and Olaparib in Patients with Advanced and Non-Resectable Bone and Soft-Tissue Sarcomas (TOMAS): An Open-

Label, Phase 1b Study from the Italian Sarcoma Group." *The Lancet Oncology* 19 (10): 1360–71. https://doi.org/10.1016/S1470-2045(18)30438-8.

Groisberg, Roman, David S. Hong, Vijaykumar Holla, Filip Janku, Sarina Piha-Paul, Vinod Ravi, Robert Benjamin, et al. 2017. "Clinical Genomic Profiling to Identify Actionable Alterations for Investigational Therapies in Patients with Diverse Sarcomas." *Oncotarget* 8 (24): 39254–67. https://doi.org/10.18632/oncotarget.16845.

Gronchi, A., A. B. Miah, A. P. Dei Tos, N. Abecassis, J. Bajpai, S. Bauer, R. Biagini, et al. 2021. "Soft Tissue and Visceral Sarcomas: ESMO–EURACAN–GENTURIS Clinical Practice Guidelines for Diagnosis, Treatment and Follow-Up☆." *Annals of Oncology* 32 (11): 1348–65. https://doi.org/10.1016/j.annonc.2021.07.006.

Gronchi, Alessandro, Stefano Ferrari, Vittorio Quagliuolo, Javier Martin Broto, Antonio Lopez Pousa, Giovanni Grignani, Umberto Basso, et al. 2017. "Histotype-Tailored Neoadjuvant Chemotherapy versus Standard Chemotherapy in Patients with High-Risk Soft-Tissue Sarcomas (ISG-STS 1001): An International, Open-Label, Randomised, Controlled, Phase 3, Multicentre Trial." *The Lancet Oncology* 18 (6): 812–22. https://doi.org/10.1016/S1470-2045(17)30334-0.

Grünewald, Thomas GP, Marta Alonso, Sofia Avnet, Ana Banito, Stefan Burdach, Florencia Cidre-Aranaz, Gemma Di Pompo, et al. 2020. "Sarcoma Treatment in the Era of Molecular Medicine." *EMBO Molecular Medicine* 12 (11): 1–33. https://doi.org/10.15252/emmm.201911131.

Guo, Xiangqian, Vickie Y. Jo, Anne M. Mills, Shirley X. Zhu, Cheng Han Lee, Inigo Espinosa, Marisa R. Nucci, et al. 2015. "Clinically Relevant Molecular Subtypes in Leiomyosarcoma." *Clinical Cancer Research* 21 (15): 3501–11. https://doi.org/10.1158/1078-0432.CCR-14-3141.

"Gynecologic Oncology_20240203." n.d.

Hattinger, Claudia Maria, Maria Pia Patrizio, Silvia Luppi, Federica Magagnoli, Piero Picci, and Massimo Serra. 2019. *Current Understanding of Pharmacogenetic Implications of DNA Damaging Drugs Used in Osteosarcoma Treatment*. *Expert Opinion on Drug Metabolism and Toxicology*. Vol. 15. Taylor & Francis. https://doi.org/10.1080/17425255.2019.1588885.

Heldt, Frank S., Alexis R. Barr, Sam Cooper, Chris Bakal, and Béla Novák. 2018. “A Comprehensive Model for the Proliferation–Quiescence Decision in Response to Endogenous DNA Dama e in Human Cells.” *Proceedings of the National Academy of Sciences of the United States of America* 115 (10): 2532–37. https://doi.org/10.1073/pnas.1715345115.

Henley, Shauna A., and Frederick A. Dick. 2012. “The Retinoblastoma Family of Proteins and Their Regulatory Functions in the Mammalian Cell Division Cycle.” *Cell Division*. https://doi.org/10.1186/1747-1028-7-10.

Hensley, Martee L. 2011. “Role of Chemotherapy and Biomolecular Therapy in the Treatment of Uterine Sarcomas.” *Best Practice and Research: Clinical Obstetrics and Gynaecology* 25 (6): 773–82. https://doi.org/10.1016/j.bpobgyn.2011.06.003.

Hijioka, Susumu, Waki Hosoda, Keitaro Matsuo, Makoto Ueno, Masayuki Furukawa, Hideyuki Yoshitomi, Noritoshi Kobayashi, et al. 2017a. “Rb Loss and KRAS Mutation Are Predictors of the Response to Platinum-Based Chemotherapy in Pancreatic Neuroendocrine Neoplasm with Grade 3: A Japanese Multicenter Pancreatic NEN-G3 Study.” *Clinical Cancer Research* 23 (16): 4625–32. https://doi.org/10.1158/1078-0432.CCR-16-3135.

———. 2017b. “Rb Loss and KRAS Mutation Are Predictors of the Response to Platinum-Based Chemotherapy in Pancreatic Neuroendocrine Neoplasm with Grade 3: A Japanese Multicenter Pancreatic NEN-G3 Study.” *Clinical Cancer Research* 23 (16): 4625–32. https://doi.org/10.1158/1078-0432.CCR-16-3135.

Hipp, Mark S., Prasad Kasturi, and F. Ulrich Hartl. 2019a. “The Proteostasis Network and Its Decline in Ageing.” *Nature Reviews Molecular Cell Biology*. Nature Publishing Group. https://doi.org/10.1038/s41580-019-0101-y.

———. 2019b. “The Proteostasis Network and Its Decline in Ageing.” *Nature Reviews Molecular Cell Biology*. Nature Publishing Group. https://doi.org/10.1038/s41580-019-0101-y.

Hoter, Abdullah, Marwan E. El-Sabban, and Hassan Y. Naim. 2018. “The HSP90 Family: Structure, Regulation, Function, and Implications in Health and Disease.” *International Journal of Molecular Sciences*. MDPI AG. https://doi.org/10.3390/ijms19092560.

Huang, Alan, Levi A. Garraway, Alan Ashworth, and Barbara Weber. 2020. “Synthetic Lethality as an Engine for Cancer Drug Target Discovery.” *Nature Reviews Drug Discovery*. Nature Research. https://doi.org/10.1038/s41573-019-0046-z.

Hughes, J. P., S. S. Rees, S. B. Kalindjian, and K. L. Philpott. 2011. “Principles of Early Drug Discovery.” *British Journal of Pharmacology*. https://doi.org/10.1111/j.1476-5381.2010.01127.x.

Itallie, Christina M. Van, Amber Jean Tietgens, Angel Aponte, Marjan Gucek, Alexander X. Cartagena-Rivera, Richard S. Chadwick, and James M. Anderson. 2018. “MARCKS-Related Protein Regulates Cytoskeletal Organization at Cell-Cell and Cell-Substrate Contacts in Epithelial Cells.” *Journal of Cell Science* 131 (3). https://doi.org/10.1242/jcs.210237.

Ito, Moriko, Louise Barys, Terence O’Reilly, Sophie Young, Bella Gorbatcheva, John Monahan, Sabine Zumstein-Mecker, et al. 2011. “Comprehensive Mapping of P53 Pathway Alterations Reveals an Apparent Role for Both SNP309 and MDM2 Amplification in Sarcomagenesis.” *Clinical Cancer Research* 17 (3): 416–26. https://doi.org/10.1158/1078-0432.CCR-10-2050.

Jackson, Stephen P., and Jiri Bartek. 2009. “The DNA-Damage Response in Human Biology and Disease.” *Nature* 461 (7267): 1071–78. https://doi.org/10.1038/nature08467.

Jan, Rehmat, and Gul e.Saba Chaudhry. 2019. “Understanding Apoptosis and Apoptotic Pathways Targeted Cancer Therapeutics.” *Advanced Pharmaceutical Bulletin*. Tabriz University of Medical Sciences. https://doi.org/10.15171/apb.2019.024.

Jensen, Michael R., Joseph Schoepfer, Thomas Radimerski, Andrew Massey, Chantale T. Guy, Josef Brueggen, Cornelia Quadt, et al. 2008. “NVP-AUY922: A Small Molecule HSP90 Inhibitor with Potent Antitumor Activity in Preclinical Breast Cancer Models.” *Breast Cancer Research* 10 (2). https://doi.org/10.1186/bcr1996.

Johnson, Amy, and Jan M. Skotheim. 2013. “Start and the Restriction Point.” *Current Opinion in Cell Biology*. https://doi.org/10.1016/j.ceb.2013.07.010.

Jones, Lyn H., and Mark E. Bunnage. 2017. “Applications of Chemogenomic Library Screening in Drug Discovery.” *Nature Reviews Drug Discovery*. Nature Publishing Group. https://doi.org/10.1038/nrd.2016.244.

Jones, Samuel E., Emmy D.G. Fleuren, Jessica Frankum, Asha Konde, Chris T. Williamson, Dragomir B. Krastev, Helen N. Pemberton, et al. 2017. “ATR Is a Therapeutic Target in Synovial Sarcoma.” *Cancer Research* 77 (24): 7014–26. https://doi.org/10.1158/0008-5472.CAN-17-2056.

Jonsson, Philip, Chaitanya Bandlamudi, Michael L. Cheng, Preethi Srinivasan, Shweta S. Chavan, Noah D. Friedman, Ezra Y. Rosen, et al. 2019. “Tumour Lineage Shapes BRCA-Mediated Phenotypes.” *Nature* 571 (7766): 576–79. https://doi.org/10.1038/s41586-019-1382-1.

Judson, Ian, Jaap Verweij, Hans Gelderblom, Jörg T. Hartmann, Patrick Schöffski, Jean Yves Blay, J. Martijn Kerst, et al. 2014. “Doxorubicin Alone versus Intensified Doxorubicin plus Ifosfamide for First-Line Treatment of Advanced or Metastatic Soft-Tissue Sarcoma: A Randomised Controlled Phase 3 Trial.” *The Lancet Oncology* 15 (4): 415–23. https://doi.org/10.1016/S1470-2045(14)70063-4.

Juhasz-Böss, Ingolf, Lena Gabriel, Rainer M. Bohle, Lars C. Horn, Erich Franz Solomayer, and Georg Peter Breitbach. 2018. “Uterine Leiomyosarcoma.” *Oncology Research and Treatment* 41 (11): 680–86. https://doi.org/10.1159/000494299.

Jusino, Shirley, Yainyrette Rivera-Rivera, Camille Chardón-Colón, Armando J. Ruiz-Justiz, Jaleisha Vélez-Velázquez, Angel Isidro, Melanie E. Cruz-Robles, Margarita Bonilla-Claudio, Guillermo N. Armaiz-Pena, and Harold I. Saavedra. 2021. “E2F3 Drives the Epithelial-to-Mesenchymal Transition, Cell Invasion, and Metastasis in Breast Cancer.” *Experimental Biology and Medicine* 246 (19): 2057–71. https://doi.org/10.1177/15353702211035693.

Jusino, Shirley, and Harold I. Saavedra. 2019. “Highlight Article: Role of E2Fs and Mitotic Regulators Controlled by E2Fs in the Epithelial to Mesenchymal Transition.” *Experimental Biology and Medicine*. SAGE Publications Inc. https://doi.org/10.1177/1535370219881360.

Kasper, Bernd, Annie Achee, Kathrin Schuster, Roger Wilson, Gerard van Oortmerssen, Rebecca A. Gladdy, Matthew L. Hemming, et al. 2021. “Unmet Medical Needs and Future Perspectives for Leiomyosarcoma Patients—A Position Paper from the National Leiomyosarcoma Foundation (NLMSF) and Sarcoma Patients Euronet (SPAEN).” *Cancers*. MDPI AG. https://doi.org/10.3390/cancers13040886.

Kaufman, Bella, Ronnie Shapira-Frommer, Rita K. Schmutzler, M. William Audeh, Michael Friedlander, Judith Balmaña, Gillian Mitchell, et al. 2015. “Olaparib Monotherapy in Patients with Advanced Cancer and a Germline BRCA1/2 Mutation.” *Journal of Clinical Oncology* 33 (3): 244–50. https://doi.org/10.1200/JCO.2014.56.2728.

Kaushik, Susmita, and Ana Maria Cuervo. 2015. “Proteostasis and Aging.” *Nature Medicine*. Nature Publishing Group. https://doi.org/10.1038/nm.4001.

Kent, Lindsey N., and Gustavo Leone. 2019. “The Broken Cycle: E2F Dysfunction in Cancer.” *Nature Reviews Cancer* 19 (6): 326–38. https://doi.org/10.1038/s41568-019-0143-7.

Kim, Sungsoo, Alessandra Leong, Minah Kim, and Hee Won Yang. 2022. “CDK4/6 Initiates Rb Inactivation and CDK2 Activity Coordinates Cell-Cycle Commitment and G1/S Transition.” *Scientific Reports* 12 (1). https://doi.org/10.1038/s41598-022-20769-5.

Kim, Yujin E., Mark S. Hipp, Andreas Bracher, Manajit Hayer-Hartl, and F. Ulrich Hartl. 2013. “Molecular Chaperone Functions in Protein Folding and Proteostasis.” *Annual Review of Biochemistry*. https://doi.org/10.1146/annurev-biochem-060208-092442.

Koivisto-Korander, R., J. I. Martinsen, E. Weiderpass, A. Leminen, and E. Pukkala. 2012. “Incidence of Uterine Leiomyosarcoma and Endometrial Stromal Sarcoma in Nordic Countries: Results from NORDCAN and NOCCA Databases.” *Maturitas* 72 (1): 56–60. https://doi.org/10.1016/j.maturitas.2012.01.021.

Koppenhafer, Stacia L., Kelli L. Goss, William W. Terry, and David J. Gordon. 2020. “Inhibition of the ATR-CHK1 Pathway in Ewing Sarcoma Cells Causes DNA Damage and Apoptosis via the CDK2-Mediated Degradation of RRM2.” *Molecular Cancer Research* 18 (1): 91–104. https://doi.org/10.1158/1541-7786.MCR-19-0585.

Kostov, Stoyan, Yavor Kornovski, Vesela Ivanova, Deyan Dzhenkov, Dimitar Metodiev, Rafał Watrowski, Yonka Ivanova, Stanislav Slavchev, Dimitar Mitev, and Angel Yordanov. 2021. "New Aspects of Sarcomas of Uterine Corpus—a Brief Narrative Review." *Clinics and Practice*. Page Press Publications. https://doi.org/10.3390/clinpract11040103.

Lancet, J. E., I. Gojo, M. Burton, M. Quinn, S. M. Tighe, K. Kersey, Z. Zhong, et al. 2010. "Phase i Study of the Heat Shock Protein 90 Inhibitor Alvespimycin (KOS-1022, 17-DMAG) Administered Intravenously Twice Weekly to Patients with Acute Myeloid Leukemia." *Leukemia* 24 (4): 699–705. https://doi.org/10.1038/leu.2009.292.

Lee, A. T.J., W. Chew, C. P. Wilding, N. Guljar, M. J. Smith, D. C. Strauss, C. Fisher, et al. 2019. "The Adequacy of Tissue Microarrays in the Assessment of Inter- and Intra-Tumoural Heterogeneity of Infiltrating Lymphocyte Burden in Leiomyosarcoma." *Scientific Reports* 9 (1). https://doi.org/10.1038/s41598-019-50888-5.

Leitao, Mario M., Martee L. Hensley, Richard R. Barakat, Carol Aghajanian, Ginger J. Gardner, Elizabeth L. Jewell, Roisin O'Cearbhaill, and Robert A. Soslow. 2012. "Immunohistochemical Expression of Estrogen and Progesterone Receptors and Outcomes in Patients with Newly Diagnosed Uterine Leiomyosarcoma." *Gynecologic Oncology* 124 (3): 558–62. https://doi.org/10.1016/j.ygyno.2011.11.009.

Leng, Xiaohong, Lisa Connell-Crowley, David Goodrich, and J. Wade Harper. 1997. "S-Phase Entry upon Ectopic Expression of G1 Cyclin-Dependent Kinases in the Absence of Retinoblastoma Protein Phosphorylation." *Current Biology* 7 (9): 709–12. https://doi.org/10.1016/S0960-9822(06)00301-0.

Lew, Daniel J, and Sally Kornbluth. 1996. "Regulatory Roles of Cyclin Dependent Kinase Phosphorylation in Cell Cycle Control Abbreviations BIME Blocked in Mitosis E Cdk Cyclin-Dependent Kinase KAP Cdk-Associated Phosphatase NIMA Never in Mitosis A PP2A Protein Phosphatase 2A." *Current Opinion in Cell Biology* 8:795–804.

Li, Hongyi, Jian Tu, Zhiqiang Zhao, Lijuan Chen, Yueting Qu, Hongbo Li, Hao Yao, et al. 2020. "Molecular Signatures of BRCAness Analysis Identifies PARP Inhibitor Niraparib as a Novel

Targeted Therapeutic Strategy for Soft Tissue Sarcomas." *Theranostics* 10 (21): 9477–94. https://doi.org/10.7150/thno.45763.

Li, Zi Nan, and Ying Luo. 2023. "HSP90 Inhibitors and Cancer: Prospects for Use in Targeted Therapies (Review)." *Oncology Reports* 49 (1). https://doi.org/10.3892/or.2022.8443.

Lin, Ann, and Jason M. Sheltzer. 2020. "Discovering and Validating Cancer Genetic Dependencies: Approaches and Pitfalls." *Nature Reviews Genetics*. Nature Research. https://doi.org/10.1038/s41576-020-0247-7.

Linch, Mark, Aisha B. Miah, Khin Thway, Ian R. Judson, and Charlotte Benson. 2014. "Systemic Treatment of Soft-Tissue Sarcoma - Gold Standard and Novel Therapies." *Nature Reviews Clinical Oncology*. Nature Publishing Group. https://doi.org/10.1038/nrclinonc.2014.26.

Liu, Hanqing, Ziwen Lu, Xiaofeng Shi, Lanlan Liu, Peishan Zhang, Erica A. Golemis, and Zhigang Tu. 2021. "HSP90 Inhibition Downregulates DNA Replication and Repair Genes via E2F1 Repression." *Journal of Biological Chemistry* 297 (2). https://doi.org/10.1016/j.jbc.2021.100996.

Liu, Jeff C., Letizia Granieri, Mariusz Shrestha, Dong Yu Wang, Ioulia Vorobieva, Elizabeth A. Rubie, Rob Jones, et al. 2018. "Identification of CDC25 as a Common Therapeutic Target for Triple-Negative Breast Cancer." *Cell Reports* 23 (1): 112–26. https://doi.org/10.1016/j.celrep.2018.03.039.

Liu, Lei, Xiujie Chen, Chunyu Hu, Denan Zhang, Zhuo Shao, Qing Jin, Jingbo Yang, et al. 2018. "Synthetic Lethality-Based Identification of Targets for Anticancer Drugs in the Human Signaling Network." *Scientific Reports* 8 (1). https://doi.org/10.1038/s41598-018-26783-w.

Liu, Quanyu, Guihui Tu, Yan Hu, Qingna Jiang, Jingwen Liu, Shanshan Lin, Zelei Yu, et al. 2022. "Discovery of BP3 as an Efficacious Proteolysis Targeting Chimera (PROTAC) Degrader of HSP90 for Treating Breast Cancer." *European Journal of Medicinal Chemistry* 228 (January). https://doi.org/10.1016/j.ejmech.2021.114013.

Lolli, Graziano, and Louise N. Johnson. 2005. “CAK-Cyclin-Dependent Activating Kinase: A Key Kinase in Cell Cycle Control and a Target for Drugs?” *Cell Cycle*. Taylor and Francis Inc. https://doi.org/10.4161/cc.4.4.1607.

Longworth, Michelle S., Anabel Herr, Jun Yuan Ji, and Nicholas J. Dyson. 2008. “RBF1 Promotes Chromatin Condensation through a Conserved Interaction with the Condensin II Protein DCAP-D3.” *Genes and Development* 22 (8): 1011–24. https://doi.org/10.1101/gad.1631508.

López-Guerrero, José Antonio, Concha López-Ginés, Antonio Pellín, Carmen Carda, and Antonio Llombart-Bosch. 2004. “Deregulation of the G1 to S-Phase Cell Cycle Checkpoint Is Involved in the Pathogenesis of Human Osteosarcoma.” *Diagnostic Molecular Pathology* 13 (2): 81–91. https://doi.org/10.1097/00019606-200406000-00004.

López-Otín, Carlos, Maria A. Blasco, Linda Partridge, Manuel Serrano, and Guido Kroemer. 2023. “Hallmarks of Aging: An Expanding Universe.” *Cell*. Elsevier B.V. https://doi.org/10.1016/j.cell.2022.11.001.

Lord, Christopher J, and Alan Ashworth. 2017. “PARP Inhibitors: Synthetic Lethality in the Clinic.” https://www.science.org.

LoRusso, Patricia M., Renzo Canetta, John A. Wagner, Erin P. Balogh, Sharyl J. Nass, Scott A. Boerner, and John Hohneker. 2012. “Accelerating Cancer Therapy Development: The Importance of Combination Strategies and Collaboration. Summary of an Institute of Medicine Workshop.” In *Clinical Cancer Research*, 18:6101–9. https://doi.org/10.1158/1078-0432.CCR-12-2455.

Lukas, Jiri, Thomas Herzinger, Klaus Hansen, Maria Cristina Moroni, Dalia Resnitzky, Kristian Helin, Steven I. Reed, and Jiri Bartek. 1997. “Cyclin E-Induced S Phase without Activation of the PRb/E2F Pathway.” *Genes and Development* 11 (11): 1479–92. https://doi.org/10.1101/gad.11.11.1479.

Lundberg, Ante S., and Robert A. Weinberg. 1998. “Functional Inactivation of the Retinoblastoma Protein Requires Sequential Modification by at Least Two Distinct Cyclin-Cdk Complexes.” *Molecular and Cellular Biology* 18 (2): 753–61. https://doi.org/10.1128/mcb.18.2.753.

Ly, Peter, Simon F. Brunner, Ofer Shoshani, Dong Hyun Kim, Weijie Lan, Tatyana Pyntikova, Adrienne M. Flanagan, et al. 2019. “Chromosome Segregation Errors Generate a Diverse Spectrum of Simple and Complex Genomic Rearrangements.” *Nature Genetics* 51 (4): 705–15. https://doi.org/10.1038/s41588-019-0360-8.

Lyu, Heather G., Adil H. Haider, Adam B. Landman, and Chandrajit P. Raut. 2019. “The Opportunities and Shortcomings of Using Big Data and National Databases for Sarcoma Research.” *Cancer* 125 (17): 2926–34. https://doi.org/10.1002/cncr.32118.

Lyu, Junfang, Eun Ju Yang, Baoyuan Zhang, Changjie Wu, Lakhansing Pardeshi, Changxiang Shi, Pui Kei Mou, Yifan Liu, Kaeling Tan, and Joong Sup Shim. 2020. “Synthetic Lethality of RB1 and Aurora A Is Driven by Stathmin-Mediated Disruption of Microtubule Dynamics.” *Nature Communications* 11 (1). https://doi.org/10.1038/s41467-020-18872-0.

Ma, Fang, Xiao Fang Jia, Xian Jun Xia, Da Ge Wu, Xiao Qian Liu, Lin Yin, Bao Chi Liu, and Li Jun Zhang. 2015. “Proteomic Analysis of 17-DMAG Effects on Colon Cancer HT-29 Cells.” *International Research Journal of Public and Environmental Health* 2 (8): 92–101. https://doi.org/10.15739/irjpeh.026.

Maccaroni, Elena, Valentina Lunerti, Veronica Agostinelli, Riccardo Giampieri, Laura Zepponi, Alessandra Pagliacci, and Rossana Berardi. 2022. “New Insights into Hormonal Therapies in Uterine Sarcomas.” *Cancers*. MDPI. https://doi.org/10.3390/cancers14040921.

Maddocks, Kami, Erin Hertlein, Timothy L Chen, Amy J Wagner, Yonghua Ling, Joseph Flynn, Mitch Phelps, Amy J Johnson, John C Byrd, and Jeffrey A Jones. 2016. “A Phase I Trial of the Intravenous Hsp90 Inhibitor Alvespimycin (17-DMAG) in Patients with Relapsed Chronic Lymphocytic Leukemia/Small Lymphocytic Lymphoma.” *Leukemia & Lymphoma* 57 (9): 2212–15. https://doi.org/10.3109/10428194.2015.1129536.

Maiani, Emiliano, Giacomo Milletti, Francesca Nazio, Søs Grønbæk Holdgaard, Jirina Bartkova, Salvatore Rizza, Valentina Cianfanelli, et al. 2021. “AMBRA1 Regulates Cyclin D to Guard S-Phase Entry and Genomic Integrity.” *Nature* 592 (7856): 799–803. https://doi.org/10.1038/s41586-021-03422-5.

Mäkinen, Netta, Mervi Aavikko, Tuomas Heikkinen, Minna Taipale, Jussi Taipale, Riitta Koivisto-Korander, Ralf Bützow, and Pia Vahteristo. 2016. “Exome Sequencing of Uterine Leiomyosarcomas Identifies Frequent Mutations in TP53, ATRX, and MED12.” *PLoS Genetics* 12 (2): 1–13. https://doi.org/10.1371/journal.pgen.1005850.

Mammadova, Aynura, Arif Mermer, and Fatih Kocabaş. 2021a. “Screening of the Small Molecule Library of Meinox Enables the Identification of Anticancer Compounds in Pathologically Distinct Cancers.” *Turkish Journal of Biology* 45 (5): 633–43. https://doi.org/10.3906/biy-2104-14.

———. 2021b. “Screening of the Small Molecule Library of Meinox Enables the Identification of Anticancer Compounds in Pathologically Distinct Cancers.” *Turkish Journal of Biology* 45 (5): 633–43. https://doi.org/10.3906/biy-2104-14.

Manning, Amity L., and Nicholas J. Dyson. 2012a. “RB: Mitotic Implications of a Tumour Suppressor.” *Nature Reviews Cancer*. https://doi.org/10.1038/nrc3216.

———. 2012b. “RB: Mitotic Implications of a Tumour Suppressor.” *Nature Reviews Cancer*. https://doi.org/10.1038/nrc3216.

Manning, Amity L., Michelle S. Longworth, and Nicholas J. Dyson. 2010. “Loss of PRB Causes Centromere Dysfunction and Chromosomal Instability.” *Genes and Development* 24 (13): 1364–76. https://doi.org/10.1101/gad.1917310.

Mantovani, Fiamma, Licio Collavin, and Giannino Del Sal. 2019. “Mutant P53 as a Guardian of the Cancer Cell.” *Cell Death and Differentiation*. Nature Publishing Group. https://doi.org/10.1038/s41418-018-0246-9.

Masuda, H., C. Miller, H. P. Koeffler, H. Battifora, and M. J. Cline. 1987. “Rearrangement of the P53 Gene in Human Osteogenic Sarcomas.” *Proceedings of the National Academy of Sciences of the United States of America* 84 (21): 7716–19. https://doi.org/10.1073/pnas.84.21.7716.

Matson, Jacob P., and Jeanette G. Cook. 2017. “Cell Cycle Proliferation Decisions: The Impact of Single Cell Analyses.” *FEBS Journal*. Blackwell Publishing Ltd. https://doi.org/10.1111/febs.13898.

Matushansky, Igor, and Robert G. Maki. 2005. “Mechanisms of Sarcomagenesis.” *Hematology/Oncology Clinics of North America* 19 (3): 427–49. https://doi.org/10.1016/j.hoc.2005.03.006.

Mbatani, Nomonde, Alexander B. Olawaiye, and Jaime Prat. 2018. “Uterine Sarcomas.” *International Journal of Gynecology and Obstetrics* 143 (October):51–58. https://doi.org/10.1002/ijgo.12613.

Merry, Callie, Kang Fu, Jingna Wang, I. Ju Yeh, and Youwei Zhang. 2010. “Targeting the Checkpoint Kinase Chk1 in Cancer Therapy.” *Cell Cycle* 9 (2): 279–83. https://doi.org/10.4161/cc.9.2.10445.

Merry, Eve, Khin Thway, Robin L. Jones, and Paul H. Huang. 2021. “Predictive and Prognostic Transcriptomic Biomarkers in Soft Tissue Sarcomas.” *Npj Precision Oncology*. Nature Research. https://doi.org/10.1038/s41698-021-00157-4.

Mertens, Fredrik, Ulf Strömberg, Nils Mandahl, Paola Dal Cin, Ivo De Wever, Christopher D.M. Fletcher, Felix Mitelman, et al. 2002. “Prognostically Important Chromosomal Aberrations in Soft Tissue Sarcomas: A Report of the Chromosomes and Morphology (CHAMP) Study Group.” *Cancer Research* 62 (14): 3980–84.

Mickler, Moritz, Martin Hessling, Christoph Ratzke, Johannes Buchner, and Thorsten Hugel. 2009. “The Large Conformational Changes of Hsp90 Are Only Weakly Coupled to ATP Hydrolysis.” *Nature Structural and Molecular Biology* 16 (3): 281–86. https://doi.org/10.1038/nsmb.1557.

Min Woo, Seon, Seung Un Seo, Peter Kubatka, Min Kyoung-Jin, and Taeg Kyu Kwon. 2019. “Honokiol Enhances TRAIL-Mediated Apoptosis through STAMBPL1-Induced Survivin and c-FLIP Degradation.” *Biomolecules* 9 (12). https://doi.org/10.3390/biom9120838.

Mohammadi, Elyas, Rui Benfeitas, Hasan Turkez, Jan Boren, Jens Nielsen, Mathias Uhlen, and Adil Mardinoglu. 2020. “Applications of Genome-Wide Screening and Systems Biology Approaches in Drug Repositioning.” *Cancers*. MDPI AG. https://doi.org/10.3390/cancers12092694.

Mollapour, Mehdi, and Len Neckers. 2012. “Post-Translational Modifications of Hsp90 and Their Contributions to Chaperone Regulation.” *Biochimica et Biophysica Acta - Molecular Cell Research*. https://doi.org/10.1016/j.bbamcr.2011.07.018.

Morimoto, Richard I., and Ana Maria Cuervo. 2014. “Proteostasis and the Aging Proteome in Health and Disease.” *Journals of Gerontology - Series A Biological Sciences and Medical Sciences*. Oxford University Press. https://doi.org/10.1093/gerona/glu049.

Mullard, Asher. 2017. “Synthetic Lethality Screens Point the Way to New Cancer Drug Targets.” *Nature Reviews Drug Discovery*. Nature Publishing Group. https://doi.org/10.1038/nrd.2017.165.

Müller, Lin, Andreas Schaupp, Dawid Walerych, Harald Wegele, and Johannes Buchner. 2004. “Hsp90 Regulates the Activity of Wild Type P53 under Physiological and Elevated Temperatures.” *Journal of Biological Chemistry* 279 (47): 48846–54. https://doi.org/10.1074/jbc.M407687200.

Nacev, Benjamin A., Kevin B. Jones, Andrew M. Intlekofer, Jamie S.E. Yu, C. David Allis, William D. Tap, Marc Ladanyi, and Torsten O. Nielsen. 2020. “The Epigenomics of Sarcoma.” *Nature Reviews Cancer*. Nature Research. https://doi.org/10.1038/s41568-020-0288-4.

Nath, Somsubhra, Abhishek Chowdhury, Sanjib Dey, Anirban Roychoudhury, Abira Ganguly, Dibyendu Bhattacharyya, and Susanta Roychoudhury. 2015. “Deregulation of Rb-E2F1 Axis Causes Chromosomal Instability by Engaging the Transactivation Function of Cdc20–Anaphase-Promoting Complex/Cyclosome.” *Molecular and Cellular Biology* 35 (2): 356–69. https://doi.org/10.1128/mcb.00868-14.

“Nature04873 (1).” n.d.

Ngo, Vy, Nadun C. Karunatilleke, Anne Brickenden, Wing Yiu Choy, and Martin L. Duennwald. 2022. “Oxidative Stress-Induced Misfolding and Inclusion Formation of Nrf2 and Keap1.” *Antioxidants* 11 (2). https://doi.org/10.3390/antiox11020243.

Noack, Sabrina, Monika Raab, Yves Matthess, Mourad Sanhaji, Andrea Krämer, Balázs Győrffy, Lars Kaderali, Ahmed El-Balat, Sven Becker, and Klaus Strebhardt. 2018. “Synthetic Lethality in CCNE1-Amplified High Grade Serous Ovarian Cancer through Combined Inhibition of Polo-like Kinase 1 and Microtubule Dynamics.” www.oncotarget.com.

Oliva, Esther. 2016. “Practical Issues in Uterine Pathology from Banal to Bewildering: The Remarkable Spectrum of Smooth Muscle Neoplasia.” *Modern Pathology* 29 (S1): S104–20. https://doi.org/10.1038/modpathol.2015.139.

Oser, Matthew G., Raquel Fonseca, Abhishek A. Chakraborty, Rachel Brough, Alexander Spektor, Rebecca B. Jennings, Abdallah Flaifel, et al. 2019a. “Cells Lacking the RB1 Tumor Suppressor Gene Are Hyperdependent on Aurora B Kinase for Survival.” *Cancer Discovery* 9 (2): 230–47. https://doi.org/10.1158/2159-8290.CD-18-0389.

———. 2019b. “Cells Lacking the RB1 Tumor Suppressor Gene Are Hyperdependent on Aurora B Kinase for Survival.” *Cancer Discovery* 9 (2): 230–47. https://doi.org/10.1158/2159-8290.CD-18-0389.

Pacey, Simon, Richard H. Wilson, Mike Walton, Martin M. Eatock, Anthea Hardcastle, Anna Zetterlund, Hendrik Tobias Arkenau, et al. 2011. “A Phase I Study of the Heat Shock Protein 90 Inhibitor Alvespimycin (17-DMAG) given Intravenously to Patients with Advanced Solid Tumors.” *Clinical Cancer Research* 17 (6): 1561–70. https://doi.org/10.1158/1078-0432.CCR-10-1927.

Pagano, Michele, Giulio Draetta, and Pidder Jansen-Dürr. 1992. “Association of Cdk2 Kinase with the Transcription Factor E2F during S Phase.” *Science* 255 (5048): 1144–47. https://doi.org/10.1126/science.1312258.

Palacios, Carmen, Rosa Martín-Pérez, Ana Isabel López-Pérez, Atanasio Pandiella, and Abelardo López-Rivas. 2010. “Autophagy Inhibition Sensitizes Multiple Myeloma Cells to 17-Dimethylaminoethylamino-17-Demethoxygeldanamycin-Induced Apoptosis.” *Leukemia Research* 34 (11): 1533–38. https://doi.org/10.1016/j.leukres.2010.07.002.

Park, Margaret A., Guo Zhang, Clint Mitchell, Mohamed Rahmani, Hossein Hamed, Michael P. Hagan, Adly Yacoub, et al. 2008. “Mitogen-Activated Protein Kinase Kinase 1/2 Inhibitors and 17-Allylamino-17-Demethoxygeldanamycin Synergize to Kill Human Gastrointestinal Tumor Cells in Vitro via Suppression of c-FLIP-s Levels and Activation of CD95.” *Molecular Cancer Therapeutics* 7 (9): 2633–48. https://doi.org/10.1158/1535-7163.MCT-08-0400.

Pasquali, Sandro, Emanuela Palmerini, Vittorio Quagliuolo, Javier Martin-Broto, Antonio Lopez-Pousa, Giovanni Grignani, Antonella Brunello, et al. 2022. “Neoadjuvant Chemotherapy in High-Risk Soft Tissue Sarcomas: A Sarculator-Based Risk Stratification Analysis of the ISG-STS 1001 Randomized Trial.” *Cancer* 128 (1): 85–93. https://doi.org/10.1002/cncr.33895.

Peng, Caiwang, Fengyan Zhao, Hengli Li, Ling Li, Yantao Yang, and Fang Liu. 2022. “HSP90 Mediates the Connection of Multiple Programmed Cell Death in Diseases.” *Cell Death and Disease*. Springer Nature. https://doi.org/10.1038/s41419-022-05373-9.

Pennycook, Betheney R., and Alexis R. Barr. 2020a. “Restriction Point Regulation at the Crossroads between Quiescence and Cell Proliferation.” *FEBS Letters*. Wiley Blackwell. https://doi.org/10.1002/1873-3468.13867.

———. 2020b. “Restriction Point Regulation at the Crossroads between Quiescence and Cell Proliferation.” *FEBS Letters*. Wiley Blackwell. https://doi.org/10.1002/1873-3468.13867.

Peron, Marica, Paolo Bonvini, and Angelo Rosolen. 2012. “Effect of Inhibition of the Ubiquitin-Proteasome System and Hsp90 on Growth and Survival of Rhabdomyosarcoma Cells in Vitro.” *BMC Cancer* 12 (June). https://doi.org/10.1186/1471-2407-12-233.

Prodromou, Chrisostomos, and Dennis M. Bjorklund. 2022. “Advances towards Understanding the Mechanism of Action of the Hsp90 Complex.” *Biomolecules*. MDPI. https://doi.org/10.3390/biom12050600.

Rahul Bhowmick, Kavi P.M. Mehta, Mads Lerdrup, and David Cortez. 2023. “Integrator Facilitates RNAPII Removal to Prevent Transcription-Replication Collisions and Genome Instability.” *Cell*.

Raish, Mohammad, Mohsin Khurshid, Mushtaq Ahmad Ansari, Pankaj Kumar Chaturvedi, Su Mi Bae, Jang Heub Kim, Eun Kyung Park, Dong Chun Park, and Woong Shick Ahn. 2012. “Analysis of Molecular Cytogenetic Alterations in Uterine Leiomyosarcoma by Array-Based Comparative Genomic Hybridization.” *Journal of Cancer Research and Clinical Oncology* 138 (7): 1173–86. https://doi.org/10.1007/s00432-012-1182-6.

Resnitzky, D, M Gossen, H Bujard, and S I Reed. 1994. “Acceleration of the G1/S Phase Transition by Expression of Cyclins D1 and E with an Inducible System.” *Molecular and Cellular Biology* 14 (3): 1669 LP – 1679. https://doi.org/10.1128/MCB.14.3.1669.

Resnitzky, D, and S I Reed. 1995. “Different Roles for Cyclins D1 and E in Regulation of the G1-to-S Transition.” *Molecular and Cellular Biology* 15 (7): 3463–69. https://doi.org/10.1128/mcb.15.7.3463.

Rosenbaum, Evan, Philip Jonsson, ; Kenneth Seier, ; Li, -Xuan Qin, Ping Chi, Mark Dickson, et al. 2020. “Clinical Outcome of Leiomyosarcomas With Somatic Alteration in Homologous Recombination Pathway Genes.” *JCO Precis Oncol* 4:1350–60. https://doi.org/10.1200/PO.20.

Rubin, Seth M., Julien Sage, and Jan M. Skotheim. 2020. “Integrating Old and New Paradigms of G1/S Control.” *Molecular Cell*. Cell Press. https://doi.org/10.1016/j.molcel.2020.08.020.

Sajjad, Humna, Saiqa Imtiaz, Tayyaba Noor, Yusra Hasan Siddiqui, Anila Sajjad, and Muhammad Zia. 2021. “Cancer Models in Preclinical Research: A Chronicle Review of Advancement in Effective Cancer Research.” *Animal Models and Experimental Medicine*. John Wiley and Sons Inc. https://doi.org/10.1002/ame2.12165.

Sanada, Sakiko, Kimio Ushijima, Hiroyuki Yanai, Yoshiki Mikami, Yoshihiro Ohishi, Hiroaki Kobayashi, Hironori Tashiro, Mikio Mikami, Shingo Miyamoto, and Hidetaka Katabuchi. 2022. “A Critical Review of ‘Uterine Leiomyoma’ with Subsequent Recurrence or Metastasis: A Multicenter Study of 62 Cases.” *Journal of Obstetrics and Gynaecology Research* 48 (12): 3242–51. https://doi.org/10.1111/jog.15426.

Santos, Reinaldo S. Dos, Laura Marroqui, Fabio A. Grieco, Lorella Marselli, Mara Suleiman, Stefan R. Henz, Piero Marchetti, Rasmus Wernersson, and Decio L. Eizirik. 2017. “Protective Role of Complement C3 against Cytokine-Mediated β-Cell Apoptosis.” *Endocrinology* 158 (8): 2503–21. https://doi.org/10.1210/en.2017-00104.

Scaltriti, Maurizio, Shaheenah Dawood, and Javier Cortes. 2012. “Molecular Pathways: Targeting Hsp90 - Who Benefits and Who Does Not.” *Clinical Cancer Research* 18 (17): 4508–13. https://doi.org/10.1158/1078-0432.CCR-11-2138.

Schwock, Jörg, Nhu An Pham, Mary P. Cao, and David W. Hedley. 2008. “Efficacy of Hsp90 Inhibition for Induction of Apoptosis and Inhibition of Growth in Cervical Carcinoma Cells in Vitro and in Vivo.” *Cancer Chemotherapy and Pharmacology* 61 (4): 669–81. https://doi.org/10.1007/s00280-007-0522-8.

Serrano, Cesar, and Suzanne George. 2013. “Leiomyosarcoma.” *Hematology/Oncology Clinics of North America*. https://doi.org/10.1016/j.hoc.2013.07.002.

Sessa, Cristiana, Geoffrey I. Shapiro, Kapil N. Bhalla, Carolyn Britten, Karen S. Jacks, Monica Mita, Vali Papadimitrakopoulou, et al. 2013. “First-in-Human Phase I Dose-Escalation Study of the HSP90 Inhibitor AUY922 in Patients with Advanced Solid Tumors.” *Clinical Cancer Research* 19 (13): 3671–80. https://doi.org/10.1158/1078-0432.CCR-12-3404.

Setton, Jeremy, Michael Zinda, Nadeem Riaz, Daniel Durocher, Michal Zimmermann, Maria Koehler, Jorge S. Reis-Filho, and Simon N. Powell. 2021a. “Synthetic Lethality in Cancer Therapeutics: The next Generation.” *Cancer Discovery*. American Association for Cancer Research Inc. https://doi.org/10.1158/2159-8290.CD-20-1503.

———. 2021b. “Synthetic Lethality in Cancer Therapeutics: The next Generation.” *Cancer Discovery*. American Association for Cancer Research Inc. https://doi.org/10.1158/2159-8290.CD-20-1503.

Sharp, Swee, Keith Jones, and Paul Workman. 2013. “Exploiting Cancer Dependence on Molecular Chaperones: HSP90 Inhibitors Past, Present, and Future.” In *Cancer Drug Design and Discovery: Second Edition*, 239–74. Elsevier Inc. https://doi.org/10.1016/B978-0-12-396521-9.00009-7.

Sherr, Charles J., and Frank McCormick. 2002. “The RB and P53 Pathways in Cancer.” *Cancer Cell* 2 (2): 103–12. https://doi.org/10.1016/S1535-6108(02)00102-2.

Shiau, Andrew K., Seth F. Harris, Daniel R. Southworth, and David A. Agard. 2006. “Structural Analysis of E. Coli Hsp90 Reveals Dramatic Nucleotide-Dependent Conformational Rearrangements.” *Cell* 127 (2): 329–40. https://doi.org/10.1016/j.cell.2006.09.027.

Simoneschi, Daniele, Gergely Rona, Nan Zhou, Yeon Tae Jeong, Shaowen Jiang, Giacomo Milletti, Arnaldo A. Arbini, et al. 2021. "CRL4AMBRA1 Is a Master Regulator of D-Type Cyclins." *Nature* 592 (7856): 789–93. https://doi.org/10.1038/s41586-021-03445-y.

Siozopoulou, Vasiliki, Andreas Domen, Karen Zwaenepoel, Annelies Van Beeck, Evelien Smits, Patrick Pauwels, and Elly Marcq. 2021. "Immune Checkpoint Inhibitory Therapy in Sarcomas: Is There Light at the End of the Tunnel?" *Cancers*. MDPI AG. https://doi.org/10.3390/cancers13020360.

Steinmann, Sara, Hala Gali-Muhtasib, Kerstin Huebner, Racha Al-Halabi, Raghida Abou Merhi, Pierre Aman, Abbas Agaimy, Florian Haller, and Regine Schneider-Stock. 2015. "Hsp90 Inhibition by AUY922 as an Effective Treatment Strategy against Myxoid Liposarcoma." *Cancer Letters* 367 (2): 147–56. https://doi.org/10.1016/j.canlet.2015.07.025.

Stevens, MCG, C Frobisher, MM Hawkins, M Jenney, ER Lancashire, RC Reulen, AJ Taylor, and DL Winter. 2008. "The British Childhood Cancer Survivor Study: Objectives, Methods, Population Structure, Response Rates and Initial Descriptive Information." *Pediatric Blood & Cancer* 50 (5): 1018–25. https://doi.org/10.1002/pbc.

Stiller, C. A., E. Desandes, S. E. Danon, I. Izarzugaza, A. Ratiu, Z. Vassileva-Valerianova, E. Steliarova-Foucher, et al. 2006. "Cancer Incidence and Survival in European Adolescents (1978-1997). Report from the Automated Childhood Cancer Information System Project." *European Journal of Cancer* 42 (13): 2006–18. https://doi.org/10.1016/j.ejca.2006.06.002.

Stiller, C. A., A. Trama, D. Serraino, S. Rossi, C. Navarro, M. D. Chirlaque, N. Zielonk, et al. 2013. "Descriptive Epidemiology of Sarcomas in Europe: Report from the RARECARE Project." *European Journal of Cancer* 49 (3): 684–95. https://doi.org/10.1016/j.ejca.2012.09.011.

Sumi, Mamta P., and Arnab Ghosh. 2022. "Hsp90 in Human Diseases: Molecular Mechanisms to Therapeutic Approaches." *Cells*. MDPI. https://doi.org/10.3390/cells11060976.

Taipale, Mikko, Daniel F. Jarosz, and Susan Lindquist. 2010. "HSP90 at the Hub of Protein Homeostasis: Emerging Mechanistic Insights." *Nature Reviews Molecular Cell Biology*. https://doi.org/10.1038/nrm2918.

Tap, William D., Andrew J. Wagner, Patrick Schöffski, Javier Martin-Broto, Anders Krarup-Hansen, Kristen N. Ganjoo, Chueh Chuan Yen, et al. 2020. “Effect of Doxorubicin Plus Olaratumab vs Doxorubicin Plus Placebo on Survival in Patients with Advanced Soft Tissue Sarcomas: The ANNOUNCE Randomized Clinical Trial.” In *JAMA - Journal of the American Medical Association*, 323:1266–76. American Medical Association. https://doi.org/10.1001/jama.2020.1707.

Taylor, Barry S., Jordi Barretina, Robert G. Maki, Cristina R. Antonescu, Samuel Singer, and Marc Ladanyi. 2011. “Advances in Sarcoma Genomics and New Therapeutic Targets.” *Nature Reviews Cancer* 11 (8): 541–57. https://doi.org/10.1038/nrc3087.

Terry, Jefferson, Joanna M Lubieniecka, Wanda Kwan, Suzanne Liu, and Torsten O Nielsen. 2005. “Hsp90 Inhibitor 17-Allylamino-17-Demethoxygeldanamycin Prevents Synovial Sarcoma Proliferation via Apoptosis in In Vitro Models.” www.aacrjournals.org.

Thanopoulou, Eirini, Khin Thway, Komel Khabra, and Ian Judson. 2014. “Treatment of Hormone Positive Uterine Leiomyosarcoma with Aromatase Inhibitors.” *Clinical Sarcoma Research* 4 (1). https://doi.org/10.1186/2045-3329-4-5.

Timmer, Tineke, Elisabeth G.E. De Vries, and Steven De Jong. 2002. “Fas Receptor-Mediated Apoptosis: A Clinical Application?” *Journal of Pathology*. https://doi.org/10.1002/path.1028.

Toro, Jorge R., Lois B. Travis, Julian Wu Hongyu, Kangmin Zhu, Christopher D.M. Fletcher, and Susan S. Devesa. 2006. “Incidence Patterns of Soft Tissue Sarcomas, Regardless of Primary Site, in the Surveillance, Epidemiology and End Results Program, 1978-2001: An Analysis of 26,758 Cases.” *International Journal of Cancer* 119 (12): 2922–30. https://doi.org/10.1002/ijc.22239.

Trepel, Jane, Mehdi Mollapour, Giuseppe Giaccone, and Len Neckers. 2010. “Targeting the Dynamic HSP90 Complex in Cancer.” *Nature Reviews Cancer*. https://doi.org/10.1038/nrc2887.

Treré, D., E. Brighenti, G. Donati, C. Ceccarelli, D. Santini, M. Taffurelli, L. Montanaro, and Massimo Derenzini. 2009. “High Prevalence of Retinoblastoma Protein Loss in Triple-Negative

Breast Cancers and Its Association with a Good Prognosis in Patients Treated with Adjuvant Chemotherapy." *Annals of Oncology* 20 (11): 1818–23. https://doi.org/10.1093/annonc/mdp209.

Tsuyoshi, Hideaki, and Yoshio Yoshida. 2018. "Molecular Biomarkers for Uterine Leiomyosarcoma and Endometrial Stromal Sarcoma." *Cancer Science* 109 (6): 1743–52. https://doi.org/10.1111/cas.13613.

Wagner, Andrew J., Rashmi Chugh, Lee S. Rosen, Jeffrey A. Morgan, Suzanne George, Michael Gordon, Joi Dunbar, Emmanuel Normant, David Grayzel, and George D. Demetri. 2013. "A Phase i Study of the HSP90 Inhibitor Retaspimycin Hydrochloride (IPI-504) in Patients with Gastrointestinal Stromal Tumors or Soft-Tissue Sarcomas." *Clinical Cancer Research* 19 (21): 6020–29. https://doi.org/10.1158/1078-0432.CCR-13-0953.

Wang, Lixia, Xiantao Ye, Yueyong Liu, Wenyi Wei, and Zhiwei Wang. 2014. "Aberrant Regulation of FBW7 in Cancer." *Oncotarget* 5 (8): 2000–2015. https://doi.org/10.18632/oncotarget.1859.

Wang, Qilin, Wendong Sun, Xuexi Hao, Tianliang Li, Ling Su, and Xiangguo Liu. 2012. "Down-Regulation of Cellular FLICE-Inhibitory Protein (Long Form) Contributes to Apoptosis Induced by Hsp90 Inhibition in Human Lung Cancer Cells." *Cancer Cell International* 12 (December). https://doi.org/10.1186/1475-2867-12-54.

Weber, Anika Maria, and Anderson Joseph Ryan. 2015. "ATM and ATR as Therapeutic Targets in Cancer." *Pharmacology and Therapeutics* 149:124–38. https://doi.org/10.1016/j.pharmthera.2014.12.001.

Weinberg, Robert A. 1995. "The Retinoblastoma Protein and Cell Cycle Control." *Cell* 81 (3): 323–30. https://doi.org/10.1016/0092-8674(95)90385-2.

Whitesell, Luke, and Susan L. Lindquist. 2005. "HSP90 and the Chaperoning of Cancer." *Nature Reviews Cancer*. https://doi.org/10.1038/nrc1716.

Wispelaere, Wout De, Daniela Annibali, Sandra Tuyaerts, Diether Lambrechts, and Frédéric Amant. 2021. "Resistance to Immune Checkpoint Blockade in Uterine Leiomyosarcoma: What Can We Learn from Other Cancer Types?" *Cancers*. MDPI AG. https://doi.org/10.3390/cancers13092040.

Witkiewicz, Agnieszka K., Sejin Chung, Rachel Brough, Paris Vail, Jorge Franco, Christopher J. Lord, and Erik S. Knudsen. 2018. “Targeting the Vulnerability of RB Tumor Suppressor Loss in Triple-Negative Breast Cancer.” *Cell Reports* 22 (5): 1185–99. https://doi.org/10.1016/j.celrep.2018.01.022.

Workman, Paul, Francis Burrows, Len Neckers, and Neal Rosen. 2007a. “Drugging the Cancer Chaperone HSP90: Combinatorial Therapeutic Exploitation of Oncogene Addiction and Tumor Stress.” In *Annals of the New York Academy of Sciences*, 1113:202–16. Blackwell Publishing Inc. https://doi.org/10.1196/annals.1391.012.

———. 2007b. “Drugging the Cancer Chaperone HSP90: Combinatorial Therapeutic Exploitation of Oncogene Addiction and Tumor Stress.” In *Annals of the New York Academy of Sciences*, 1113:202–16. Blackwell Publishing Inc. https://doi.org/10.1196/annals.1391.012.

Würl, Peter, Axel Meye, Christine Lautenschläger, Hannelore Schmidt, Matthias Bache, Holger Kalthoff, Manfred Schönfelder, Friedrich Wilhelm Rath, and Helge Taubert. 1999. “Clinical Relevance of PRb and P53 Co-Overexpression in Soft Tissue Sarcomas.” *Cancer Letters* 139 (2): 159–65. https://doi.org/10.1016/S0304-3835(99)00034-8.

Yang, Jilong, Xiaoling Du, Kexin Chen, Antti Ylipää, Alexander J.F. Lazar, Jonathan Trent, Dina Lev, et al. 2009. “Genetic Aberrations in Soft Tissue Leiomyosarcoma.” *Cancer Letters* 275 (1): 1–8. https://doi.org/10.1016/j.canlet.2008.06.013.

Yun, Chul Won, Hyung Joo Kim, Ji Ho Lim, and Sang Hun Lee. 2020. “Heat Shock Proteins: Agents of Cancer Development and Therapeutic Targets in Anti-Cancer Therapy.” *Cells*. MDPI. https://doi.org/10.3390/cells9010060.

Zecha, Jana, Chen Meng, Daniel Paul Zolg, Patroklos Samaras, Mathias Wilhelm, and Bernhard Kuster. 2018. “Peptide Level Turnover Measurements Enable the Study of Proteoform Dynamics.” *Molecular and Cellular Proteomics* 17 (5): 974–92. https://doi.org/10.1074/mcp.RA118.000583.

Zetterberg, Anders, Olle Larsson, and G Wiman. 1995. “What Is the Restriction Point?” *Current Opinion in Cell Biology*. Vol. 7.

Zhang, Jian, Houde Li, Yu Liu, Kejia Zhao, Shiyou Wei, Eric T. Sugarman, Lunxu Liu, and Gao Zhang. 2022. “Targeting HSP90 as a Novel Therapy for Cancer: Mechanistic Insights and Translational Relevance.” *Cells*. MDPI. https://doi.org/10.3390/cells11182778.

Zhang, Jianming, Huadan Li, Zhizhou Huang, Yangfan He, Xueqiong Zhou, Tingyuan Huang, Peijuan Dai, et al. 2016. “Hypoxia Attenuates Hsp90 Inhibitor 17-DMAG-Induced Cyclin B1 Accumulation in Hepatocellular Carcinoma Cells.” *Cell Stress and Chaperones* 21 (2): 339–48. https://doi.org/10.1007/s12192-015-0664-2.

Zhang, Zhiwei, Chenggong Sun, Chengcheng Li, Xinlin Jiao, Brannan B. Griffin, Samina Dongol, Huan Wu, et al. 2020. “Upregulated MELK Leads to Doxorubicin Chemoresistance and M2 Macrophage Polarization via the MiR-34a/JAK2/STAT3 Pathway in Uterine Leiomyosarcoma.” *Frontiers in Oncology* 10 (April). https://doi.org/10.3389/fonc.2020.00453.

Zheng, Yuan-Yin, Xiao-Bin Liu, Ying-Yu Mao, and Mao-Hua Lin. 2020. “Smooth Muscle Tumor of Uncertain Malignant Potential (STUMP): A Clinicopathologic Analysis of 26 Cases.” *Int J Clin Exp Pathol*. Vol. 13. www.ijcep.com/.

Zhu, Chunxiao, Xiaoqing Guan, Xinuo Zhang, Xin Luan, Zhengbo Song, Xiangdong Cheng, Weidong Zhang, and Jiang Jiang Qin. 2022a. “Targeting KRAS Mutant Cancers: From Druggable Therapy to Drug Resistance.” *Molecular Cancer*. BioMed Central Ltd. https://doi.org/10.1186/s12943-022-01629-2.

———. 2022b. “Targeting KRAS Mutant Cancers: From Druggable Therapy to Drug Resistance.” *Molecular Cancer*. BioMed Central Ltd. https://doi.org/10.1186/s12943-022-01629-2.

ZI-NAN LI and YING LUO. 2023. “HSP90 Inhibitors and Cancer: Prospects for use in Targeted Therapies (Review).” *ONCOLOGY REPORTS*.

APPENDICES

Compound Screening Library – The small Oncology Library tested at 30 nM in SK-LMS-1 cell line.

DRUG	Delta-Zeta Value
17-DMAG (Alvespimycin)	-1.011655531
ABT-888 (Veliparib)	-1.001154057
CAL-101	-0.982901401
Carfilzomib	-0.84463279
Methylprednisolone	-0.836476476
Flutamide	-0.833112881
Lenvatinib	-0.833035979
OSI-906_Linsitinib	-0.82157632
Clofarabine	-0.796810452
EMPTY	-0.776895749
*Simvastatin***	-0.74808822
*S-trityl-L-cysteine, 40 mM**	-0.735169394
Olaparib	-0.731011544
DMSO	-0.716802444
PF670462	-0.715553603
Mitotane	-0.707239633
LY2784544_Gandotinib	-0.688099882
EMPTY	-0.681962056
Fludarabine phosphate	-0.679602024
Anastrozole	-0.676942068
AZ 3146	-0.653347735
ZSTK474	-0.632846797
Triethylenemelamine	-0.625464959
DMSO	-0.614976877
Toremifene citrate	-0.599453699
Letrozole	-0.590316448
EMPTY	-0.586755874
BIBF 1120_Nintedanib	-0.560922456

Allopurinol	-0.553938439
Oxaliplatin	-0.54864604
EMPTY	-0.540078729
ABT-263 (Navitoclax)	-0.530964016
EMPTY	-0.528622705
Carboplatin	-0.527451149
Erismodegib	-0.515238167
Obatoclax Mesylate (GX15-070)	-0.509002305
Cytarabine hydrochloride	-0.49979937
Alectinib	-0.480661113
DCC-2036_Rebastinib	-0.473754405
Lenalidomide	-0.472355955
ARRY-162_MEK-162	-0.472153929
PF-04708671	-0.459696205
Motesanib Diphosphate (AMG-706)	-0.456589774
CI-994_Tacedinaline	-0.454233329
PCI-32765_Ibrutinib	-0.446382245
EMPTY	-0.439121053
Dacomitinib (monohydrate) (PF-00299804)	-0.439117211
1-methyl-D-tryptophan, 95%	-0.431094314
BIIB021	-0.426154362
Crenolanib	-0.424998659
Abitrexate/Methotrexate	-0.421832965
VER 155008	-0.421408698
PF-3845	-0.420476272
PLX4032_Vemurafenib	-0.41852021
DMSO	-0.414069494
TAK-901	-0.409362588
EMPTY	-0.406525979
Methoxsalen	-0.404508088
Dabrafenib Mesylate	-0.399720551
Dexamethasone (Decadron)	-0.398829061
EMPTY	-0.392779334

LY2228820 (CP868569)	-0.39134701
MLN4924	-0.382056606
NVP-BGJ398	-0.379730298
Trifluridine	-0.379461735
Valrubicin	-0.375961282
Lomustine	-0.372558718
Ifosfamide	-0.372309613
MK-2206	-0.369281655
BI 6727_Volasertib	-0.368751446
Dasatinib	-0.364171153
Thiotepa	-0.362549587
Uracil mustard	-0.362001652
AZD1480	-0.358863067
EMPTY	-0.352986466
Rofecoxib (Vioxx)	-0.3524936
Prima-1 Met	-0.346903171
Vincristine Sulfate (Oncovin)	-0.342301014
Finasteride	-0.340948423
EMPTY	-0.337512795
Indibulin	-0.332752513
AV-951 (Tivozanib)	-0.332351284
EMPTY	-0.330976325
GDC-0980	-0.328057469
Erlotinib hydrochloride	-0.32726444
Plicamycin	-0.324299483
Pomalidomide	-0.324204939
Ponatinib	-0.323504552
EMPTY	-0.321565886
Pazopanib	-0.31616749
AG-014699_Rucaparib	-0.315274134
SR1 HCl	-0.315051543
Belinostat (PXD101)	-0.30895532
Temozolomide	-0.306869564

Romidepsin	-0.296009345
Etoposide	-0.295837712
Tasocitinib_Tofacitinib	-0.293468007
Uridine triacetate	-0.285207102
DMSO	-0.281222796
BMS-754807	-0.281043866
Dexrazoxane	-0.280383413
GSK1120212_Trametinib	-0.276481335
MK-0752	-0.274063117
Gefitinib	-0.271545931
Idelalisib	-0.270557986
Varespladib	-0.269873403
Vatalanib	-0.269097297
Sorafenib	-0.2690603
EMPTY	-0.265077874
Azacitidine	-0.258462493
EMPTY	-0.257276923
Perifosine aq/PBS	-0.254833901
Atorvastatin Ca	-0.254284893
Lasofoxifene	-0.253519287
4nM E7107	-0.247365068
RD162	-0.245884385
Deferoxamine mesylate	-0.245649786
Idarubicin HCl	-0.242196138
DMSO	-0.240068333
DMSO	-0.237886755
Mercaptopurine	-0.232855461
Gefitinib	-0.229517042
DMSO	-0.229324882
Celecoxib	-0.218769827
Goserelin acetate	-0.218007359
Entinostat	-0.216208304
GDC-0941_Pictilisib	-0.215716697

PAC-1	-0.214143579
FK 506_Tacrolimus	-0.21325925
EMPTY	-0.209607293
AC220_Quizartinib	-0.209514691
LY2157299	-0.208267353
DMSO	-0.207034694
DMSO	-0.206892234
MK-4827, HCl salt	-0.202861112
EMPTY	-0.198171717
EMPTY	-0.197290968
EMPTY	-0.19579124
MGCD-265	-0.194400472
Pipobroman	-0.193979611
EMD1214063	-0.192031212
17-AAG (Tanespimycin, Geldanamycin)	-0.189685182
Bortezomib	-0.187905938
BMS-911543	-0.186758805
DMSO	-0.186552651
EMPTY	-0.185034147
CUDC-101	-0.183938796
MLN8237_Alisertib	-0.179825257
AZD1152-HQPA	-0.178777814
DMSO	-0.178691813
Melphalan	-0.174016629
AP24534 (Ponatinib)	-0.167494218
Clafen (Cyclophosphamide, Endoxan)	-0.162562258
DMSO	-0.158647155
Roscovitine_Selicilib	-0.153440401
Dasatinib	-0.150037844
Vandetanib	-0.149258515
Aminolevulinic acid hydrochloride	-0.143919958
GSK 650394	-0.143727192
RDEA119_Refametinib	-0.139735878

Thio-TEPA	-0.136875136
DMSO	-0.136420238
Nelarabine	-0.130625374
Mechlorethamine hydrochloride	-0.128406813
GDC-0068	-0.127679557
Tipifarnib (Zarnestra)	-0.113285853
Imiquimod	-0.111474513
DMSO	-0.106323789
Exemestane	-0.102591518
Decitabine (Dacogen)	-0.102258953
EMPTY	-0.101184394
AVN944	-0.09826212
5uM GEM	-0.092802933
Amifostine	-0.092228605
Megestrol acetate	-0.09063696
GSK2636771	-0.090081992
4-hydroxytamoxifen	-0.080721457
Thioguanine	-0.076452887
EMPTY	-0.073392059
CHR 2797_Tosedostat	-0.071452805
*Epirubicin HCl***	-0.067488777
*Ribociclib**	-0.060235163
YM155	-0.057911953
Venetoclax	-0.055403245
Epothilone B (Patupilone)	-0.055108607
Prednisolone	-0.054193467
Altretamine	-0.053761391
Brivanib	-0.048667385
DMSO	-0.047863257
EMPTY	-0.04550812
DMSO	-0.04461761
5uM GEM	-0.044057682
Bexarotene	-0.041198143

EMPTY	-0.0384341
BAY 73-4506_Regorafenib	-0.036078025
Ixabepilone	-0.035611576
HA-1077 (Fasudil)	-0.03509124
Nutlin-3	-0.034512584
Sunitinib	-0.029296731
EMPTY	-0.028668411
Capecitabine	-0.028065112
AT-406	-0.026188809
DMSO	-0.022143579
NVP-LDE225 (Diphosphate salt)	-0.021794745
EMPTY	-0.02076542
Omacetaxine mepesuccinate	-0.013370149
5uM GEM	-0.013283128
Bimatoprost	-0.010428169
MK1775	-0.007164034
Hydroxyurea	-0.005833876
Aminoglutethimide	-0.004152657
Palbociclib	0.002305499
Tretinoin	0.009023471
JNJ 26854165 (Serdemetan)	0.012988406
Floxuridine	0.013674205
Masitinib	0.016791992
Pentostatin	0.016857826
5uM GEM	0.021639473
XL184_Cabozantinib	0.022514761
PX-866_Sonolisib	0.02556995
Homoharringtonine	0.026755523
Tandutinib	0.028650314
5uM GEM	0.029470992
Arsenic(III) oxide	0.030415618
Paclitaxel	0.031602581
(5Z)-7-Oxozeaenol	0.033349323

MGCD0103_Mocetinostat	0.033438736
EMPTY	0.034487796
5uM GEM	0.036785388
Vorinostat	0.038205707
Tubacin	0.038908044
DMSO	0.040608406
XL-147	0.041919578
PF-04691502	0.045346426
Dactinomycin	0.046090843
Sotrastaurin	0.046725948
EMPTY	0.046986297
Everolimus	0.048614292
PF 431396	0.053155177
Vinblastine sulfate	0.053514948
Ixazomib citrate	0.05417661
NVP-AUY922	0.054751636
Cabazitaxel	0.055985813
Chlorambucil	0.060520918
Prednisone	0.062046082
5uM GEM	0.067814015
(R)-Flurbiprofen (Tarenflurbil)	0.072678014
Anagrelide	0.07344511
AZD6244 (Selumetinib)	0.076392694
Busulfan	0.079738022
Auranofin	0.080254589
Bosutinib	0.088896357
Clomifene citrate	0.091309236
Pralatrexate	0.09201793
BIBW2992 (Tovok)_Afatinib	0.092193782
TAK-733	0.104217477
Galiellalactone	0.114567161
Camptothecin	0.116026115
EMPTY	0.116818106

Mithramycin A	0.116857494
EMPTY	0.118170862
Tetramisole HCl	0.120104648
Valproic acid	0.121820387
5uM GEM	0.125661898
Procarbazine hydrochloride	0.133831319
DMSO	0.146401194
R406_Tamatinib	0.149869899
EMPTY	0.157789042
Niraparib hydrochloride	0.159521947
Streptozocin	0.16027612
Osimertinib	0.162970872
DMSO	0.163113186
PF 477736	0.163639612
DMSO	0.167549548
Dacarbazine	0.171839155
Capecitabine	0.178027296
DMSO	0.178058827
Vinorelbine tartrate	0.181499345
Dinaciclib (SCH727965)	0.186041631
Temsirolimus	0.199756162
JNJ-26481585_Quisinostat	0.211870715
Docetaxel	0.221272951
Thalidomide	0.230636889
I-BET151 (GSK1210151A)	0.232997836
BIRB 796 (Doramapimod)	0.23551662
ABT-199	0.239959067
Crizotinib	0.24204311
Pravastatin	0.242920347
AT 101	0.245198639
Carmustine	0.254166171
Zoledronic acid	0.254191969
CHIR-258 (Dovitinib)	0.255683382

PF-2341066 (Crizotinib)	0.256145819
PD-0332991	0.257123069
Nilutamide	0.258199285
EMPTY	0.263491186
Ceritinib	0.265472612
Doxorubicin	0.272736904
Iniparib (BSI-201, IND-71677)	0.273660374
Tubastatin A HCl	0.27718152
ABT-869_Linifanib	0.280176957
XAV-939	0.282140564
XL880 (Foretinib)	0.284046067
Cobimetinib	0.284202185
Cisplatin aq	0.287680113
DMSO	0.301786315
Pemetrexed	0.302575698
Daunorubicin hydrochloride	0.303797892
Fluorouracil	0.311020232
CPI-613	0.312738652
DMSO	0.313393573
LY2603618_Rabusertib	0.317106411
Chloroquine diphosphate	0.318692471
Cladribine	0.321977156
SB 743921	0.326838329
Lomeguatrib	0.327153698
Imatinib	0.330828829
INCB018424 (free base, Ruxolitinib)	0.33793895
EMPTY	0.346131195
AZD 7762 hydrochloride	0.350157595
NVP-BEZ235_Dactolisib	0.357657688
Cyclophosphamide	0.377782792
Pilocarpine	0.382300701
AT9283	0.382970507
ABT-751	0.386718831

EMPTY	0.399196988
Aspirin (Acetylsalicylic Acid)	0.419126281
Fulvestrant	0.420417574
FG-4592	0.42402601
Teniposide	0.424186004
Panobinostat	0.425011354
Axitinib	0.429012102
AS703026_Pimasertib	0.438609017
Canertinib	0.445738017
ARQ 197_Tivantinib	0.446057374
Irinotecan	0.446809781
KX2-391	0.449237194
Rapamycin (sirolimus)	0.449846814
Lapatinib, di-p-toluenesulfonate salt	0.47544607
Enzastaurin	0.482340709
Stattic	0.494947384
AZD4547	0.506820951
PKC412_Midostaurin	0.50707004
UCN-01	0.508118518
VX-11e	0.515591392
TGX-221	0.519284492
Mitomycin	0.527644033
Bleomycin sulfate	0.536002176
Metformin hydrochloride aq	0.53643117
BKM-120_Buparlisib	0.549436259
Gemcitabine hydrochloride	0.556554046
Estramustine sodium phosphate	0.577687523
RAF265	0.585340193
EMPTY	0.587101584
LY 333531 mesylate_Ruboxistaurin	0.588960367
GSK2126458	0.590655362
Quinacrine HCl	0.605443663
2-methoxyestradiol (Panzem)	0.616585503

Nilotinib	0.644675148
OSI-027	0.648610432
MDV3100_Enzaluamide	0.66071761
CYT-387_Momelotinib	0.67883565
AZD8055	0.692877645
Vorinostat	0.695613864
BI 2536	0.710124218
PHA-739358 (Danusertib)	0.723597343
Arsenic trioxide	0.730358231
Plerixafor	0.735723203
Ridaforolimus	0.762292113
Topotecan hydrochloride	0.779169847
PIK-75 HCl	0.784843318
AZD2014	0.786863162
Bicalutamide	0.813699899
Abiraterone	0.866493976
INK128	0.873064183
Lestaurtinib	0.877051362
Enzalutamide	0.925829107
Amonafide	0.934537677
Mitoxantrone	1.087769366
PF4800567 hydrochloride	1.109930454
Bendamustine hydrochloride	1.161778631
FK-866 HCl_Daporinad	1.239281268
GSK 269962	2.739359326
Vismodegib	2.739359326